

1991

Intelligent chip control and tool wear estimation in automated machining systems

Xiang Dong Fang
University of Wollongong

Recommended Citation

Fang, Xiang Dong, Intelligent chip control and tool wear estimation in automated machining systems, Doctor of Philosophy thesis, Department of Mechanical Engineering, University of Wollongong, 1991. <http://ro.uow.edu.au/theses/1585>

Research Online is the open access institutional repository for the University of Wollongong. For further information contact the UOW Library: research-pubs@uow.edu.au

NOTE

This online version of the thesis may have different page formatting and pagination from the paper copy held in the University of Wollongong Library.

UNIVERSITY OF WOLLONGONG

COPYRIGHT WARNING

You may print or download ONE copy of this document for the purpose of your own research or study. The University does not authorise you to copy, communicate or otherwise make available electronically to any other person any copyright material contained on this site. You are reminded of the following:

Copyright owners are entitled to take legal action against persons who infringe their copyright. A reproduction of material that is protected by copyright may be a copyright infringement. A court may impose penalties and award damages in relation to offences and infringements relating to copyright material. Higher penalties may apply, and higher damages may be awarded, for offences and infringements involving the conversion of material into digital or electronic form.

ERRATA TABLE

Page	Line	Corrections	
		was	to be corrected as
32	5	we	was
120	5 from foot	form	from
135	2 from foot	much a	much
141	3 from foot	grooves' spacing	the spacing of the grooves
176	11	This work	This work is
179	11	to modify tool	to modify the tool
190	11	Reconnition	Recognition

**INTELLIGENT CHIP CONTROL AND TOOL WEAR
ESTIMATION IN AUTOMATED MACHINING SYSTEMS**

A thesis submitted in fulfilment of the
requirements for the award of the degree

DOCTOR OF PHILOSOPHY

from

THE UNIVERSITY OF WOLLONGONG

by

XIANG DONG FANG

B.E. (Hons.), M.E. (Hons.), Tsinghua

Department of Mechanical Engineering
June, 1991

DECLARATION

This is to certify that the work presented in this thesis was carried out by the author in the Department of Mechanical Engineering of the University of Wollongong, Australia and has not been submitted for a degree to any other university or institution.

Xiang Dong FANG

ACKNOWLEDGEMENTS

The author is greatly indebted to his supervisors Dr. Y. Yao and Professor G. Arndt for their excellent guidance, close supervision and generous help during the course of this thesis.

The author is also deeply grateful to the invaluable guidance and help from his former supervisor, Associate Professor I.S. Jawahir, currently in the University of Kentucky, U.S.A.

The author is very thankful to the University of Wollongong as well as CAMIA, the Centre for Advanced Manufacturing and Industrial Automation, for providing him with postgraduate scholarships.

Acknowledgement is also given to all the staff in the Department, in particular to Professor P. C. Arnold for his encouragement and all sorts of help; Dr. E. Siores for his useful advice on artificial intelligence techniques; Mr. D. Jamieson, Mr. I. Kirby, Mr. T. Kent and Mr K. Maywald for their assistance in using computer and instrument facilities.

Many thanks are also due to the workshop staff, especially Mr. M. Morillas and Mr. R. Marshall, for their many days with the assistance to the machining experiments.

Finally, the author expresses his heartfelt thanks to his wife Na Lin for her consistent encouragement and help during his PhD study.

ABSTRACT

Chip control and tool wear estimation are two major concerns in automated machining systems. Chip control is essential for the safety of the machining operation, the maintenance of good surface finish on the machined part, the convenience of chip disposal, and possible power reduction; while tool wear estimation is vital to an effective tool change policy and quality control strategy, especially in finish-machining.

This thesis first presents a new method for quantifying chip breaking and chip shapes with a fuzzy rating system, and further for predicting the chip breakability for arbitrary combinations of machining conditions through a fuzzy-set mathematical model. A predictive expert system for off-line assessment of machining performance, with chip control as a major criterion and due consideration to surface finish and power consumption, is then developed.

A knowledge-based system for designing optimum chip breakers is set up with a criterion of efficient chip breaking at reduced power consumption. The method is based on the analysis of three-dimensional chip flow in oblique machining for a wide range of work materials, cutting conditions, tool geometries, chip breaker styles/sizes and restricted contact lengths.

Experimental results of tool wear patterns in finish-machining show that estimation of more than one type of tool wear is required to assure the quality of a finished product. In order to achieve this, a dispersion analysis algorithm, derived from the established

multivariate time series models, is used for the overall estimation of tool wear, including major flank wear, crater wear, minor flank wear and groove wear at the minor cutting edge.

Finally, neural network techniques are used for modelling the dynamic interrelationship between the chip forming behaviour and different tool wear states. By integrating the developed methods for predicting chip breakability/shapes and for estimating comprehensive tool wear, the initially-predicted chip forming/breaking patterns can be updated with tool wear progression during the machining process through the use of neural network techniques.

The results show that the methods developed in this thesis, for predicting chip breaking and shapes, and for evaluating machining performance, including chip control, surface finish and power consumption, may be used to form a basis for the off-line assessment of "total machinability" for automated machining systems. The strategy of comprehensive tool wear estimation provides a feasible means for on-line tool wear monitoring to assure product quality, especially under finish-machining conditions. The results also show that by using neural networks, chip forming behaviour with tool wear progression can be evaluated in-process, thus providing a feasible approach for achieving the on-line assessment of machining performance including chip forming patterns, surface finish and overall tool wear progression.

TABLE OF CONTENTS

DECLARATION	i.
ACKNOWLEDGEMENTS	ii.
ABSTRACT	iii.
TABLE OF CONTENTS	v.
LIST OF TABLES	xii.
LIST OF FIGURES	xiii.
NOMENCLATURE	xvii.
PUBLICATIONS WHILE STUDYING FOR PHD COURSE	xxii.

Chapter	Title	Page
1.	INTRODUCTION	1.
1.1	The Importance of the Current Research Project and Its Objective	1.
1.1.1	Significance of Chip Control in Automated Machining	1.
1.1.2	The Need for Developing a Knowledge-based Expert System for Effective Chip Control	1.
1.1.3	Strategies of Tool Wear Estimation in Finish-Machining	2.
1.1.4	Multivariate Time Series Modelling for Comprehensive Tool Wear Estimation	4.
1.1.5	Integrating Chip Control and Tool Wear Estimation for On-line Assessment of Machining Performance	6.
1.2	Scope of Thesis	6.

1.3	Literature Survey	9.
2.	PREDICTING CHIP BREAKABILITY IN MACHINING WITH A FUZZY SET-BASED EXPERT SYSTEM	10.
2.1	Introduction	10.
2.2	Fuzzy Description of Chip Breakability	12.
2.3	Machining Experiments for Setting up the Basic Chip Database	15.
2.4	Factors Affecting Chip Breakability : An Experimental Analysis	17.
2.4.1	Effect of Cutting Conditions	20.
2.4.2	Effect of Work Materials	24.
2.4.3	Effect of Tool Inserts	29.
2.4.4	Effect of Tool Geometries	31.
2.5	Foundation of a Fuzzy-set Mathematical Model	33.
2.6	Establishment of an Expert System for Predicting Chip Breakability	37.
2.6.1	Knowledge Representation	37.
2.6.2	Examples of Knowledge Rules for Chip Breakability	39.
2.6.3	Schematic Diagram of the Expert System	44.
2.7	Prolog Programming Architecture	45.
2.8	Summary and Concluding Remarks	46.
3.	A PREDICTIVE EXPERT SYSTEM FOR THE ASSESSMENT OF MACHINING PERFORMANCE WITH CHIP CONTROL AS A MAJOR CRITERION	48.
3.1	Introduction	48.
3.2	Foundation of Machining Performance Database	49.

3.3	Assessment of Machining Performance	50.
3.3.1	Assessment of Chip Control	50.
3.3.2	Assessment of Surface Finish	53.
3.3.3	Assessment of Power Consumption	53.
3.4	An Investigation of the Influencing Factors on Machining Performance	54.
3.4.1	Effect of Tool Insert Types	54.
3.4.2	Effect of Work Materials	56.
3.4.3	Effects of Cutting Conditions and Tool Geometries	56.
3.5	Evaluation of Work Material Properties	58.
3.6	Knowledge Representation	60.
3.6.1	Basic Facts Based on the Database	60.
3.6.2	Knowledge from Expert's Experience	61.
3.7	Establishment of a Predictive Expert System	64.
3.8	Summary and Concluding Remarks	65.
4.	A KNOWLEDGE-BASED SYSTEM FOR DESIGNING EFFECTIVE GROOVED CHIP BREAKERS BASED ON THREE-DIMENSIONAL CHIP FLOW IN MACHINING	67.
4.1	Introduction	67.
4.2	Present Knowledge of Chip Control with Grooved Chip Breakers	68.
4.2.1	Tool Restricted Contact Effect on Chip Breaking	68.
4.2.2	Three-dimensional Chip Flow	69.
4.2.3	Power Consumption Rate	70.
4.3	Establishment of a Database System	71.
4.3.1	Reference Database	71.

4.3.2	Grooved Chip Breaker Database	71.
4.3.3	Three-dimensional Chip Flow Database	72.
4.4	Summary of Present Knowledge for Setting up a Knowledge Base	72.
4.4.1	Analysis of Chip Breaking	73.
4.4.2	Analysis of Grooved Chip Breakers and Power Consumption Rate	80.
4.5	Analysis of 3-D Chip Flow and Chip Curling with Grooved Chip Breakers	83.
4.5.1	Effect of the Chip Backflow Angle	83.
4.5.2	Effect of the Chip Sideflow Angle	85.
4.6	The Establishment of a Knowledge Base	86.
4.6.1	Knowledge Rules for Predicting the Natural Contact Length	86.
4.6.2	Knowledge Rules for Predicting the Chip Backflow Angle	88.
4.6.3	Knowledge Rules for Predicting the Chip Sideflow Angle	90.
4.6.4	Knowledge Rules for Determining the Minimum Power Consumption	92.
4.6.5	Knowledge Rules for Selecting the Effective Groove Profile	93.
4.7	A Strategy for Designing Effective Grooved Chip Breakers	94.
4.7.1	Determining the Optimum Restricted Contact Length	94.
4.7.2	Determining the Effective Groove Parameters	96.
4.7.3	Schematic Diagram for Designing Effective Grooved Chip Breakers	97.
4.8	Summary and Concluding Remarks	99.
5.	COMPREHENSIVE TOOL WEAR ESTIMATION IN FINISH-MACHINING BY MULTIVARIATE TIME SERIES ANALYSIS	100.
5.1	Introduction	100.
5.2	Tool Wear Experiments	102.

5.2.1	Description of Experiments	102.
5.2.2	Definition of Comprehensive Tool Wear Parameters	105.
5.2.3	Tool Wear Measurement and Wear Development Patterns	106.
5.3	Multivariate Time Series Techniques	110.
5.3.1	Trivariate ARMAV Models	110.
5.3.2	Dispersion Analysis	112.
5.4	Tool Wear Estimation by Dispersion Analysis based on ARV Models	114.
5.4.1	ARV Modelling of 3-D Dynamic Cutting Forces	114.
5.4.2	Patterns of Dispersion Development	115.
5.4.3	Analysis Associated with Physical Interpretation	119.
5.4.4	Strategies of Tool Wear Estimation in Finish-Machining	121.
5.4.5	Structural Dynamics and Idle Disturbances	122.
5.5	Summary and Concluding Remarks	122.
6.	MONITORING GROOVE WEAR DEVELOPMENT IN FINISH-MACHINING BY ARV MODEL-BASED MULTIPLE DISPERSION ANALYSIS	124.
6.1	Introduction	124.
6.2	Investigation in to the Patterns of Groove Wear Development	126.
6.2.1	Tool Wear Experiments	126.
6.2.2	Development of Groove Wear	127.
6.2.3	Patterns of Groove Wear Development	131.
6.3	ARV Model-based Multiple Dispersion Analysis	135.
6.3.1	Application of Autoregressive Vector Time Series Modelling	135.
6.3.2	Multiple Dispersion Analysis	136.

6.4	Strategy for Groove Wear Monitoring by Multiple Dispersion Analysis	138.
6.4.1	Groove Wear Monitoring for the Lower Feed Condition	138.
6.4.2	Groove Wear Monitoring for the High Feed Condition	140.
6.5	Physical Interpretations	141.
6.6	Summary and Concluding Remarks	143.
7.	INTEGRATING CHIP CONTROL AND TOOL WEAR THROUGH NEURAL NETWORKS FOR THE ON-LINE ASSESSMENT OF MACHINING PERFORMANCE	145.
7.1	Introduction	145.
7.2	Description of Machining Experiments	147.
7.2.1	Machining Conditions	147.
7.2.2	Comprehensive Tool Wear Patterns	148.
7.2.3	Chip Breakability Assessment	149.
7.2.4	Surface Finish Assessment	152.
7.3	Feature Extraction from 3-D Dynamic Cutting Forces	153.
7.4	Architecture of Neural Networks	155.
7.4.1	Neural Network Techniques Used	155.
7.4.2	Selection of Input Features	158.
7.5	Analysis of Results from Neural Networks	161.
7.5.1	Training Strategy with Neural Networks	161.
7.5.2	Analysis of Results for Training and Testing Effects	162.

7.6	Extension : Future Directions and Developments	169.
7.6.1	Real-time Application of Chip Control and Tool Wear Estimation in Automated Machining Systems	169.
7.6.2	Developing a Self-organising Neural Network	171.
7.7	Summary and Concluding Remarks	171.
8.	CONCLUSIONS	173.
8.1	A New Approach for the Quantitative Prediction of Chip Breakability and Chip Forming Patterns	174.
8.2	A Scientifically-based Method for the Effective Design of Chip Breakers	175.
8.3	A New Strategy for Comprehensive Tool Wear Estimation	176.
8.4	A New Attempt at Estimating Chip Forming Patterns with Tool Wear Progression for On-line Assessment of Machining Performance	177.
8.5	Suggestion for Future Work	178.
	REFERENCES	181.
	APPENDIX	
A	Standard Fuzzy Membership Values for Chip Breakability	
B	Representative Data of Surface Finish when Machining with Different Tool Chip Breakers	
C	Overall Groove Wear Data from Groove Wear Experiments	
D	Input/Output Training and Testing Data in Neural Network Experiments	

LIST OF TABLES

TABLE		PAGE
1.1	ARMA modelling of machining process for condition monitoring	5.
2.1	Membership values for most common chip shapes/sizes	15.
2.2	Machining conditions used for setting up the basic chip database	16.
2.3	Conditions used for the extensive machining experiments	19.
2.4	Fuzzy linguistic values	35.
2.5	Predicting chip breakability with fuzzy ratings	36.
3.1	Chip acceptable factor $g(x)$ in automated machining systems	51.
3.2	Integrated assessment for chip control in automated machining systems	52.
3.3	An example of work material effect table	58.
3.4	Fuzzy ratings of surface finish and power consumption	59.
5.1	Machining conditions used in tool wear experiments	103.
5.2	Tool wear measurement result for cutting condition Group 4	106.
5.3	Tool wear measurement results for cutting condition Groups 1-3	107.
5.4	Dispersion analysis results	116.
5.5	Tool wear analysis for cutting condition Group 1	121.
6.1	Machining conditions used in groove wear experiments	127.
6.2	Relationship between surface roughness and dispersion pattern	141.
6.3	Comparison between dispersion analysis results and physical quantities	143.
7.1	Machining conditions used in neural network experiments	148.
7.2	Chip forming behaviour in machining process while tool wear	150.
7.3	The training data under Training Cutting Conditions 1-3	160.

LIST OF FIGURES

FIGURE		PAGE
2.1	Classification of chip shapes	15.
2.2	Two examples of chip breakability diagrams	18.
2.3	Factors affecting chip breakability	18.
2.4	The effect of depth of cut on chip breakability	21.
2.5	The effect of feed on chip breakability	22.
2.6	The effect of cutting speed on chip breakability	23.
2.7	The effect of carbon content on chip breakability	25.
2.8	The effect of Cr-Mo alloying on chip breakability	26.
2.9	The effect of low-carbon-based alloying on chip breakability	27.
2.10	The effect of different work materials on chip breakability	28.
2.11	Chip breakability diagrams for six different work materials	28.
2.12	Chip breakability diagram for different tool inserts at a high cutting speed	29.
2.13	Chip breakability diagrams for different tool inserts at a low cutting speed	30.
2.14	Comparison of cutting speed effect with different chip breakers	31.
2.15	The effect of cutting edge angle on chip breakability	32.
2.16	The effect of tool nose radius on chip breakability	33.
2.17	Fuzzy exponential functions	35.
2.18	The expert system schematic diagram	44.
2.19	PROLOG program structure diagram	46.
3.1	Surface finish comparison for four tool inserts	54.
3.2	Power consumption comparison for five tool inserts	55.
3.3	Surface finish comparison for four work materials	56.
3.4	Power consumption comparison for four work materials	57.

3.5	Integrated effects of cutting conditions and tool geometries	57.
3.6	Flow chart for selecting efficient feed value	63.
3.7	A schematic diagram for setting up the predictive expert system	64.
3.8	The predictive expert system acting as an auxiliary for APP system	65.
4.1	Three chip streaming models	69.
4.2	Three dimensional chip flow with a grooved chip breaker	70.
4.3	Configurations of grooved chip breakers	72.
4.4	Typical relationship diagrams for restricted contact tools	74.
4.5	The effect of tool restricted contact length on chip up-curl and chip breaking	75.
4.6	The effect of tool restricted contact length on chip up-curl radius for three chip-breaker groove sizes	75.
4.7	The effect of chip-breaker groove style on chip breaking	76.
4.8	The effects of depth of cut	77.
4.9	The effects of feed	78.
4.10	The effects of tool nose radius	79.
4.11	The effect of inclination angle on chip sideflow	80.
4.12	The effect of cutting speed on chip sideflow	80.
4.13	The effects of work material (carbon steels)	81.
4.14	The effect of tool/chip contact length on power consumption	82.
4.15	The effect of tool restricted contact length on specific cutting pressure in machining with grooved chip breakers	83.
4.16	The chip backflow effect on tool groove utilisation	84.
4.17	The chip sideflow effect on the effective tool groove parameters	85.
4.18	Determination of tool/chip natural contact length	86.
4.19	Determining the optimum restricted contact length	95.
4.20	Flow chart for the knowledge-based system developed	98.
5.1	Experiment setup	102.
5.2	Dynamic cutting force measured in terms of its three orthogonal components	104.

5.3	Definition of comprehensive tool wear parameters	105.
5.4	Tool wear development for cutting condition Group 1	108.
5.5	Tool wear development for cutting condition Groups 2 & 3	109.
5.6	Tool wear observed under a scanning electron microscope (SEM)	110.
5.7	Dispersion diagram for cutting condition Group 1	117.
5.8	Dispersion diagrams for cutting condition Groups 2 & 3	118.
5.9	The model for the forces acting on different tool faces	119.
6.1	Groove wear at the minor cutting edge	125.
6.2	Number of grooves at the minor cutting edge	128.
6.3	Development of groove depth	128.
6.4	Development of the maximum groove length	129.
6.5	Development of groove wear area	129.
6.6	Development of nose wear	130.
6.7	Surface roughness for five cutting conditions	130.
6.8	Groove wear development under the lower feed condition	132.
6.9	Groove wear development under the higher feed condition	133.
6.10	Dispersion patterns for the lower feed condition	139.
6.11	Dispersion patterns for the higher feed condition	140.
7.1	Development patterns of comprehensive tool wear	149.
7.2	Change of chip shapes/sizes with tool wear progression	150.
7.3	Change of chip breakability under Training Cutting Conditions 2-6	151.
7.4	Change of surface finish with tool wear rates for Training Cutting Condition 1	152.
7.5	Development of surface finish for Training Cutting Conditions 2-6	153.
7.6	A typical relationship between tool wear and dispersion patterns	154.
7.7	Back-propagation neural network with one hidden layer	156.
7.8	The function of artificial neuron	157.
7.9	Description of three basic transfer functions	158.
7.10	Feature selection for neural network	159.

7.11	Effect of the number of hidden neurons for three transfer functions	163.
7.12	Evaluation of training effect of chip breakability	164.
7.13	Evaluation of training effect of surface finish	166.
7.14	Neural network performance in predicting patterns of chip breakability	167.
7.15	Neural network performance in predicting patterns of surface finish	168.
7.16	Proposed schematic diagram of an integrated system for chip control and tool wear estimation based on the G2 Real-time Expert System	170.
8.1	A proposed schematic diagram for an expert system-supported tool wear estimation system	180.

NOMENCLATURE

a_t	white noise
B	groove width of tool chip breaker
B_e	equivalent groove width of tool chip breaker
B_j	bias of the j th neuron in a neural network
C_s	cutting edge angle
d	depth of cut or groove depth of tool chip breaker
d_1	raised height of groove back wall
d_2	reduced height of groove back wall
d_i	dispersion
D_i	dispersion percentage
D_{xy}	cross-dispersion between x and y series signals
D_{xz}	cross-dispersion between x and z series signals
D_{yz}	cross-dispersion between y and z series signals
$D'_x(\text{LF})$	rate of low frequency (LF) dispersion of the feed force (in x direction)
$D'_x(\text{HF})$	rate of high frequency (HF) dispersion of the feed force (in x direction)
$D'_y(\text{HF})$	rate of high frequency (HF) dispersion of the thrust force (in y direction)
$D'_z(\text{HF})$	rate of high frequency (HF) dispersion of the main cutting force (in z direction)
f	feed
f_n	frequency corresponding to a pair of complex conjugate eigenvalues
F_c	main cutting force
F_t	thrust cutting force
F_x	cutting force in feed (x) direction or feed cutting force
F_y	cutting force in thrust (y) direction or thrust cutting force

F_z	cutting force in main cutting (z) direction or main cutting force
F_α	tangential (friction) force to major flank
$F_{\alpha n}$	normal force to major flank
$F_{\beta h}$	horizontally tangential (friction) force to minor flank
$F_{\beta n}$	normal force to minor flank
$F_{\beta v}$	vertically tangential (friction) force to minor flank
F_γ	tangential (friction) force to crater face
$F_{\gamma n}$	normal force to crater face
$g(x)$	chip acceptability factor
G_k	explicit Green's function
$\overline{G_k}$	the complex conjugate of G_k
h	tool restricted contact length
h_c	tool/chip contact length
h_e	effective tool restricted contact length
h_n	tool/chip natural contact length
h_p	tool restricted contact length with minimum power consumption
h_η	tool restricted contact length with effective chip breaking
i	tool inclination angle
KB	crater width on tool rake face
KK	crater length on tool rake face
KS	retract of tool cutting edge
KT	crater depth on tool rake face
N	tool nose wear
O_j	output pattern of a neural network
P_s	specific power consumption
P_{se}	efficient specific power consumption
q	exponent decided by fuzzy linguistic values
q_1, \dots, q_5	exponents decided by fuzzy linguistic values (corresponding to each machining parameter)

r	tool nose radius
R_a	arithmetic mean deviation of surface roughness
R_k	standard chip breakability matrix
R_o	groove radius of tool chip breaker
r_u	chip up-curl radius
r_{ui}	radius of initial chip curvature
r_{uf}	radius of final chip curvature
t_1	undeformed chip thickness
t_2	chip thickness
T_i	eigenvector
T_j	target pattern of a neural network
u	exponent for determining the variations of chip breakability membership values due to the change of tool geometry
v	exponent for determining the variations of surface finish membership values due to the change of tool geometry
V	cutting speed
V_c	chip velocity
VB	major flank wear
VB'	minor flank wear
VG	length of the groove (notch)
w	exponent for determining the variations of power consumption membership values due to the change of tool geometry or width of cut in orthogonal cutting
W_{ji}	weight between the j th neuron and its i th input in a neural network
W_L	work material evaluation matrix
x	chip shape/type
X	chip shape set
X_i	the i th input of a neural network
X_t	discrete series of observation vectors
Y_j	output of the j th neuron activated by a non-linear transfer function

Z_j	linear summation of the total inputs to the j th neuron
α	tool rake angle
γ_o	process variation
γ_{o-vec}	vector auto-covariance matrix
γ_k	correlation matrix of measured variables
δ_k	Kronecker delta function
Δ	uniform sample interval
Δh_{nV}	increment of tool/chip natural contact length due to the variations of cutting speed
$\Delta h_{n\alpha}$	increment of tool/chip natural contact length due to the variations of tool rake angle
ΔP_h	increment of power consumption
$\Delta \eta_{bh}$	increment of chip backflow angle due to the variations of tool restricted contact length
$\Delta \eta_{bf}$	increment of chip backflow angle due to the variations of feed
$\Delta \eta_{bV}$	increment of chip backflow angle due to the variations of cutting speed
$\Delta \eta_{b\alpha}$	increment of chip backflow angle due to the variations of tool rake angle
$\Delta \eta_{sd}$	increment of chip sideflow angle due to the variations of depth of cut
$\Delta \eta_{sf}$	increment of chip sideflow angle due to the variations of feed
$\Delta \eta_{sr}$	increment of chip sideflow angle due to the variations of tool nose radius
ϵ_b	ultimate strain of the chip material
θ	groove tangent angle of tool chip breaker
θ_i	moving average parameter matrix
λ_i	eigenvalue
$\mu(x)$	fuzzy membership value
$\mu^*(x)$	modified fuzzy membership value
$\mu_i(k)$	input of fuzzy membership values for chip breakability to the neural networks used
$\mu_k(i, j)$	fuzzy membership value of the standard chip breakability matrix

$\mu_o(k)$	output of fuzzy membership values for chip breakability from the neural networks used
μ_P	membership value of power consumption
μ_s	membership value of surface finish
σ_a	covariance of white noise a_t
σ_a^2	residual matrix
Φ_i	autoregressive parameter matrix
η_b	chip backflow angle
$\eta_{b \text{ std}}$	standard chip backflow angle in the 3-D chip flow database
η_{be}	effective chip backflow angle
η_s	chip sideflow angle
η_{si}	increment of chip sideflow angle due to the variations of tool inclination angle compared with that at the standard 0 degree
$\eta_{s \text{ std}}$	standard chip sideflow angle in the 3-D chip flow database

PUBLICATIONS WHILE STUDYING FOR PHD COURSE

I. Journal Papers

1. Y. Yao, X. D. Fang and G. Arndt, "Comprehensive Tool Wear Estimation in Finish-machining via Multivariate Time-Series Analysis of 3-D cutting Forces", *Annals of CIRP*, Vol. 39(1), 1990, pp. 57-60.
2. X. D. Fang and I. S. Jawahir, "On Predicting Chip Breakability in Machining of Steels with Carbide Tool Inserts Having Complex Chip Groove Geometries", to appear in *J. Materials Processing Technology*, Vol. 26, Issue 2, selected from the papers in *Proc. 7th International Conference on Computer-Aided Production Engineering*, Tennessee, USA, August 13-14, 1991, pp. 37-48.
3. Y. Yao, X. D. Fang and G. Arndt, "On-line Estimation of Groove Wear in the Minor Cutting Edge for Finish-machining", to appear in *Annals of CIRP*, Vol. 40(1), 1991.
4. Y. Yao and X.D. Fang, "Modelling of Multivariate Time Series for Tool Wear Estimation in Finish-Turning", paper accepted for publication in *Int. J. Machine Tools & Manufacturing*.

II. Papers in International Conference Proceedings

5. I. S. Jawahir and X. D. Fang, "A Knowledge-based Approach for Improved Performance with Grooved Chip Breakers in Metal Machining", *Proc. 3rd International Conference on Advances in Manufacturing Technology*, Organised by *IProDE*, Singapore, August 14-16, 1989, pp. 130-144.
6. X. D. Fang and I. S. Jawahir, "An Expert System Based on A Fuzzy Mathematical Model for Chip Breakability Assessments in Automated

- Machining", *Proc. Int. Conf., ASME, MI'90*, Vol. IV, Atlanta, Georgia, U. S. A., March 25-28, 1990, pp. 31-37.
7. Y. Yao, I. S. Jawahir, D. Jamieson and X. D. Fang, "Computer Animation of Chip Flow and Chip Curl in an Expert Process Planning System for Metal Machining", *Transactions of the North American Manufacturing Research Conference(NAMRC /SME)*, Pennsylvania, USA, May 23-25, 1990, pp. 161-166.
 8. I. S. Jawahir and X. D. Fang, "Some Guidelines on the Use of a Predictive Expert System for Chip Control in Automated Process Planning", *Proc. Fifth International Conference on Manufacturing Engineering*, Vol.1,Wollongong, Australia, July 11-13, 1990, pp. 288-292.
 9. Y. Yao, X. D. Fang and R. Rudziejewski, "Analysis of Dynamic Components of 3-D Cutting Forces in Oblique Machining", *Proc. Fifth International Conference on Manufacturing Engineering*, Vol.2,Wollongong, Australia, July 11-13, 1990, pp. 349-353.
 10. X. D. Fang and Y. Yao, "Expert System-Supported On-line Tool Wear Monitoring", *Proc. of International Conference on Artificial Intelligence in Engineering - AIE'90*, Sponsored by I.E.E.(UK), August 21-22, 1990, Kuala Lumpur, Malaysia, pp. 77-84.
 11. X. D. Fang, Y. Yao and G. Arndt, "Tool Wear Estimation by Multidimensional Autoregressive Spectral Analysis", *Proc. 1990 Pacific Conference on Manufacturing*, Vol. 2, Sydney & Melbourne, Australia, December 17-21, 1990, pp. 834-841.
 12. E. Siores, X. D. Fang and Y. Yao, "Intelligent Design for Manufacturing Employing Knowledge Based Expert System", accepted for publication in *International Conference on Information Technology for Advanced Manufacturing Systems*, organised by IFIP, Nanjing, P.R. China, Sep., 17-19, 1991.

CHAPTER 1

INTRODUCTION

1.1 THE IMPORTANCE OF THE CURRENT RESEARCH PROJECT AND THE ITS OBJECTIVE

1.1.1 Significance of Chip Control in Automated Machining

It has been long known that chip control in metal machining, particularly in continuous mode operations such as turning, is vital due to its significant role in producing small and handleable sized chips for disposal, and in protecting the machined work surface, cutting tool, machine tool and operator (in manual operation) from long, snarled, hard and hot unbroken chips. With the advent of automated manufacturing technologies involving unattended machining operations, the need for chip control has grown into significant proportions. In order to achieve total chip control in automated manufacture, the predictability of chip shapes/breaking is essential. Recently, effective chip control has been recognised by the International Institution for Production Engineering Research (CIRP) as one of the most urgent technical problems needed to be solved to improve machining quality [1].

1.1.2 The Need for Developing a Knowledge-based Expert System for Effective Chip Control

Since the present knowledge of chip control is inadequate to describe quantitatively the processes of chip flow, chip curl and chip breaking, it becomes very difficult to predict chip forming behaviour in the actual machining process with a certain degree

of accuracy. Indeed, the present knowledge of chip control is found to be segmented and scattered; and currently available machinability database systems have not incorporated the chip control factor either. Individual factors influencing chip breakability, such as tool chip breaker configurations, tool geometries, work material properties and cutting conditions, have not been fully studied to provide a basis for optimal chip breaking. Although several hundred types of cutting tools with different toolface configurations involving various chip groove profiles, obstruction lumps, wavy cutting edges and curved rake faces have become commercially available, most of these cutting tools are designed on the basis of the traditional "try and see" experimental methods. Thus it is apparent that a more scientific methodology is required to avoid these time-consuming and less-accurate methods.

It is noticed, however, that much of the knowledge and many practical techniques about machining have not been fully utilised in assessing the chip control effects. Therefore it is imperative to develop a knowledge-based expert system, integrating experts' rich experience, empirical rules, experimental results and the existing qualitative knowledge and theories. The need for developing knowledge-based systems to address the problems concerning chip control has been highlighted based on the results of an extensive survey on chip control covering over 160 published papers [2].

1.1.3 Strategies of Tool Wear Estimation in Finish-Machining

In automated machining, on-line tool wear estimation plays an important role in establishing an efficient tool change policy and an effective quality control strategy. Numerous methods have been developed, as reviewed in several survey papers [3-6]. Most of them, however, are concerned with the estimation of major flank wear alone

[7-17] or with major flank and crater wear combined [18-21]. In actual machining operations, especially in a finish-machining process, minor flank wear, groove wear at the minor cutting edge and nose wear are crucial to dimensional accuracy and surface quality. It is likely that in finish-machining, the wear state at the minor cutting edge reaches its critical point earlier than those in the major flank and crater, such that the tool monitoring policy should be established on the basis of the wear state at the minor cutting edge.

The mechanism of minor flank wear and groove wear at the minor cutting edge is complex. Minor flank wear will always form in machining process, while under certain cutting conditions, the grooves, spaced at a distance equal to feed, may appear and become the dominant type of wear at the minor cutting edge. When no grooves form at the minor cutting edge, the machined work surface is further shaped by the minor cutting edge, thus causing minor flank wear mainly due to high-speed friction. Surface finish and dimensional accuracy are affected by the severity of minor flank wear.

Although minor flank wear and groove wear at the minor cutting edge have been recognised long ago to be crucial to the surface quality in finish-machining and much work has been done on their mechanism [22-26], almost no work has been reported on the detection and estimation methods for these types of tool wear, presumably due to the complexity involved in interpreting multivariate signals and resolving them for estimation of more than one type of wear. Therefore, a more effective monitoring strategy involving multi-sensor and/or multi-modelling is called for in order to estimate more than one type of tool wear simultaneously.

1.1.4 Multivariate Time Series Modelling for Comprehensive Tool Wear Estimation

Autoregressive moving average (ARMA) time series analysis has been used in modelling machining processes during the past decade. As it does not require much prior knowledge about the underlying system physics, ARMA modelling is most suitable for cutting processes which are stochastic in nature. By using ARMA modelling techniques, a mathematical model which describes the internal system dynamics can be established solely based on experimentally measured data. Once the ARMA models are established, feature extraction can be developed in different ways, such as, residual analysis [27], parametric spectral analysis [28-29], dispersion analysis [28, 30-32], damping ratio calculation [9, 33], model parameters [7-8, 34], etc. When more than one series of data is involved, multivariate ARMA vector models [30, 32, 35-36] may be developed to reveal the interactive characteristics between different series. Table 1.1 summarises applications of ARMA modelling in on-line monitoring concerning machining processes.

As seen from Table 1.1, most methods use only the univariate time series model to estimate tool wear. If more than one quantity is to be estimated, more complexity will be encountered. Thus a higher demand is placed on effective signal processing and analysis techniques which shall be able to single out particular signal ingredients sensitive to particular quantities to be estimated.

Table 1.1 ARMA modelling of machining processes for condition monitoring

References	Year	Specifications of Application	Signals Used	Model Dimensions	Diagnostic Methods and Feature Extraction
[7]	1987	major flank wear estimation in turning	acoustic emission	1-D	model parameters
[8]	1989	major flank wear estimation in turning	acoustic emission	1-D	model parameters
[9]	1980	major flank wear estimation in turning	vibration	1-D	damping ratio
[10]	1982	major flank wear estimation in turning	2-D forces & 1-D vibration	1-D	actual power contribution of ARMA spectral analysis
[27]	1986	tool breakage detection	cutting torque	1-D	residual analysis
[28]	1980	on-line identification of chatter in turning	2-D vibration & cutting forces	1-D	autoregressive spectral density & dispersion analysis
[29]	1990	estimations of crater wear and minor flank wear	3-D dynamic cutting forces	3-D	autoregressive spectral analysis
[30]	1990	comprehensive tool wear estimation in finish-turning	3-D dynamic cutting forces	3-D	dispersion analysis
[31]	1977	chatter identification	vibration	1-D	dispersion analysis
[32]	1991	estimation of groove wear at the minor cutting edge	3-D vibration	3-D	multiple (cross) dispersion analysis
[33]	1985	estimation of average flank wear in drilling process	thrust torque	1-D	normalised damping ratio
[34]	1986	tool breakage detection in milling process	cutting force	1-D	prediction errors based on model parameters

1.1.5 Integrating Chip Control and Tool Wear Estimation for On-line Assessment of Machining Performance

Chip control and tool wear estimation are two vital yet closely interrelated concerns in automated machining systems. The dynamic chip forming behaviour will vary significantly at different tool wear stages, thus resulting in the changeable performance of the undergoing machining operation, such as chip breaking/chip forms and surface finish. Although much work has been done on them individually, no work has been reported to integrate them for on-line monitoring of machining process or optimal control of machining operation. In fact, all the present machining theories and machinability database are based on unworn or fresh cutting tools. Due to the extreme complexity involved, it is very difficult at present to model analytically the dynamic interrelations between the overall machining performance in terms of chip control and tool wear development.

The recent advent of neural network techniques provides a suitable tool for analysing such a complicated process by extracting knowledge only based on the observations of experimental input-output data, and further using this knowledge to synthesise an optimal predicting model. Some work has been reported on using neural network in modelling of machining process, such as tool wear monitoring [11-12, 37] and optimisation of machining process [38].

1.2 SCOPE OF THESIS

The work described in this thesis is devoted to developing an effective means for chip control and tool wear estimation, two vital concerns in automated machining systems.

The research has been focused on the following four aspects :

- (a) Predictions of chip breakability for a wide range of machining conditions through a fuzzy-set mathematical model and further predictions of the machining performance including chip breakability/chip forming patterns, surface finish and power consumption.
- (b) Development of a knowledge-based system for optimal design of conventional groove-type chip breaker in the point of view of three-dimensional chip flow in oblique machining process.
- (c) Development of dispersion analysis algorithm, derived from the established multivariate time series models, for the comprehensive tool wear (major flank wear, crater wear, minor flank wear and groove wear at the minor cutting edge) estimation in finish-machining.
- (d) Integration of chip control and comprehensive tool wear estimation, with consideration of surface finish as well, by the use of neural network techniques, aiming at developing an effective strategy for on-line assessment of machining performance.

The thesis is organised into 8 chapters, the outline of each chapter is given below.

Chapter 1 highlights the significance of the research project and describes the objectives to be achieved. The outline of the thesis is also included.

Chapter 2 presents a new approach of a fuzzy rating mechanism to predict the chip breakability for various chip shapes/sizes produced in the machining process. A fuzzy-set mathematical model is developed to describe the variations of chip breakability at different input machining conditions.

Chapter 3 is devoted to developing an off-line predictive expert system for the machining performance involving chip control as well as surface finish and power consumption based on the extensive machining experiments.

Chapter 4 describes the development of a knowledge-based system for optimal design of a groove-type chip breaker based on the analysis of three-dimensional chip flow (sideflow & backflow) and the results of the machining experiments.

Chapter 5 is devoted to investigating the comprehensive tool wear (major flank, crater & minor flank wear) patterns in finish-machining, and to developing a multivariate modelling algorithm, aiming at providing an effective estimation strategy which is able to single out particular signal ingredients sensitive to particular quantities to be estimated. Dispersion analysis algorithm based on the multivariate ARMA vector models of 3-D dynamic cutting force is established for extracting features sensitive to the development of various types of tool wear.

Chapter 6 describes the experimental investigation of the patterns of groove wear at the minor cutting edge in finish-machining as well as the relationship between groove formation and surface roughness development. Multiple (cross) dispersion analysis is developed to analyse quantitatively not only the characteristics of individual variables from 3-D tool vibration produced in the machining process, but also the interactions among different variables, providing effective detection and estimation of groove wear at the minor cutting edge.

Chapter 7 aims at integrating chip control and comprehensive tool wear estimation for on-line assessment of dynamic machining performance, including chip breaking/chip forms, surface finish and tool wear states. Neural network techniques are used to

model the dynamic characteristics of chip forming behaviour as well as surface roughness development during the process of tool wear.

Chapter 8 presents concluding remarks and summarises the achievements described in the thesis. Suggestions for future work are also given in this chapter.

1.3 LITERATURE SURVEY

Since each chapter of this thesis is relatively independent, the relevant literature survey has been integrated into each chapter (from Chapters 1 to 7).

CHAPTER 2

PREDICTING CHIP BREAKABILITY IN MACHINING WITH A FUZZY SET-BASED EXPERT SYSTEM

2.1 INTRODUCTION

Chip breaking is essential in metal machining. The advent of automated machining systems has placed even more emphasis on the need for controlling the chip. Therefore, developing feasible means for predicting chip breakability and forms/shapes is highly called for. Due to a great number of interacting process variables involved, predicting chip breakability has been a major yet complicated problem for many years. It has been shown, when machining with a conventional flat-faced tool or a tool with simple chip-breaker configuration, the prediction of chip breakability can be made with some accuracies under certain machining conditions [39-41]. However, when tool inserts with complex chip forming toolface configurations, most of which have been commercially available, are used, predicting chip breaking becomes much more difficult. This is attributed to the very complex nature of chip flow mechanics on the toolface, which results in non-uniquely definable chip curvatures. In this case, it is almost impossible to predict chip breakability with sufficient accuracy in machining with tools having such complicated chip breaker configurations. As such, the need for adopting non-algorithmic means of predicting chip breakability has been felt by the research workers for quite some time [2] but it is recently that the problem has been addressed.

Henriksen's [42-43] early works on obstruction-type and integral groove-type chip breakers laid the foundation for applied research on chip breaking. Following Colwell's chip flow investigation [44], Stabler [45] established his still famous chip

flow law, in which he derived an expression for the direction of chip flow in terms of the cutting edge inclination angle and showed the validity of this relationship with a material factor added.

Cook et al [46] explained various chip flow and chip curl mechanisms and showed that reducing the average friction on the toolface will produce thinner chips. They also reported that a toolface crater and Built-up Edge (BUE) determine the initial chip curl which was shown to vary from one material to another. Nakayama, in his over 25 years of experimental and analytical work on metal machining, published a number of papers on chip breaking [39-40, 47-52]. The most notable early work by Nakayama [39] in 1962 presented the very first criterion for chip breaking. In this work he showed that the chip will break when the strain on the chip surface exceeds the ultimate strain of chip material (ϵ_b), and that chip breakability depends on the chip thickness (t_2) and the radii of initial and final chip curvature (r_{ui} and r_{uf}), in a combined up and side curling mode, as shown in Equation (2.1).

$$\epsilon_b \leq \frac{t_2}{2} \left(\frac{1}{r_{ui}} - \frac{1}{r_{uf}} \right) \quad (2.1)$$

Worthington et al [41, 53-55] conducted a series of experimental work on chip breaker geometry and presented their results, which highlight the actual action of a chip-breaker tool, by showing the effect of a grooved toolface on chip curl and chip breaking. Johnson [56] reported the applicability of a slip-line field for machining with restricted contact tools using a velocity diagram (hodograph). Based on this slip-line field theory, Usui et al [57-58] expanded the basic knowledge on machining with restricted contact tools. However, the effect of chip streaming (i.e. chip backflow) which would primarily determine the chip breaker parameters needed for an effective chip breaking operation, was paid far less attention in research for about 25

years. This vital effect exists, as shown in recent work [59-62], for tools with a restricted contact length (on the toolface) less than the tool/chip natural contact length under a given set of cutting conditions. Subsequently, Jawahir [2] in an extensive survey on chip breaking identified the need for knowledge-based systems and continuous process monitoring for "total chip control" in unmanned machining systems.

In this chapter, a new approach of fuzzy rating mechanism is presented to quantify the chip breakability for various chip shapes/sizes produced in the machining processes. A fuzzy mathematical model was developed to describe the variations of chip breakability at different input machining conditions. Using the basic representative experimental results that are stored in the chip database, in conjunction with a set of appropriate knowledge-rules summarised on the basis of the extensive machining experiments on chip breaking and chip shapes, the predictability of chip breaking can be made through the use of an expert system with quite reasonable accuracy. Knowledge-rules are developed by using Turbo PROLOG language. The application of a fuzzy-set mathematical model provides the basis for the establishment of the expert system.

2.2 FUZZY DESCRIPTION OF CHIP BREAKABILITY

As a result of surveying the development history of predicting chip breakability, it is apparent that no quantitative methods have been presented on the prediction of chip breaking and classification of chip shapes although much work has been done on their analysis [51, 55, 61-63]. In fact, chip breakability is a concept involving many uncertainties without well-defined boundaries. In industrial practice, when we explain chip breakability, descriptive words, such as good, moderate, poor, are usually used. Therefore, the fuzzy set theory, apparently very applicable to the problem concerned,

is selected to describe quantitatively different levels of chip breakability. In this way, a description of chip breakability may be expressed in terms of linguistic values based on the recorded observations. Figure 2.1 shows a detailed classification of chip shapes produced from machining operations, which we define as a chip shape set X :

$$X = \{ x \}, \quad \text{where } x \text{ is a chip shape/type} \quad (2.2)$$

In order to describe the chip breakability for different chip shapes, we introduce a fuzzy membership function $\mu(x)$ within the interval $[0,1]$:

$$\mu(x) \in [0, 1], \quad x \in X \quad (2.3)$$

In this way, each chip shape is assigned to a fuzzy membership value $\mu(x)$ which represents the membership grade of the chip shape x . Taking $\mu(x) = 1.0$ as the most ideally broken chip shape, the membership value $\mu(x_i) = 0.7$ means that the breakability rating for chip shape x_i is 0.7. The larger the membership value, the better the chip breakability. A range of approximate chip breakability ratings (membership values) has been assigned to various common chip shapes obtainable, based on the relative ease/difficulty of producing them. Table 2.1 shows the membership value (representing chip breakability) for each chip shape shown in Figure 2.1.























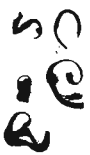






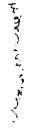
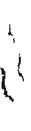





TUBULAR CHIPS	Large Dia. 	Snarled 	Cont. Long 	Broken Long 	Medium 	Short 
RIBBON CHIPS	Snarled 	Long 	Small Snarled 			
HELICAL CHIPS	Large Dia. 	Snarled 	Cont. Long 	Broken Long 	Medium 	Short 
CORK-SCREW CHIPS	Snarled 	Cont. Long 	Broken Long 	Medium 	Short 	
SPIRAL CHIPS	Wavy 	Few Turns 	Full Turn 	Flat 	Conical 	
ARC CHIPS	Up-curl 	Side-curl 	Connected 			
STRING CHIPS	Cont. Long 	Broken Long 	Medium 	Short 		
TOOTHED-EDGE CHIPS	Long 	Short 	Arc 	Connected 		

Figure 2.1 Classification of chip shapes

Table 2.1 Membership values for most common chip shapes/sizes

Tubular Chips	Large Diameter 0.10	Snarled 0.28	Continuous Long 0.35	Broken Long 0.43	Medium 0.46-0.48	Short 0.64
Ribbon Chips	Snarled 0.20	Long 0.30	Small Snarled 0.3-0.45			
Helical Chips	Large Diameter 0.08	Snarled 0.20	Continuous Long 0.30	Broken Long 0.38	Medium 0.44-0.46	Short 0.60
Cork Screw Chips	Snarled 0.25	Continuous Long 0.32	Broken Long 0.41	Medium 0.45-0.47	Short 0.62	
Spiral Chips	Wavy 0.44-0.48	Few Turns 0.42-0.48	Full Turn 0.65-0.67	Flat 0.57-0.60	Conical 0.67-0.70	
Arc Chips	Up-curl 0.88-0.92	Side-curl 0.85-0.90	Connected 0.92-0.95			
String Chips	Continuous Long 0.35	Broken Long 0.42	Medium 0.49	Short 0.64		
Tooth-Edged Chips	Long 0.28	Short 0.60	Side-curl Arc 0.86	Connected Arc 0.92		

2.3 MACHINING EXPERIMENTS FOR SETTING UP THE BASIC CHIP DATABASE

A series of experimental work was conducted for setting up the basic chip database to be used as the primary standard (i.e. reference) for chip breakability. In the basic chip database, combinations of tool inserts and work materials together with a fairly wide range of cutting conditions, as shown in Table 2.2, are used.

Table 2.2 Machining conditions used for setting up the basic chip database

TOOL INSERT	TNMG160408 (ENZ, ENA & ENT) with tool geometry : 0°, 5°, -6°, 90°, 60°, 0.8
WORK MATERIAL	CS1020 K1040 EN25
CUTTING SPEED	50, 75, 100, 150, 200 m/min
DEPTH OF CUT	0.25, 0.5, 1.0, 2.0, 3.0, 4.0 mm
FEED	0.06, 0.1, 0.2, 0.3, 0.4, 0.5 mm/rev

Based upon the basic chip database the standard chip breakability matrices R_k 's are set up under the five specified machining parameters (i.e. tool inserts, work materials, cutting speeds, depths of cut and feeds) as follows :

$$R_k = \begin{pmatrix} \mu_k(1,1) & \mu_k(1,2) & \dots & \dots & \dots & \mu_k(1,6) \\ \mu_k(2,1) & \mu_k(2,2) & \dots & \dots & \dots & \mu_k(2,6) \\ \cdot & \cdot & \dots & \dots & \dots & \cdot \\ \cdot & \cdot & \dots & \mu_k(i,j) & \dots & \cdot \\ \cdot & \cdot & \dots & \dots & \dots & \cdot \\ \mu_k(6,1) & \mu_k(6,2) & \dots & \dots & \dots & \mu_k(6,6) \end{pmatrix} \quad (2.4)$$

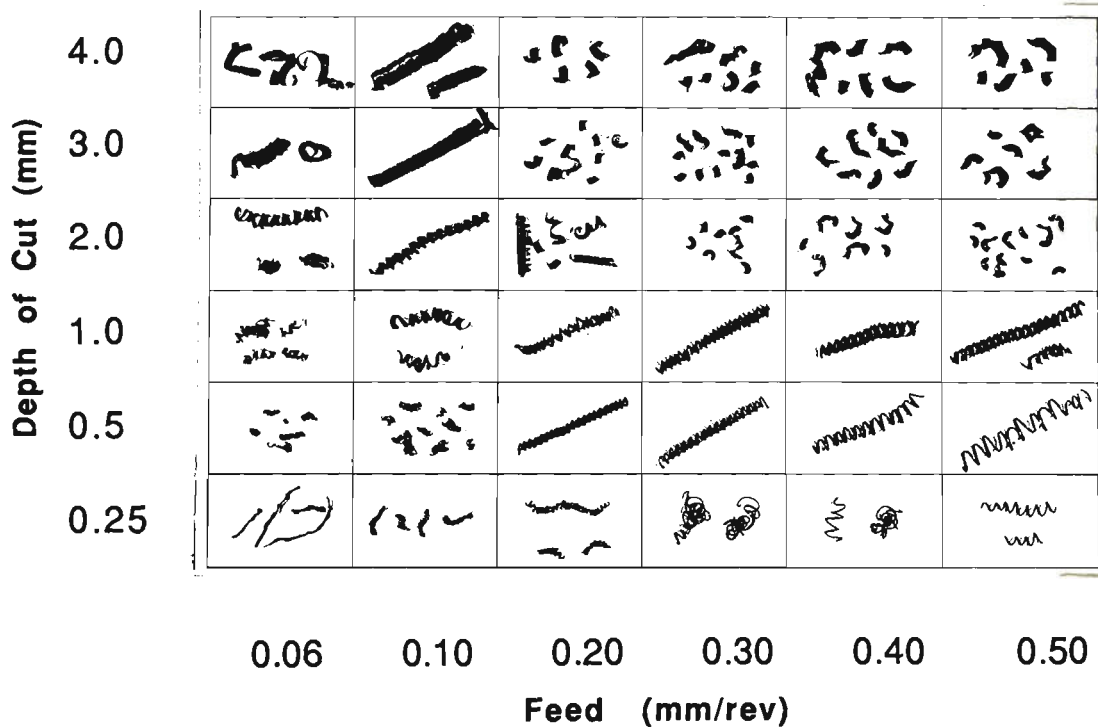
where $\mu_k(i, j)$ provides the fuzzy membership values of chip breakability, $i = 1, \dots, 6$ and $j = 1, \dots, 6$ represent various depths of cut (6 values) and feeds (6 values) respectively, and $k = 1, \dots, 45$ represents combinations of tool inserts (3 values), work materials (3 values) and cutting speeds (5 values). In effect, 45 individual matrices were compiled using the experimental results. All these standard fuzzy membership values for chip breakability are given in Appendix A.

Figure 2.2 shows two samples of photographs from the machining experiments which correspond to two of the above standard chip breakability matrices, in the form of feed-depth of cut relationships at two typical cutting speeds (i.e. at 50 and 100m/min).

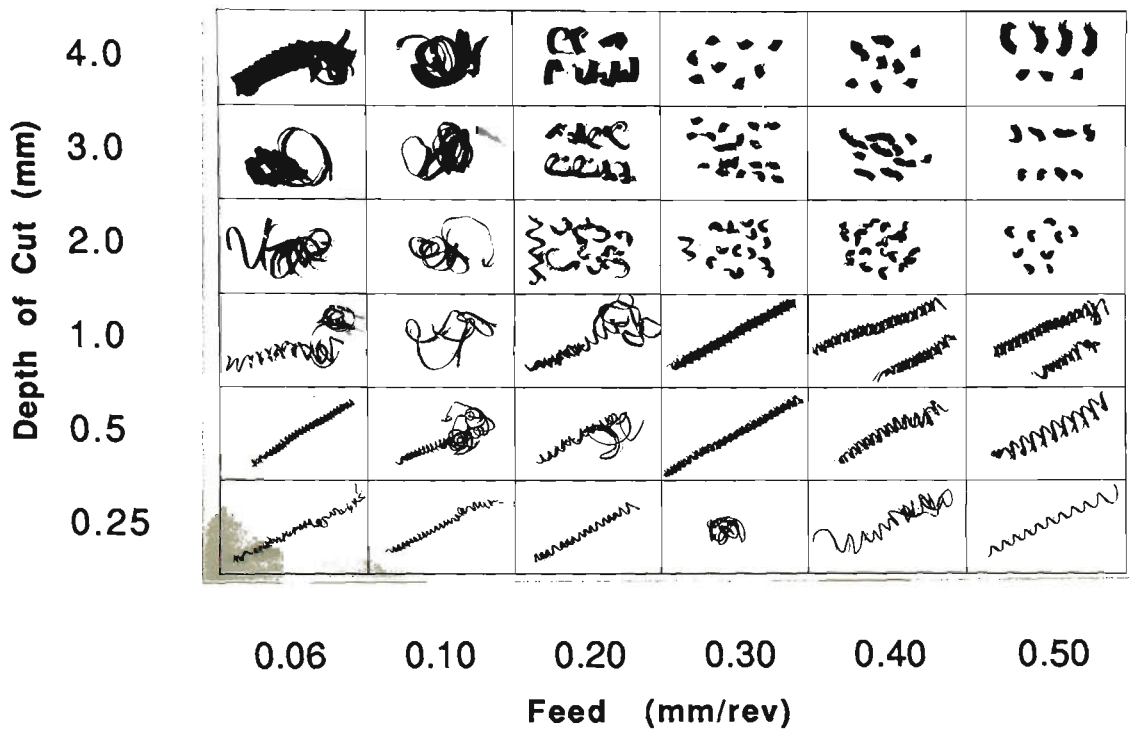
2.4 FACTORS AFFECTING CHIP BREAKABILITY : AN EXPERIMENTAL ANALYSIS

Chip breakability is affected by many factors (Figure 2.3), of which the most significant factors considered in the present work are :

- Cutting conditions (cutting speed, depth of cut and feed)
- Work material (7 different work materials used)
- Chip breaker type (8 different chip breaker configurations used)
- Tool geometry (cutting edge angle and tool nose radius variations considered)



- (a) Cutting Conditions : Tool Insert : TNMG160408ENZ
Work Material : K1040
Cutting Speed : 50 m/min



(b) Cutting Conditions : Tool Insert : TNMG160408ENZ
 Work Material : K1040
 Cutting Speed : 100 m/min

Figure 2.2 Two examples of chip breakability diagrams (Feed-Depth of Cut Relationship)

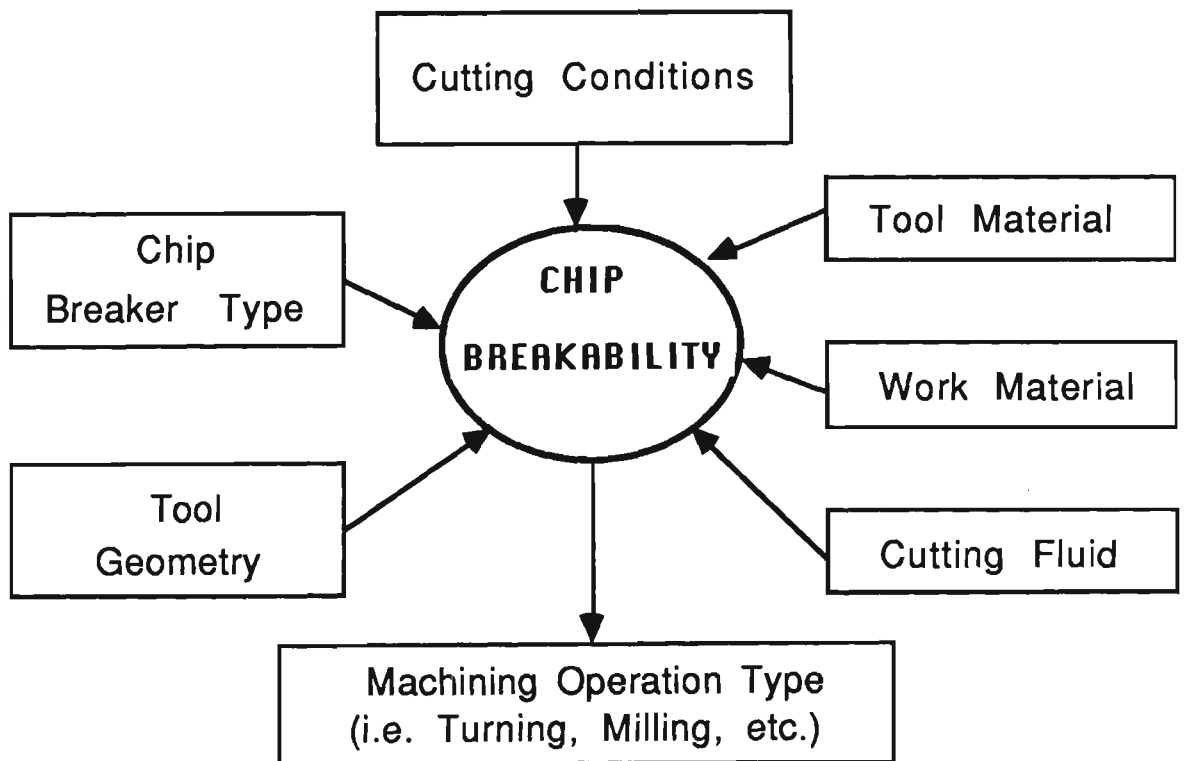


Figure 2.3 Factors affecting chip breakability

The basic chip database is only used as a primary criterion to provide the standard chip breakability for the machining conditions exactly the same as those in the basic chip database. As chip breakability is a complicated physical phenomenon, influenced by numerous factors, only the basic chip database established under the selected machining conditions may not be accurate enough to describe the chip breakability under arbitrary machining conditions/parameters. In order to extend the prediction range to any combinations of machining conditions, further justification is required.

Table 2.3 Conditions used for the extensive machining experiments

CUTTING CONDITIONS	V=30--300 m/min d=0.25--5 mm f=0.06--1.0 mm/rev
CUTTING TOOLS	<ol style="list-style-type: none"> 1. flat-face (without chip breaker) 2. ENA type: chip breaker with varying widths and wavy cutting edge 3. ENZ type: straight-style grooved chip breaker with raised back wall 4. ENT type: conventional grooved chip breaker 5. ENK type: multiple-lumps chip breaker 6. ENG type: chip breaker configuration combining groove with lump 7. ENJ type: grooved chip breaker with smaller restricted contact length 8. EFJ type: grooved chip breaker with larger restricted contact length 9. EFB type: double-step chip breakers
WORK MATERIALS	<ol style="list-style-type: none"> 1. low carbon steel <u>CS1020</u> : C 0.2% Mn 0.6% (BHN=185) 2. medium carbon steel <u>K1040</u> : C 0.4% Mn 0.6% (BHN=198) 3. high carbon carbon steel <u>K1055</u> : C 0.55% Mn 0.6% (BHN=220) 4. Ni-Mo-Cr alloy <u>EN25</u> : C 0.3% Mn 0.6% Ni 2.5% Mo 0.5% Cr 0.5% (BHN=240) 5. Mo-Cr alloy <u>AISI 4140</u> : C 0.4% Mn 0.8% Mo 0.2% Cr 0.9% (BHN=300) 6. Ni-Cr alloy <u>EN36A</u> : C 0.12% Mn 1.0% Ni 3.2% Cr 0.9% (BHN=210) 7. free-machining steel <u>S12L14</u> : C 0.15% Mn 1.0% S 0.3% Pb 0.25% (BHN=168)
TOOL GEOMETRIES	<ol style="list-style-type: none"> 1. nose radius, r = 0.4, 0.8, 1.2 & 1.6 mm 2. cutting edge angle, Cs = 90, 75, 60 & 45°

Therefore, extensive machining experiments, as shown in Table 2.3, were conducted to analyse the effect of each machining parameter, i.e., work materials, cutting conditions, tool chip breakers and tool geometries, on chip breakability, aiming at providing a quantitative reference for determining the interrelationships between chip breakability and various machining parameters.

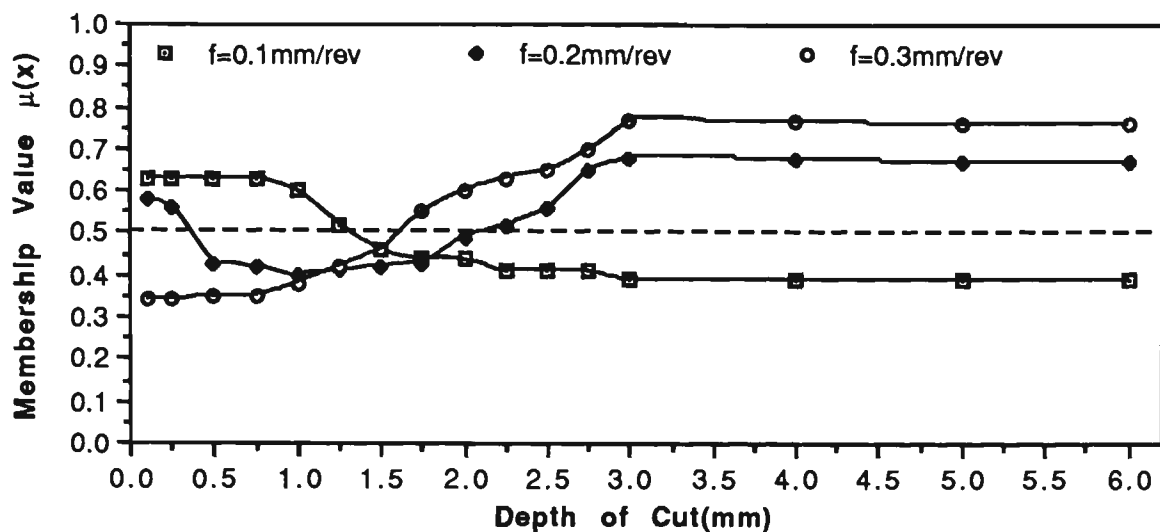
Some results of the experimental work and analysis are presented below as representatives to show the effects of these four factors through the chip breakability rating (i.e. fuzzy membership value).

2.4.1 Effect of Cutting Conditions

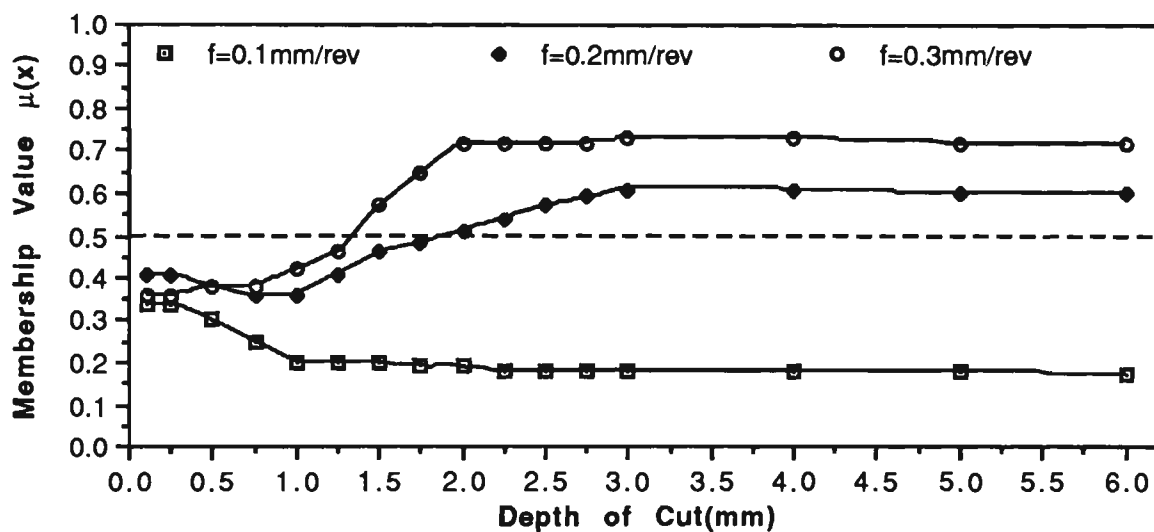
2.4.1-1 Analysis of depth of cut

Three feed values (0.1, 0.2 and 0.3 mm/rev) and three cutting speeds (50, 100 and 200 m/min, representing low, medium and high speeds) were used in the analysis of chip breakability, represented by membership values $\mu(x)$, at varying depths of cut.

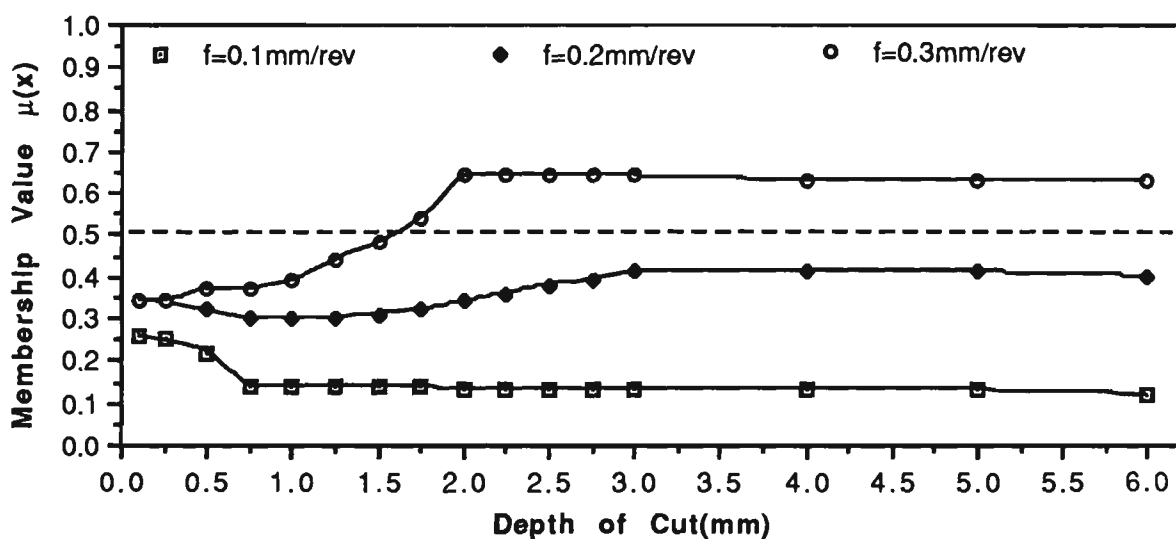
The effect of depth of cut varies at different feeds. As shown in Figure 2.4 for a typical ENZ type tool insert when machining work material K1040, at a low feed, such as 0.1mm/rev, the chip breakability decreases with the increase in depth of cut but the effect is opposite when the feed is increased up to 0.3 mm/rev. The reason for this is that, in general, as the depth of cut is increased, the chip shapes produced at low feeds change from long to snarled chips, while at a higher feed ($f = 0.3$ mm/rev) from long to small chips. When the depth of cut is larger than 3 mm, in general, there is virtually no change in chip breakability within the range tested. At lower depths of cut the chip breakability is generally poor.



(a) Low Cutting Speed (50m/min)



(b) Medium Cutting Speed (100m/min)



(c) High Cutting Speed (200m/min)

Figure 2.4 The effect of depth of cut on chip breakability
(Tool Insert : TNMG160408ENZ, Work Material : K1040)

2.4.1-2 Analysis of feed

Chip breakability ($\mu(x)$) with varying feeds was estimated at three values of cutting speeds and two values of depths of cut (see Figure 2.5). Feed plays a very important role in determining chip breakability. In general, the higher the feed, the better the chip breakability except at low cutting speeds due to the possible formation of Built-up Edge (see Figure 2.5). For a larger depth of cut ($d = 2$ mm), when the feed goes up from 0.2 to 0.3 mm/rev, there is a steep increase in chip breakability, while for a smaller depth of cut ($d = 1$ mm), only a slight increase being noted. At low depths of cut, the chip breakability is found to be poor for all feed values.

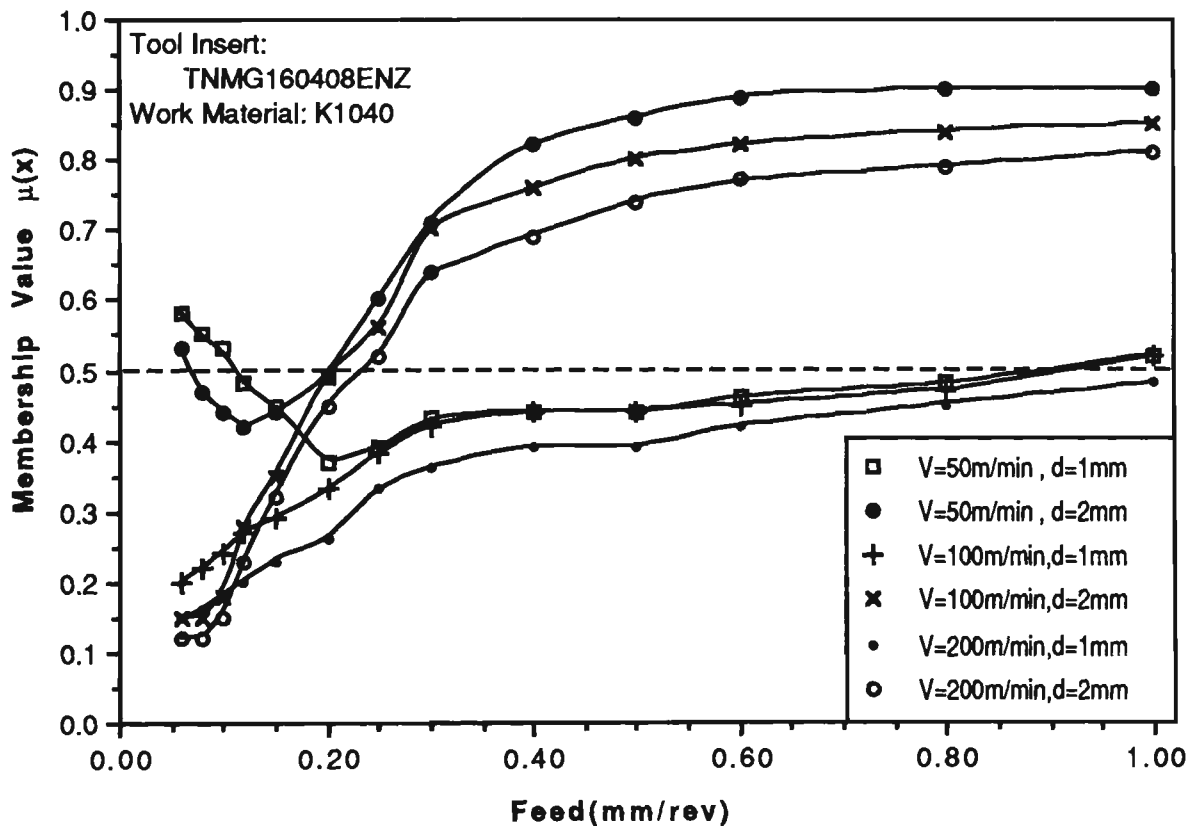
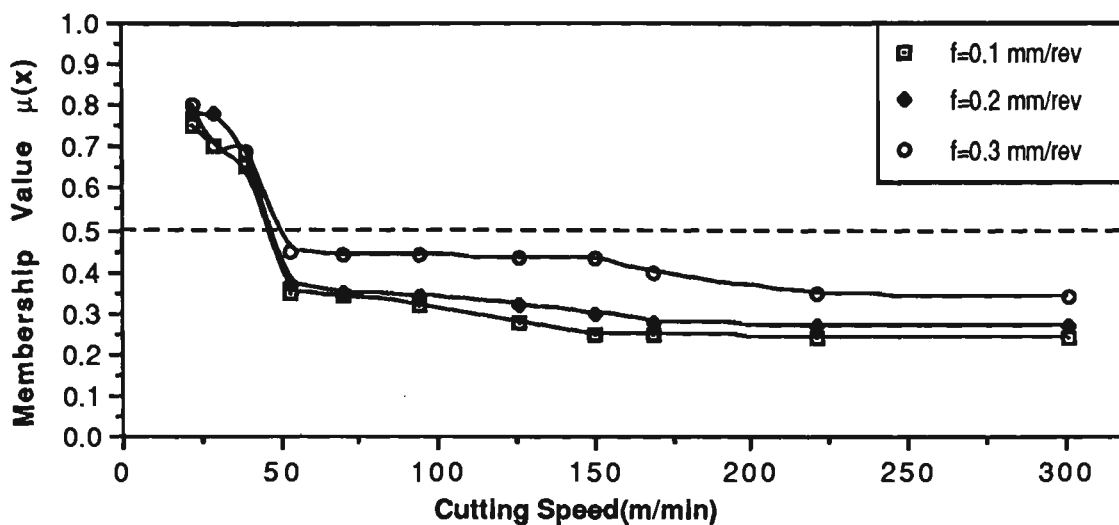


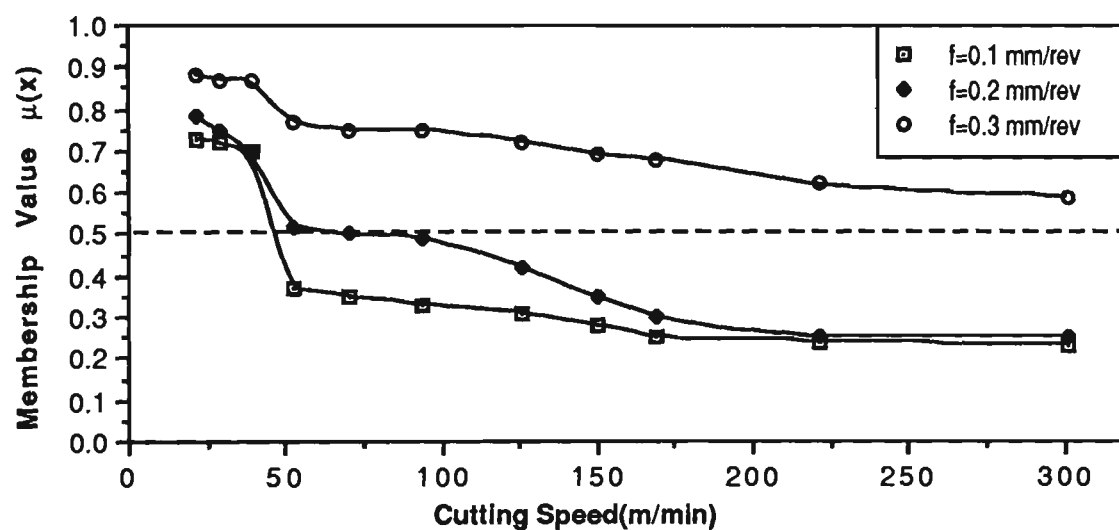
Figure 2.5 The effect of feed on chip breakability

2.4.1-3 Analysis of cutting speed

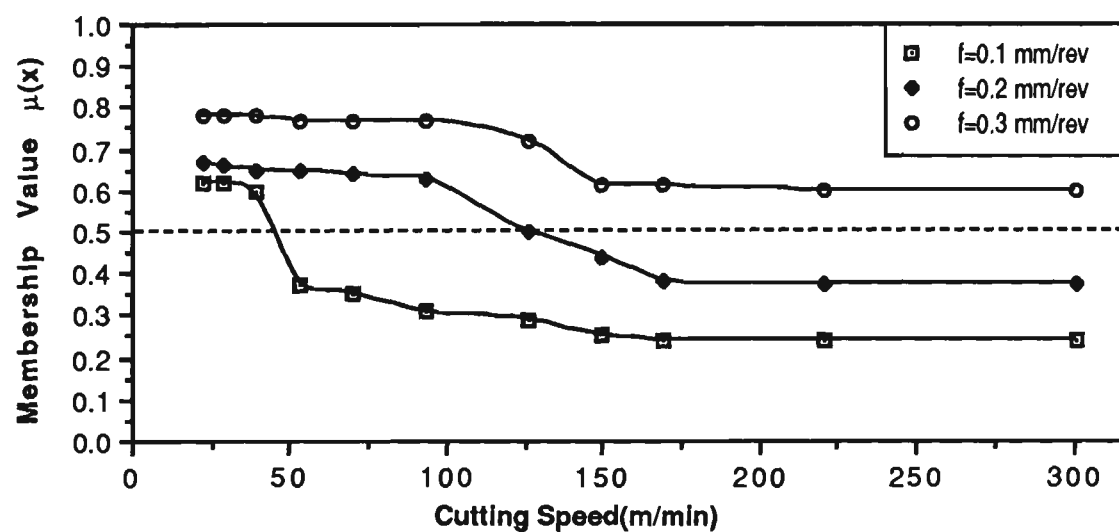
The chip breakability ratings were estimated for three values of depth of cut (1, 2 & 4 mm) and three values of feed (0.1, 0.2 & 0.3 mm/rev) at varying cutting speeds. Shown in Figure 2.6 is a sample result produced for machining of material K1040



(a) Low Depth of Cut (1mm)



(b) Medium Depth of Cut (2mm)



(c) High Depth of Cut (4mm)

Figure 2.6 The effect of cutting speed on chip breakability

with an ENZ tool insert. As seen, the lower the cutting speed the better the chip breakability, because higher cutting speeds produce thinner chips which are more difficult to break (see Equation 2.1). When the cutting speed is lower than 50 m/min, the chip breakability appears to be very good at all depths of cut for all feed values tested due to the apparent existence of BUE. When the cutting speed is larger than 50m/min, there are different effects at different depths of cut. For small depth of cut (Figure 2.6(a)), there is a sharp decrease in chip breakability at all feeds, while for high depth of cut (see Figure 2.6(c)), significant decrease occurs only at low feeds. When the cutting speed is beyond 150m/min, there is virtually no change in chip breakability.

2.4.2 Effect of Work Materials

In the present analysis seven different work materials were considered. The chemical composition is a major factor which determines the mechanical properties of a work material, this in turn affects the chip breakability. Several chip breakability diagrams for conditions using different work materials were plotted and some of the representative diagrams are shown in Figures 2.7 to 2.11.

2.4.2-1 Analysis of carbon content on chip breakability

Three carbon steels, with the same chemical composition but different carbon contents, were selected to investigate the influence of carbon content on chip breakability. In Figures 2.7(a), (b) and (c), the change of membership values was plotted with varying cutting speeds, feeds and depths of cut respectively. The results show that the relationships among different carbon contents are consistent in all the cases, i.e. a steel with higher carbon content is more difficult to break, thus with smaller membership value.

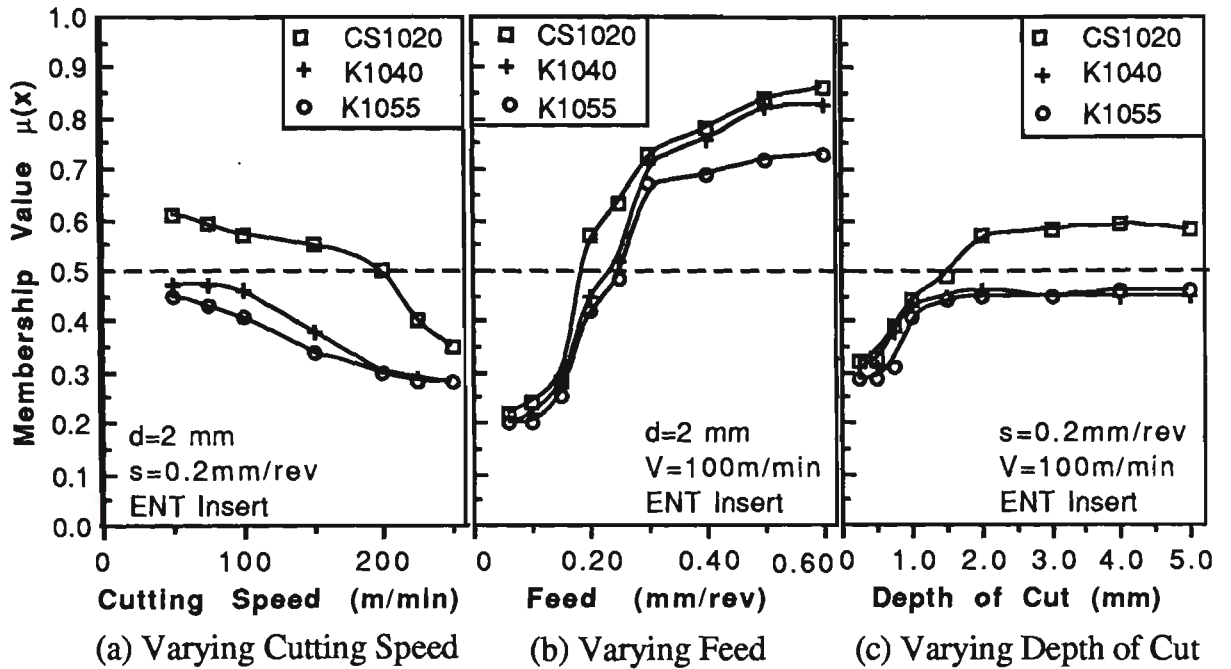


Figure 2.7 The effect of carbon content on chip breakability

2.4.2-2 Analysis of Cr-Mo alloy steel

The work material AISI4140 is a typical Cr-Mo alloy steel widely used in industrial practice. In order to study the effect of Cr-Mo alloy element, a comparison was made with plain carbon steel, K1040, both having the same carbon content. As shown in Figure 2.8, there are generally no significant difference in chip breakability at low (0.1 mm/rev) and high (0.3 mm/rev) feeds because the chip breakability of both materials is poor at low feeds and good at high feeds with the selected cutting speed (200 m/min). However, when the feed is at its medium value (0.2 mm/rev), there is an abrupt increase in chip breakability for material K1040, while for material AISI4140, the change occurs only when the feed goes up to 0.3 mm/rev, due to its higher chip ultimate strain than that of material K1040.

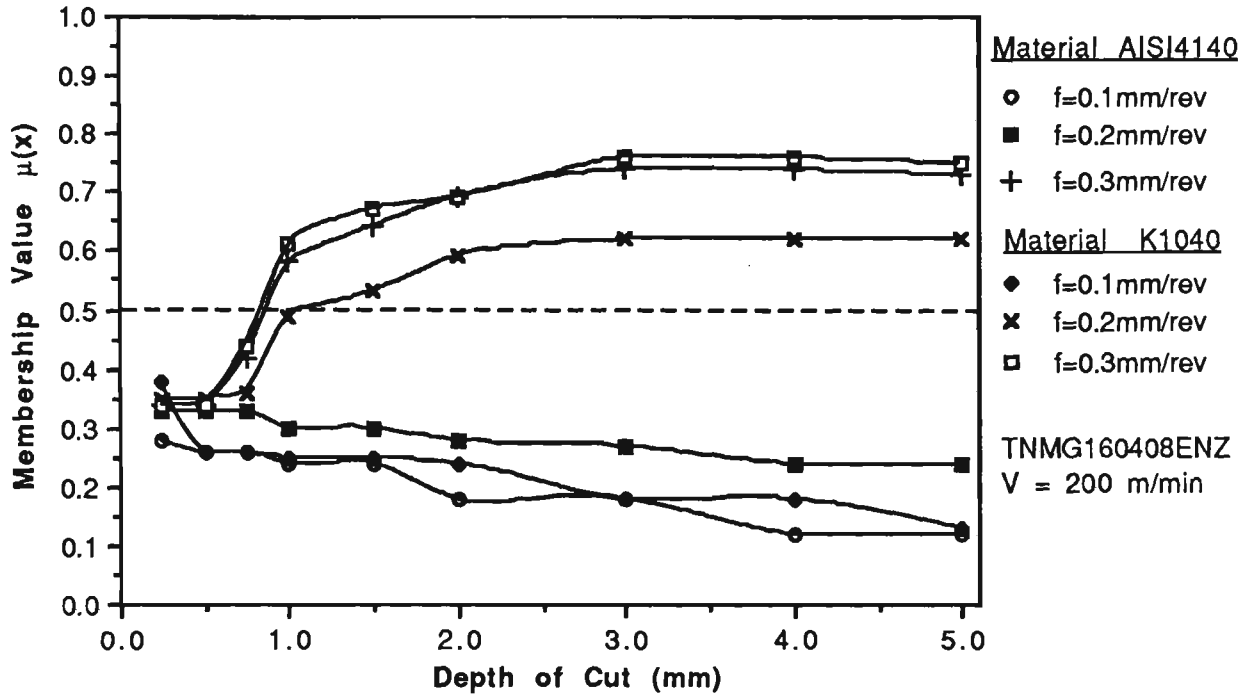


Figure 2.8 The effect of Cr-Mo alloying on chip breakability

2.4.2-3 Comparative analysis for three low-carbon-based alloy steels

The membership values of three work materials with approximately equal low carbon content yet different alloy elements were shown in Figure 2.9 at varying depths of cut. Generally speaking for all three materials, with the increase of depth of cut (up to 3 mm), the chip breakability increases at the higher feed (0.2 mm/rev) while decreases at the lower feed (0.1 mm/rev). Among the three work materials, it is clear that the chip breakability of free-machining steel S12L14 is remarkably good mainly due to the fact that the addition of Lead (P_b) to steel largely reduces the shear strength in the workpiece and subsequently results in tighter chip curling. At lower feeds (0.1 mm/rev), the effect of free-machining steel is even more significant in comparison with the other two materials. Between materials CS1020 and EN36A, it can be concluded that the chip breakability is lower if the work material contains Chromium (Cr) and Nickel (Ni) due to the increased chip ultimate strain.

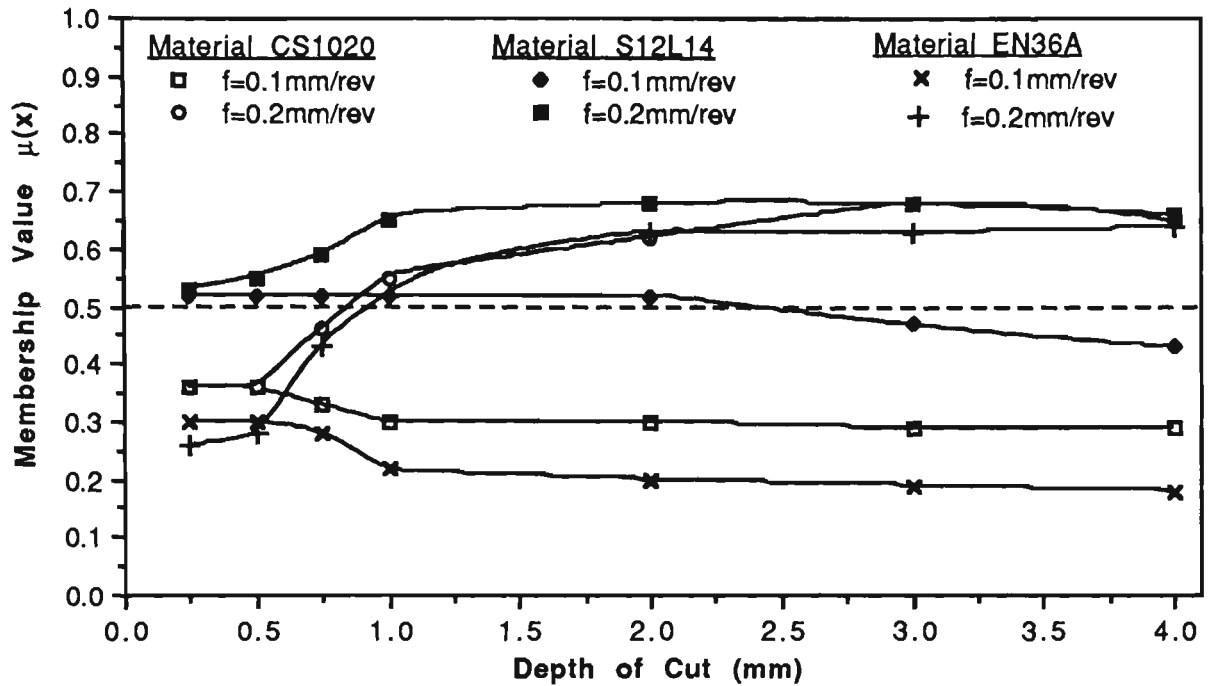


Figure 2.9 The effect of low-carbon-based alloying on chip breakability (Tool Insert : TNMG160408ENA, Cutting Speed = 200 m/min)

2.4.2-4 Comparative analysis of six different work materials

Figure 2.10 shows the effect of feed on chip breakability for six work materials at varying feeds with a typical cutting speed. In all cases except material S12L14, there exists a sensitive feed range between 0.2 to 0.3 mm/rev, during which a small change in feed has a significant effect on chip breakability. When the feed is higher than 0.3 mm/rev, there is no significant effect on chip breakability with the increase in feed. Furthermore, a representative set of chip breakability diagrams in terms of standard feed-depth of cut relationship is shown in Figure 2.11 for six work materials with membership values $\mu(x) = 0.5$ as the boundary lines.

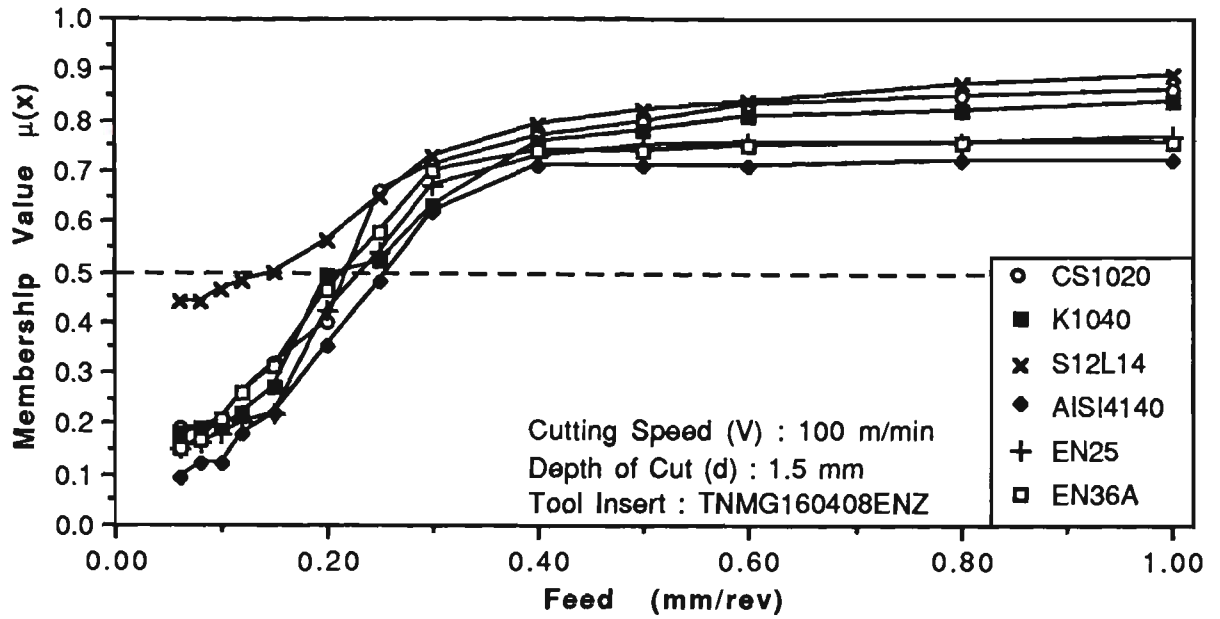


Figure 2.10 The effect of different work materials on chip breakability

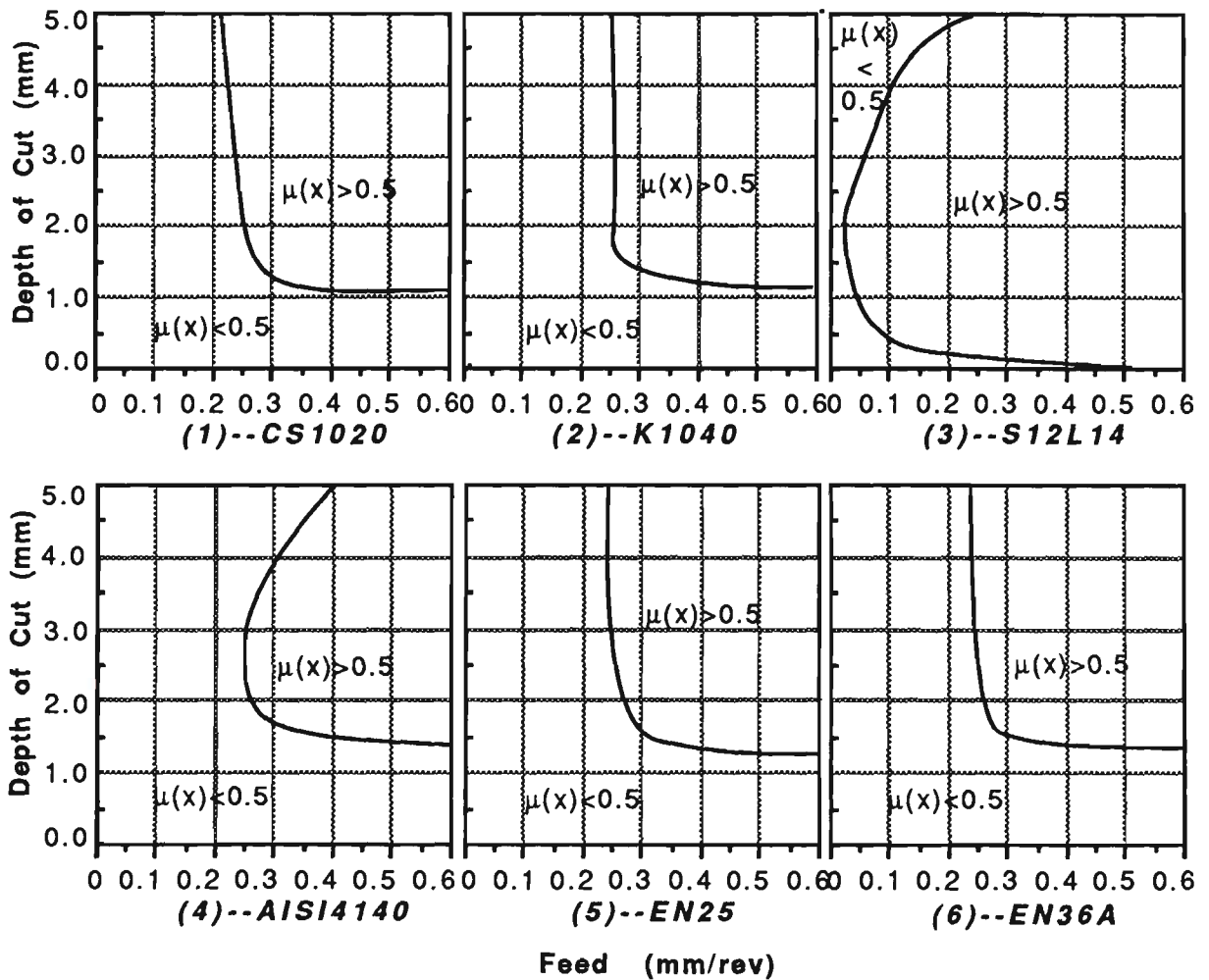


Figure 2.11 Chip breakability diagrams for six different work materials (Tool Insert : TNMG160408, Cutting Speed = 200 m/min)

2.4.3 Effect of Tool Inserts

Different chip breakers have different regions of chip breakability. Figure 2.12 shows the boundary lines with membership values $\mu(x) = 0.5$ for the seven tool inserts in the feed-depth of cut relationship diagram at higher cutting speeds (200 m/min). With the same method, Figure 2.13 shows the diagrams for six tool inserts at lower cutting speeds (50 m/min). It is noticed that there are two boundary lines at the low cutting speed, mainly due to the complex BUE formation.

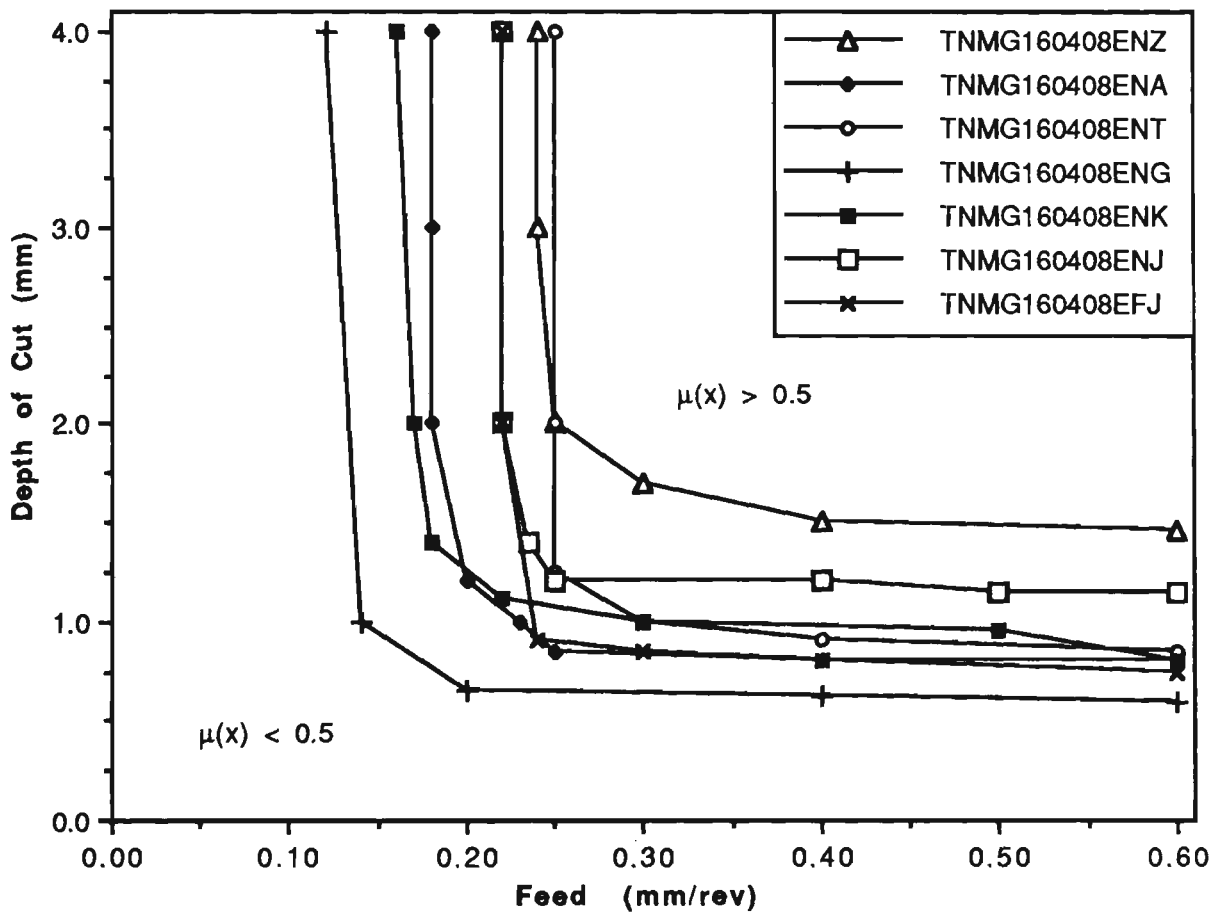


Figure 2.12 Chip breakability diagram for different tool inserts at a high cutting speed (Work Material : K1040, Cutting Speed = 200 m/min)

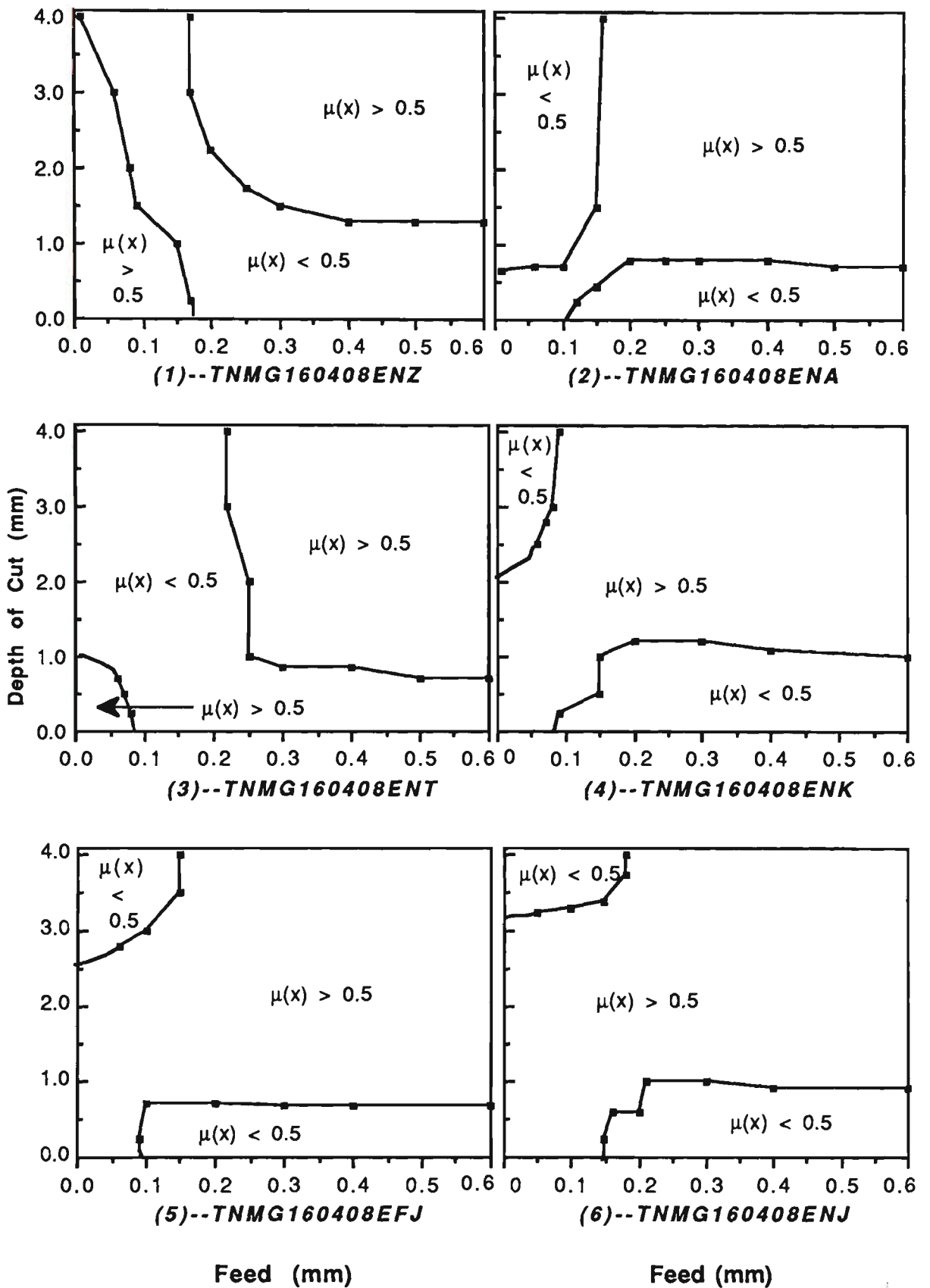


Figure 2.13 Chip breakability diagrams for different tool inserts at a low cutting speed (Work Material : K1040, Cutting Speed = 50 m/min)

As discussed before, the chip breakability decreases with the increase of cutting speed, however, the extent to which it is affected by the cutting speed varies with different chip breakers. As shown in Figure 2.14, ENA, ENG and EFJ types of tool inserts appear to be less affected by the increase of cutting speed, giving a much better chip breakability than the other three types.

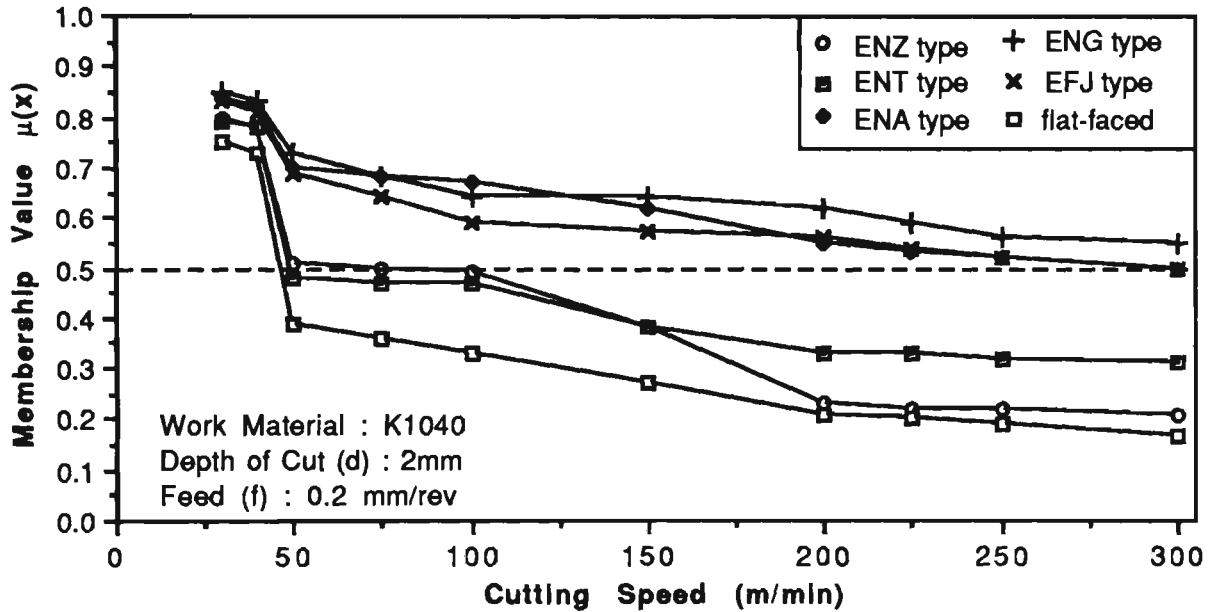


Figure 2.14 Comparison of cutting speed effect with different chip breakers

2.4.4 Effect of Tool Geometries

Variations in cutting tool geometry such as the rake angle, clearance angle and cutting edge inclination angle are found to be less common against the variations in the cutting edge angle (C_s) and tool nose radius (r) for a given cutting tool of defined specifications and thus were not considered in the initial analysis.

2.4.4-1 Analysis of cutting edge angle

As shown in Figure 2.15, the cutting edge angle, defined as the angle between the feed direction and the straight part of major cutting edge, has a significant influence on

chip breakability. At a high cutting speed (200 m/min), chip breakability is almost the same in the low feed region for all cutting edge angles, while in the high feed region, higher cutting edge angles in general produce better chip breakability. When both cutting speed and feed are very low, a rather complex effect occurs which is much the same as what we described before about the effect of feed at a low cutting speed (50 m/min), i.e. the likely formation of BUE. Overall, the decrease in cutting edge angle reduces the effectiveness of chip breakers and thus lowers the chip breakability.

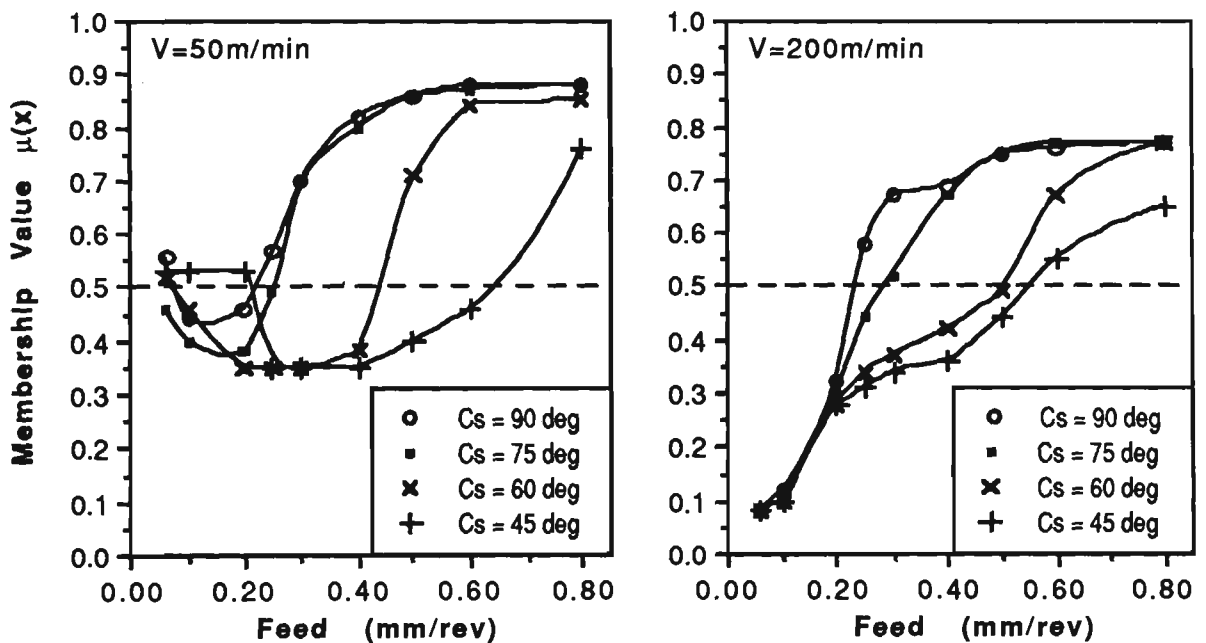


Figure 2.15 The effect of cutting edge angle on chip breakability
(Tool Insert : TNMG160408ENZ, Work Material : K1040, Depth of Cut : 2mm)

2.4.4-2 Analysis of tool nose radius

The relationship between tool nose radius and chip breakability is shown in Figure 2.16. Generally speaking, the smaller the tool nose radius, the better the chip breakability, while at the low cutting speed (50 m/min), larger tool nose radius appears to have better chip breakability within the low feed range ($f < 0.1\text{mm/rev}$).

The effect of tool nose radius tends to be less significant with the increase in cutting speed.

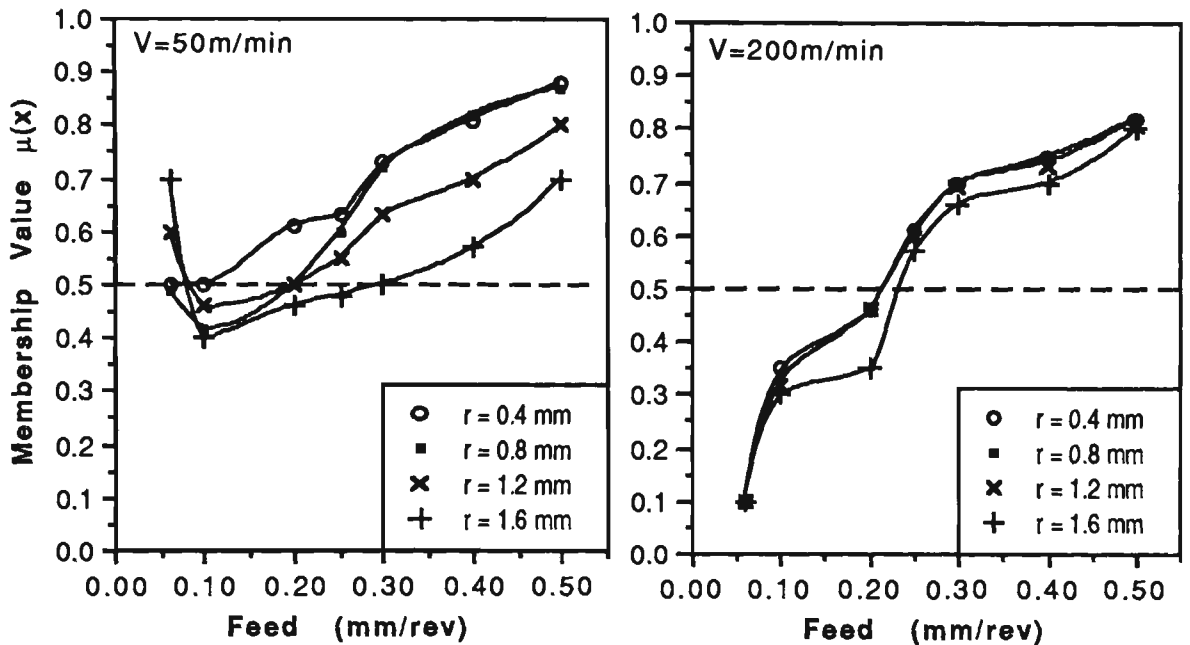


Figure 2.16 The effect of tool nose radius on chip breakability (Tool Insert : ENT-type, Work Material : K1040, Depth of Cut : 2mm)

2.5 FOUNDATION OF A FUZZY-SET MATHEMATICAL MODEL

Factors affecting chip breakability have been studied in detail by the extensive machining experiments. However, a quantitative utilisation of these results is required in order to extend the prediction range of chip breakability to arbitrary combinations of machining parameters. Therefore a fuzzy-set mathematical model is introduced because of its ability to quantify the usually adopted descriptive words, such as slight increase, large decrease, etc., for the effect of each machining parameter on chip breakability. The detailed procedure for establishing such a fuzzy-set model is described below.

The membership value $\mu_k(i, j)$ will vary when the combinations of five machining parameters (see Table 2.2) are different from those in the standard chip breakability matrices. Knowledge rules are used to deduce the chip breakability for any combinations of machining parameters on the basis of the established standard chip breakability matrices. For each machining parameter, there are corresponding groups of knowledge rules developed by using fuzzy logics. The following is an example for such a rule used in the present work for **feed**:

IF	Tool insert	is	ENT type	and
	Material	is	K1040 or EN25	and
	Cutting speed	is	≥ 40 m/min	and
	Depth of Cut	is	> 0.8 mm	and
	while Feed varies between 0.23 and 0.25 mm/rev			

THEN the chip breakability, i.e. the membership value $\mu(x)$ will have a large increase comparing with that at the standard feed value $f = 0.2$ mm/rev in the standard chip breakability matrix.

With the quantitative representation of chip breakability by giving membership value $\mu(x)$ for each chip shape/size, it becomes feasible to structure and describe the machining conditions which differ from those involved in the basic chip database, and to formulate these varying conditions in models. Fuzzy exponential function, as shown in Figure 2.17, is used to quantify the variation of the membership value corresponding to each different machining parameter,

$$\mu^*(x) = [\mu(x)]^q \quad (2.5)$$

where the exponent q is decided by the fuzzy linguistic values shown in Table 2.4, and $\mu^*(x)$ is the modified membership value indicating the variation of chip breakability.

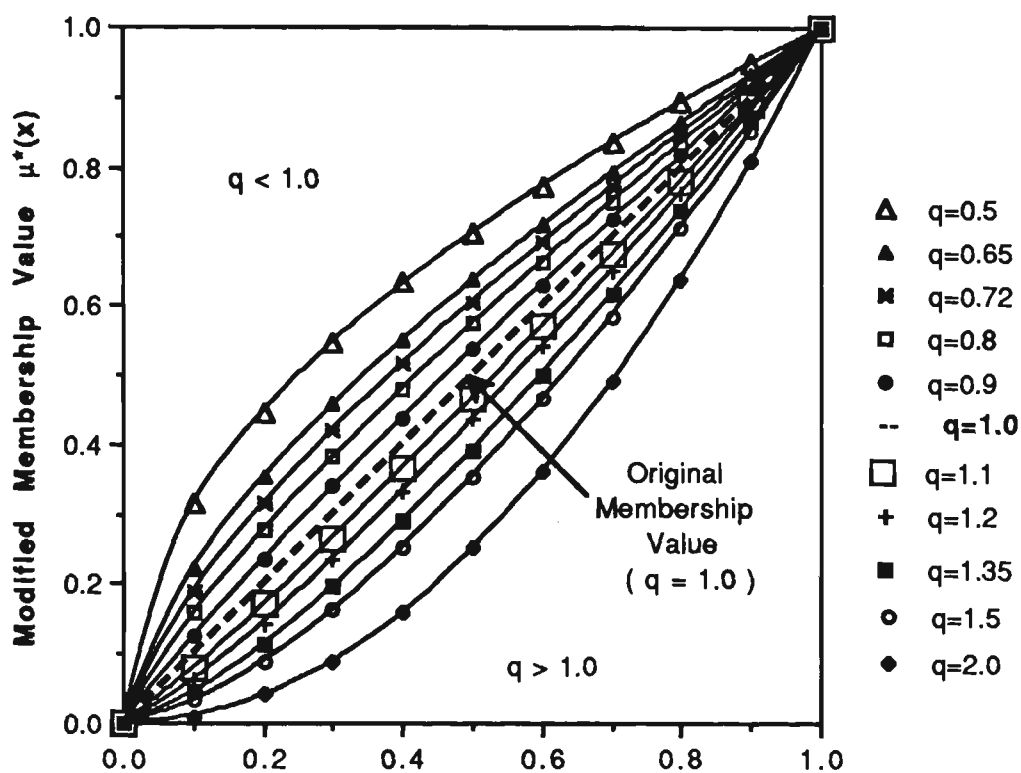


Figure 2.17 Fuzzy exponential functions

Table 2.4 Fuzzy linguistic values

Chip Breakability ($\mu^*(x)$)	Exponent q
very rapid increase	0.50
rapid increase	0.65
large increase	0.72
moderate increase	0.80
slight increase	0.90
no change	1.0
slight decrease	1.10
moderate decrease	1.20
large decrease	1.35
rapid decrease	1.50
very rapid decrease	2.0

For the assessment of chip breakability involving more changeable machining parameters, membership values, $\mu(i, j)$, can be modified by the integrated effects of these parameters. The modified membership value, $\mu^*(i, j)$, can be determined by the following fuzzy-set mathematical model,

$$\mu_k^*(i, j) = \left[\mu_k(i, j) \right]^{\prod_{n=1}^5 q_n} \quad (2.6)$$

$$i = 1, \dots, 6; \quad j = 1, \dots, 6; \quad \text{and} \quad k = 1, \dots, 45;$$

where q_1, q_2, q_3, q_4 and q_5 are the exponents corresponding to the tool insert, work material, cutting speed, depth of cut and feed respectively, and are determined from the knowledge-rules that summarise all the effects of each machining parameter. On the basis of this fuzzy-set mathematical model, a predicting output for chip breakability is derived with fuzzy ratings. Table 2.5 shows the likely outputs for chip breakability as well as the corresponding chip shapes/sizes.

Table 2.5 Predicting chip breakability with fuzzy ratings

Output Ratings	$\mu_k^*(i, j)$	Fuzzy Definition of Chip Breakability	The Most Likely Chip Shapes/Sizes Produced in Machining
1	0.0-0.2	absolutely unbroken	large snarled continue and long size with large diameter
2	0.2-0.3	very difficult to break	continue long size snarled with medium or large size
3	0.3-0.45	usually difficult to break	long size (continue or broken) snarled often with few turns or small size
4	0.45-0.5	maybe broken (about 40% probability)	medium size spiral with few turns
5	0.5-0.58	maybe broken (about 60% probability)	short to medium size flat spiral with medium size conical spiral with medium size
6	0.58-0.7	usually easy to break	short size, full turn flat or conical spirals with short size
7	0.7-0.9	very easy to break	side-curl arcs or up-curl arcs
8	0.9-1.0	always broken	up-curl arcs or connected side-curl arcs

2.6 ESTABLISHMENT OF AN EXPERT SYSTEM FOR PREDICTING CHIP BREAKABILITY

Expert systems are computer programs that can help advise, diagnose, analyse, consult and categorise. They simulate the problem-solving process of a human expert on the basis of rules obtained by developing the knowledge of experts and the database which collects facts or the relationships of facts. The programming language used in developing the expert system is Turbo Prolog.

2.6.1 Knowledge Representation

2.6.1-1 Basic facts about chip breakability

Since the knowledge is expressed as facts and rules in Prolog, the basic chip database is composed of 1620 facts about chip breakability. The data structure is described by the following Prolog code:

database :

chip (membership_value, std_tool, std_material, std_speed, std_depth, std_feed)

where std_tool = standard tool inserts : ENZ type, ENA type, ENT type
 std_material = standard work materials : CS1020, K1040, EN25
 std_speed = standard cutting speeds : 50, 75, 100, 150, 200 m/min
 std_depth = standard depths of cut : 0.25, 0.5, 1.0, 2.0, 3.0, 4.0 mm
 std_feed = standard feeds : 0.06, 0.1, 0.2, 0.3, 0.4, 0.5 mm/rev

With the above membership_value considered as elements, depth of cut as row variable, feed as column variable, 45 standard chip breakability matrices are set up under each combination of the above tool inserts, work materials and cutting speeds (see Equation 2.4).

2.6.1-2 Knowledge rules for the effects of machining parameters

Based upon the standard chip breakability matrices and the analysis of results from the experiments for investigating factors affecting chip breakability, knowledge rules are summarised for each machining parameter. These rules are used to infer one fact from the given facts in the basic chip database. The inference engine is based on the established fuzzy-set mathematical model, i.e. Equation 2.6 from which a modified membership value $\mu_k^*(i,j)$ is obtained. A knowledge rule takes the following general form :

$$P \text{ if } (P_1 \text{ and } P_2 \text{ and } P_3 \text{ and } \dots \text{ and } P_n) \quad (2.7)$$

where P is the head of a rule which is the hypothesis and represents the goal to be achieved, (P₁ and P₂ and P₃ and and P_n) is the body of a rule which is a subgoal consisting of several conditions. The head of the rule for each machining parameter is given as follows :

tool(tool, material, speed, depth, feed, std_tool, tool_exponent)

material(std_tool, material, speed, depth, feed, std_material, material_exponent)

speed(std_tool, std_material, speed, depth, feed, std_speed, speed_exponent)

depth(std_tool, std_material, speed, depth, feed, std_depth, depth_exponent)

feed(std_tool, std_material, speed, depth, feed, std_feed, feed_exponent)

tool_Cs(std_tool, cs_angle, speed, depth, feed, cs_factor)

tool_NR(nose_radius, speed, feed, nr_factor)

where std_tool, std_material, std_speed, std_depth and std_feed are the standard values in the basic chip database, and tool_exponent, material_exponent, speed_exponent, depth_exponent and feed_exponent correspond to q_1 , q_2 , q_3 , q_4 and q_5 in Equation 2.6 respectively. The symbols cs_factor and nr_factor are the factors to modify the tool_exponent .

2.6.2 Examples of Knowledge Rules for Chip Breakability

Two examples of the knowledge rules for each machining parameter are given below :

(1) Rules for Tool Inserts

Example 1

----- In	Prolog -----	----- Read	As -----
tool(T,M,V,D,F,ena,0.8):-		IF	Tool insert is ENG and
	T=eng,		Work material is any and
	M=M,		Cutting speed is $V < 60$ m/min and
	V<60,		Depth of cut is $D = \text{any}$ and
	D=D,		Feed is $F < 0.15$ mm/rev
	F<0.15.	THEN	membership value $\mu(x)$ has a moderate increase, i.e. exponent $q_1 = 0.8$, comparing with that at the standard tool insert ENA.

Example 2

----- In	Prolog -----	----- Read	As -----
tool_Cs(StdT,Tcs,V,D,F,1.5):-		IF	Standard tool insert is ENZ type
	StdT=enz,		Cutting edge angle $Cs = 45^\circ$ and

$D > 2.5$,
 $F < 0.2$.
 THEN membership value $\mu(x)$ has a rapid increase, i.e. exponent $q_2 = 0.65$, comparing with that at the standard work material CS1020.

(3) Rules for Cutting Speeds

Example 1

<pre> ----- In Prolog ----- depth(StdT,StdM,V,D,F,150,0.9):- StdT=enx, StdM=k1040, V>=130, V<145, D>2.0, F>=0.2, F<=0.23. </pre>	<pre> ----- Read As ----- IF Standard tool insert is ENZ and Standard work material is K1040 and Cutting speed is 130 ≤ V < 145 m/min and Depth of cut is D > 2.0 mm and Feed is 0.2 ≤ F ≤ 0.23 mm/rev THEN membership value μ(x) has a slight increase, i.e. exponent q₃ = 0.9, comparing with that at the standard cutting speed V = 150 m/min. </pre>
---	---

Example 2

<pre> ----- In Prolog ----- depth(StdT,StdM,V,D,F,50,1.1):- StdT=StdT, StdM=StdM, V>=52, V<60, </pre>	<pre> ----- Read As ----- IF Standard tool insert is any and Standard work material is EN25 and Cutting speed is 52 ≤ V ≤ 60 m/min and Depth of cut is D = any and Feed is F ≤ 0.1mm/rev </pre>
---	---

D=D,
F<0.1. THEN membership value $\mu(x)$ has a slight decrease (i.e., exponent $q_3 = 1.1$) comparing with that at the standard cutting speed V=50 m/min.

(4) Rules of Depths of Cut

Example 1

```

----- In   Prolog -----           ----- Read   As -----
depth(StdT,StdM,V,D,F,2.0,1.35):-  IF   Standard tool insert is ENZ       and
      StdT=enz,                       Standard work material is any       and
      StdM=StdM,                       Cutting speed is V = any and
      V=V,                               Depth of cut is  $1.6 < D \leq 1.8$  mm and
      D>1.6,                             Feed is  $F \geq 0.25$  mm/rev
      D<=1.8,                             THEN membership value  $\mu(x)$  has a large
      F>=0.25.                           decrease (i.e., exponent  $q_4 = 1.35$ )
                                           comparing with that at the standard
                                           depth of cut D = 2.0 mm.

```

Example 2

```

----- In   Prolog -----           ----- Read   As -----
depth(StdT,StdM,V,D,F,1.0,0.8):-  IF   Standard tool insert is ENT       and
      StdT=ent,                       Standard work material is CS1020 and
      StdM=cs1020,                   Cutting speed is V=any             and
      V=V,                               Depth of Cut is  $1.5 < D < 2.0$  mm and
      D>1.5,                             Feed is  $0.2 \leq F < 0.25$  mm/rev
      D<2.0,                             THEN membership value  $\mu(x)$  has a moderate
      F>=0.2,                           increase, i.e. exponent  $q_4 = 0.8$ ,

```


2.6.3 Schematic Diagram of the Expert System

On the basis of what was discussed before, a schematic diagram of the expert system can be drawn as shown in Figure 2.18.

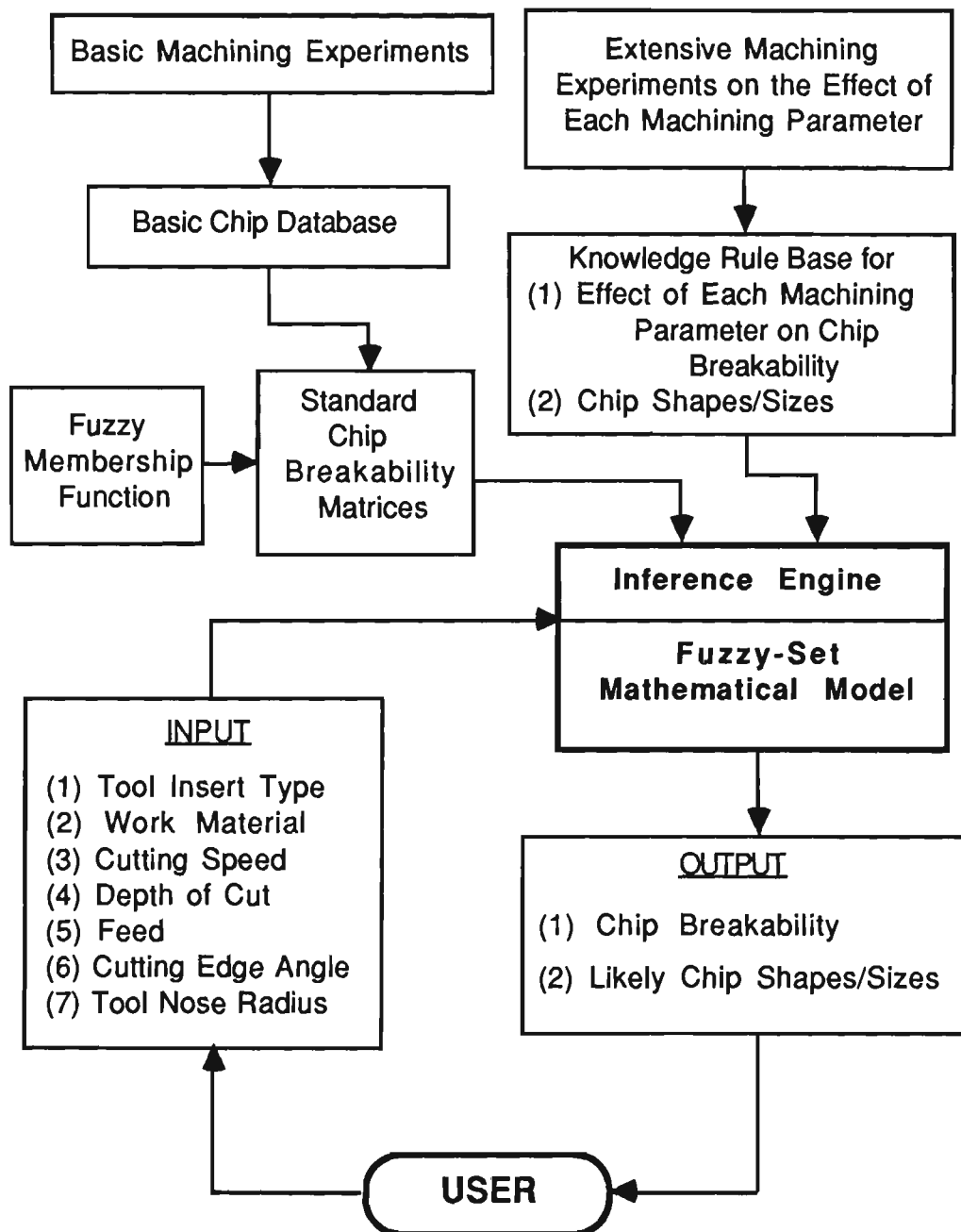


Figure 2.18 The expert system schematic diagram

2.7 PROLOG PROGRAMMING ARCHITECTURE

Prolog stands for "PROgramming in LOGic" and is a computer programming language which was invented in 1970s. Prolog is powerful in handling logic problems and particularly well suited for applications in the artificial intelligence systems, such as, expert systems. Turbo Prolog is one of Prolog versions used on an IBM PC computer (or compatible) system.

Considering the large scope of the expert system program, a modular architecture is introduced in programming, i.e. the whole program is divided into several modules according to their functions. Then a global method is used to communicate across module boundaries. All the data items are stored in the external database in the form of chains which allow the expert system to access the data items very quickly. Figure 2.19 shows the programming structure of the expert system.

In this way, the program structure has the following advantages:

- (a) With the basic chip database as external database in files, the only limit on the database size is the available computer disk space which is usually large enough to hold any practical database.
- (b) With all the data stored as chains in the external database, the expert system is able to handle efficiently even a very large amount of data on disk.
- (c) With modular programming, the expert system is very easy to develop new functions only by creating new modules without influencing on other modules.

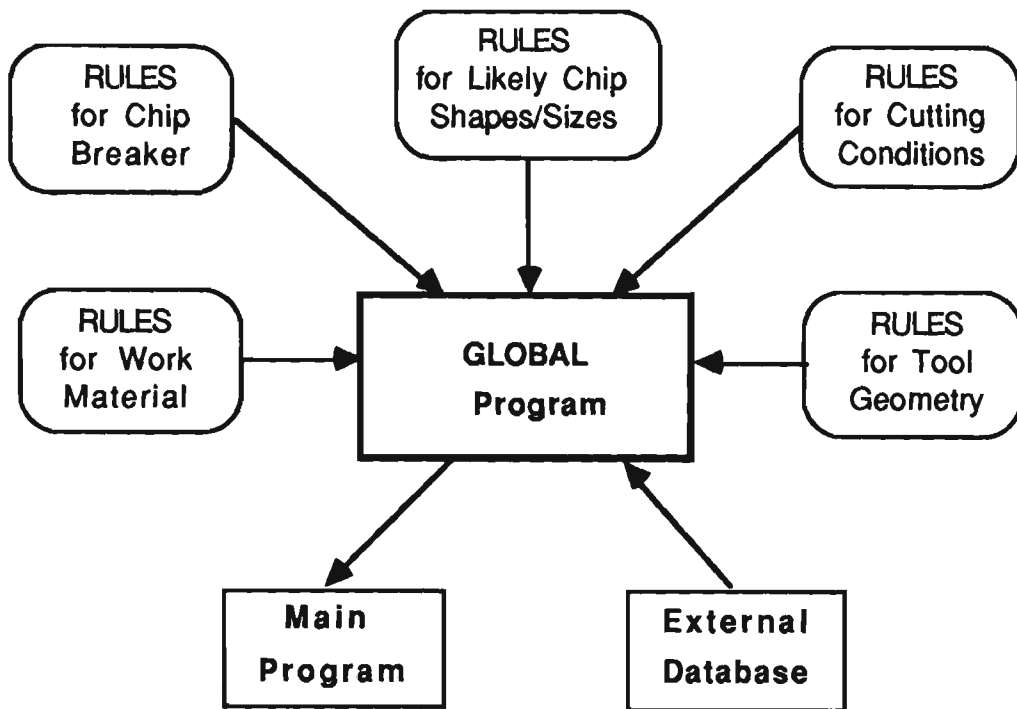


Figure 2.19 PROLOG program structure diagram

2.8 SUMMARY AND CONCLUDING REMARKS

- (1). Advances in automated machining systems inevitably require more effective chip control. Particularly, predictability of chip breaking has been identified as vital since the performance of chip control greatly depends on the chip breakability in machining of steel.
- (2). Chip breaking is a complicated process, influenced by a great number of interacting process variables. The theory and knowledge to date about metal cutting and chip control are not available to predict quantitatively the chip breakability for the application to workshop environments.
- (3) By introducing a fuzzy membership function, this chapter has presented a new method to quantify chip breakability according to the chip shapes/sizes produced in the machining process. Based on the basic chip database for

providing the standard chip breakability and the extensive machining experiments for evaluating the effect of each machining parameter, an expert system has been developed using a fuzzy-set mathematical model for quantitatively predicting the chip breakability under any combinations of cutting conditions, work materials and tool design features including tool geometry.

- (4). The prediction accuracy of chip breakability depends heavily on the range of experimental results available in the "knowledge-base" and on the quality of knowledge rules that could be developed.
- (5). The method for predicting chip breakability presented in this chapter may provide a quantitative reference for optimal machining process control or machinability assessment, and also will provide a feasible application to total chip control in unmanned machining systems in the future.

CHAPTER 3

A PREDICTIVE EXPERT SYSTEM FOR THE ASSESSMENT OF MACHINING PERFORMANCE WITH CHIP CONTROL AS A MAJOR CRITERION

3.1 INTRODUCTION

The development of automated process planning (APP) is of great interest to CAD/CAM integration. Developing expert systems for machining parameter selection is an effective approach for improving APP [64-66]. However, chip control is seldom selected as a criterion for APP mainly due to its complexity. Aiming at providing an effective auxiliary to APP system, this chapter presents the development of a predictive expert system for the assessment of machining performance with chip control, including chip breakability/chip forming patterns, as a major criterion and with due consideration of surface finish and power consumption.

The predictive expert system is set up based on the results of a series of experimental work, the knowledge rules derived from the present knowledge on chip control and machining, and the expert's knowledge and findings. The knowledge-base created includes a comprehensive database containing basic facts about chip breakability, surface finish and power consumption, and a set of knowledge rules covering the effects of different tool inserts, work materials, cutting conditions and tool geometries.

3.2 FOUNDATION OF MACHINING PERFORMANCE DATABASE

A database is an essential part of the predictive expert system and has the following functions :

- (a) storing basic facts about machining performance based on machining experimental results;
- (b) being used as a primary standard for assessing machining performance;
- (c) being used as an analytical criterion for the knowledge rule summary; and
- (d) providing referable information during the expert's consultation process.

A series of machining experiments on chip control, surface finish and power consumption was conducted to set up the machining performance database for a wide range of cutting tools, work materials, cutting conditions and major tool geometries, shown as follows.

(1) Cutting Tools :

- (i) one conventional flat-faced tool (without chip breaker);
- (ii) eight commercial tool inserts with different types of chip breakers (ENA, ENZ, ENT, ENK, ENG, ENJ, EFJ and EFB types).

(2) Work Materials :

- (i) low carbon steel - CS1020 (BHN=185)
- (ii) medium carbon steel - K1040 (BHN=198)
- (iii) high carbon steel - K1055 (BHN=220)
- (iv) free-machining steel - S12L14 (BHN=168)
- (v) Ni-Cr alloy steel - EN36A (BHN=210)
- (vi) Mo-Cr alloy steel - AISI 4140 (BHN=300)
- (vii) Ni-Mo-Cr alloy steel - EN25 (BHN=240)

(3) Cutting Conditions :

- (i) cutting speed = 100 -- 350 m/min
- (ii) depth of cut = 0.25 -- 5 mm
- (iii) feed = 0.06 -- 1.0 mm/rev

(4) Tool Geometries :

- (i) tool nose radius = 0.4, 0.8, 1.2 & 1.6 mm
- (ii) cutting edge angle = 90, 75, 60 & 45 degrees
- (iii) tool rake angle = -5 & +5 degrees
- (iv) tool inclination angle = -12, -6, 0 & +5 degrees

3.3 ASSESSMENT OF MACHINING PERFORMANCE

Chip control, including chip breakability/chip forming patterns, combined with the power consumption and surface finish will give a better assessment for machining performance.

3.3.1 Assessment of Chip Control

The major objective of chip breaking is to facilitate effective and hazard-free chip disposal. In fact, the chip control operation requires efficient breaking of the chips into *acceptable* sizes and shapes for disposal in automated machining systems. Introducing a factor for chip acceptability therefore becomes vital from the point of view of chip disposal and safe machining. Chip acceptability can also be related to the chip shapes/sizes produced. Let us define the chip acceptability factor $g(x)$ as follows :

$$g(x) = k, \quad k = 1, \dots, 7 \quad (3.1)$$

where x is the chip shape (the same as that shown in Equation 2.2 in Chapter 2) and k is a positive integer representing the different grade of chip acceptability. The larger the chip acceptability factor $g(x)$, the more acceptable is the chip for chip disposal. A range of $g(x)$ is shown in Table 3.1.

Table 3.1 Chip acceptability factor $g(x)$ in automated machining systems

Chip Shapes/sizes	$g(x)$	Definition and Explanation
large snarled chips continuous chips	1	most unacceptable due to the main reason for inducing tangled chips
tooth-edged chips	2	unacceptable even if the chips are broken chips due to high cutting force, poor surface finish, etc.
long size size chips broken medium snarled chips	3	usually unacceptable
broken long size chips medium size chips	4	maybe acceptable depending on the practical machining requirements
small snarled chips	5	acceptable although chips are not broken due to easiness of chip disposal
short size broken chips	6	usually acceptable
small arc chips	7	most acceptable

Chip acceptability factor $g(x)$ can be deduced from the knowledge rules for chip shapes. Table 3.2 shows the integrated (combined) assessments for chip control after considering both the chip breakability and the chip acceptability. The most likely chip shapes/sizes are also provided to complement the basic understanding.

Table 3.2 Integrated assessment for chip control in automated machining systems

No.	$\mu(x)$	$g(x)$	Integrated Outputs	Most Likely Chip Shapes/sizes
1	0.0--0.2	1	absolutely unbroken and most unacceptable	large snarled chip infinite chip tubular chip with large diameter
2	0.2--0.3	1	very difficult to break and unacceptable	continuous long size chip medium-large size snarled chip
3	0.3--0.45	3	usually difficult to break and usually unacceptable	long size (continuous or broken) snarled (often with few turns)
4	0.45--0.5	4	maybe broken (about 40% probability) and maybe acceptable	medium size chip spiral chip with few turns
5	0.5--0.58	4	maybe broken (about 60% probability) and probably acceptable	short to medium size chip medium size flat spiral chip medium size conical spiral chip
6	0.58--0.7	6	usually easy to break and usually acceptable	short size chip full turn chip short size flat spiral chip short size conical spiral chip
7	0.7--0.9	7	very easy to break and most acceptable	side-curl arcs up-curl arcs
8	0.9--1.0	7	always broken and often overbroken; though most acceptable for disposal, usually not suggested	very tight up-curl arcs connected side-curl arcs
9	0.0--0.5	2	unbroken and unacceptable	long size tooth-edged chip
10	0.5--0.85	2	broken but unacceptable	short to medium size and tooth-edged chip
11	0.85--1.0	2	overbroken and absolutely unacceptable due to very harmful to the machining system	connected side-curl arc type with heavily tooth-edged chip
12	0.3--0.45	5	unbroken but acceptable	small snarled chip

3.3.2 Assessment of Surface Finish

The quality of machined surface is very closely associated with the chip shapes produced. Steady and continuous chips will produce a better surface finish while broken and tightly curled chips result in worse surface finish. In general, the formation of built-up edge (BUE) will cause deterioration of surface finish due to the effect of BUE fragments being randomly deposited on the machining surface. Furthermore, poor chip control results in tangled chips which, in turn, will scratch the machined workpiece surface and even lead to unexpected machine tool or cutting tool damage.

The surface finish was measured by Surfcom Model 550AD Surface Measuring Equipment, with the arithmetic mean deviation, R_a , as an assessment criterion. Four R_a values on the periphery, but along the same circle of workpiece, were taken to obtain an average R_a value. Some representative data of surface finish for different tool chip breakers are given in Appendix B.

3.3.3 Assessment of Power Consumption

The power consumption has a direct effect on the heat production, further influencing tool wear, tool life and the machined surface quality. It has been shown that the effective chip breaking at reduced power consumption can be achieved by means of efficient tool groove geometries [60].

Power consumption rate was assessed by evaluating the main cutting force measured by the KISTLER Dynamometer (Type 9257A).

3.4. AN INVESTIGATION OF THE INFLUENCING FACTORS ON MACHINING PERFORMANCE

As the factors influencing chip breakability have been investigated in detail in Chapter 2, in this section, the analysis will be emphasised on surface finish and power consumption.

3.4.1 Effect of Tool Insert Types

The performance of each tool insert was tested through machining experiments for chip breakability, power consumption and surface finish. Different chip breakers give different chip forms for a given set of cutting conditions, while producing varying surface finish. Figure 3.1 shows a representative result reflecting this.

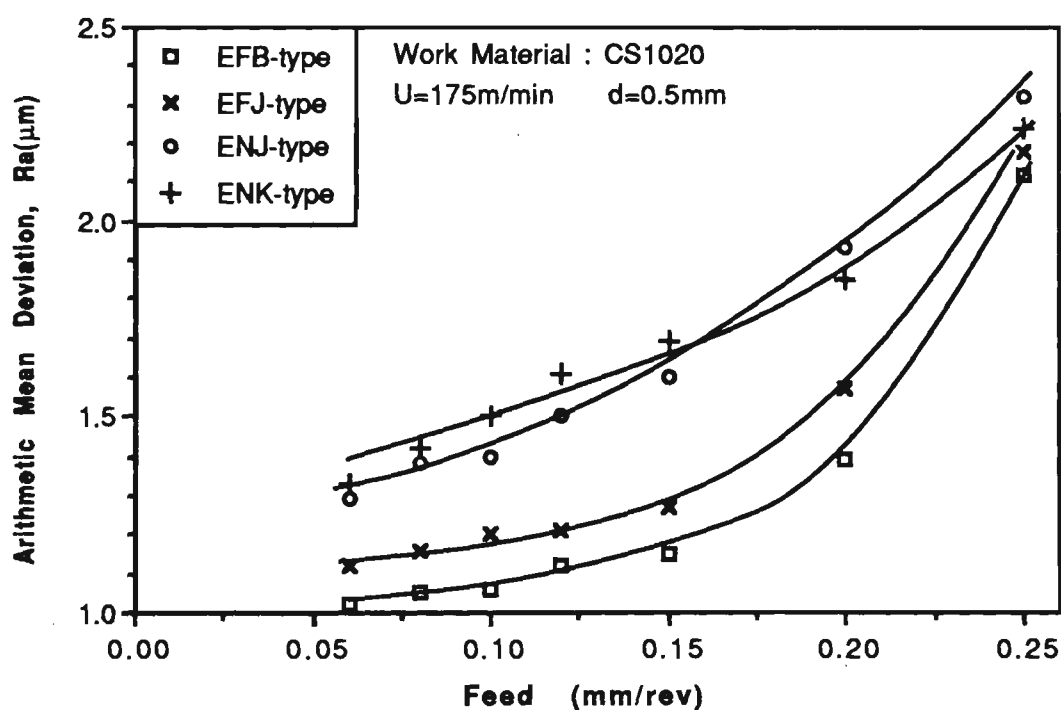


Figure 3.1 Surface finish comparison for four tool inserts

As shown in Figure 3.1, the groove-type chip breaker with the smaller restricted contact length (EFJ, $h = 0.1\text{mm}$) has a better surface finish than that of the larger

restricted contact length (ENJ, $h = 0.25\text{mm}$). EFB type has the best surface finish mainly due to its special configuration of chip breaker.

Reducing power consumption is of great importance for achieving improved tool life and efficient production. The chip breaker configuration and the restricted contact length are the two major factors to be considered in the design of efficient chip breakers. Shown in Figure 3.2 is the power comparison made among several representative tools.

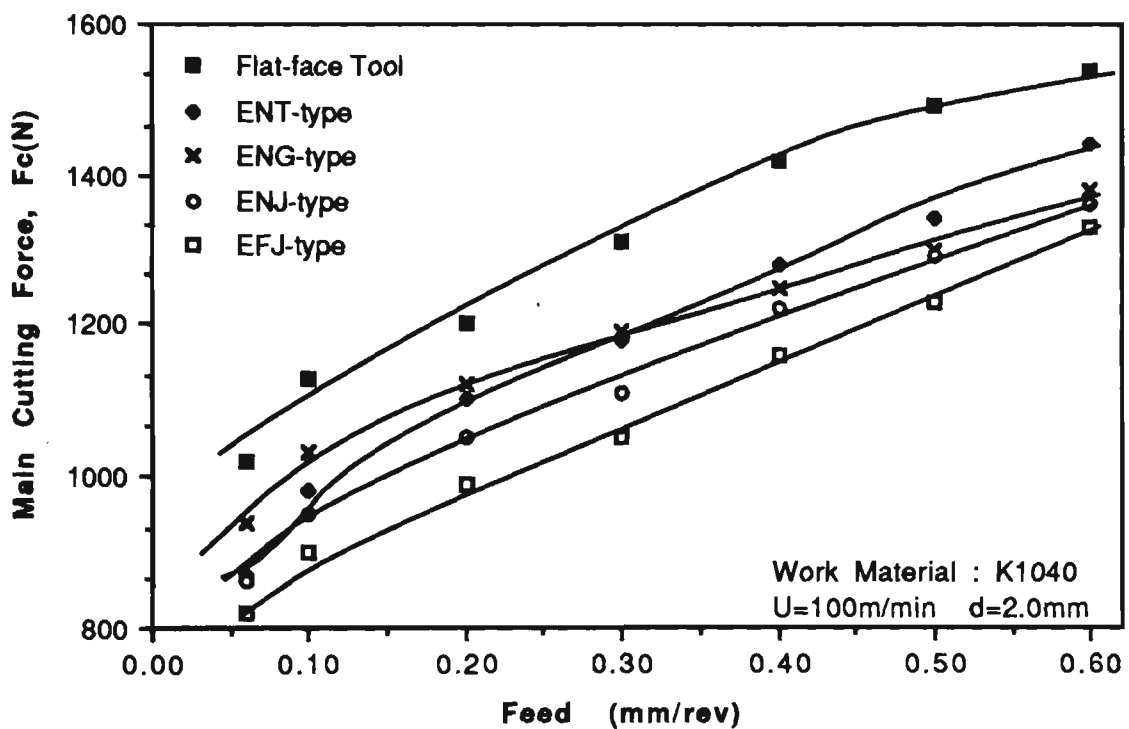


Figure 3.2 Power consumption comparison for five tool inserts

It is apparent from Figure 3.2 that the flat-faced tool consumes the highest power while the groove-type tool with smaller restricted contact length (EFJ) consumes the least power. Between the two representative chip breakers, i.e., the groove-type (ENT) and the obstruction-type (ENG), ENT proves to be better for low feed rates while ENG is better for high feed rates.

3.4.2 Effect of Work Materials

The effect of work material properties including chemical composition and material hardness on machining performances is very complex to investigate due to the difficulties in isolating the effects of various alloying elements in the work specimens. In this section, six typical work materials were selected for analysis. As given below in Figure 3.3 and 3.4 are two representative experimental results of surface finish and power consumption for different work materials.

3.4.3 Effects of Cutting Conditions and Tool Geometries

On the basis of the machining experiments and the knowledge derived from the published work, an integrated summary for the effects of cutting conditions and major tool geometries on machining performance is given in Figure 3.5.

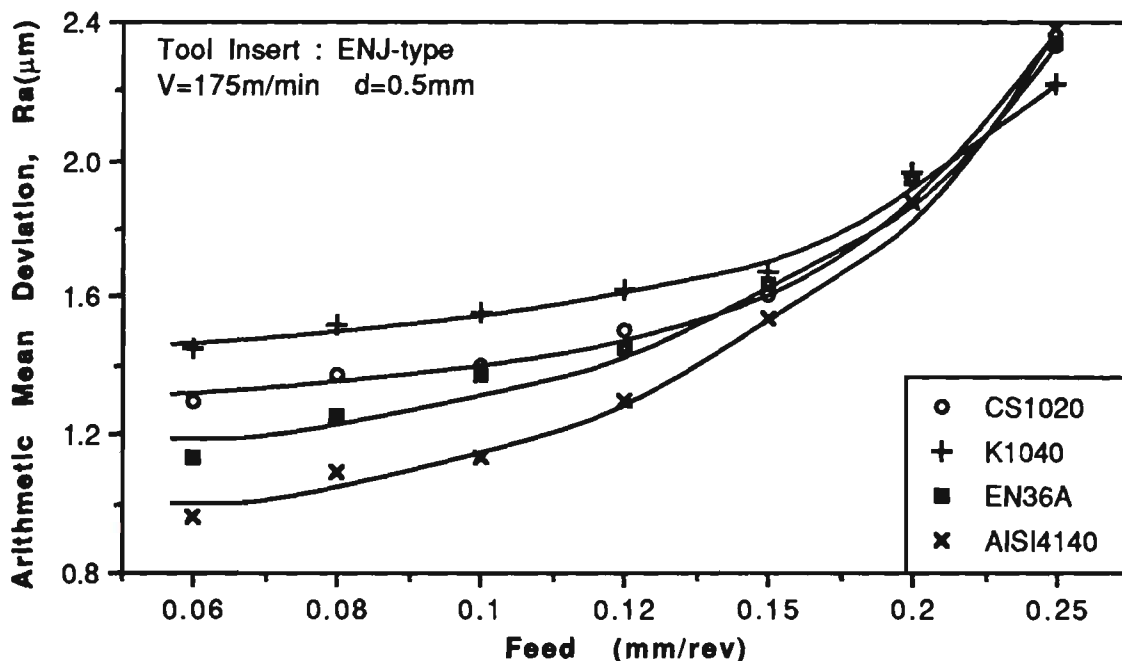


Figure 3.3 Surface finish comparison for four work materials

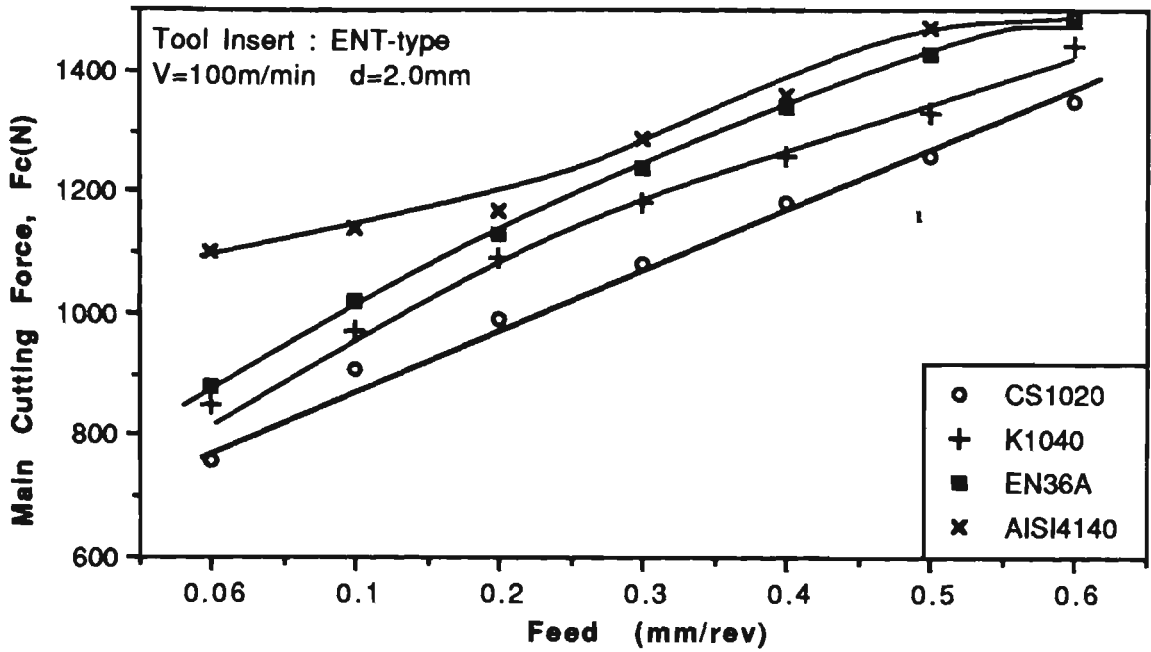


Figure 3.4 Power consumption comparison for four work materials

Parameters (X-axis)	Chip Breakability $\mu(x)$ (Y-axis)	Surface Finish $Ra(\mu m)$ (Y-axis)	Power Consumption $F_c(N)$ (Y-axis)
Cutting Speed	significant	significant	slight
Feed	very significant	significant	very significant
Depth of Cut	significant for small d	significant for very small d	very significant
Nose Radius	significant	significant	significant
Cutting Edge Angle	significant	slight	significant
Rake Angle	slight	slight	significant
Inclination Angle	nearly constant	slight	significant

Figure 3.5 Integrated effects of cutting conditions and tool geometries

3.5 EVALUATION OF WORK MATERIAL PROPERTIES

The properties of work materials have significant yet complicated effects on machining performance including chip breakability, surface finish and power consumption. In Chapter 2, the effect of work material on chip breakability has been studied sufficiently. In order to describe comprehensively the effects of work materials, a work material effect table is introduced for various classes of machining conditions, aiming at providing referable information for automated process planning systems. Shown in Table 3.3 is an example of work material EN25 when machining with a conventional groove-type tool insert (ENT type).

Table 3.3 An example of work material effect table (Tool Insert : ENT type)

The Classes of Machining Conditions		Chip Breakability	Surface Finish	Power Consumption
1	Precision Finishing	very difficult to break	good	low
2	Normal Finishing	very difficult to break	fair	moderate
3	Semi-Finishing	usually difficult to break	fair	moderate
4	Light Roughing	maybe or partly broken	acceptable	moderate
5	Normal Roughing	usually easy to break	poor	high
6	Heavy Roughing	very easy to break	very poor	very high

Furthermore, the effects of work materials on surface finish and power consumption can be quantitatively evaluated by introducing a fuzzy membership function. Table 3.4 shows the fuzzy ratings of surface finish and power consumption based on the conventional machining requirements.

Table 3.4 Fuzzy ratings of surface finish and power consumption

Assessment of Surface Finish			Assessment of Power Consumption*		
Range R_a (μm)	Fuzzy Description	Membership Value μ_s	Range F_{cutting} (N)	Fuzzy Description	Membership Value μ_p
≤ 0.6	excellent	0.85 - 1.0	≤ 300	very low	0.9 - 1.0
0.6 - 1.1	good	0.7 - 0.85	300 - 700	low	0.8 - 0.9
1.1 - 1.5	fair	0.6 - 0.7	700 - 1200	moderate	0.65 - 0.8
1.5 - 2.0	acceptable	0.5 - 0.6	1200 - 1500	high	0.50 - 0.65
2.0 - 3.0	poor	0.25 - 0.5	1500 - 2000	very high	0.3 - 0.5
> 3.0	very poor	0 - 0.25	> 2000	unacceptable	0 - 0.3

* The ratings of power consumption may change with different machine-tool structures.

In this way, the work material effect table can be formulated into a work material evaluation matrix, providing an approach to assessing the deviation of membership value due to the change of conditions. The work material evaluation matrix, W_L , is constructed with its column representing different classes of machining conditions (Table 3.3), and its row representing the fuzzy ratings of chip breakability ($\mu(x)$), surface finish (μ_s) and power consumption (μ_p) respectively, corresponding to a specific combination of one work material and one tool insert with the standard tool geometry.

$$W_L = \begin{bmatrix} \mu_1^u(x) & \mu_2^u(x) & \mu_3^u(x) & \mu_4^u(x) & \mu_5^u(x) & \mu_6^u(x) \\ \mu_{s1}^v & \mu_{s2}^v & \mu_{s3}^v & \mu_{s4}^v & \mu_{s5}^v & \mu_{s6}^v \\ \mu_{p1}^w & \mu_{p2}^w & \mu_{p3}^w & \mu_{p4}^w & \mu_{p5}^w & \mu_{p6}^w \end{bmatrix} \quad (3.2)$$

$$L = 1, 2, \dots, 63$$

The meaning of each symbol in the matrix is defined as follows :

integer L : combinations of different work materials and the tool inserts with
standard tool geometry (0° , 5° , -6° , 90° , 60° , 0.8)

subscript number 1 to 6 : six different classes of machining conditions

exponents u, v and w : exponents for determining the variations of membership
values due to the change of tool geometry.

3.6 KNOWLEDGE REPRESENTATION

3.6.1 Basic Facts Based on the Database

A database was established using the results from selected machining experiments, providing the basic facts about machining performance including chip breakability, surface finish and power consumption. The database structure developed in PROLOG is shown as follows :

```
machining_performance_data ( output (chip_breakability_membership_value,
                                     surface_finish, main_cutting_force), tool_insert_type,
                             work_material, cutting_conditions (speed, depth,
                                                                feed), tool_geometry (nose_radius, rake_angle,
                                                                inclination_angle, cutting_edge_angle) ).
```

Given below is an example for one of the facts established :

```
machining_performance_data ( output(0.7, 1.65, 1.2), ena_type_insert,
                             k1040, cutting_conditions(100, 2.0, 0.2),
                             tool_geometry(0.8,-5, -6, 90) ).
```

The fact is explained as if the tool insert type is ENA-type, work material is medium carbon steel K1040, cutting speed =100 m/min, depth of cut =2.0 mm, feed =0.2 mm/rev, tool nose radius =0.8 mm, tool rake angle = -5° , tool inclination angle = -6°

and tool cutting edge angle $=90^\circ$, then the chip breakability (membership value) $\mu(x) = 0.7$, surface finish $R_a = 1.65 \mu\text{m}$ and main cutting force $F_c = 1.2 \text{ KN}$.

3.6.2 Knowledge from Expert's Experience

The major objective of the expert system is to formalise the experience of human experts and make it scientifically useable. The rule-based approach is an effective method which uses a large storage of IF-THEN rules simulating the expert's reasoning. Given below are some examples of expert's knowledge and experience on machining operation and chip control.

(1) Example of expert's knowledge for the effect of feed on surface finish

It is well known that the lower the feed rate, the better the surface finish. However, the expert's knowledge is not limited to this. From his experience on machining, more knowledge rules can be developed as follows :

IF the cutting speed is high enough to eliminate the formation of built-up edge

THEN the surface finish will be improved with the decrease of feed rates

BUT

IF the cutting speed is not high enough

THEN within the low feed range, decreasing feed rate will give adverse results on surface finish due to the marks of BUE fragments on the machined surface.

(2) Example of expert's experience for using tool inclination angles

The appropriate use of tool inclination angle is important to the machining process.

Given below are some of the expert's strategies for using tool inclination angles:

- (a) Use positive inclination angles for fine machining so that the chip will flow towards the unmachined surface.
- (b) Use negative inclination angles for interrupted machining to protect the tool tips.
- (c) Use negative inclination angles for tempered and hardened materials to enhance the tool strength.
- (d) Use positive inclination angles when the system setup lacks rigidity and strength to reduce the possible vibration in machining.

(3) Example of knowledge rules for answering questions

Knowledge rules are summarised to response to some specific questions, such as "why unbroken", "why tooth-edged chips", "why poor surface finish" etc. The following is an example of these rules (written in Prolog).

why_unbroken (Tool, Material, Speed, Depth, Feed):-

Tool = enz, Material = en25, Speed = Speed,

Depth <= 1.5, Feed >= 0.3,

write("--Because depth of cut is too small for cutting"),nl,

write("--EN25 alloy steel when using ENZ type tool."),nl,

write("--We suggest that at least d > 1.5 mm should"),nl,

write("--be used to make the chip break efficiently.").

(4) Guidance for Selecting Efficient Cutting Conditions

The optimal selection of cutting conditions is very complicated due to numerous factors involved. The predictive expert system has the function to help users select efficient cutting conditions in terms of machining performance. For example, in some cases, the chip is broken but it is not an efficient machining due to too high cutting

force, while in the other cases, such as in finishing-machining, the chip is very difficult to break due to the small chip thickness. In order to resolve these sorts of problems, some useful knowledge rules have been developed and summarised to give a general guidance for the user to choose the most effective tool insert, tool geometry and cutting conditions to satisfy his/her specific machining requirements. Given below in Figure 3.6 is a sample for the selection of efficient feed value.

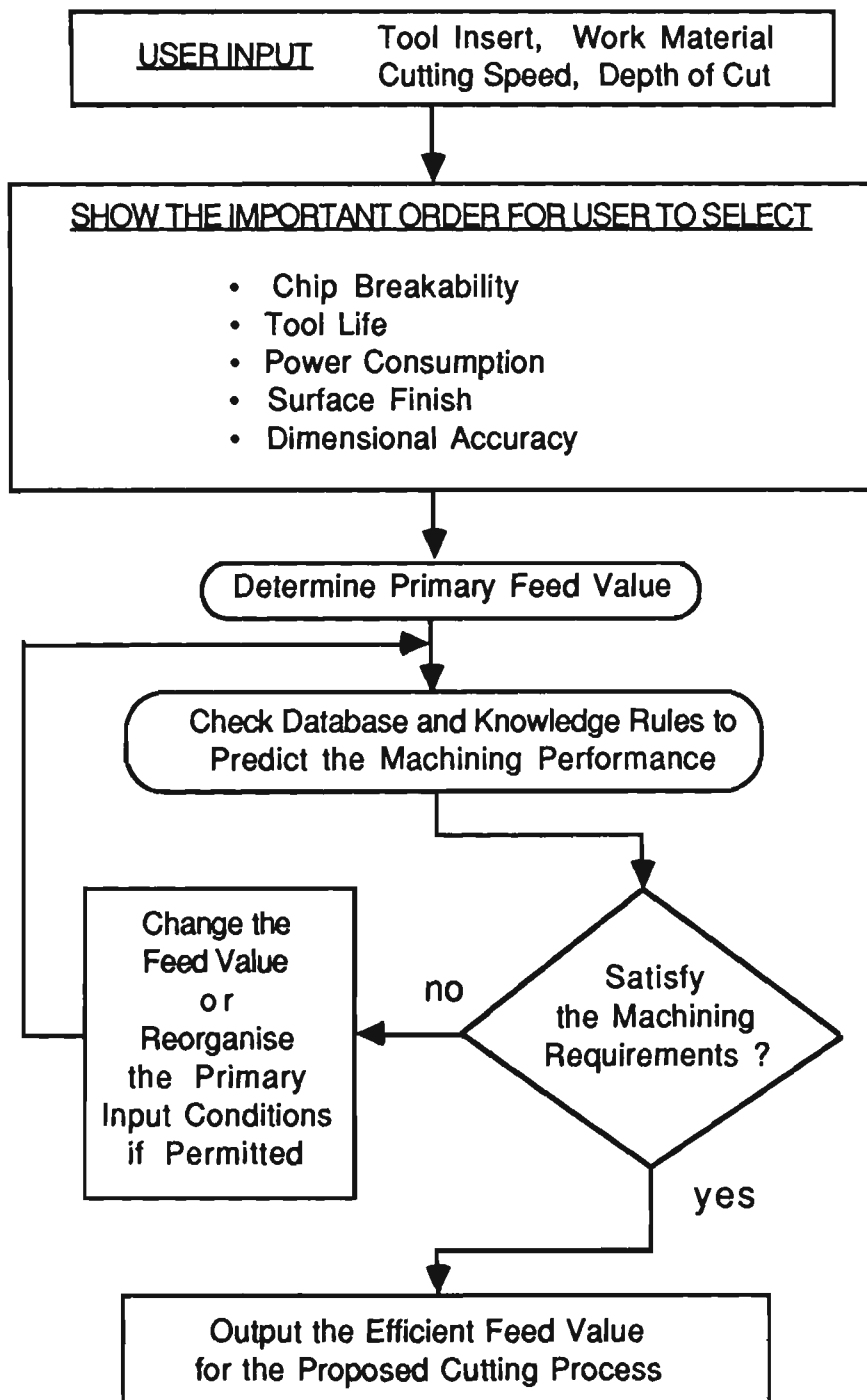


Figure 3.6 Flow chart for selecting efficient feed value

3.7 ESTABLISHMENT OF A PREDICTIVE EXPERT SYSTEM

Figure 3.7 shows a simplified schematic diagram for establishing the predictive expert system for the assessment of machining performance. The machining performance database created based on the machining experiments and the expert's knowledge and experience are combined to set up the knowledge base.

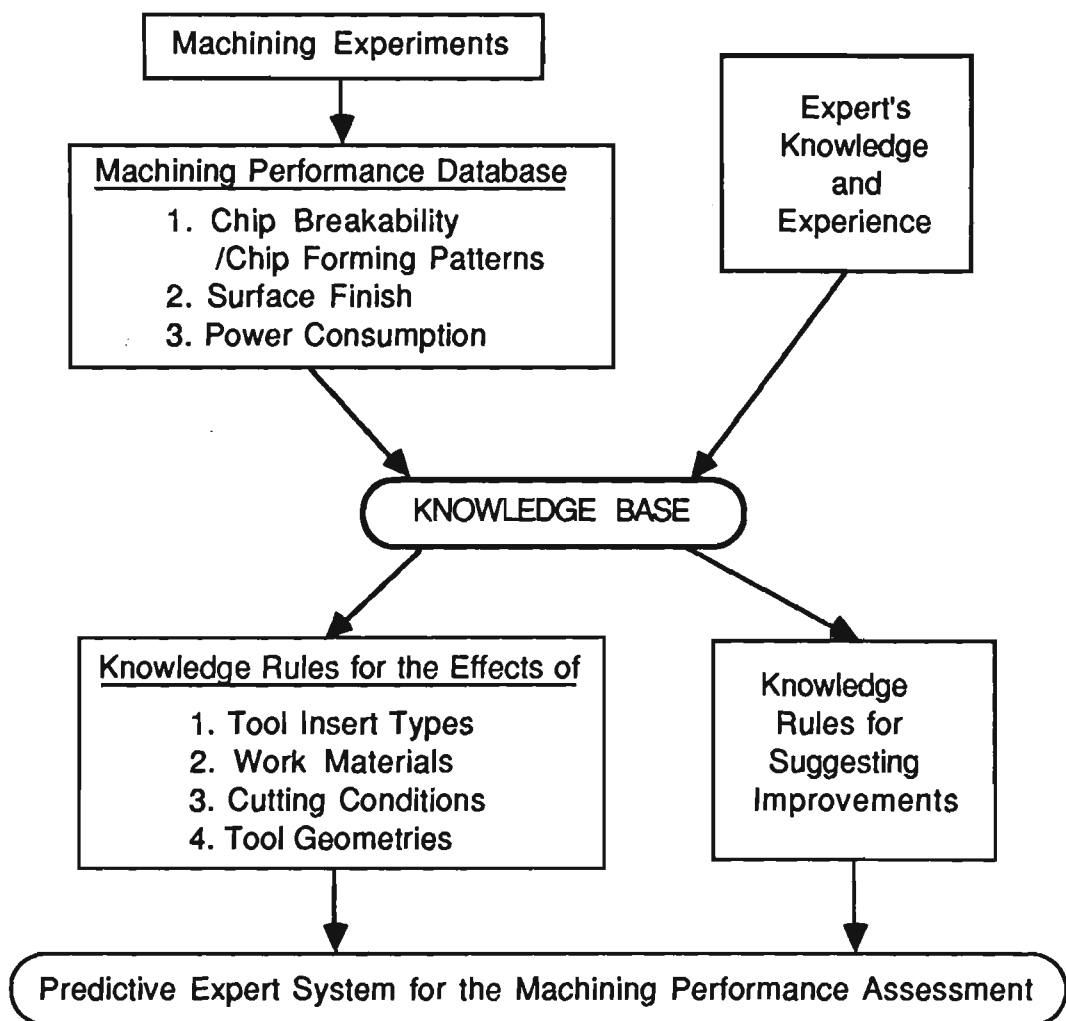


Figure 3.7 A schematic diagram for setting up the predictive expert system

The established expert system provides three major functions as shown in Figure 3.8, i.e., assessment of machining performances for user's self-selected input machining

parameters; suggestions for improvement on the initial input parameters according to the user's requirement; reply to user's questions and explain the output results. In this way, the predictive expert system provides quantitative evaluations for the automated process planning (APP) system.

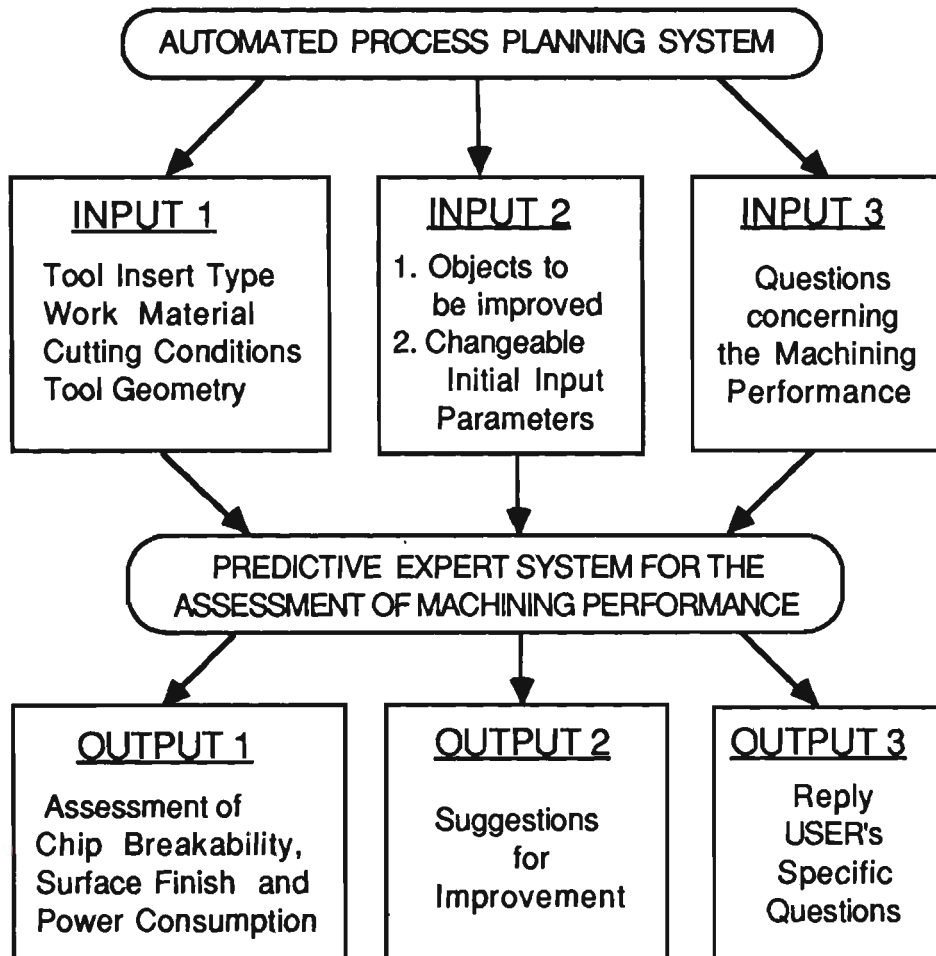


Figure 3.8 The predictive expert system acting as an auxiliary for APP system

3.8 SUMMARY AND CONCLUDING REMARKS

- (1) A new approach for evaluating machining performance (i.e. assessing chip breakability/chip forming patterns with due consideration to power consumption rates and the surface finish produced) has been presented in this chapter. The

method uses a predictive expert system which was developed by using expert's knowledge on machining operation and the results of extensive experimental work.

- (2) An interactive user-friendly program is added to this predictive system to help the user with his/her specific queries and aimed at improving machining performance. The basic guidelines presented in this chapter are designed to emphasise the need for implementing this predictive expert system in an automated process planning system.
- (3) The success of this expert system depends very heavily on the applicability range of experimental results covering all likely combinations of work materials, tool inserts, cutting conditions and tool geometries. Therefore it is essential to have "dedicated knowledge pools" to suit the individual requirements; and this can be done without significant effort using the guidelines given in this chapter.

CHAPTER 4

A KNOWLEDGE-BASED SYSTEM FOR DESIGNING EFFECTIVE GROOVED CHIP BREAKERS BASED ON THREE-DIMENSIONAL CHIP FLOW IN MACHINING

4.1. INTRODUCTION

Continuing R & D efforts on cutting tools have now produced a great number of different chip breaker configurations. However, the current practice in tool chip breaker design and application is very heavily dependent upon the arbitrary experimental work, which is primarily based on the historically known "try and see" methodology. This practice is very time-consuming and does not always produce the most desirable results in terms of the chip breakability aspect at optimum chip breaker utilisation and the associated minimum power consumption. Therefore, a more scientific and effective approach for designing tool chip breakers is highly called for, against the current practice of "try and see" methods. The need for developing a knowledge-base from a database system has been shown as essential both for designing effective chip breakers and for achieving the total chip control in automated machining [2].

The first attempt has been made to develop a knowledge-based approach to designing grooved chip breakers for providing effective chip breaking at minimum power consumption in two-dimensional chip up-curl modes in a recent work [67]. This work has now been extended to include a more common three-dimensional chip flow, i.e. combined chip sideflow and chip backflow (or chip streaming), for various work materials at a much wider range of tool geometries and cutting conditions.

It has also been shown that the basic mechanism of chip flow in a majority of commercial grooved chip breakers can be explained as resulting from the combined effects of tool restricted contact and toolface configurations, which quite often represent a groove with varying sizes and profiles [61]. Therefore, in the present work, typical grooved chip breakers (i.e. groove profiles with raised back wall, standard back wall, reduced back wall & no back wall) with various sizes and restricted contact lengths are selected to form a reference model for a primary systematic analysis, which could then be extended to more complicated toolface configurations.

4.2 PRESENT KNOWLEDGE OF CHIP CONTROL WITH GROOVED CHIP BREAKERS

4.2.1 Tool Restricted Contact Effect on Chip Breaking

The chip streaming (i.e. chip backflow) effect has been found to be playing a significant role in chip curling and subsequent chip breaking when machining with grooved chip breakers having a tool restricted contact adjacent to the grooved profile [61]. For a given set of cutting conditions, the tool restricted contact length h is the most important factor in determining the chip backflow angle η_b . Machining experiments with restricted contact tools have shown that there exist the following three basic models for chip streaming (backflow) [67], as shown in Figure 4.1.

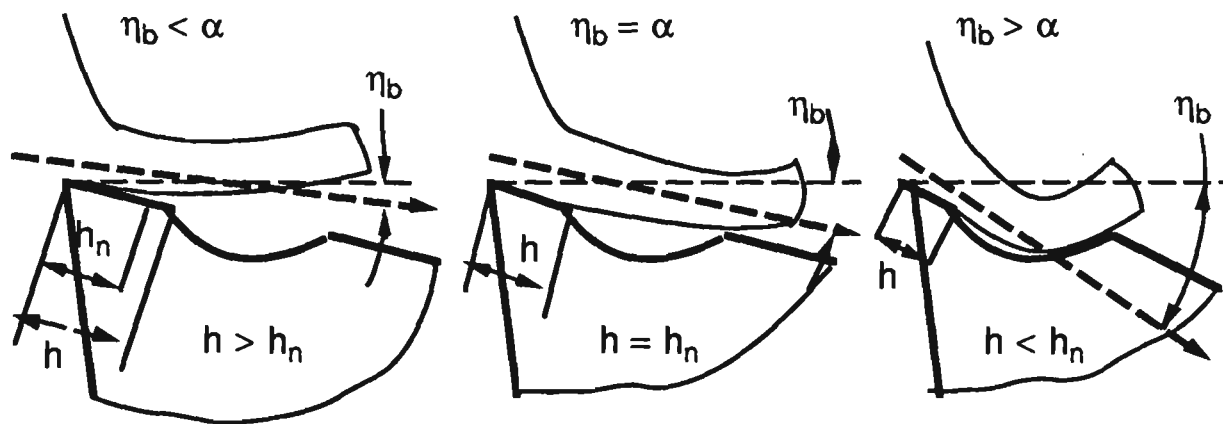


Figure 4.1 Three chip streaming models

These three chip streaming models can be summarised into the following equation :

$$\begin{aligned}
 &\eta_b < \alpha, \text{ when } h > h_n \\
 &\quad \text{(chip curls upwards before reaching the chip groove);} \\
 &\eta_b = \alpha, \text{ when } h = h_n \\
 &\quad \text{(chip straightening occurs);} \\
 &\eta_b > \alpha, \text{ when } h < h_n \\
 &\quad \text{(chip enters the chip groove as a result of chip streaming).}
 \end{aligned} \tag{4.1}$$

where h is the tool restricted contact length, h_n is the tool/chip natural contact length and α is the tool rake angle.

4.2.2 Three-dimensional Chip Flow

Many researchers have presented cutting models for predicting chip flow in machining [44-45, 68-72]. All these investigations were based on the use of flat-faced cutting tools. However, the chip flow in practical oblique machining for the grooved tools with varying tool nose radii, tool inclination angles and rake angles, is far more

complex than that for the flat-faced tools. Furthermore, the chip flow when machining with the grooved tools having various toolface configurations is even more complicated. When dealing with a grooved chip breaker with varying tool restricted contact lengths, the effect of three-dimensional chip flow can be presented by two components, chip sideflow angle η_s and chip backflow (stream) angle η_b . As shown in Figure 4.2, η_s is the angle formed by the chip side-curling projected onto the X-Y plane, while η_b is the angle formed by the chip up-curling projected onto the X-Z plane.

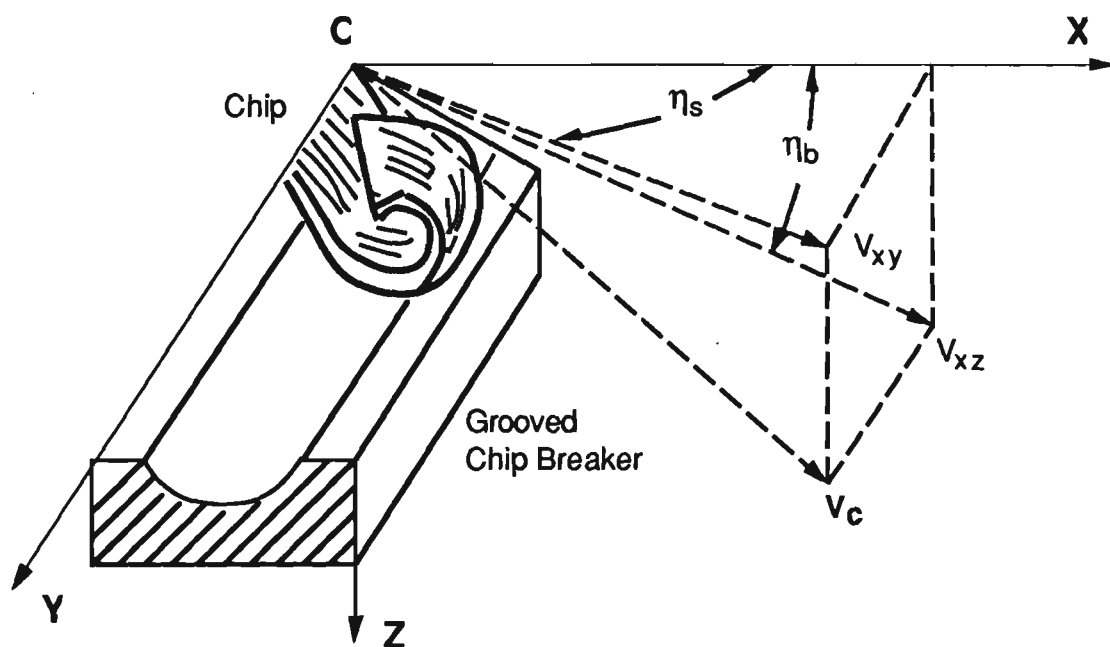


Figure 4.2 Three dimensional chip flow with a grooved chip breaker

4.2.3 Power Consumption Rate

The aim of studying power consumption rate is to provide design criteria for achieving efficient chip control at reduced power consumption. Early work has emphasised the possibility of reducing power consumption with grooved chip breakers [68, 73-76]. The tool restricted contact effect has been shown to be the most important factor for

achieving efficient chip breaking and reduced power consumption with grooved chip breakers [60, 67, 77-78].

4.3 ESTABLISHMENT OF A DATABASE SYSTEM

The basic database established in this chapter is mainly based on the previous work [59-60, 63, 67] and provides the analytical foundation for chip breaking performance, power consumption, knowledge rules and designing criteria for grooved chip breakers. The database consists of three parts : Reference Database, Grooved Chip Breaker Database and 3-D (three-dimensional) Chip Flow Database.

4.3.1 Reference Database

A series of experiments was conducted using the secondary rake type restricted contact tools as the standard tools representing a wide range of cutting speeds (4 values), undeformed chip thicknesses (3 values), tool rake angles (5 values) and tool restricted contact lengths (4 values). Medium carbon steel was used as the work material in the experiments. The chip backflow angle η_b , chip thickness t_2 and the cutting forces F_C and F_t measured from the experiments, were recorded to set up the Reference Database.

4.3.2 Grooved Chip Breaker Database

Four chip groove styles (A, B, C & D) as shown in Figure 4.3, each with three groove sizes (GT1, GT2 & GT3), were used in the experiments on establishing the effects of different groove profiles for various t_1 and h values at the cutting speed $V = 100$ m/min, rake angle $\alpha = 0^\circ$ and depth of cut $w = 3.0$ mm. The cutting forces F_C and F_t , chip breaking performance and chip shape were recorded to set up the Grooved Chip Breaker Database.

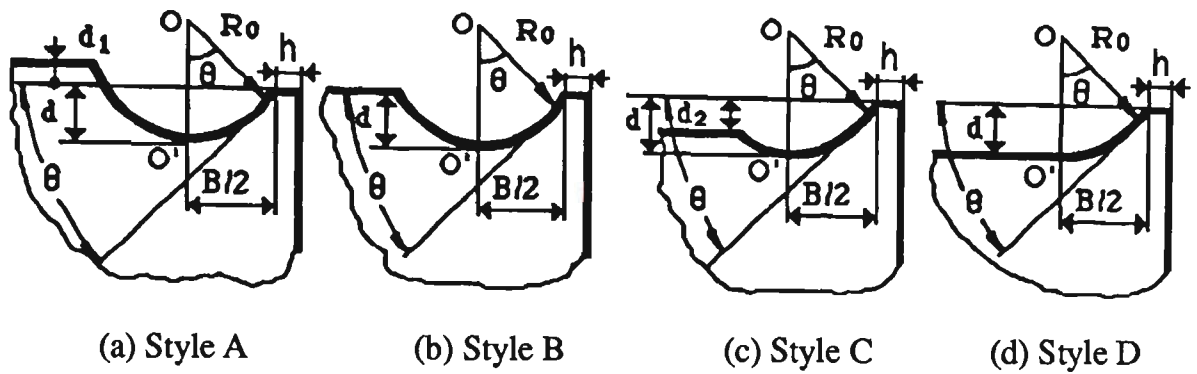


Figure 4.3 Configurations of grooved chip breakers (based on [67])

4.3.3 3-D Chip Flow Database

A series of oblique cutting experiments was conducted with standard grooved chip breakers for combinations of 3 work materials, 3 tool nose radii, 5 depths of cut and 6 feeds at a cutting speed $V = 100\text{m/min}$, tool inclination angle $i = -6^\circ$ and rake angle $\alpha = -5^\circ$. The chip sideflow angle η_s , chip backflow angle η_b and chip thickness t_2 , were measured to set up the 3-D Chip Flow Database.

A second series of experiments was conducted to establish the effects of tool inclination angle i , cutting speed V on chip sideflow angle η_s . These results are included in the 3-D chip flow database.

4.4 SUMMARY OF PRESENT KNOWLEDGE FOR SETTING UP A KNOWLEDGE BASE

An attempt was made to integrate the results derived from the databases established with the present knowledge and research findings on chip control, and then to

summarise the total knowledge into two major groups, i.e. chip breaking and power consumption.

4.4.1 Analysis of Chip Breaking

It has been found that the chip breaking is generally influenced by the combined effects of the chip backflow angle η_b , chip sideflow angle η_s , chip thickness t_2 and the chip shape produced.

4.4.1-1 Results of machining with the secondary rake restricted contact tools

A series of machining experiments with secondary rake restricted contact tools was conducted to study the individual effects of undeformed chip thickness t_1 , restricted contact length h , rake angle α and cutting speed V . The knowledge acquired was incorporated into the database for grooved chip breakers. The relationships between these parameters and the chip backflow angle η_b and chip thickness t_2 were plotted for all combinations and a representative diagram is shown in Figure 4.4 to give a general understanding of these effects.

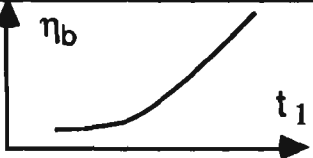

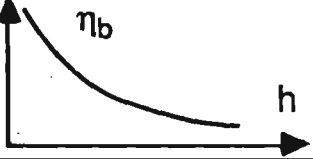

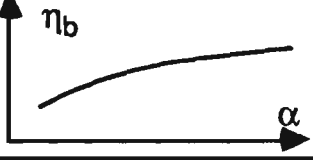

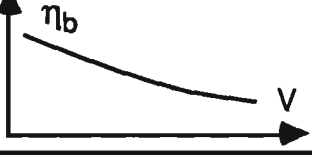
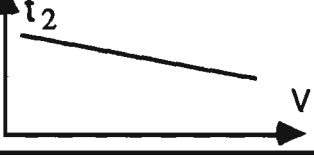
VARIABLE	EFFECT ON CHIP BACKFLOW ANGLE		EFFECT ON CHIP THICKNESS	
	RELATIONSHIP	EFFECT RATING	RELATIONSHIP	EFFECT RATING
Undeformed Chip Thickness		Significant		Significant
Restricted Contact Length		Significant		small
Tool Rake Angle		small		small
Cutting Speed		small		small

Figure 4.4 Typical relationship diagrams for restricted contact tools

4.4.1-2 Results of machining with different configurations of grooved chip breakers

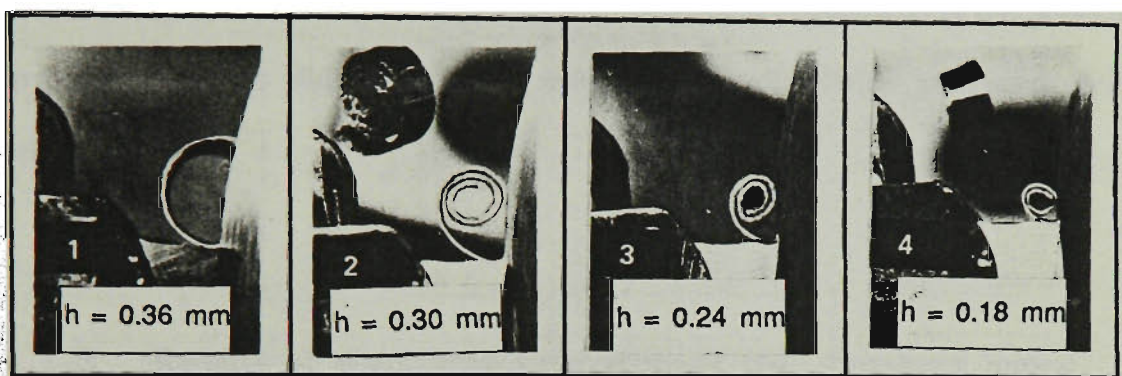
(a) Effect of restricted contact length, h

As seen from Figure 4.5, lower h values associated with higher chip backflow angles result in reduced chip up-curl radius, thus producing tighter and more efficiently broken chips.

(b) Effect of groove sizes

On the basis of the analysis of chip up-curl radius, it has been seen that the chip breaker with smaller groove size has a better chip breakability due to the smaller chip up-curl radius which facilitates the chip breaking. Figure 4.6 shows the variation of

chip up-curl radius with tool restricted contact length for the three chip-breaker groove sizes tested. It also appears that the minimum chip up-curl radius r_u equal to the tool groove radius R_o will occur when the restricted contact length h is small enough to make the chip utilise the entire tool groove.



Orthogonal Cutting : $V = 100\text{m/min}$, $t_1 = 0.2\text{mm}$, $w = 3.0\text{mm}$
 Tool Groove Size : Medium (GT2)
 Tool Groove Style : Style B (with standard back wall)
 Work Material : Medium Carbon Steel

Figure 4.5 The effect of tool restricted contact length on chip up-curl and chip breaking (based on [67])

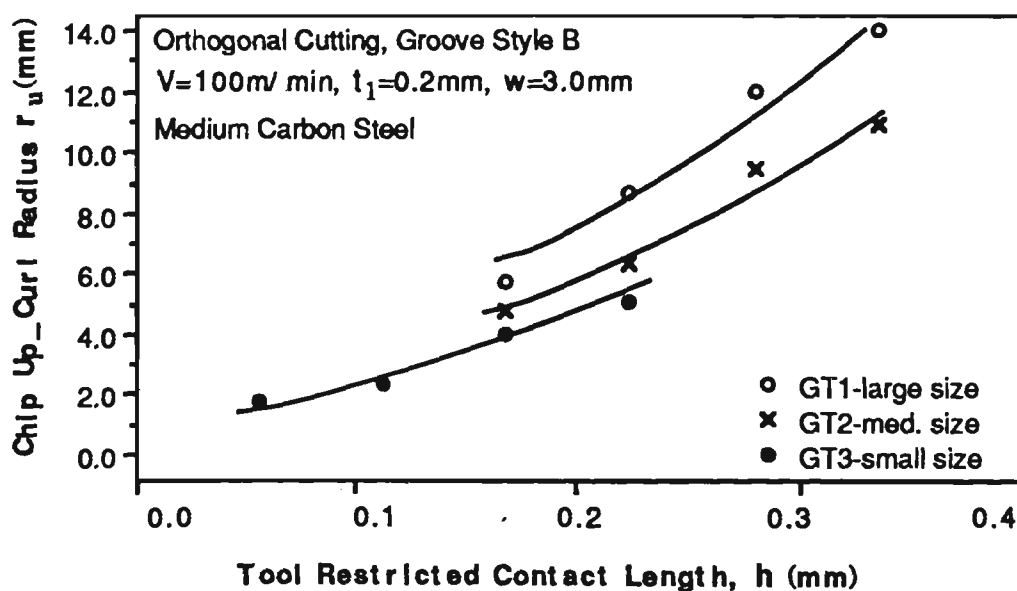


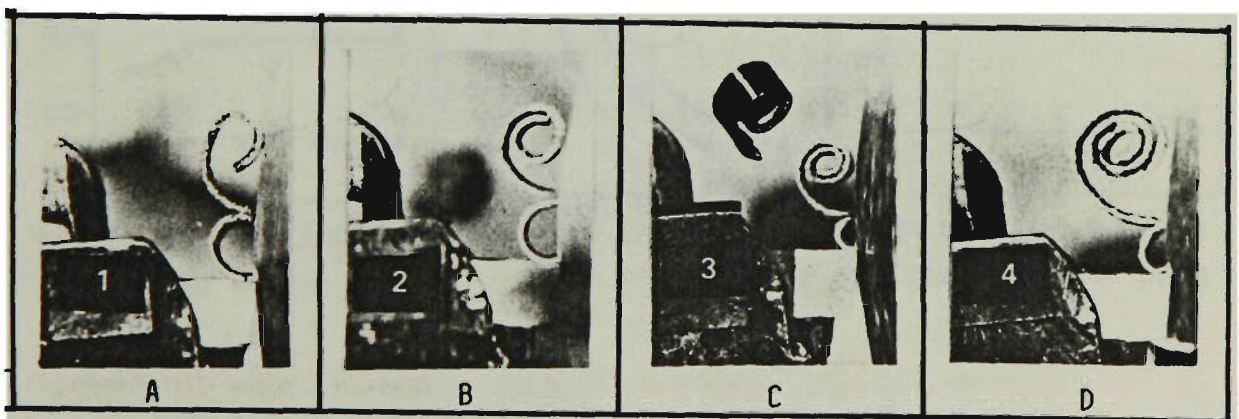
Figure 4.6 The effect of tool restricted contact length on chip up-curl radius for three chip-breaker groove sizes

(c) Effect of groove styles

A representative photograph of the chip breaking patterns with varying chip-breaker groove styles is given in Figure 4.7. The chip breaker with a raised back wall (i.e. Style A in Figure 4.3) has the best chip breakability with only one full turn chip, while, the chip breaker without backwall (i.e. Style D in Figure 4.3) is the poorest in chip breakability as shown, requiring more turns in the chips produced, before breakage occurs.

4.4.1-3 Results of machining with grooved chip breakers based on 3-D chip flow

Analytical results are derived based on the oblique machining experiments with different work materials, cutting speeds, depths of cut, feeds, tool nose radii and tool inclination angles.

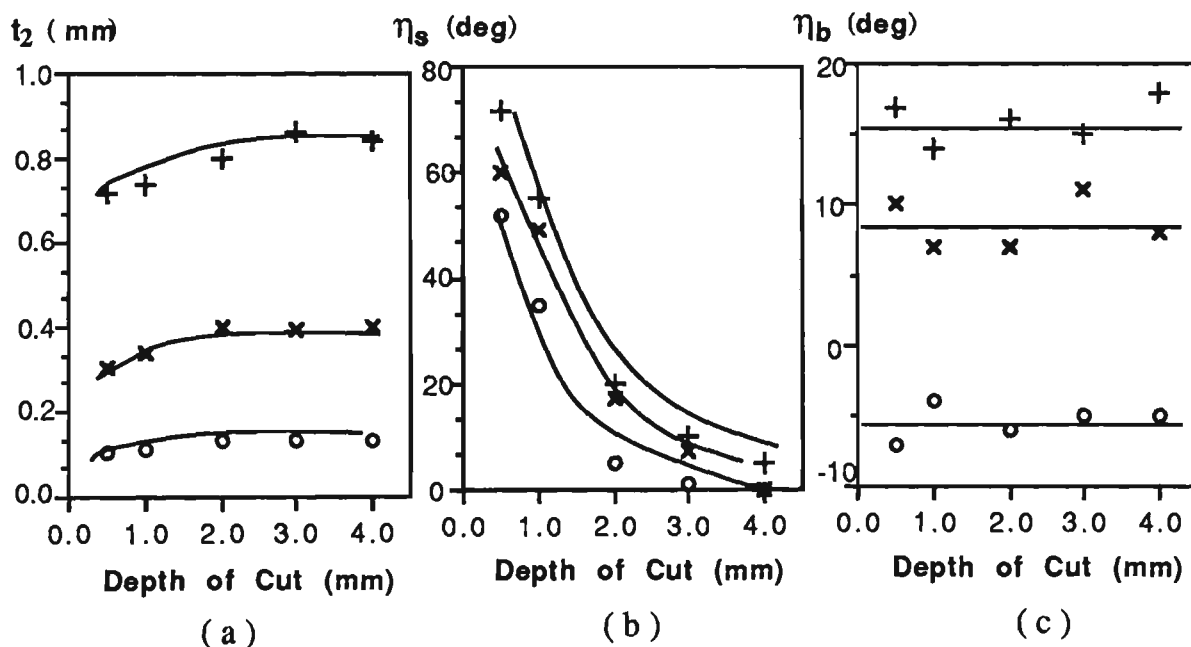


Orthogonal Cutting: $V = 100\text{m/min}$, $t_1 = 0.2\text{mm}$, $w = 3.0\text{mm}$
 Tool Groove Size : Medium (GT2), $h = 0.3\text{mm}$
 Work Material : Medium Carbon Steel

Figure 4.7 The effect of chip-breaker groove style on chip breaking (based on [67])

(a) The effects of depth of cut , d

As seen from Figure 4.8(a), an incremental in depth of cut increases the chip thickness, and thus improves the chip breakability at low depths of cut, but when depth of cut is larger than 2 mm, this effect is insignificant. Depth of cut has a greater influence on chip sideflow angle η_s . When the depth of cut is less than or around the tool nose radius, the chip sideflow angle η_s has a very large value, while at larger depths of cut, there is a very rapid decrease in η_s (see Figure 4.8(b)). Variations of depth of cut basically have no influence on chip backflow angle η_b (Figure 4.8(c)).

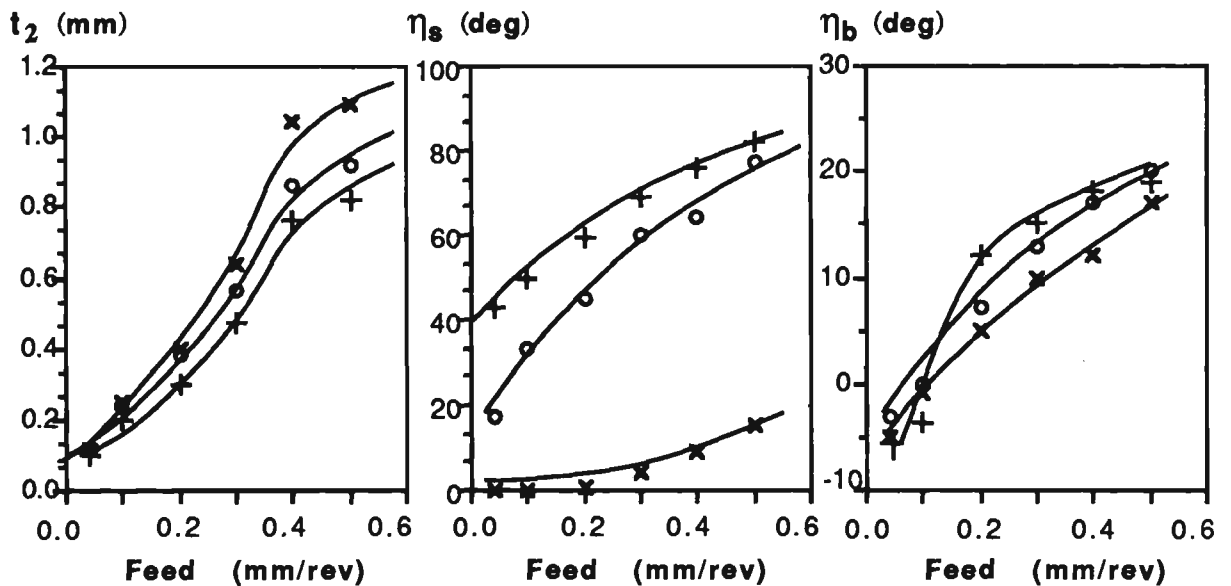


Work Material : Medium Carbon Steel o Feed (f) = 0.04 mm/rev
 Tool Nose Radius (r) = 1.2 mm x Feed (f) = 0.20 mm/rev
 Cutting Speed (V) = 100 m/min + Feed (f) = 0.40 mm/rev

Figure 4.8 The effects of depth of cut

(b) The effects of feed, f

Feed plays a significant role in the chip breaking performance. Increasing the feed increases chip sideflow angle η_s , chip backflow angle η_b and chip thickness t_2 for all cutting conditions tested (see a typical set of results in Figure 4.9).



Work Material : Medium Carbon Steel

Tool Nose Radius (r) = 0.8 mm

Cutting Speed (V) = 100 m/min

o Depth of Cut (d) = 0.5 mm

x Depth of Cut (d) = 2.0 mm

+ Depth of Cut (d) = 4.0 mm

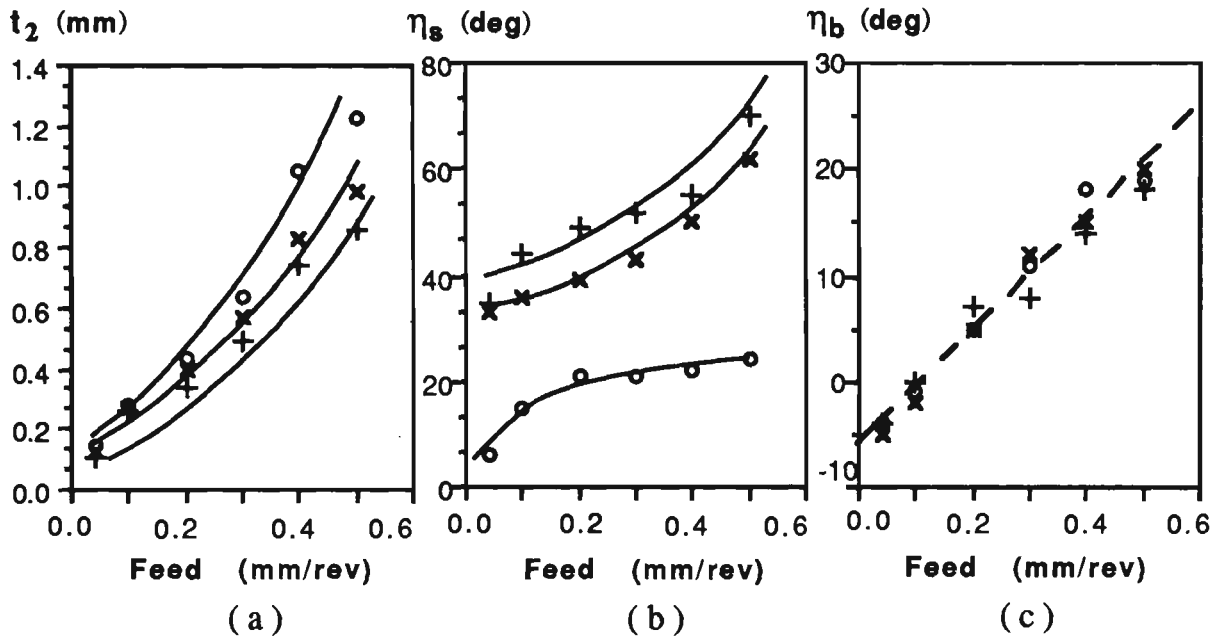
Figure 4.9 The effects of feed

(c) The effects of tool nose radius, r

The effects of tool nose radius on chip breakability is closely associated with the depth of cut which determines the effectiveness of tool nose radius, i.e., the effect of tool nose radius is reduced as the depth of cut increases.

As shown in Figure 4.10(a), the cutting tool with a sharper nose has better chip breakability due to the larger chip thickness produced. For a given depth of cut, the

influence of tool nose radius on chip sideflow angle η_s increases as the feed increases (Figure 4.10(b)). The larger the tool nose radius, the greater the chip sideflow angle η_s . The effect of tool nose radius on chip backflow angle η_b is insignificant.



Work Material : Medium Carbon Steel o Tool Nose Radius (r) = 0.4 mm
 Depth of Cut (d) = 1.0 mm x Tool Nose Radius (r) = 0.8 mm
 Cutting Speed (V) = 100 m/min + Tool Nose Radius (r) = 1.2 mm

Figure 4.10 The effects of tool nose radius

(d) The effects of tool inclination angle, i

The relationship between inclination angle i and chip sideflow angle η_s appears to be approximately linear, as shown in Figure 4.11.

(e) The effects of cutting speed, V

Chip backflow angle η_b and chip thickness t_2 have been shown that they decrease with the increase in cutting speed (see Figure 4.4). However, chip sideflow angle η_s appears to be not sensitive to variations of cutting speed V (see Figure 4.12).

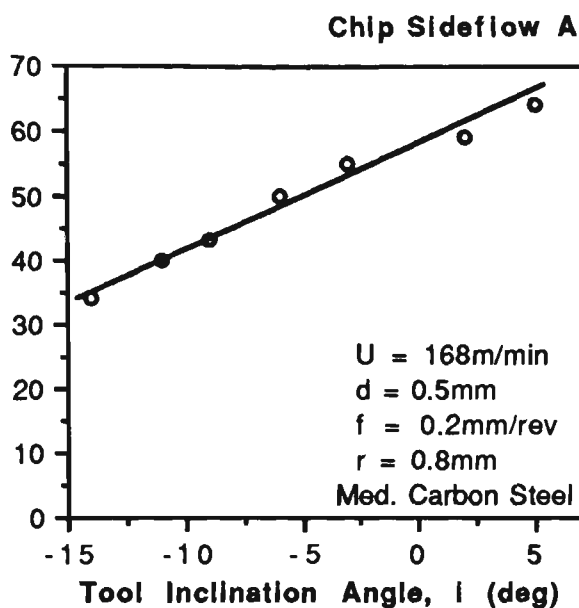


Figure 4.11 The effect of inclination angle on chip sideflow

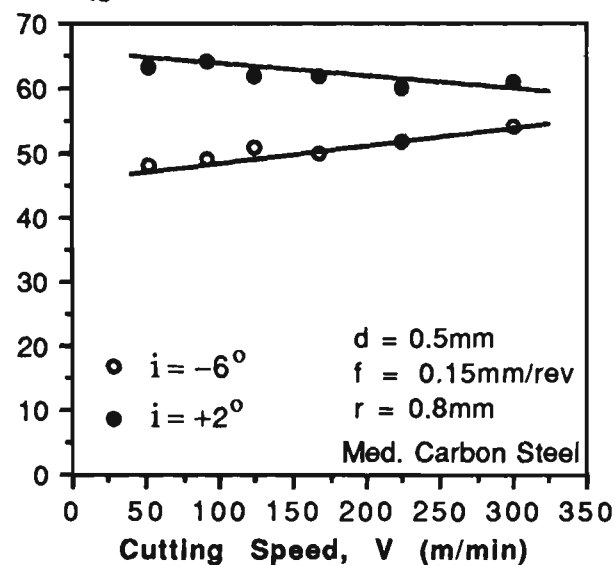


Figure 4.12 The effect of cutting speed on chip sideflow

(f) The effects of work material

In general, higher carbon steel produces thinner chips which are more difficult to break (see Figure 4.13). Chip thickness variations are significant at high feeds. However, the chip sideflow angle η_s and chip backflow angle η_b are not sensitive to variations of the work materials tested (low, medium & high carbon steels).

4.4.2 Analysis of Grooved Chip Breakers and Power Consumption Rate

For a given set of cutting conditions, the minimum power consumption for grooved chip breakers can be achieved by selecting the appropriate restricted contact length h , groove size and groove style.

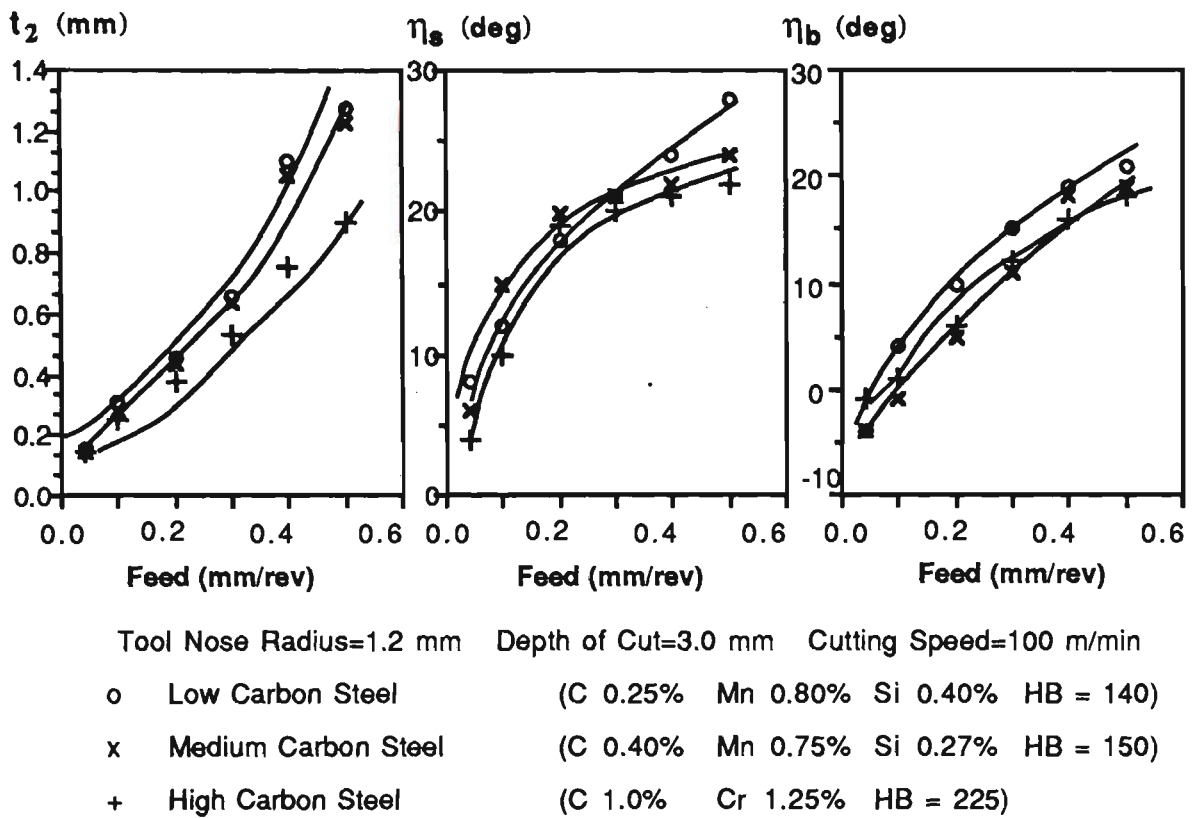


Figure 4.13 The effects of work material (carbon steels)

Machining experiments with a secondary rake restricted contact tool were conducted to study the effect of tool/chip contact length on power consumption under a fairly wide range of undeformed chip thickness t_1 , tool/chip contact length h_c , rake angle α and cutting speed V . Figure 4.14 gives a representative result. At a given t_1 value, an increase in the tool/chip contact length causes the increase in cutting force within the restricted contact region, while the cutting forces remain constant with the increase in contact length within the natural contact region. Experiments at varying cutting speeds and tool rake angles have shown this effect consistently, indicating that the reduced contact length within the restricted contact region is the key to reduced power consumption.

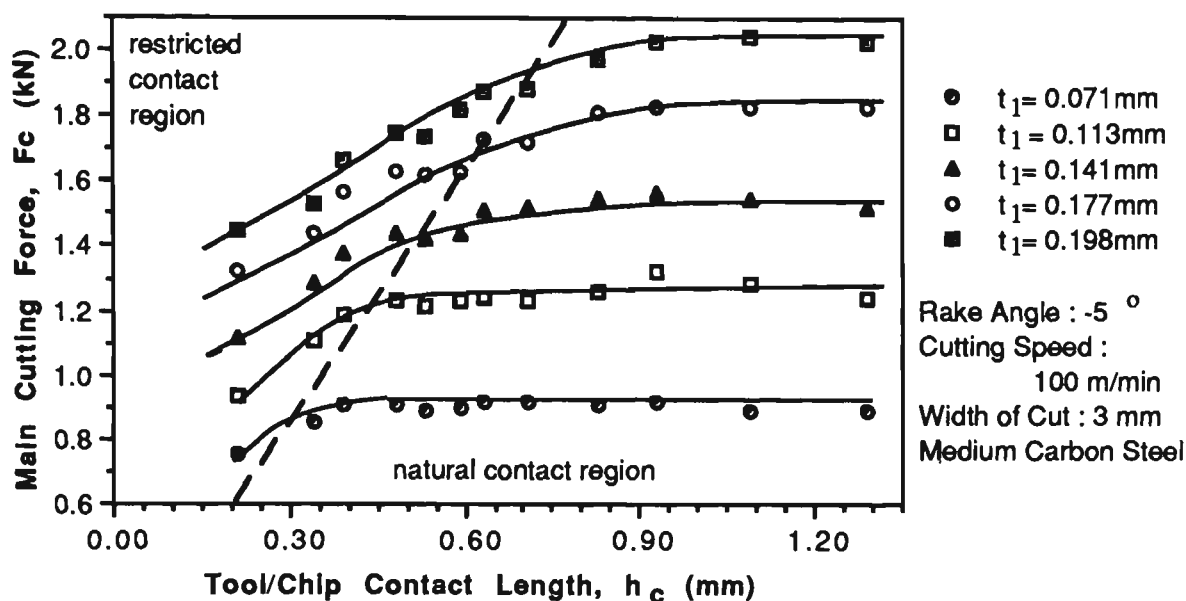


Figure 4.14 The effect of tool/chip contact length on power consumption

However, when machining with a grooved chip-breaker tool, the power consumption rate is different. As shown in Figure 4.15 for a set of typical specific cutting pressure P_s - restricted contact length h relationships, there exist minimum power regions for all three tool groove sizes, depending on the tool groove utilisation rate. The restricted contact length h is a major factor in determining tool groove utilisation due to its significant effect on chip backflow angle η_b . For all three tool groove sizes, the differences in power consumption among all the groove styles (A, B, C and D) are very explicit and this effect can be explained in terms of the geometry of the grooves and the corresponding utilisation of these grooves by the chip.

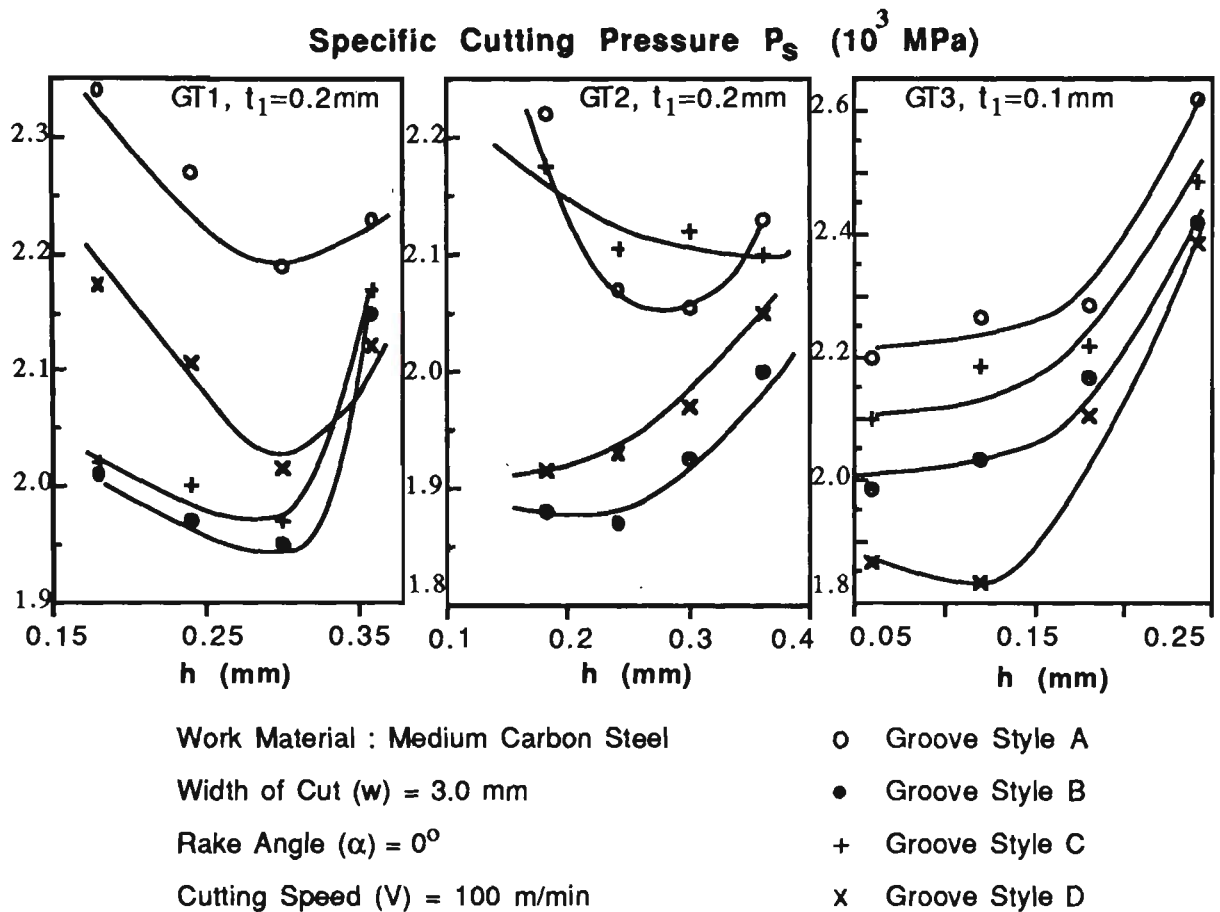


Figure 4. 15 The effect of tool restricted contact length on specific cutting pressure in machining with grooved chip breakers

4.5 ANALYSIS OF 3-D CHIP FLOW AND CHIP CURLING WITH GROOVED CHIP BREAKERS

4.5.1 Effect of the Chip Backflow Angle, η_b

Chip backflow angle η_b plays a key role in tool groove utilisation, which determines the chip breakability and power consumption rates. Figure 4.16 shows a typical chip curling pattern in the case of a grooved chip breaker with restricted contact length (i.e. $h < h_n$). It is apparent from the figure that the smaller the chip curl radius r_u , the greater is the tool groove utilisation. The chip may fully utilise the groove profile when the chip curl radius r_u is equal to the groove radius R_0 ,

$$r_u = r_{u\min} = R_0 = B/(2\sin\theta) \quad (4.2)$$

where θ is the groove tangent angle which has a very close relationship with the chip backflow angle η_b . From the relationships shown in Figure 4.16, it can be derived that if $(\eta_b - \alpha) < \theta$, the chip can not fully utilise the tool groove profile; while if $(\eta_b - \alpha) > \theta$, the chip will "overuse" the groove profile, which would unnecessarily consume more power due to the increased friction between the chip and the tool groove surface. However, in designing, the ratio $(\eta_b - \alpha)/\theta = 1.2$ may be taken as a reasonable basis to guarantee the best utilisation of the tool groove profile.

It has been shown that the chip up-curl radius (r_u) varies within a chip breaking cycle from the use of high speed filming techniques for the actual chip breaking process [79]. This variation results in the variation of tool groove utilisation. Therefore the term "full utilisation of the groove" has to be interpreted as the "maximum possible utilisation of the chip breaker groove".

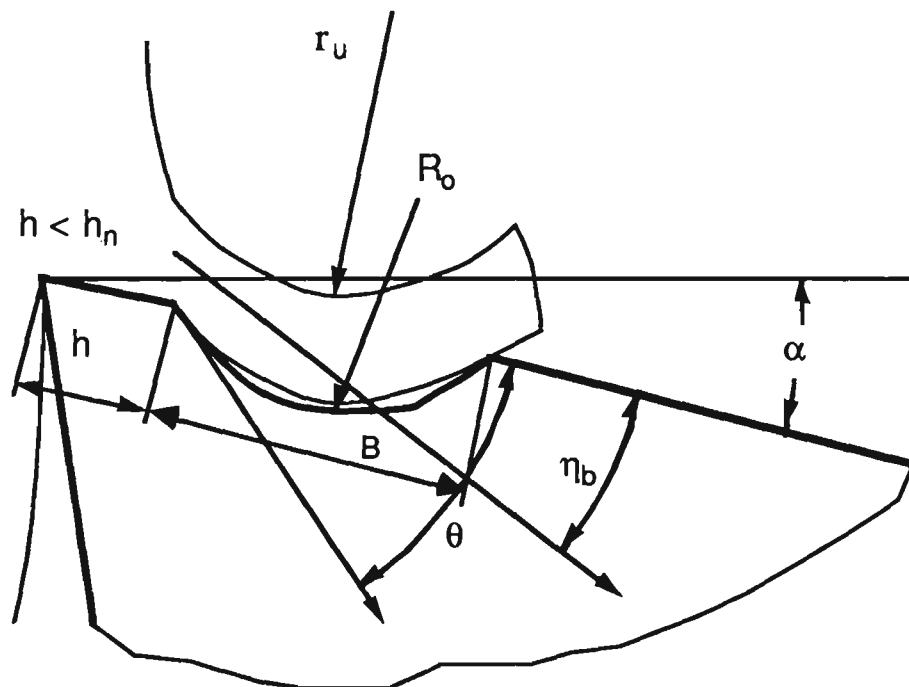


Figure 4.16 The chip backflow effect on tool groove utilisation

4.5.2 Effect of the Chip Sideflow Angle η_s

In three-dimensional oblique cutting, the effectiveness of grooved chip breakers is reduced due to the associated chip sideflow angle η_s . As shown in Figure 4.17, when chip sideflow angle η_s is not equal to zero, the equivalent tool restricted contact length h_e and the equivalent groove width B_e become larger, i.e.,

$$\begin{aligned} h_e &= h/\cos\eta_s \\ B_e &= B/\cos\eta_s \end{aligned} \quad (4.3)$$

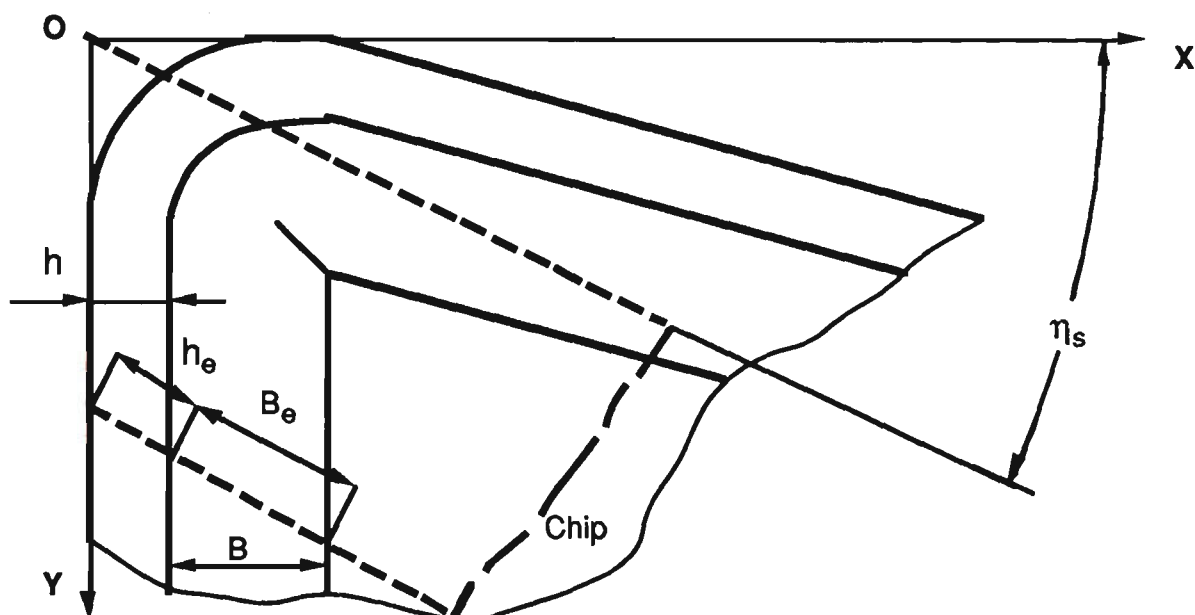


Figure 4.17 The chip sideflow effect on the effective tool groove parameters

The groove profile will be of no use if the equivalent restricted contact length h_e is larger than the tool natural contact length h_n , and when η_s is larger than, say, 75 degrees, h_e and B_e will go up rapidly with a small increase in η_s . In this case, the

direction of chip sideflow will be nearly parallel to the cutting edge, therefore a standard grooved chip breaker is no longer useable for chip curling.

4.6. THE ESTABLISHMENT OF A KNOWLEDGE BASE

The knowledge base is used for predicting the tool/chip natural contact length h_n , chip sideflow angle η_s , chip backflow angle η_b and for selecting the groove parameters for effective chip breaking and minimum power consumption.

4.6.1 Knowledge Rules for Predicting the Natural Contact Length h_n

The groove effect of a restricted contact tool is operational only when the tool contact length h is smaller than the natural tool/chip contact length h_n , for a given set of cutting conditions. The h_n value can be determined by the experimental η_b - h relationship diagram for orthogonal cutting conditions or η_b - h_e relationship diagram for oblique cutting conditions. Figure 4.18 shows a typical diagram that can be used for determining h_n .

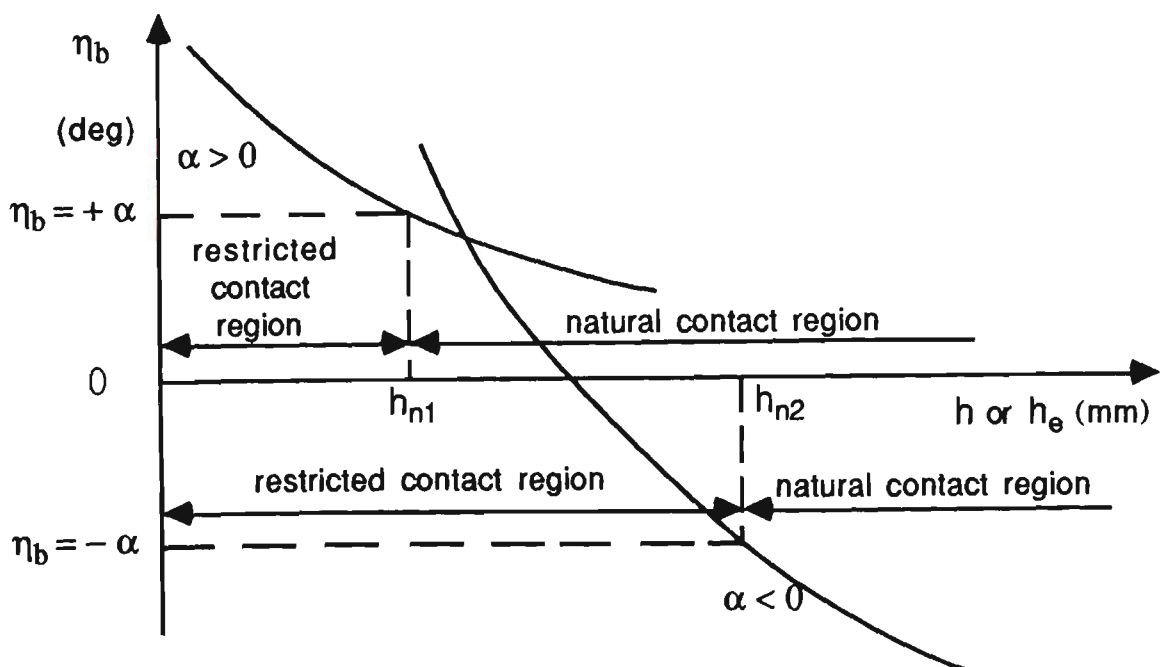


Figure 4.18 Determination of tool/chip natural contact length h_n

On the basis of 3-D Chip Flow Database, h_n values can be estimated directly for the combinations of 3 work materials, 3 tool nose radii, 5 depths of cut and 6 feeds with cutting speed $V = 100\text{m/min}$ and tool rake angle $\alpha = -5^\circ$. The effects of V and α can be derived by knowledge rules based upon the Reference Database.

(a) Rules for the effect of V

The h_n value increases with the increase in cutting speed V for all the cutting conditions tested. Given below is a representative rule for the effect of V on h_n with $V = 100\text{ m/min}$ as the standard value for comparison.

IF $150 < V \leq 180\text{ m/min}$

THEN the natural tool/chip contact length h_n will have a
 15% increase ($\Delta h_{nV} = +15\%$) at low feeds ($f \leq 0.15\text{mm/rev}$) or
 18% increase ($\Delta h_{nV} = +18\%$) at medium feeds ($0.15 < f < 0.3\text{mm/rev}$) or
 22% increase ($\Delta h_{nV} = +22\%$) at high feeds ($f \geq 0.3\text{mm/rev}$).

(b) Rules for the effect of α

The effect of α on h_n is very little. In general, the h_n value will have a slight decrease with the increase in α . An example of the rules for the effect of α on h_n is given below with $\alpha = -5^\circ$ as the standard value for comparison.

IF $0 < \alpha < 5^\circ$

THEN the natural tool/chip contact length will have a
 9% decrease ($\Delta h_{n\alpha} = -9\%$) at low feeds ($f \leq 0.15\text{mm/rev}$) or
 7% decrease ($\Delta h_{n\alpha} = -7\%$) at medium feeds ($0.15 < f < 0.3\text{mm/rev}$) or
 5% decrease ($\Delta h_{n\alpha} = -5\%$) at high feeds ($f \geq 0.3\text{mm/rev}$).

4.6.2 Knowledge Rules for Predicting the Chip Backflow Angle η_b

The restricted contact length h , tool rake angle α , feed f (or undeformed chip thickness t_1) and cutting speed V have significant influence on chip backflow angle η_b .

(a) Rules for the effect of h :

The chip backflow angle η_b is sensitive to small variations of h values. Knowledge rules have been derived to predict η_b for all possible h values under various cutting conditions based on the Reference Database. The standard h value is different at different machining conditions. One of these rules is shown below.

IF $0.15 < h < 0.19$ mm, $\alpha = 0^\circ$, $V = 100$ m/min

THEN Chip backflow angle η_b will have a

40% increase ($\Delta\eta_{bh} = +40\%$) at low feeds ($f \leq 0.15$ mm/rev) or

38% increase ($\Delta\eta_{bh} = +38\%$) at medium feeds ($0.15 < f < 0.3$ mm/rev) or

28% increase ($\Delta\eta_{bh} = +28\%$) at high feeds ($f \geq 0.3$ mm/rev)

comparing with that at the standard value $h = 0.226$ mm.

(b) Rules for the effect of α :

Knowledge rules for the effect of rake angle α on chip backflow angle η_b are summarised based on the comparison with the standard rake angle value, $\alpha = 0$ degree, at different machining conditions. Given below is an example.

IF $8^\circ < \alpha \leq 10^\circ$, $f \leq 0.15$ mm/rev, $h < h_n$

THEN Chip backflow angle η_b will have a

3% increase ($\Delta\eta_{b\alpha} = +3\%$) at low cutting speeds ($V \leq 100\text{m/min}$) or
 8% increase ($\Delta\eta_{b\alpha} = +8\%$) at med. cutting speeds ($100 < V \leq 200\text{m/min}$) or
 12% increase ($\Delta\eta_{b\alpha} = +12\%$) at high cutting speeds ($200 < V \leq 300\text{m/min}$) or
 18% increase ($\Delta\eta_{b\alpha} = +18\%$) at very high cutting speeds ($V > 300\text{m/min}$).

(c) Rules for the effect of cutting speed V

Taking cutting speed $V = 100\text{m/min}$ as the standard value for comparison, knowledge rules for the effect of V on η_b are developed. A representative rule is shown as follows :

IF $200 < V \leq 250\text{m/min}$, $f \leq 0.15\text{mm/rev}$, $h < h_n$

THEN Chip backflow angle η_b will have a

10% decrease ($\Delta\eta_{bV} = -10\%$)	at	$\alpha \geq 10^\circ$	or
14% decrease ($\Delta\eta_{bV} = -14\%$)	at	$5^\circ \leq \alpha < 10^\circ$	or
16% decrease ($\Delta\eta_{bV} = -16\%$)	at	$2^\circ \leq \alpha < 5^\circ$	or
20% decrease ($\Delta\eta_{bV} = -20\%$)	at	$-2^\circ \leq \alpha < 2^\circ$	or
32% decrease ($\Delta\eta_{bV} = -32\%$)	at	$-5^\circ \leq \alpha < -2^\circ$	or
50% decrease ($\Delta\eta_{bV} = -50\%$)	at	$-8^\circ \leq \alpha < -5^\circ$	or
58% decrease ($\Delta\eta_{bV} = -58\%$)	at	$-15^\circ \leq \alpha < -8^\circ$	or
65% decrease ($\Delta\eta_{bV} = -65\%$)	at	$\alpha \leq -15^\circ$.	

(d) Rules for the effect of feed f

The feed rate has a significant effect on chip backflow angle η_b . Six feed values (0.04, 0.1, 0.2, 0.3, 0.4, 0.5 mm/rev) are selected as the standard values in the established 3-D Chip Flow Database. A typical rule for the effect of feed on η_b is as follows :

IF Work material is low carbon steel and
 Tool nose radius is $r = 0.8\text{mm}$ and
 Depth of cut is $1.0 < d < 2.0$ and
 While feed value is $0.2 < f \leq 0.25\text{mm/rev}$

THEN Chip backflow angle will have a 30% increase ($\Delta\eta_{bf} = +30\%$)
 comparing with that at the standard feed value $f = 0.2\text{mm/rev}$
 in the 3-D Chip Flow Database.

4.6.3 Knowledge Rules for Predicting the Chip Sideflow Angle η_s

The tool nose radius r , tool inclination angle i , depth of cut d and feed f are the major factors influencing the chip sideflow angle η_s in oblique machining.

(a) Rules for the effect of tool nose radius r

The tool nose radius r plays a significant role in determining chip sideflow angle η_s . Given below is a sample of such rules for its effect on η_s .

IF Work material is high carbon steel and
 Feed is $0.3 < f \leq 0.4\text{mm/rev}$ and
 Depth of cut is $d \leq 0.5\text{mm}$ and
 While tool nose radius is $1.4 \leq r < 1.6\text{mm}$

THEN Chip sideflow angle η_s will have a 25% increase ($\Delta\eta_{sr} = +25\%$)
 comparing with that at the standard tool nose radius value $r = 1.2\text{mm}$
 in the 3-D Chip Flow Database.

(b) Rules for the effect of tool inclination angle i

In formulating the knowledge rules for the effect of inclination angle, $i = 0^\circ$ is taken as the standard value for comparison, an example of such rules is shown as follows :

IF Work material is medium carbon steel and $i = i_1 > 0^\circ$
 THEN Chip sideflow angle η_s will have an increment $\eta_{si} = 1.15i_1$.

(c) Rules for the effect of depth of cut d

The depth of cut has the most significant influence on chip sideflow angle η_s . Five depth of cut values (0.5, 1.0, 2.0, 3.0, 4.0 mm) are selected as the standard values. One of the knowledge rules for depth of cut is given below :

IF Work material is medium carbon steel and
 Feed is $0.1 < f < 0.2\text{mm/rev}$ and
 Tool nose radius is $r = 1.2\text{mm}$ and
 While depth of cut is $1.2 < d \leq 1.5\text{mm}$

THEN Chip sideflow angle η_s will have a 22% decrease ($\Delta\eta_{sd} = -22\%$)
 comparing with that at the standard value $d = 1.0\text{mm}$ in the 3-D
 Chip Flow Database.

(d) Rules for the effect of feed f

Knowledge rules for the effect of feed f on chip sideflow angle η_s are derived based on the selected six standard feed values. Given below is an example of the rules used:

IF Work material is low carbon steel and
 Tool nose radius is $r = 0.4\text{mm}$ and
 Depth of cut is $0.8 \leq d < 1.2\text{mm}$ and
 While feed is $0.35 < f < 0.4\text{mm/rev}$

THEN Chip sideflow angle η_s will have an 18% decrease ($\Delta\eta_{sf} = -18\%$)
 comparing with that at the standard value $f = 0.4\text{mm/rev}$ in the 3-D Chip
 Flow Database.

4.6.4 Knowledge Rules for Determining the Minimum Power Consumption

(a) Rules for setting up the restricted contact length - power consumption relationship

In the experiments for setting up the Grooved Chip Breaker Database, six standard h values (0.36, 0.30, 0.24, 0.18, 0.12 & 0.06 mm) were used at $V = 100 \text{ m/min}$, $\alpha = 0^\circ$. The effect of different h values on power consumption under various cutting conditions can be summarised into knowledge rules on the basis of the Reference Database. One example of such rules is given below.

IF $0.3 < h < 0.33 \text{ mm}$ at high feed value ($f \geq 0.3 \text{ mm/rev}$)

THEN power consumption will have a 3% increase ($\Delta P_h = +3\%$) comparing with
 that at standard value $h = 0.3\text{mm}$ in the Grooved Chip Breaker Database.

(b) Rules for determining the h values for minimum power consumption

The restricted contact length h is the most important parameter for grooved chip breakers. Generally speaking, the smaller the h value, the lower the power

consumption. However, a too small h value may give rise to an adverse effect. The reason for this is that a decrease in h may cause an increase in η_b and if the η_b value is excessive it will consume more power. Based upon the established Grooved Chip Breaker Database, the rules for determining h values for minimum power consumption are summarised. Given below is one of the samples.

IF tool groove size is large (GT1) and groove style is A
 THEN power consumption is minimum for
 $h = 0.30 \text{ mm}$ at medium feeds ($0.15 < f < 0.3 \text{ mm/rev}$) or
 $h = 0.36 \text{ mm}$ at high feeds ($f \geq 0.3 \text{ mm/rev}$).

4.6.5 Knowledge Rules for Selecting the Effective Groove Profile

(a) Rules for the selection of tool groove sizes (GT1, GT2 & GT3)

- (i) IF feed value is low (i.e. $f \leq 0.15 \text{ mm/rev}$)
 THEN small groove size (GT3) must be selected with $h = 0.5h_n$.
- (ii) IF feed value is medium (i.e. $0.15 < f < 0.3 \text{ mm/rev}$)
 THEN medium groove size (GT2) is selected with $h = 0.6h_n$ or
 small groove size (GT3) is selected with $h = 0.7h_n$.
- (iii) IF feed value is high (i.e. $f \geq 0.3 \text{ mm}$)
 THEN large groove size (GT1) is selected with $h = 0.7h_n$ or
 medium groove size (GT2) is selected with $h = 0.8h_n$.

(b) Rules for the selection of tool groove styles (A, B, C & D)

- (i) IF all the cutting conditions are same
 THEN the chip breakability is in decreasing order for tool groove styles

(from A to D) for any given tool groove size.

- (ii) IF feed value is low ($f \leq 0.15\text{mm/rev}$), the chip breaking is usually a problem.
THEN the preferential selection of tool groove styles is from A to D.
- (iii) IF feed value is high ($f \geq 0.3\text{mm/rev}$), the chip breaking is usually not a problem.
THEN the tool groove style with minimum power consumption is preferred.
- (iv) IF feed value is medium ($0.15 < f < 0.3\text{mm/rev}$), the integrated effects of chip breakability and power consumption should be considered.
THEN when the difference in power consumption is less than 25%, the tool groove style with better chip breakability is preferred.

4.7 A STRATEGY FOR DESIGNING EFFECTIVE GROOVED CHIP BREAKERS

The design of an effective grooved chip breaker greatly depends on the optimum groove utilisation, i.e. effective chip breaking and minimum power consumption.

4.7.1 Determining the Optimum Restricted Contact Length h

As discussed before, an appropriate selection of h value is very important. A very small h value will weaken the strength of the tool cutting edge, furthermore, it might consume more power when machining with the specific grooved chip breakers, mainly due to the excessive chip backflow angle η_b . Figure 4.19(a) shows a typical $\eta_b - h$ relationship from the experiments, when $h < h_n$, the chip will flow towards

the groove with an effective chip backflow angle η_{be} and h_η is the assumed h value from the point of view of effective chip breaking. Figure 4.19(b) shows another typical $P_s - h$ relationship from the experiments, where there exists a specific h value (h_p) at which the power consumption reaches its minimum value. In the region where $h > h_p$, the power consumption reduces with the decrease in h , while in the region for $h < h_p$, the effect is opposite. The curve in this region is not as steep as that in the region for $h > h_p$. Therefore, the optimum h value is determined by the following relationship (h_η and h_p are determined by the associated rules),

$$h = \{ \min(h_\eta , h_p) \} \cos \eta_s \quad (4.4)$$

where the chip sideflow angle η_s is predicted based on the 3-D Chip Flow Database and the associated knowledge rules. If we assume $\eta_{s\ std}$ is the standard chip sideflow angle in the 3-D Chip Flow Database, η_s can be determined by the following equation,

$$\eta_s = \eta_{si} + (1 + \Delta\eta_{sr}) (1 + \Delta\eta_{sd}) (1 + \Delta\eta_{sf}) \eta_{s\ std} \quad (4.5)$$

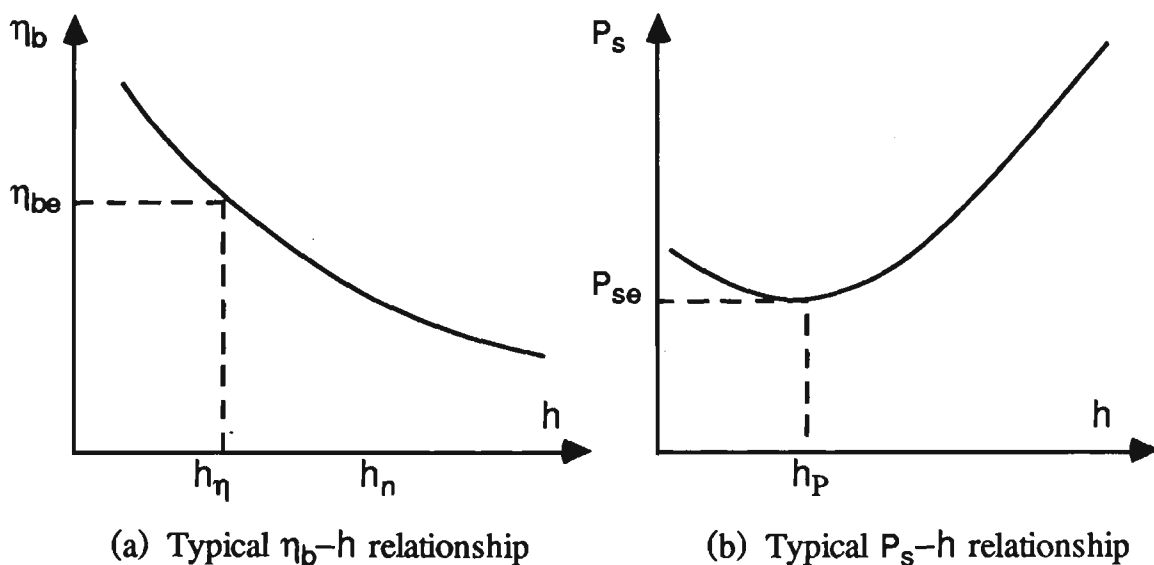


Figure 4.19 Determining the optimum restricted contact length

4.7.2 Determining the Effective Groove Parameters

From the selected restricted contact lengths h associated with the input cutting conditions, the chip backflow angle η_b can be predicted using the knowledge rules and the established 3-D Chip Flow Database. If $\eta_{b\text{ std}}$ is assumed to be the standard chip backflow angle in the 3-D Chip Flow Database, the predicted chip backflow angle is determined as follows :

$$\eta_b = (1 + \Delta\eta_{bh})(1 + \Delta\eta_{bv})(1 + \Delta\eta_{b\alpha})(1 + \Delta\eta_{bf})\eta_{b\text{ std}} \quad (4.6)$$

On the basis of this predicted chip backflow angle η_b , the groove parameters (refer to Figure 4.3) are calculated by the following set of equations :

Groove Tangent Angle (θ) :

$$\theta = (\eta_b - \alpha)/1.2 \quad (4.7)$$

Groove Width (B) :

$$B = \begin{cases} 2.0 \text{ mm,} & \text{for large groove size (GT1)} \\ 1.5 \text{ mm,} & \text{for medium groove size (GT2)} \\ 1.0 \text{ mm,} & \text{for small groove size (GT3)} \end{cases} \quad (4.8)$$

Groove Radius (R_o) :

$$R_o = B / 2\sin\theta \quad (4.9)$$

Groove Depth (d) :

$$d = R_0 - \left[R_0^2 - (B/2)^2 \right]^{1/2} \quad (4.10)$$

Raised Height of Groove Back Wall (d₁) :

$$d_1 = 0.5d \quad (4.11)$$

Reduced Height of Groove Back Wall (d₂) :

$$d_2 = 0.3d \quad (4.12)$$

4.7.3 Schematic Diagram for Designing Effective Grooved Chip Breakers

On the basis of the established knowledge-based system for designing effective grooved chip breakers, a schematic diagram for determining the most effective tool restricted contact length h as well as the groove parameters has been prepared and is shown in Figure 4.20. This system has been developed by using Turbo PROLOG language.

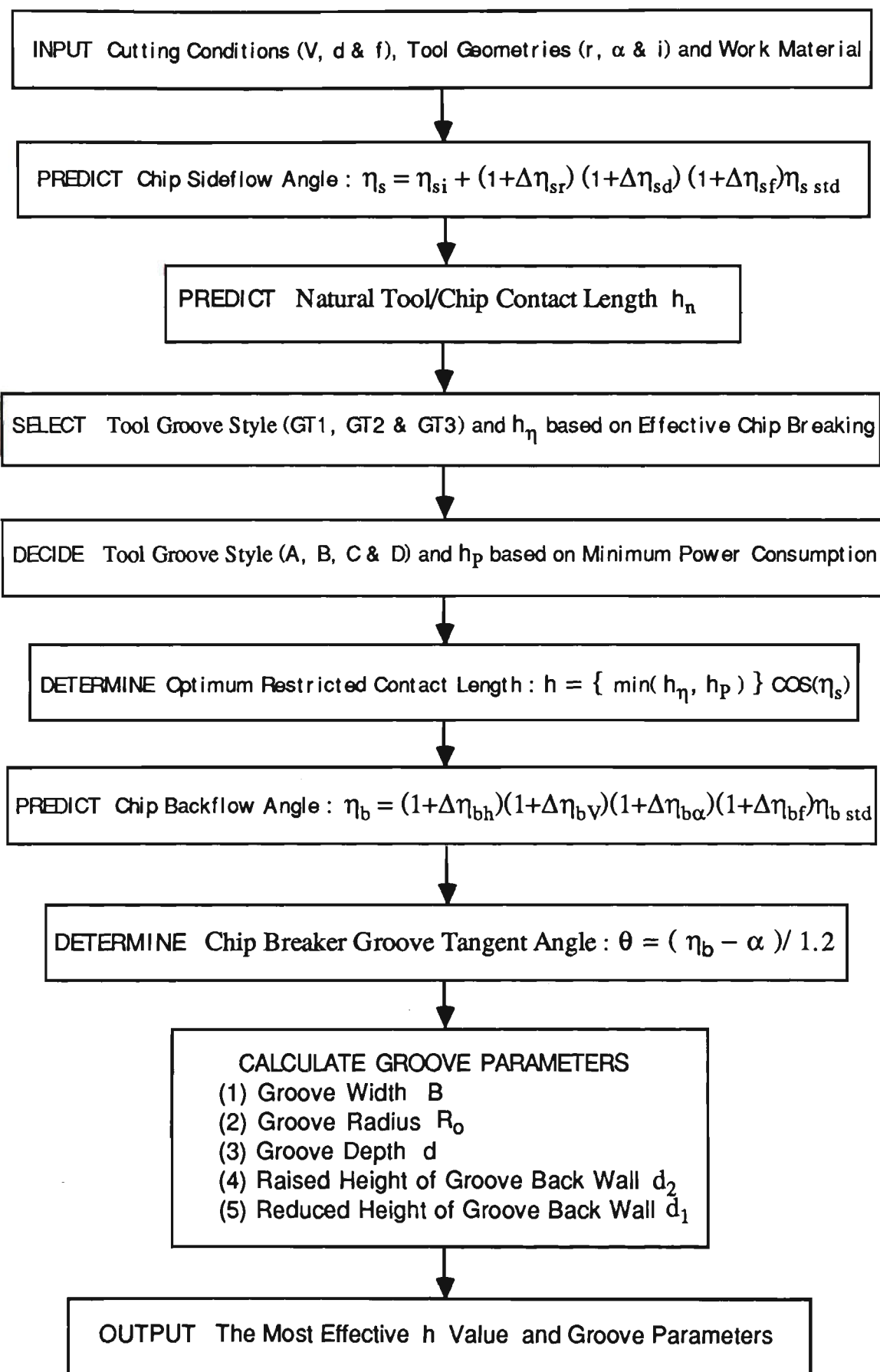


Figure 4.20 Flow chart for the knowledge-based system developed

4.8 SUMMARY AND CONCLUDING REMARKS

- (1) Most commercially available cutting tools are designed on the basis of the traditional "try and see" methods which very often do not provide the best results. Therefore, it is imperative to explore a more scientific design strategy in order to improve the performance of cutting tools in machining.
- (2) An alternative to the traditional design of chip breakers is presented in this chapter in the form of knowledge-based system incorporating a well established database system including Reference Database, Grooved Chip Breaker Database and 3-D Chip Flow Database.
- (3) In the present work, conventional grooved chip breakers are selected as the typical tools since the analysis of them could be regarded as a suitable basis for the general chip breaker design. The combined effects of tool restricted contact and groove configurations have been studied systematically in terms of three-dimensional chip flow. It has been shown that efficient chip breaking at the minimum power consumption can be achieved through the optimum groove utilisation of the chip breakers.
- (4) Although the knowledge-based system is only for designing effective grooved chip breakers, the methodology described in this chapter could be extended to the design of a more complicated toolface configuration.

CHAPTER 5

COMPREHENSIVE TOOL WEAR ESTIMATION IN FINISH-MACHINING BY MULTIVARIATE TIME SERIES ANALYSIS

5.1 INTRODUCTION

In finish-machining, the traditional (major) flank or crater wear estimation alone is no longer adequate and the wear on the minor flank face, such as minor flank wear or groove wear at the minor cutting edge, is of more importance since it directly affects the surface quality and dimensional accuracy of a finished product. It is obviously desirable for these wear states to be effectively monitored as well, because it is likely that wear in these areas may reach critical points earlier than those in the major flank and crater, such that the optimum cutting conditions or tool change policy in a finish-machining has to be set based on these wear types. Therefore, a more comprehensive monitoring strategy involving multi-sensor or multi-modelling is called for in order to estimate more than one type of tool wear, or comprehensive tool wear estimation.

Employing multi-sensor or multi-modelling strategies has been identified in a recent survey conducted for CIRP [5] as one of the three promising directions in machining process monitoring and control research. Interesting work has been reported in integrating force and acoustic emission (AE) signals via neural networks [11-12, 80]. Chryssolouris [37] evaluated the effectiveness of sensor integration for tool wear estimation by neural network, least-squares regression, and the group method of data handling (GMDH) algorithm using simulation data. Both papers reported better estimation of flank wear by integrating multi-sensory information than by using a single sensor. For finish-machining where more than one quantity is to be estimated, however, a multi-sensor and multi-modelling strategy as suggested in [5] becomes necessary.

The "comprehensive" monitoring strategy has been addressed less frequently, perhaps because of the complexity of the machining process. If more than one quantity is to be estimated, more complexity will be encountered. This places higher demands on signal processing and analysis techniques which shall be able to "single out", from the signals, particular ingredients sensitive to particular quantities to be estimated. Otherwise, multi-sensory techniques will do more harm than help. The spectrum analysis is a technique commonly used to single out frequency components to be correlated to tool wear [81-83]. Time domain methods, such as using autocorrelation coefficients of cutting force signals have been reported [13]. It, however, has been recognised that the cutting process is a stochastic process due to the existence of inevitable material property variations and other uncertainties. The necessity of employing stochastic analysis for cutting dynamics was emphasised in [84]. Interesting work on correlating coefficients of Autoregressive (AR) models of AE signals to flank wear was reported [7], though appreciation of the results is impaired by inadequate physical interpretations. Another example of using stochastic analysis is to detect tool breakage by monitoring the residuals of an AR model obtained from cutting torque signals [27]. The residual analysis has been proven to be very effective to detect abrupt changes in the cutting process, such as tool breakage.

Since groove formation at the minor cutting edge occurs only under certain cutting conditions, in this chapter, minor flank wear is first estimated along with major flank and crater wear, aiming at developing a comprehensive estimation strategy for tool wear in finish-machining. As using 3-D dynamic cutting force is an effective means for providing necessary information about wear states at different tool faces, the estimation strategy is based on the cutting force measured in terms of its three orthogonal components, from which trivariate Autoregressive Moving Average Vector (ARMAV) models [35] were developed. The dispersion analysis (DA) [35, 85] based on ARMAV models led to the discrimination between various modes of force

variations in a quantitative way, such that correlating them to various quantities to be estimated was made possible. The correlation results were supported by physical interpretations.

5.2 TOOL WEAR EXPERIMENTS

5.2.1 Description of Experiments

Dynamic components of the cutting force were measured by using a tool dynamometer (KISTLER 9257A). Figure 5.1 shows the experiment setup used. The data acquisition system used in the experiment is a Macintosh-based 12-bit A/D converter (MacADIOS II with MacInstrument software).

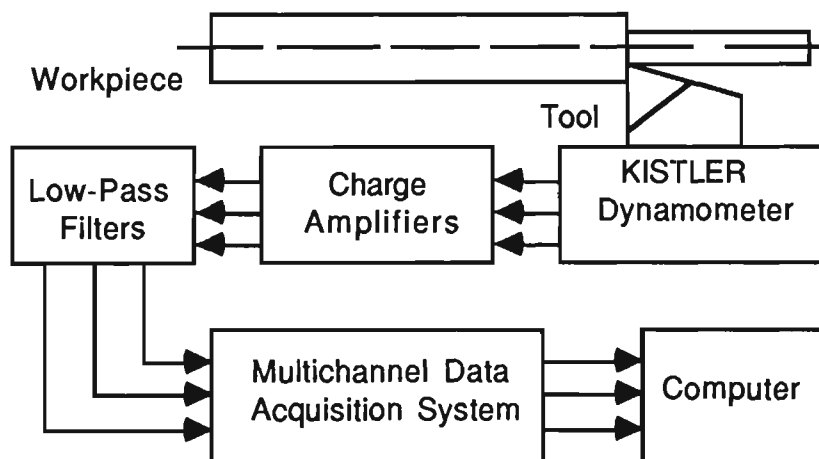


Figure 5.1 Experiment setup

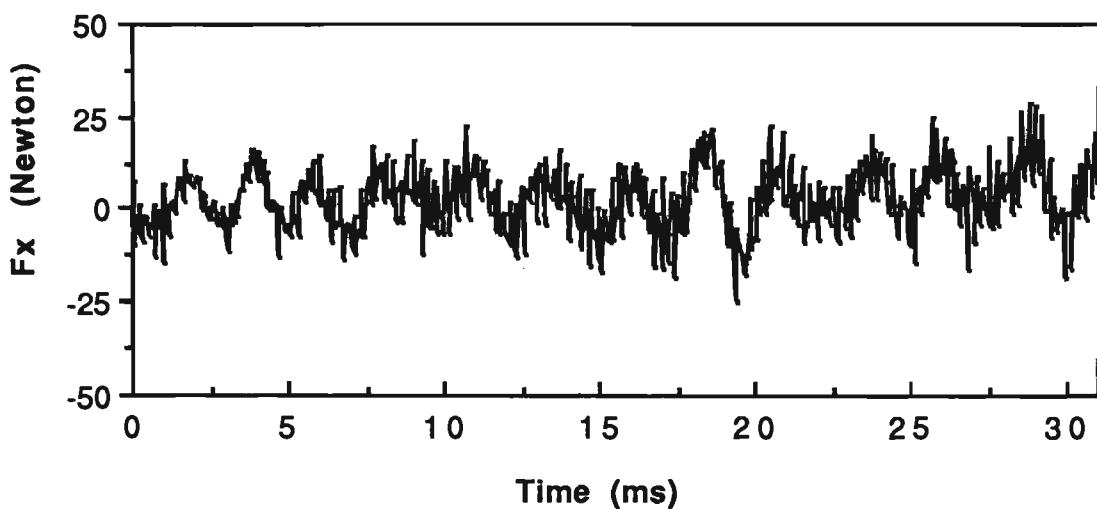
Four typical cutting conditions are selected for tool wear experiments as shown in Table 5.1. As we are only interested in the development patterns of particular types of tool wear, the degraded tool tests, i.e. using relatively softer tools as recommended in [86], are adopted to shorten the time-consuming and costly tool wear experiments.

Table 5.1 Machining conditions used in tool wear experiments

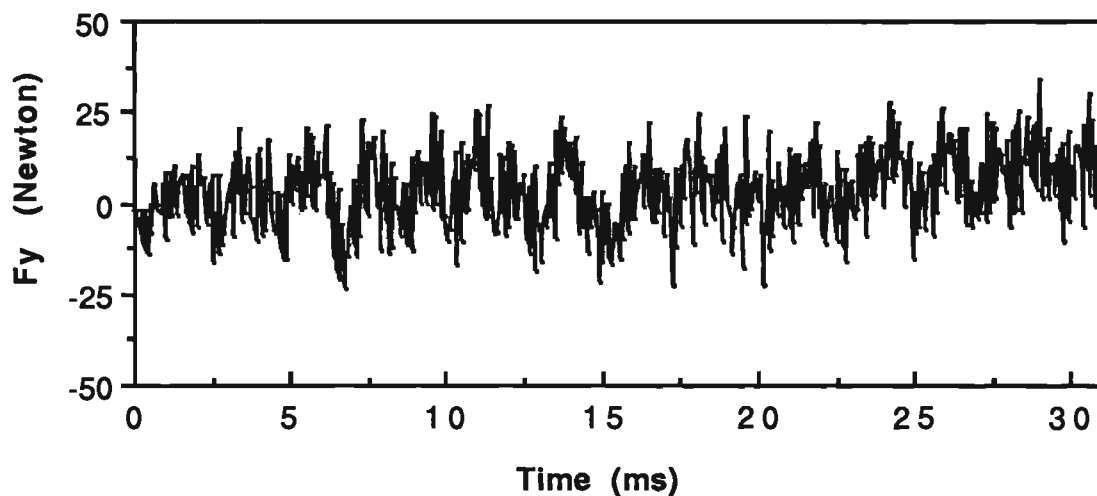
Machine Tool	Colchester Mascot 1600 (9.3 KW)
Tool Insert Type	TNMA160408F (flat-faced tool)
Tool Material	Carbide : Grade 883, SECO
Tool Geometry	0°, 5°, -6°, 90°, 60°, 0.8
Work Material	AISI4140 (BHN=275-320)
Workpiece Size	Length =1m and Diameter =100mm
Cutting Conditions	1. V=115 m/min f=0.1 mm/rev d=0.5mm 2. V=145 m/min f=0.1 mm/rev d=0.5mm 3. V=145 m/min f=0.06 mm/rev d=0.5mm 4. V=145 m/min f=0.06 mm/rev d=0.25
Cutting Fluid	No

A typical record of the dynamic cutting force is illustrated in Figure 5.2 in terms of its three orthogonal components, i.e., F_x , F_y and F_z .

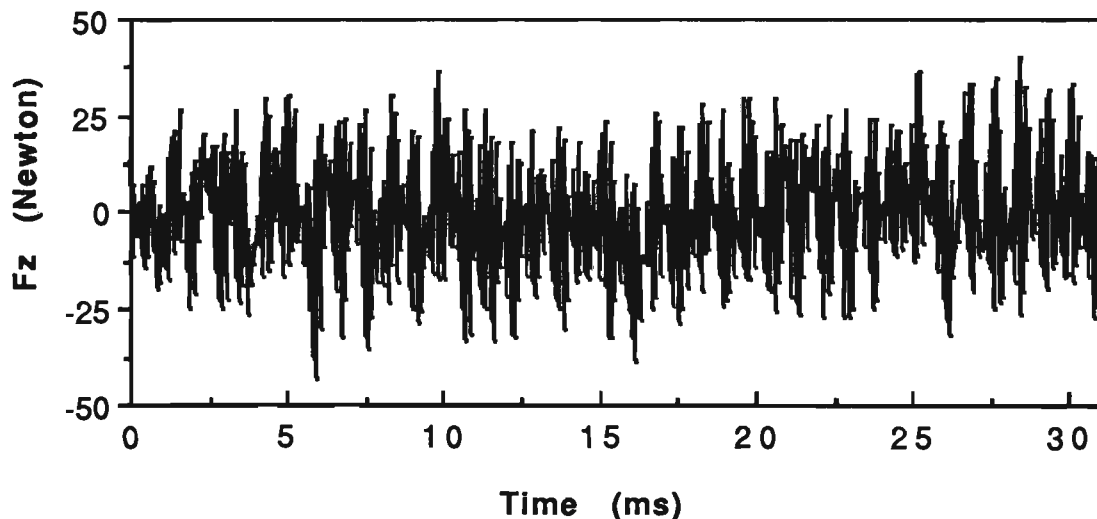
In order to assure that the experimental conditions are as close as possible to practical machining operations, the machining process was interrupted periodically with an increment in period of about 5 minutes under cutting condition Group 1, and 2.5 minutes under Groups 2-4. The tool was replaced by a fresh one at each interruption such that every tool remained in thermal continuity until it was replaced. Just before each tool replacement, a set of 524 data points was sampled for each channel. Therefore, the experimental results consist of 8 tools and 8 sets of data from each channel under Group 1, and 7 tools and 7 sets of data from each channel under Groups 2-4. Before the dynamic cutting force in terms of its three orthogonal components was sampled into a multi-channel data acquisition system with a sample interval equal to 60 μ s (about 16.7 KHz), low-pass filters with a cut-off frequency of 4 KHz were applied, considering the 4 KHz resonant frequency of the dynamometer.



(a) Dynamic Cutting Force in Feed Direction



(b) Dynamic Cutting Force in Thrust Direction

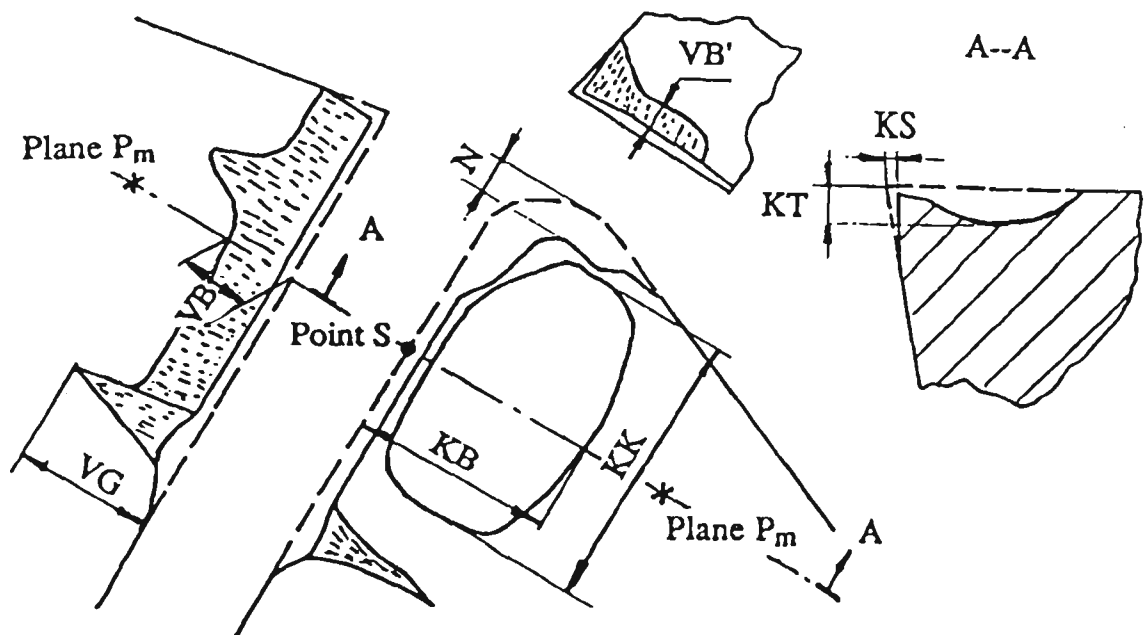


(c) Dynamic Cutting Force in Main Cutting Direction

Figure 5.2 Dynamic cutting force measured in terms of its three orthogonal components

5.2.2 Definition of Comprehensive Tool Wear Parameters

Eight parameters were selected to describe the tool wear states as shown in Figure 5.3, primarily in accordance with CIRP tool wear terminology [87]. The eight tool wear parameters are roughly classified into three categories with respect to different tool faces, i.e., the major flank area (VB, KS & VG), crater area (KT, KB & KK) and minor flank area (VB' & N).



S : the point on the original major cutting edge at the middle of depth of cut

P : the plane perpendicular to the major cutting edge through Point **S**

VB : major flank wear

VG : length of the groove (notch)

KS : retract of the cutting edge

KT : crater depth on the rake face

KB : crater width on the rake face

KK : crater length on the rake face

VB' : minor flank wear

N : nose wear

Figure 5.3 Definition of comprehensive tool wear parameters (based on [87])

5.2.3 Tool Wear Measurement and Wear Development Patterns

The scanning electron microscope (SEM), stereo microscope with camera attachment, surfcom (a surface roughness measuring instrument) and coordinate measuring machine (CMM) were used jointly to measure wear parameters selected.

Table 5.2 gives the measurement results of VB, KT and VB' for cutting condition Group 4. Table 5.3 tabulates the measurement results of the all eight types of wear for cutting condition Groups 1-3 and the developments of these types of tool wear were plotted in Figures 5.4 and 5.5. A typical group of tool wear photographs taken by SEM is shown in Figure 5.6, indicating the wear situations on different tool faces.

The formation of groove wear at the minor cutting edge (see Figure 5.6(d)) was noticed but not selected for investigation because of its inconsistent appearance under the machining conditions used in the experiment and it will be addressed separately in the following chapter.

Table 5.2 Tool wear measurement result for cutting condition Group 4

Time (min)	0	2.45	5.1	7.6	10	12.4	15
VB (mm)	0	0.15	0.19	0.26	0.46	0.50	0
KT (μm)	0	23.9	37.2	48.1	53.8	108	119
VB' (μm)	0	15.1	17.5	58.3	99.5	186	19

Table 5.3 Tool wear measurement results for cutting condition Groups 1-3

Tool Wear Measurement for Cutting Condition Group 1								
Time (min)	VB (mm)	KS (μm)	VG (mm)	KT (μm)	KB (mm)	KK (mm)	VB' (μm)	N (μm)
0	0	0	0	0	0	0	0	0
2.67	0.12	12.8	0.09	22.2	1.1	0.4	15.3	7.1
5	0.16	25.7	0.10	33.3	1.2	0.60	28.6	21.4
10	0.26	47.1	0.40	38.8	1.2	0.63	71.4	32.8
15	0.34	80.0	0.70	66.7	1.2	0.64	186	54.3
20	0.58	104	0.75	167	1.4	0.66	229	91.4
25	0.64	127	0.80	206	1.4	0.68	236	113
34	0.73	143	0.84	222	1.5	0.70	243	136
Tool Wear Measurement for Cutting Condition Group 2								
Time (min)	VB (mm)	KS (μm)	VG (mm)	KT (μm)	KB (mm)	KK (mm)	VB' (μm)	N (μm)
0	0	0	0	0	0	0	0	0
2.58	0.17	0.30	0.20	25.2	1.0	0.48	10.0	5.2
5.08	0.23	83.3	0.26	38.3	1.05	0.64	18.6	16.5
7.5	0.30	100	0.45	48.3	1.15	0.66	69.3	34.1
10	0.48	108	0.69	63.2	1.20	0.70	101	72.4
12.42	0.57	150	0.73	104	1.30	0.72	203	101
15.16	0.80	200	0.94	144	1.40	0.76	211	105
Tool Wear Measurement for Cutting Condition Group 3								
Time (min)	VB (mm)	KS (μm)	VG (mm)	KT (μm)	KB (mm)	KK (mm)	VB' (μm)	N (μm)
0	0	0	0	0	0	0	0	0
2.5	0.15	28.3	0.17	24.8	0.9	0.46	33.3	5.6
5	0.20	81.7	0.21	35.7	1.0	0.58	36.7	15.6
7.67	0.28	100	0.44	47.2	1.1	0.60	83.3	35.3
10.08	0.46	103	0.64	55.6	1.1	0.62	117	68.2
12.5	0.52	153	0.74	114	1.2	0.65	197	93.5
15	0.74	166	0.88	131	1.3	0.69	202	96.7

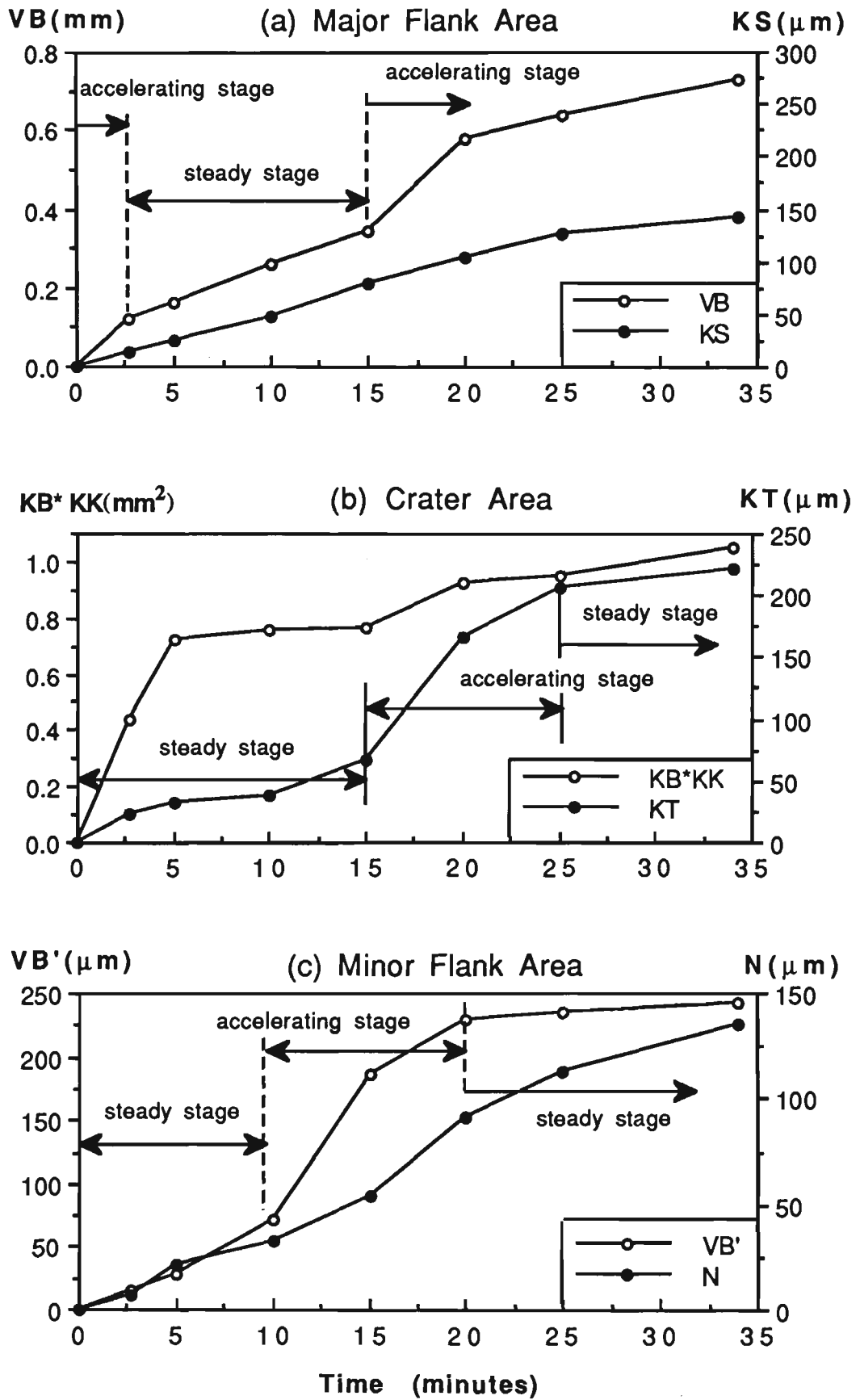


Figure 5.4 Tool wear development for cutting condition Group 1 (V=115 m/min, f=0.1 mm/rev, d=0.5 mm)

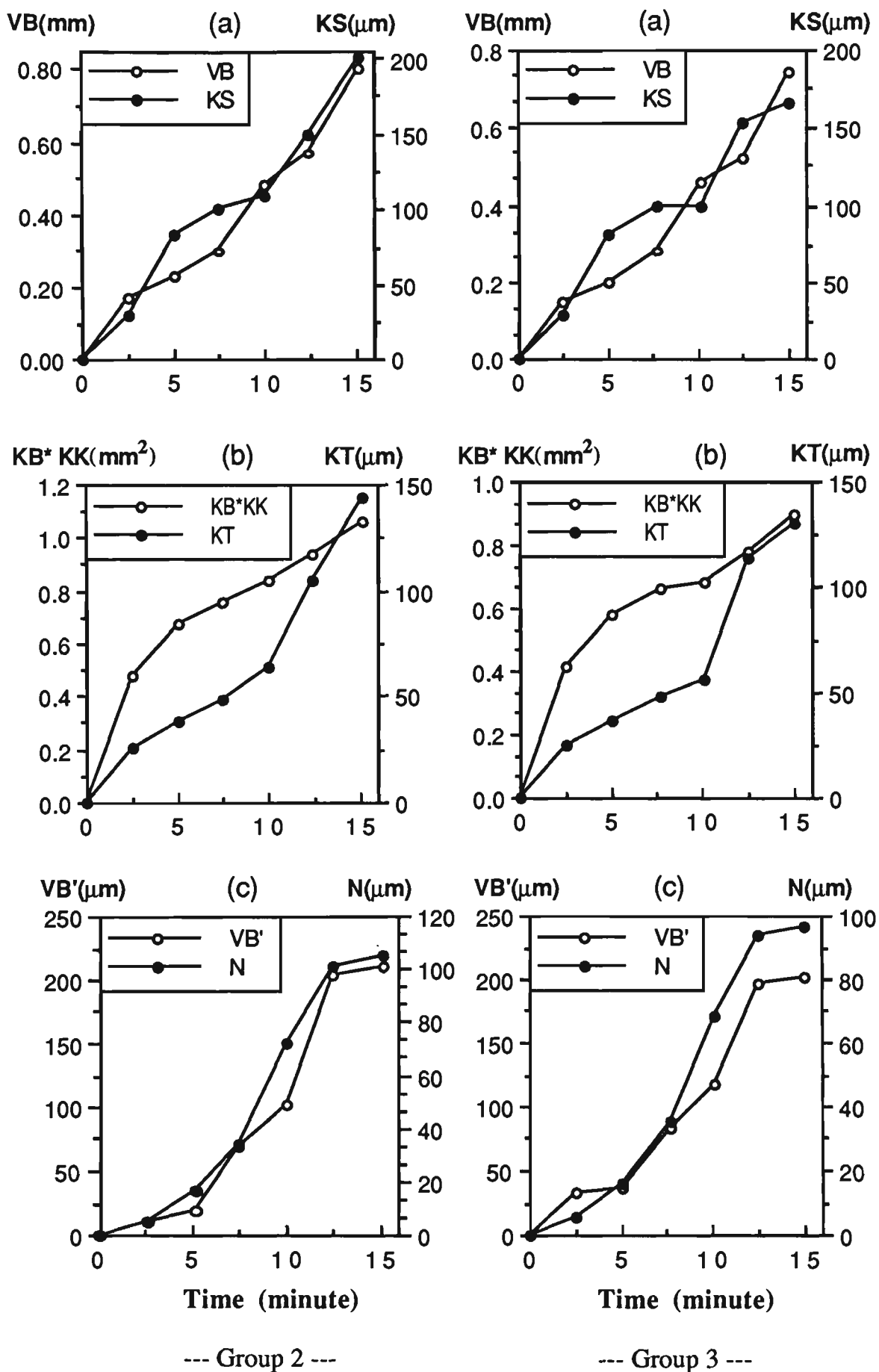


Figure 5.5 Tool wear development for cutting condition Groups 2 & 3

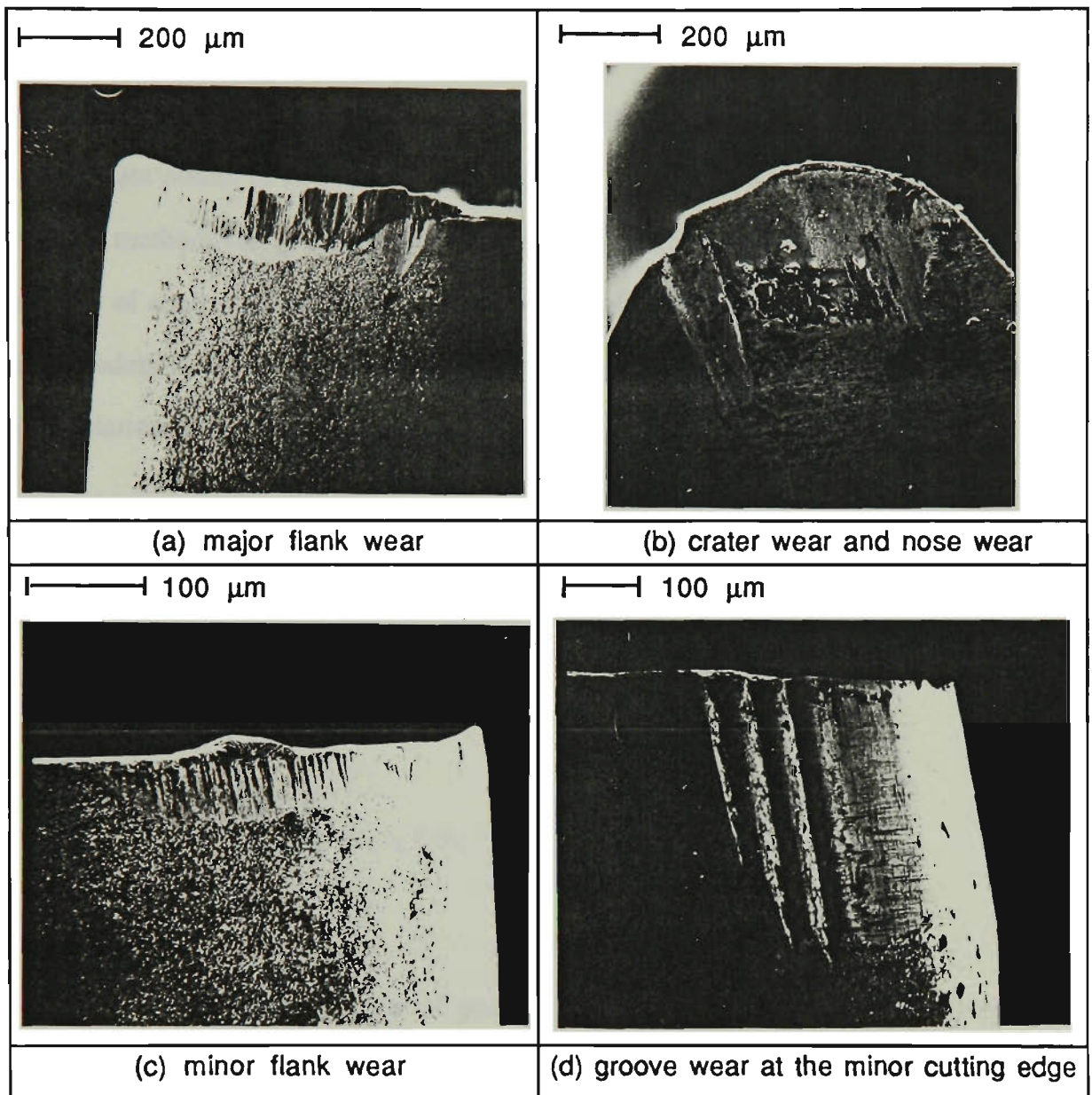


Figure 5.6 Tool wear observed under a scanning electron microscope (SEM)

5.3 MULTIVARIATE TIME SERIES TECHNIQUES

5.3.1 Trivariate ARMAV Models

It is known that the dynamic cutting force, which is the variation from the average cutting force, contains richer information about tool/workpiece interactions during machining than the latter alone [84]. It has been shown that the dynamic cutting force

is a stochastic signal which roughly obeys the normal distribution [88]. It is also appropriate to regard the dynamic force as stationary processes at different stages of wear development, because it takes only a fraction of a second for a set of a few hundred data points to be sampled each time. In summary, it is appropriate to apply statistical methods for stationary normal processes to the dynamic cutting force signal. As a way of analysing the dynamics in the cutting force measurements, trivariate time series models, developed from the data, are used, since they give a concise parametric representation of the signals.

When a dynamic process represented by its p -components is sampled at uniform intervals, Δ , the resulting discrete series of observation vectors, \mathbf{X}_t , $t=1, 2, \dots, N$; can be represented by

$$\mathbf{X}_t = \sum_{k=1}^n \Phi_k \mathbf{X}_{t-k} + \mathbf{a}_t - \sum_{k=1}^m \theta_k \mathbf{a}_{t-k} \quad (5.1)$$

where the p -dimensional vector of process variables is given by the observation vectors $\mathbf{X}_t = [X_{1t}, X_{2t}, \dots, X_{pt}]^T$, and the white noise $\mathbf{a}_t = [a_{1t}, a_{2t}, \dots, a_{pt}]^T$, with the properties of $E[\mathbf{a}_t] = 0$ and $E[\mathbf{a}_t \mathbf{a}_{t-k}^T] = \delta_k \sigma_a$. Superscript T denotes vector transpose, E expectation, δ_k the Kronecker delta function and σ_a the covariance of \mathbf{a}_t .

The model in Equation 5.1 is termed as Autoregressive Moving Average Vector model of autoregressive order n and moving average order m denoted by ARMAV(n, m). The parameter matrices Φ_k 's and θ_k 's are estimated based on the observation vectors. The orders of an adequate model can be determined by the F-test [35] or by the Akaike's Information Criterion (AIC) [89]. It can be shown that an ARMAV(n, m) model can be approximated by an autoregressive model, i.e., ARV(n) of a sufficiently high order [35]. An ARV model requires much less computations than an ARMAV

model does, such that it is more attractive for on-line implementations. When applied to the oblique machining process, an ARV(n) model has a much simpler form :

$$\mathbf{X}_t = \sum_{k=1}^n \Phi_k \mathbf{X}_{t-k} + \mathbf{a}_t \quad (5.2)$$

where $\mathbf{X}_t = (\mathbf{X}_{1t}, \mathbf{X}_{2t}, \mathbf{X}_{3t})^T$,

$$\Phi_k = \begin{pmatrix} \Phi_{11k} & \Phi_{12k} & \Phi_{13k} \\ \Phi_{21k} & \Phi_{22k} & \Phi_{23k} \\ \Phi_{31k} & \Phi_{32k} & \Phi_{33k} \end{pmatrix} \text{ and } \mathbf{a}_t = (a_{1t}, a_{2t}, a_{3t})^T$$

Such a model expresses the observed trivariate series, $\mathbf{X}_{1t} = F_{xt}$ = feed force, $\mathbf{X}_{2t} = F_{yt}$ = thrust force, and $\mathbf{X}_{3t} = F_{zt}$ = main cutting force, as linear combinations of past observation vectors \mathbf{X}_{t-k} plus the white noise \mathbf{a}_t and therefore describes the instantaneous dynamics of the cutting process.

5.3.2 Dispersion Analysis

Once an adequate ARMAV model is determined, the dispersion analysis (DA) can be introduced to make discrimination among various modes of dynamic force variations in a quantitative way. It can be shown [35] that the correlation matrix of the measured variables is a weighted linear combination of the eigenvalues, λ_i , ($i=1,2, \dots, n$, for each series) as follows,

$$\gamma_k = E[\mathbf{X}_t \mathbf{X}_{t+k}^T] = \sum_{i=1}^n d_i \lambda_i^k \quad (5.3)$$

If $k = 0$, one obtains the process variance for the measured variables as

$$\gamma_0 = E[\mathbf{X}_t \mathbf{X}_t^T] = \sum_{i=1}^n d_i \quad (5.4)$$

where d_i is the dispersion associated with eigenvalue λ_i and given by

$$d_i = g_i \sum_{k=1}^n \frac{\sigma_a g_k}{1 - \lambda_i \lambda_k} \quad (5.5)$$

and g_i is calculated by the following equation,

$$g_i = \frac{\lambda_i^{n-1}}{n \prod_{k=1, k \neq i} (\lambda_i - \lambda_k)} \quad (5.6)$$

The dispersion percentage, D_i , describes the contribution of the roots or ultimately the frequencies in the series to the process variation γ_0 and given as :

$$D_i = \frac{d_i}{\gamma_0} \quad (5.7)$$

In this way the process variation γ_0 is decomposed into contributions of process eigenvalues in terms of dispersion (D_i) quantitatively. Of particular interest are the dispersion percentages (D_i) associated with eigenvalues (λ_i) occurring in complex conjugate pairs (λ_1 and λ_2) which describe the oscillating variation of the machining process. The frequency corresponding to a pair of complex conjugate eigenvalues is given by [35],

$$f_n \text{ (Hz)} = \frac{1}{2\pi\Delta} \sqrt{\frac{[\ln(\lambda_1 \lambda_2)]^2}{4} + \left[\cos^{-1} \left(\frac{\lambda_1 + \lambda_2}{2\sqrt{\lambda_1 \lambda_2}} \right) \right]^2} \quad (5.8)$$

where Δ is the sample interval in seconds.

The significance of dispersion analysis lies in that the relative importance of the oscillating mode of each existing frequency can be established such that analysis and interpretation in terms of physical phenomena, such as natural frequencies of the tool/tool holder system and machine tool structural frequencies, can be carried out in a quantitative manner.

5.4. TOOL WEAR ESTIMATION BY DISPERSION ANALYSIS BASED ON ARV MODELS

5.4.1 ARV Modelling of 3-D Dynamic Cutting Forces

Each set of 3-D dynamic cutting force was used to develop ARV(n) models first. ARV(9) models were found adequate for the data collected under cutting condition

Group 1 in Table 5.1 and ARV(11) models for the data collected under cutting condition Groups 2-4. Given below is an example of ARV(9) model.

$$\mathbf{X}_t = \begin{bmatrix} .448 & -.063 & -.020 \\ .140 & .808 & -.018 \\ -.034 & .128 & .333 \end{bmatrix} \mathbf{X}_{t-1} + \begin{bmatrix} -.129 & .115 & -.108 \\ -.063 & -.349 & -.062 \\ -.043 & -.083 & .265 \end{bmatrix} \mathbf{X}_{t-2} + \begin{bmatrix} .262 & .013 & .193 \\ -.169 & .092 & .010 \\ .164 & -.060 & .052 \end{bmatrix} \mathbf{X}_{t-3} +$$

$$\begin{bmatrix} .342 & -.023 & -.073 \\ .103 & -.034 & -.021 \\ -.085 & .105 & .048 \end{bmatrix} \mathbf{X}_{t-4} + \begin{bmatrix} .187 & -.001 & .005 \\ -.162 & .188 & .088 \\ -.061 & -.054 & .047 \end{bmatrix} \mathbf{X}_{t-5} + \begin{bmatrix} .018 & .059 & .099 \\ .084 & -.058 & -.045 \\ .004 & .011 & -.105 \end{bmatrix} \mathbf{X}_{t-6} +$$

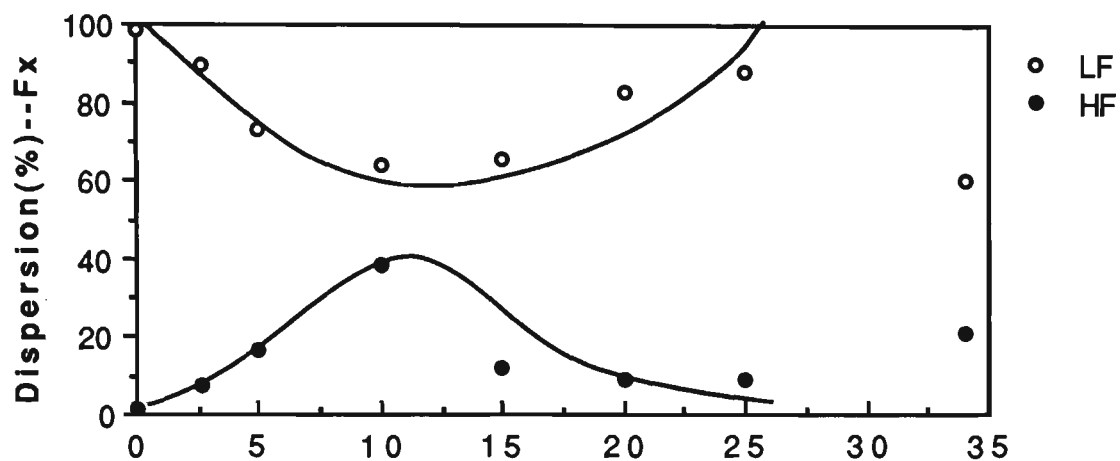
$$\begin{bmatrix} -.200 & -.161 & .010 \\ .035 & -.021 & -.016 \\ -.108 & .054 & .179 \end{bmatrix} \mathbf{X}_{t-7} + \begin{bmatrix} -.086 & .158 & -.028 \\ .054 & -.064 & -.035 \\ .086 & -.161 & -.131 \end{bmatrix} \mathbf{X}_{t-8} + \begin{bmatrix} -.084 & -.057 & -.010 \\ -.003 & .012 & .105 \\ -.044 & .060 & -.003 \end{bmatrix} \mathbf{X}_{t-9} + \mathbf{a}_t$$

5.4.2 Patterns of Dispersion Development

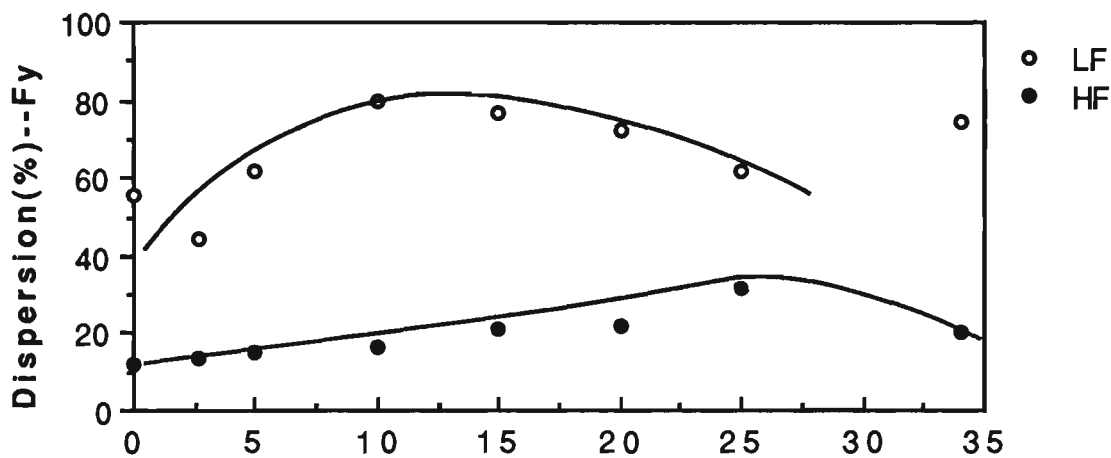
After an adequate ARV(n) model was determined, dispersion d_i 's and corresponding frequencies were calculated according to Equations 5.4 to 5.8. The dominant dispersions d_i 's, i.e., the ones with larger percentage D_i 's, and the associated frequencies under cutting condition Groups 1-3 are tabulated in Table 5.4. It is seen that the most significant dispersions are associated with a lower frequency (LF) range, and the second most significant dispersions related to a higher frequency (HF) range. The dominant dispersions for all the first three cutting conditions are plotted in Figures 2.7 and 2.8, from which recognisable trends are observed which will be exploited in the following section.

Table 5.4 Dispersion analysis results (only dominant terms listed)

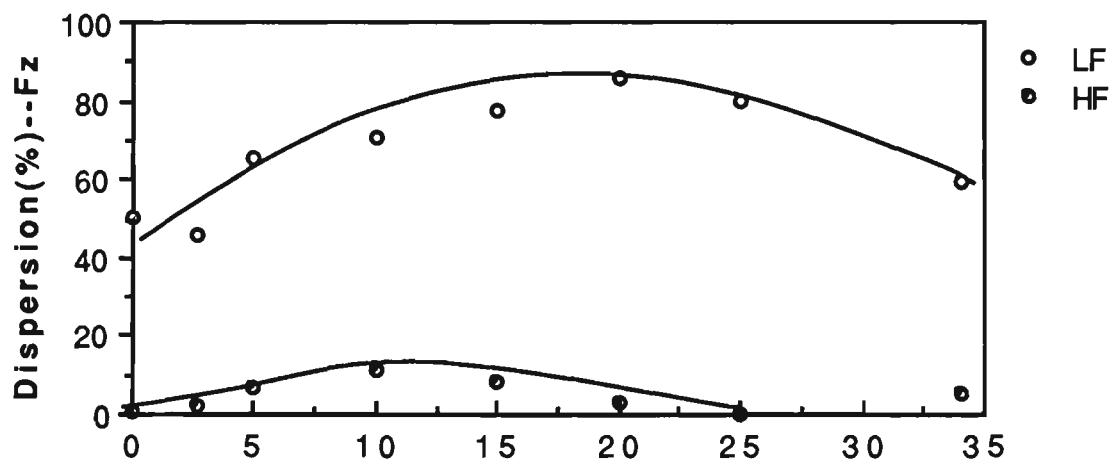
Dispersion Percentages D_i (%) for Cutting Condition Group 1						
Time (minute)	Feed Force F_x		Thrust Force F_y		Main Cutting Force F_z	
	500-550 (HZ)	3.4-3.5 (KHZ)	650-750 (HZ)	3.3-3.5 (KHZ)	950-1050 (HZ)	2.6-2.8 (KHZ)
0	98.28	1.35	55.43	12.11	50.20	0.80
2.67	89.37	7.28	44.66	13.42	46.22	2.53
5	72.77	16.79	61.60	14.77	65.4	6.50
10	63.96	38.25	79.84	16.22	70.70	11.23
15	65.14	11.68	76.43	20.80	77.49	8.53
20	82.90	9.21	72.39	21.90	85.85	2.70
25	87.74	8.80	61.98	31.74	80.00	0.01
34	60.00	20.83	74.32	20.32	59.17	5.36
Dispersion Percentages D_i (%) for Cutting Condition Group 2						
Time (minute)	Feed Force F_x		Thrust Force F_y		Main Cutting Force F_z	
	450-550 (HZ)	3.3-3.5 (KHZ)	600-700 (HZ)	3.3-3.5 (KHZ)	900-1200 (HZ)	3.0-3.5 (KHZ)
0	86.06	8.57	75.98	11.24	27.70	1.59
2.58	66.5	10.20	82.90	12.44	39.53	1.75
5.08	61.3	21.35	77.06	11.80	57.38	7.78
7.5	50.50	20.36	67.92	20.96	24.15	2.54
10	35.50	24.20	44.15	44.24	40.54	19.64
12.42	65.5	15.57	49.81	46.05	66.28	16.61
15.16	75.20	6.72	56.43	30.14	81.53	1.03
Dispersion Percentages D_i (%) for Cutting Condition Group 3						
Time (minute)	Feed Force F_x		Thrust Force F_y		Main Cutting Force F_z	
	400-500 (HZ)	3.3-3.5 (KHZ)	550-650 (HZ)	3.3-3.5 (KHZ)	800-1200 (HZ)	3.0-3.5 (KHZ)
0	81.82	8.68	78.71	12.99	28.00	0.68
2.58	70.47	15.58	81.99	11.05	39.56	8.28
5	66.17	18.13	76.05	14.97	48.36	7.09
7.5	66.93	24.67	61.54	28.60	48.32	15.33
10	68.10	17.32	46.10	37.97	57.94	21.93
12.67	84.17	1.60	47.14	42.51	61.2	7.82
15	96.34	0.82	38.68	12.96	90.66	3.31



(a) LF=500-550Hz, HF=3.4-3.5KHz



(b) LF=650-750Hz, HF=3.3-3.5KHz



(c) LF=950-1050Hz, HF=2.6-2.8KHz

Time (minutes)

Figure 5.7 Dispersion diagram for cutting condition Group 1

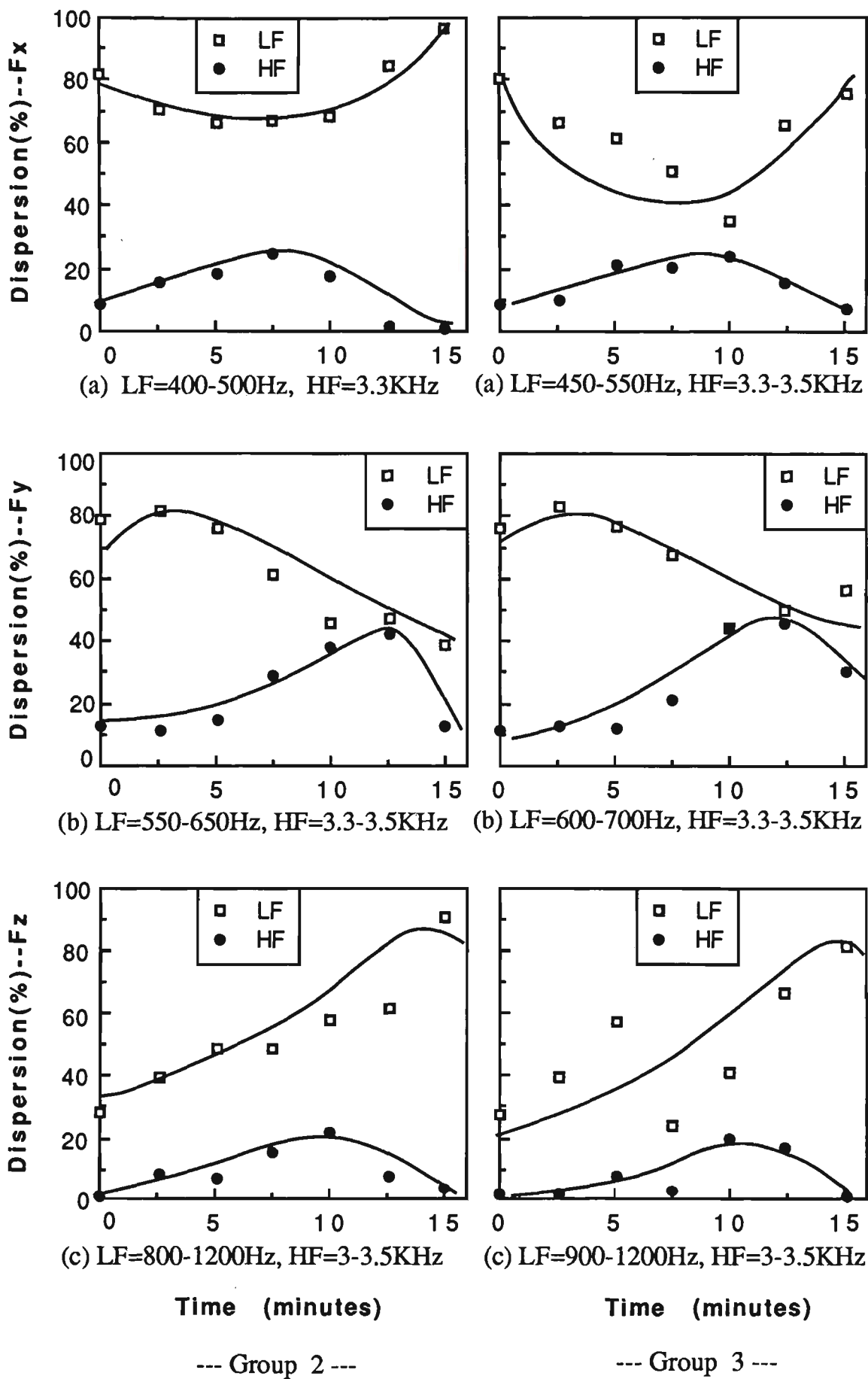


Figure 5.8 Dispersion diagrams for cutting condition Groups 2 & 3

5.4.3 Analysis Associated with Physical Interpretation

Feed Direction: For an oblique turning operation of a bar, it is known that the feed force F_x is primarily associated with the normal force acting on the major flank $F_{\alpha n}$ and the horizontal friction force acting on the minor flank $F_{\beta h}$ (Figure 5.9). Therefore, the tool/workpiece interactions on both flanks should be reflected in the dynamic feed force characteristics.

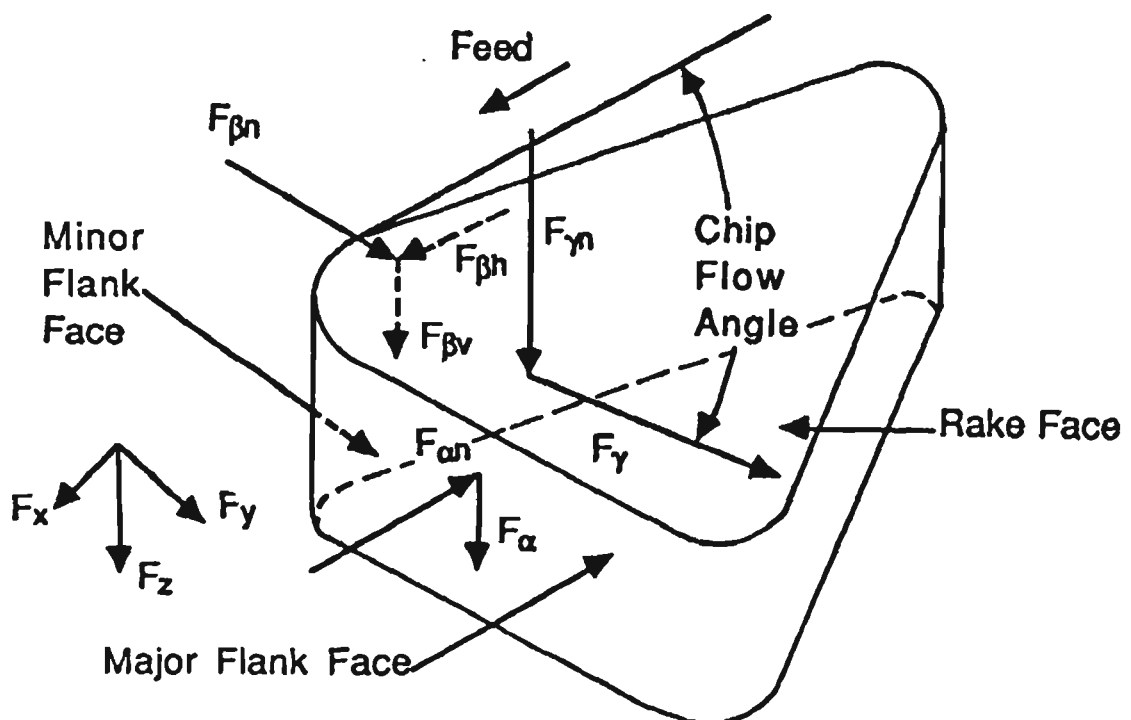


Figure 5.9 The model for the forces acting on different tool faces

By examining the trend of LF dispersions of 500-550Hz for cutting condition Group 1 shown in Figure 5.7(a), it is found that the percentage values decrease to a minimum between 10 to 15 minutes (major flank wear $VB = 0.35$ mm, Figure 5.4(a)), after which they increase. It is well known from experience that cutting tools are replaced or changed when the major flank wear reaches the critical values of 0.25-0.38 mm [10, 86]. Beyond this critical wear, the rate of wear increases very rapidly, below it the rate first decreases and then becomes constant. Thus, the behaviour of the LF dispersions isolated from the dynamic feed force is very similar to the well-known rate

of major flank wear curves and could be used as a good indicator for major flank wear.

By comparing the HF dispersion curve of 3.4-3.5 KHz shown in Figure 5.7(a) with the minor flank wear VB' curve shown in Figure 5.4(c), it is again found the former resembles the slope (rate) of the latter. The acceleration of VB' at about 10 minutes could be detected by the maximum value of the HF dispersions.

Thrust Direction: The dynamic thrust force F_y mainly reflects the tool/workpiece interactions on both the rake face and the minor flank. The small depth of cut used in finish-machining produces a large chip flow angle such that the rake face friction force F_γ is almost along the y direction. The normal force acting on the minor flank $F_{\beta n}$ is also associated with F_y . In a similar manner, the HF dispersions of 3.3-3.5 KHz shown in Figure 5.7(b) can be related to the rate of crater wear KT shown in Figure 5.4(b), and the LF dispersions of 650-750 Hz shown in Figure 5.7(b) related to the rate of the minor flank wear VB' shown in Figure 5.4(c). Therefore, they can be used for minor flank and crater wear monitoring purposes.

Cutting Direction: The dynamic cutting force F_z is primarily associated with the normal force acting on the rake face $F_{\gamma n}$, the friction force acting on the major flank F_α , and the vertical friction force on the minor flank $F_{\beta v}$. By examining the LF and HF dispersions of 950-1,050 Hz and 2.6-2.8 KHz shown in Figure 5.7(c), it was found that they reflect the rate of the crater wear KT and the minor flank wear VB' shown in Figures 5.4(b) and 5.4(c), respectively.

As summarised in Table 5.5, the trends of the LF dispersions isolated from all three components of the dynamic cutting force reflect the wear rate mechanism associated with normal forces, and the HF dispersions reflect the wear rate mechanism associated with tangential (friction) forces. Similar results were obtained for experiments under cutting condition Groups 2 and 3 as shown in Figures 5.5 and 5.8.

Table 5.5 Tool wear analysis for cutting condition Group 1

F_x	$F_{\alpha n}$ (Normal to Major Flank) ↔ VB, KS ↔ LF Dispersions (500-550 Hz)
	$F_{\beta h}$ (Tangential to Minor Flank) ↔ VB', N ↔ HF Dispersions (3.4-3.5 KHz)
F_y	$F_{\beta n}$ (Normal to Minor Flank) ↔ VB', N ↔ LF Dispersions (650-750 Hz)
	F_{γ} (Tangential to Crater Face) ↔ KT ↔ HF Dispersions (3.3-3.5 KHz)
F_z	$F_{\gamma n}$ (Normal to Crater Face) ↔ KT ↔ LF Dispersions (950-1050 Hz)
	$F_{\beta v}$ (Tangential to Minor Flank) ↔ VB', N ↔ HF Dispersions (2.6-2.8 KHz)
	F_{α} (Tangential to Major Flank) No recognisable trend was found.

5.4.4 Strategies of Tool Wear Estimation in Finish-Machining

Major Flank Wear : Based on the discussion above, it can be concluded that the LF dispersion of feed force F_x is in agreement with the rate patterns of major flank wear VB, thus giving a good indication for the major flank wear.

Minor Flank Wear : Among the three dispersion patterns for minor flank wear, i.e. the LF dispersion of F_y , the HF dispersion of F_x and the HF dispersion of F_z , the last two are found to exhibit a consistent pattern under all the three cutting conditions, Groups 1-3. The HF dispersion of F_x , however, is more a static than a dynamic one, because of the slow feed motion. Therefore, HF dispersion of F_z can be used as the main indicator of minor flank wear VB', and the HF dispersion of F_x as auxiliary one. When one of them reaches the maximum, the accelerated minor flank wear is indicated.

Crater Wear : For the crater depth, it can be seen that both LF dispersion of F_z and HF dispersion of F_y under all the three cutting conditions, Groups 1-3, reach their maximum values as the crater depth KT, falls into the accelerating stage. Thus both of them could be used as an indicator for the detection of the accelerating state of crater depth.

5.4.5 Structural Dynamics and Idle Disturbances

Clear patterns linking the force variations in terms of dispersions and associated frequencies, isolated from dynamic cutting force, to the various wear development rates have been identified. However, the physical nature of the relationships is unclear and it is the purpose of this section to identify physical origins of these relationships and interpret accordingly.

Since almost the same HF's appear in all three groups, these frequencies are then inherent in the tool holder and hence may be conjectured to relate to its natural frequencies. Tests revealed that the natural frequencies of the tool holder/dynamometer system were 3,320 Hz in the x-, 3,300 Hz in the y-, and 2,847 Hz in the z- directions, respectively. These values match reasonably well with the HF's isolated from the dynamic cutting force (Table 5.4).

Tests on dynamometer frequency response to idle speed excitation alone revealed idle frequencies of 575 Hz for x, 715 Hz for y, and 975 Hz for z under cutting condition Group 1. These frequencies are reasonably close to the LF's listed in Table 5.4. From the above tests, it becomes clear that tool/workpiece interaction at the LF's are related to the idle frequencies, and the HF's are mainly associated with the natural frequencies of the tool-holder/dynamometer system.

5.5 SUMMARY AND CONCLUDING REMARKS

- (1) Dispersion analysis based on trivariate ARMAV time series models was used to decompose quantitatively the dynamic cutting force in terms of dispersions (relative importance of modes of force variation) and the associated frequencies. The merit of the method is its ability to isolate, from the dynamic cutting force, the ingredients, each of which is sensitive to a particular wear state, thereby

providing much more comprehensive yet sensitive estimates than those possible by using the force signal in a lump-sum manner.

- (2) The patterns of change of the dispersions resemble the rate of various wear parameters and the resemblance is physically interpreted. The rapidly increasing rate of minor flank wear occurring before the accelerating stage of major flank wear is due to the fact that the gradually increasing major flank wear, and retreat of the cutting edge, sharpens the nose and puts more burden on the minor flank and edge, to a point where drastic minor flank wear is inevitable. Therefore, for operations such as a finish-turning of a bar, optimum cutting conditions or effective tool change strategies have to be determined based on the minor flank wear instead of others, to assure geometric accuracy and surface quality of the finished workpiece.
- (3) From a practical machining viewpoint, the algorithm introduced is feasible for on-line tool wear estimation after reformulation and simplification because it is sufficiently fast to determine tool wear states in real time.
- (4) Different machine tools or dynamometers certainly have different frequency characteristics which, however, can be determined with reasonable ease. The trends identified by using dispersion analysis in this chapter remain the same while the specific values of these structurally-determined frequencies may vary. In this sense, the approach is applicable to the general case of finish-machining.

CHAPTER 6

MONITORING GROOVE WEAR DEVELOPMENT IN FINISH-MACHINING BY ARV MODEL-BASED MULTIPLE DISPERSION ANALYSIS

6.1 INTRODUCTION

As described in Chapter 5 for finish-machining the well-known types of tool wear, such as major flank wear and crater wear, are often not the wear types which lead to tool failure first. Instead, minor flank wear, nose wear and groove wear at the minor cutting edge are recognised as being more important in determining the tool life, due to their greater influence on dimensional accuracy and surface quality of the finished product [87]. Particularly, groove wear at the minor cutting edge, once formed, will cause significant deterioration of surface quality and shorten tool-life [23-25]. Therefore, it is obvious that for finish-machining, monitoring of the minor flank, major flank and crater wear is not sufficient and monitoring of the groove wear at the minor cutting edge must be incorporated. Since the groove wear often induces high frequency vibration, 3-D vibration signal is chosen for monitoring purpose.

The study of groove wear at the minor cutting edge can be dated back to 1960's [23-26, 90-92]. Most work then focused on explaining the phenomena and conjecturing the mechanism of formation. The formation of the groove is mainly due to the rubbing action at the minor cutting edge from a mechanical point of view. The workpiece, with a work-hardened layer, can be compared to a grinding wheel. Groove wear will occur under certain combinations of tool and work materials, and it can be observed that a series of grooves will form at the minor cutting edge which in fact does not take part in cutting directly. The depth of groove wear directly influences the surface roughness produced. Shown in Figure 6.1 is a pictorial description of the groove wear at the

minor cutting edge in accordance with CIRP terminology [87]. It was found that when enough grooves have been formed and developed to a certain degree, severe vibration may be induced, which disturbs the formed groove pattern and wipes out the grooves eventually, resulting in a rapid deterioration of surface finish [26]. In other words, groove wear reaches its critical point and the cutting tool should be replaced when the grooves are being wiped out.

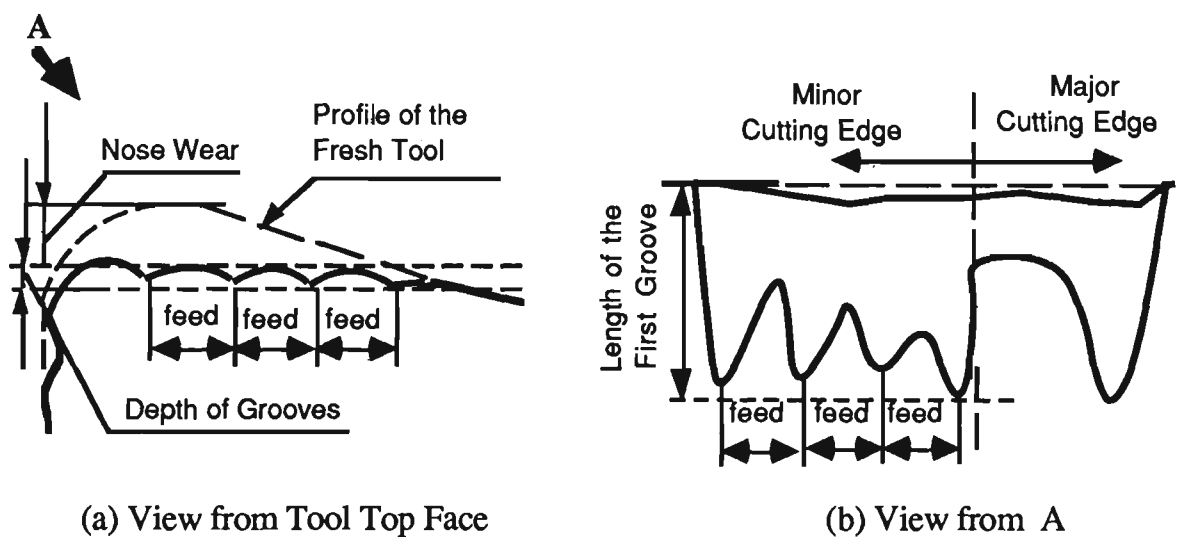


Figure 6.1 Groove wear at the minor cutting edge

Although vibrations induced by groove wear at the minor cutting edge have been observed long ago [23], no further work has been reported on investigating the possibility of using it for on-line monitoring purposes, mainly due to the complexity involved in groove wear formation and the difficulty involved in effective signal analysis and interpretation. The study of on-line groove wear monitoring, however, is of significance in automated machining systems, not just because of its influence on surface quality, but also because of the fact that groove wear is often one of the factors inducing unfavourable chatter [25]. Although it was reported that superimposing a minor vibration in the feed direction hindered groove formation [25-26], this is not economically justifiable for conventional machine-tool structures.

The purpose of this chapter is to develop an effective method to detect and monitor the formation and development of groove wear. The experimental results of groove wear development and investigation results concerning the detection of the critical point at which severe vibration is induced by the groove wear, i.e. at which the finishing tool needs to be replaced, are presented first. Due to the fact that the vibration occurring in the neighbourhood of that point in time is extremely complicated and that very little is known about it, a miniature 3-D accelerometer, mounted in close vicinity to the tool tip, was used to capture multi-dimensional vibration signals. Since more than one quantity is needed to describe the groove wear, and the formation of groove wear is related to all three orthogonal cutting directions, multivariate autoregressive time series models (ARV) are adopted. Based on the stochastic ARV models developed directly from the vibration signals, a quantitative analysis was made possible by employing multiple dispersion analysis, which discriminates features which are sensitive to various aspects of the formation of groove wear.

6.2 INVESTIGATION INTO THE PATTERNS OF GROOVE WEAR DEVELOPMENT

6.2.1 Tool Wear Experiments

In the experiments 3-D vibration signals were measured by a miniature 3-D accelerometer (PCB Model 306A06), mounted in close vicinity of the tool tip, aiming at capturing original signals with minimum distortion. The machining conditions used in the experiments are shown in Table 6.1, all the conditions being within the range recommended by the tool manufacturer.

Table 6.1 Machining conditions used in groove wear experiments

Machine Tool	HITEC-20SII CNC Lathe (18 KW)		
Tool Insert Type	TNMG160408 (Carbide P10 and groove-type chip breakers)		
Tool Geometry	0°, 5°, -6°, 90°, 60°, 0.8		
Work Material	AISI4140 (BHN=320)		
Cutting Conditions :			
Group A :	V=160m/min	f=0.08 mm/rev	d=0.25mm
Group B :	V=160m/min	f=0.04 mm/rev	d=0.25mm
Group C :	V=125m/min	f=0.08 mm/rev	d=0.25mm
Group D :	V=190m/min	f=0.08 mm/rev	d=0.25mm
Group E :	V=190m/min	f=0.04 mm/rev	d=0.25mm

The machining process was interrupted periodically in order to measure tool wear and surface roughness. Two sets of 524 data points each, one with a sample interval of 30 μ s and the other with 3.13ms, were taken from the vibration signal in each of the three orthogonal directions, just before each interruption. An extra two sets of data were also recorded between consecutive interruptions to provide more information for signal processing.

6.2.2 Development of Groove Wear

In order to describe quantitatively the development of groove wear at the minor cutting edge four parameters were selected, viz. the number of grooves at the minor cutting edge, the depth of grooves, the maximum length of grooves, and the groove wear area (defined as the product of the maximum groove length and the distance between the first and the last grooves on the minor flank). Nose wear was also selected due to its relevance to groove wear. Figures 6.2 to 6.6 show the measurement results of these wear parameters under all five cutting conditions. The surface roughness was plotted in Figure 6.7. All these data are listed in Appendix C for details.

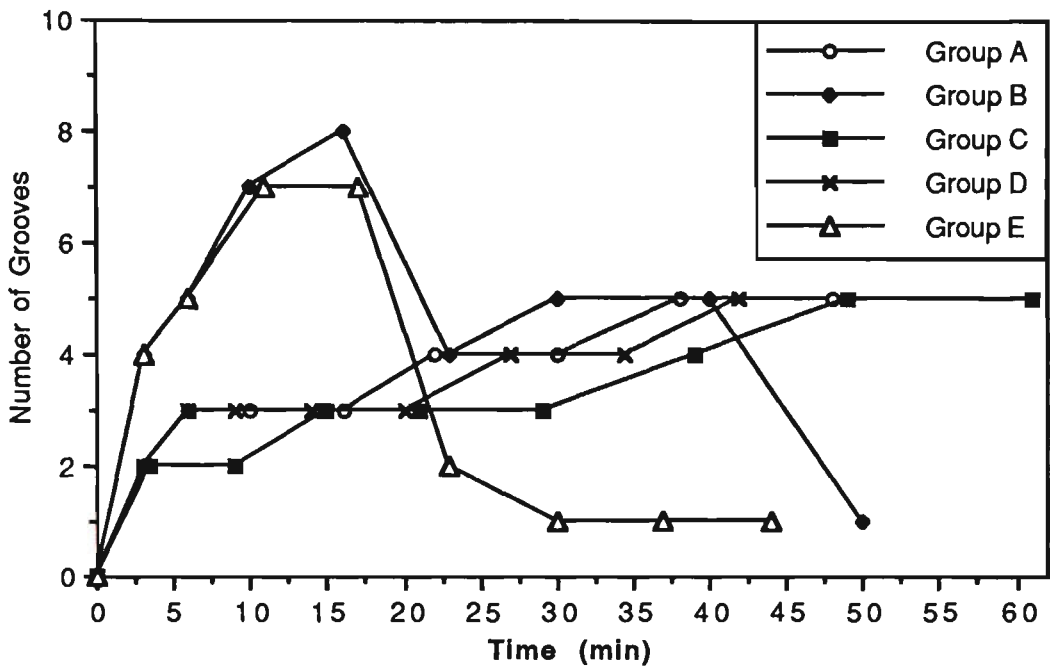


Figure 6.2 Number of grooves at the minor cutting edge

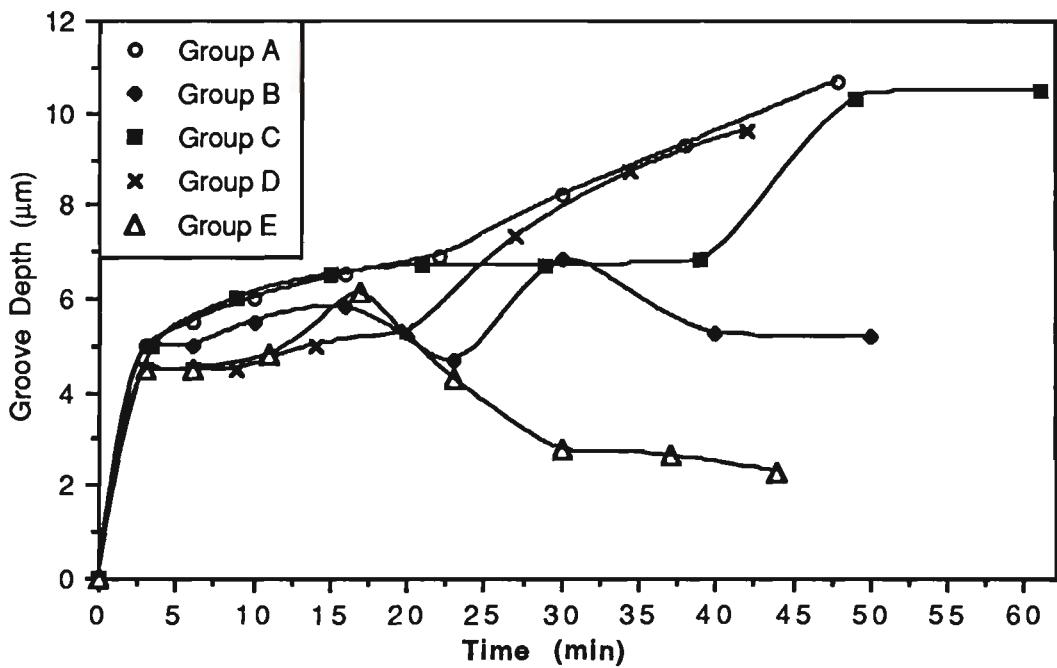


Figure 6.3 Development of groove depth

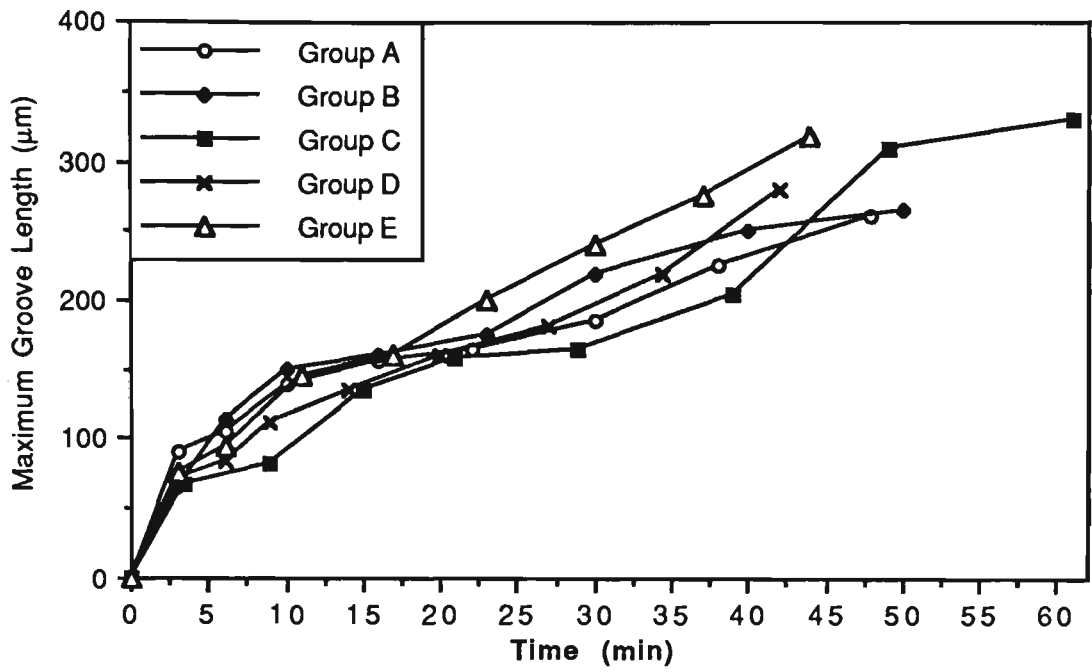


Figure 6.4 Development of the maximum groove length

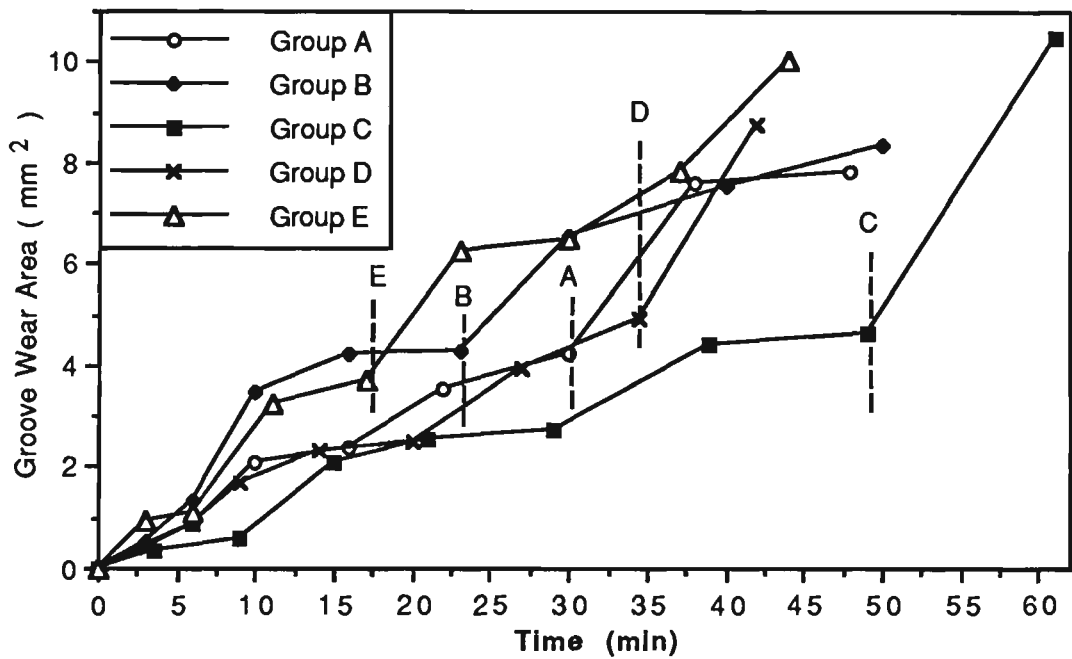


Figure 6.5 Development of groove wear area

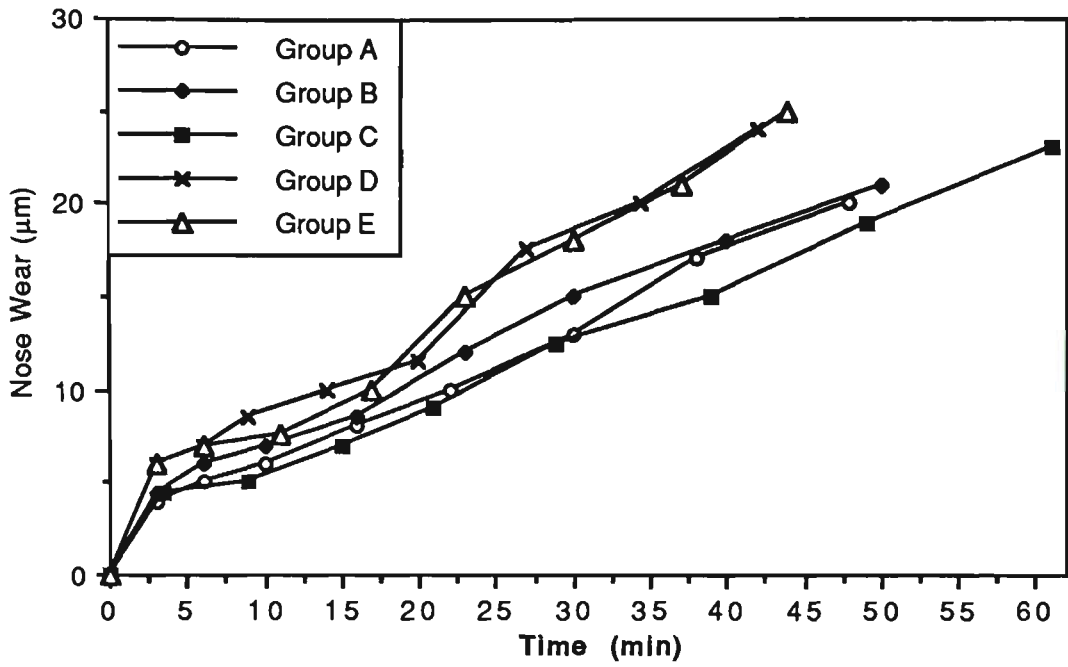


Figure 6.6 Development of nose wear

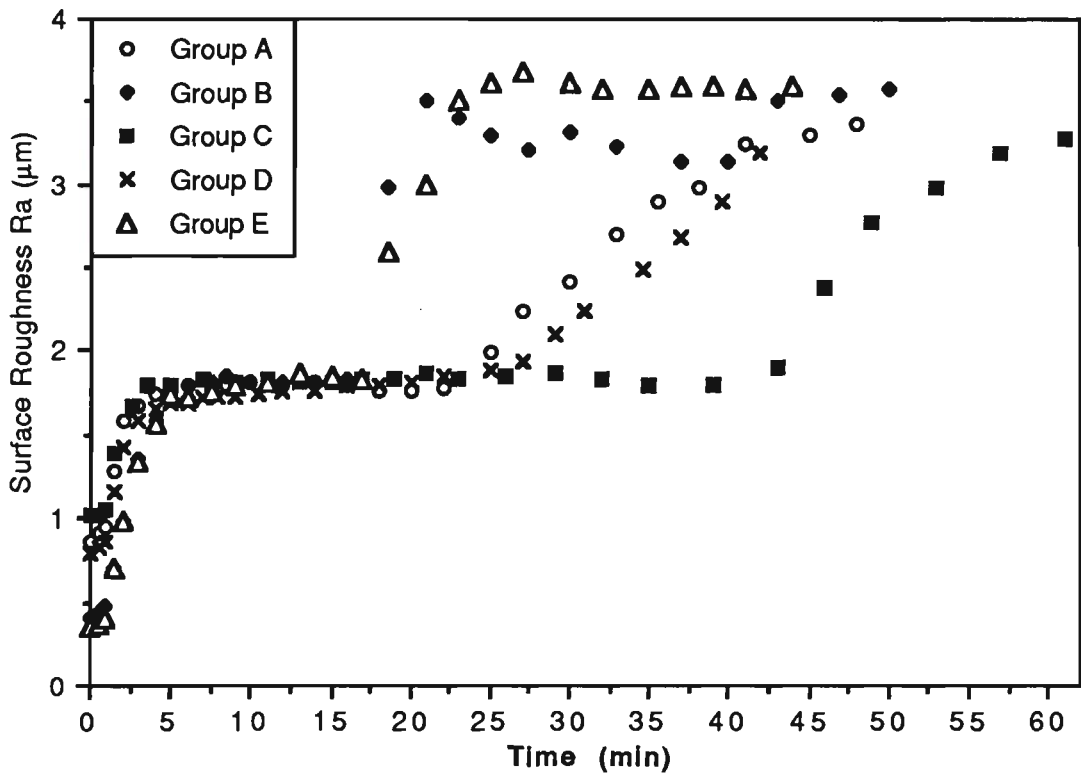


Figure 6.7 Surface roughness for five cutting conditions

6.2.3 Patterns of Groove Wear Development

From an analysis of the above figures, it is seen that two different groove wear patterns can be identified, one for the lower feed (0.04 mm/rev), designated as Groups B & E, and the other for higher feed (0.08 mm/rev), designated as Groups A, C & D. For the lower feed, it can be seen the number of grooves decreases at a certain point (Figure 6.2) and the surface finish deteriorates sharply at the same time (Figure 6.7). It is evident that the wipe-out of grooves causes the deterioration. It is also seen that the depths of grooves fluctuates for the low-feed Group B (Figure 6.3) because of the concurrence of the formation of new grooves and the wipe-out of formed grooves, while for the higher feed no decrease in the number of grooves nor a sharp increase in surface roughness are observed, even after machining for over 45 minutes (Figure 6.2). This may be due to the fact that the higher feed rate results in wider ridges between adjacent grooves, and thus in better wear-resistance.

It is consistently observed for all five cutting conditions that when the groove wear at the minor cutting edge has developed to a point at which tool failure is indicated, the major flank wear is still far below its critical value. Therefore, it can be concluded that the groove wear, once formed at the minor cutting edge, will largely dictate the tool life in finish-machining. A scanning electron microscope (SEM) was used for a more detailed analysis, with some results being shown in Figures 6.8 and 6.9.

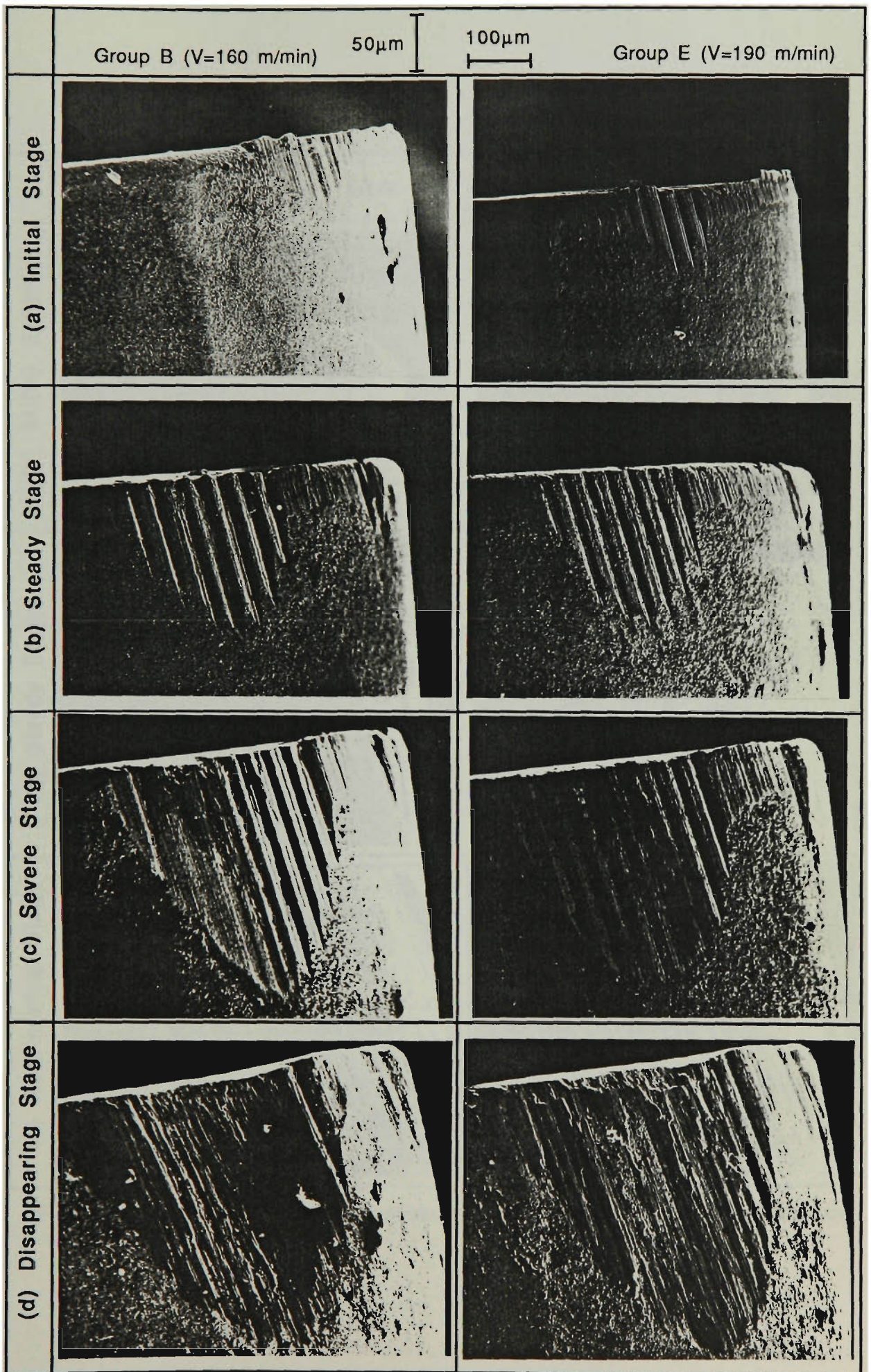


Figure 6.8 Groove wear development under the lower feed condition (0.04 mm/rev)

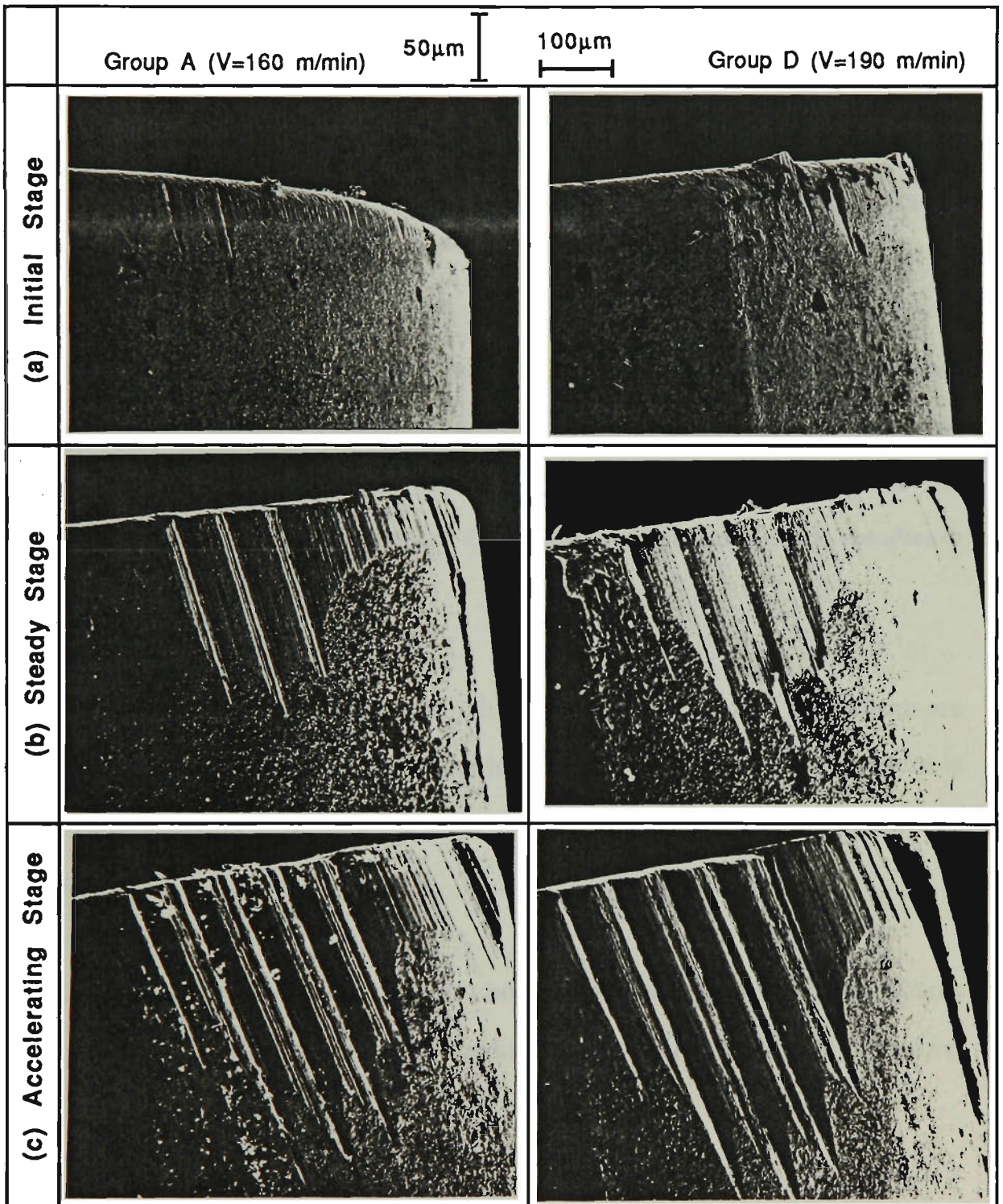


Figure 6.9 Groove wear development under the higher feed condition (0.08 mm/rev)

Lower feed (Groups B & E)

Four typical stages are found under the lower feed condition, as shown in Figure 6.8.

(a) *Initial stage* -- Before the grooves are formed, the surface roughness is mainly determined by the tool geometry of the fresh tool as well as the cutting conditions used, usually representing the best possible surface roughness condition in finish-machining.

(b) *Steady stage* -- In the next few minutes, the grooves will form at the minor cutting edge under certain machining conditions. Once these grooves are formed, the surface roughness will increase and largely depend on the depth of the grooves. As the depth of grooves develops slowly during this period, the surface roughness remains constant.

(c) *Severe stage* -- From Figure 6.8(c), it is clear that at this stage the grooves are being wiped out due to the induced vibration. When the regular groove pattern is disturbed, the surface roughness increases sharply, resulting in a very poor surface quality.

(d) *Disappearing stage* -- At this stage, most grooves have been wiped out and the minor flank face is left in a very rough condition and loses its function as a finishing tool.

Higher feed (Groups A, C & D)

For the higher feed, no decrease in the number of grooves occurs and three typical stages as shown in Figure 6.9 may be identified.

(a) *Initial stage* -- At this stage, groove wear development is similar to that under the lower feed, while the surface finish is poorer due to the higher feed used.

(b) *Steady stage* -- There seems to be no significant difference in surface roughness compared with the lower feed group. However, the grooves formed at the minor cutting edge are fewer due to the higher feed used.

(c) *Accelerating stage* -- Shown in Figure 6.9(c) is the accelerating stage of groove wear, during which the surface roughness (Figure 6.7) begins to increase quickly and soon becomes unsuitable for finish-machining. Viewed together with Figure 6.5, which shows the development of groove wear area, it is found that the starting point of rapid deterioration of surface finish always corresponds to the beginning of acceleration of the groove wear area, indicated by the dotted lines in Figure 6.5. Therefore, it is conjectured that the rapid increase of surface roughness at the high feed is due to the larger contact area between the tool minor flank and the machined workpiece surface.

6.3 ARV Model-based Multiple Dispersion Analysis

6.3.1 Application of Autoregressive Vector Time Series Modelling

Autoregressive vector time series models were developed to quantify statistically the dynamics embedded in the 3-D vibration data. It has been shown in Chapter 5 that the merit of employing such a technique lies in the fact that it provides a mathematical model primarily based on the observed data, and does not require much a prior knowledge or assumptions about the underlying system dynamics. The vibration

signals, recorded in three orthogonal directions and sampled at uniform intervals, can be represented in the form of vector difference equations, i.e. either in an explicit Green's function or in a stochastic ARV(n) model with autoregressive order n [35] :

$$\mathbf{X}_t = \sum_{k=1}^n \Phi_k \mathbf{X}_{t-k} + \mathbf{a}_t \quad \text{or} \quad \mathbf{X}_t = \sum_{k=0}^{\infty} \mathbf{G}_k \mathbf{a}_{t-k} \quad (6.1)$$

where $\mathbf{X}_t = [X_{1t}, X_{2t}, X_{3t}]^T$ and $\mathbf{a}_t = [a_{1t}, a_{2t}, a_{3t}]^T$.

In this way, the observed trivariate series, $X_{1t} = V_{xt}$ = vibration in the feed direction, $X_{2t} = V_{yt}$ = vibration in the thrust direction, and $X_{3t} = V_{zt}$ = vibration in the main cutting direction, are expressed either as linear combinations of past observation vectors \mathbf{X}_{t-k} with parameter matrices Φ_k 's ($k=1, 2, \dots, n$) plus the white noise \mathbf{a}_t , or in terms of the Green's function \mathbf{G}_k by convolution with the white noise vectors \mathbf{a}_{t-k} [35, 93].

6.3.2 Multiple Dispersion Analysis

In Chapter 5 the use of dispersion analysis provides an effective means for quantitative model decomposition in order to identify particular variations convolved in the recorded data of 3-D dynamic cutting force. Since the formation of groove wear may stem from complex interactions among all three dimensional vibrations and much about it is still not clear, multiple dispersion analysis is used to quantify not only the

contribution of individual variables, but also the interactions among different variables. Using the explicit Green's function of Equation 6.1, the vector auto-covariance matrix $\gamma_{0\text{-vec}}$ can be determined as follows :

$$\gamma_{0\text{-vec}} = E [\mathbf{X}_t \cdot \mathbf{X}_t^T] = \sum_{k=0}^{\infty} \mathbf{G}_k \cdot \sigma_a^2 \cdot \overline{\mathbf{G}_k}^T \quad (6.2)$$

where σ_a^2 is the residual matrix and $\overline{\mathbf{G}_k}$ is the complex conjugate of \mathbf{G}_k . It has been shown that the explicit Green's function can be obtained from the established ARV(n) model under the assumption of distinct eigenvalues [93] as follows,

$$\mathbf{G}_k = \sum_{i=1}^n \mathbf{T}_i \lambda_i^{k+n-1} \mathbf{U}^{-1} \mathbf{U}_i \mathbf{T}_i^{-1} \quad (6.3)$$

$$\text{where } \mathbf{U} = \prod_{i,j=1 \ \& \ i>j}^n (\lambda_i - \lambda_j) \text{ and } \mathbf{U}_i = (-1)^i \prod_{i,j=1 \ \& \ i>j \ \& \ i,j \neq k}^n (\lambda_i - \lambda_j)$$

The eigenvalue matrices $\lambda_i = \text{diag}[\lambda_{xi}, \lambda_{yi}, \lambda_{zi}]$ and eigenvector matrix \mathbf{T}_i , $i=1, \dots, n$, are found by adjoining the parameter matrices Φ_k 's of the ARV(n) model, and finally the following form of the equation for a symmetric vector auto-covariance matrix $\gamma_{0\text{-vec}}$ can be derived:

$$\gamma_{o\text{-vec}} = \begin{bmatrix} \gamma_{\text{Oxx}} & \gamma_{\text{Oxy}} & \gamma_{\text{Oxz}} \\ & \gamma_{\text{Oyy}} & \gamma_{\text{Oyz}} \\ & & \gamma_{\text{Ozz}} \end{bmatrix} = \begin{bmatrix} \sum_{i=1}^n \sum_{j=i}^n D_{\text{ixxj}} & \sum_{i=1}^n \sum_{j=1}^n D_{\text{ixyj}} & \sum_{i=1}^n \sum_{j=1}^n D_{\text{ixzj}} \\ & \sum_{i=1}^n \sum_{j=i}^n D_{\text{iyyj}} & \sum_{i=1}^n \sum_{j=1}^n D_{\text{iyzj}} \\ & & \sum_{i=1}^n \sum_{j=i}^n D_{\text{izzj}} \end{bmatrix} \quad (6.4)$$

Thus the vector auto-covariance of the entire process is decomposed into the contributions of process eigenvalues as well as the complex interactions among various eigenvalues in terms of multiple dispersion D_{ixxj} , D_{ixyj} , etc. Of particular interest are the multiple dispersions corresponding to the complex eigenvalues which reflect the oscillating characteristics of the machining process.

6.4 STRATEGY FOR GROOVE WEAR MONITORING BY MULTIPLE DISPERSION ANALYSIS

The 3-D vibration signals were modelled as a stochastic ARV(n) model. The multivariate time series analysis and the results of multiple dispersion analysis are presented below in relation to the detection and monitoring of groove wear development at the minor cutting edge.

6.4.1 Groove Wear Monitoring for the Lower Feed Condition

Three distinctive dispersions were found as being related to the development of groove wear, as shown in Figure 6.10 for Group B as a representative of the lower feed condition (0.04 mm/rev). The first two patterns are associated with high-frequency dispersions. One is the dispersion in the thrust direction (D_{yy}) at around 9.3 KHz and

another is that in the main cutting direction (D_{zz}) at around 2.5 KHz. It was found that when the number of grooves decreased from about 16 to 23 minutes (Figure 6.2), D_{yy} and D_{zz} reached their maximum values, signifying the severe vibration occurring under these frequencies. The third pattern is the cross-dispersion D_{yz} in the low-frequency range between the vibrations in the thrust direction at 150Hz and the main cutting direction at 145Hz (Figure 6.10). The moment at which D_{yz} reaches its peak value also matches with that when the number of grooves decreases and the roughness deteriorates rapidly. If one compares the times of peak dispersions, it is seen that D_{yy} occurred at about 19 minutes and D_{zz} and D_{yz} at about 22 minutes. This may indicate that vibration is first induced in the thrust direction which disturbs the regular grooves formed. The disturbed minor cutting edge in turn excites vibration in the main cutting direction. Therefore, the following criterion can be established: the peak value of D_{yy} indicates the commencement of groove wipe-out, while those of D_{zz} and D_{yz} indicates the ending of groove wipe-out. This criterion can be used in finish-machining to determine the necessity of tool replacement for the lower feed condition.

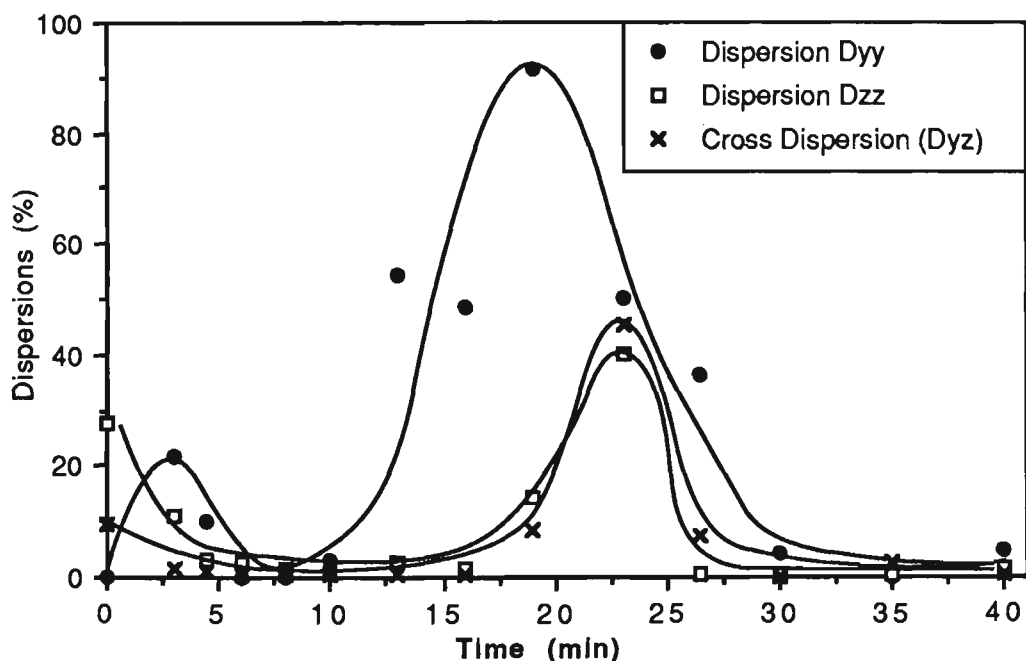


Figure 6.10 Dispersion patterns for the lower feed condition (0.04 mm/rev)

6.4.2 Groove Wear Monitoring for the Higher Feed Condition

For this condition, the dispersion pattern found is totally different from that for the lower feed, due to the difference in groove wear development. A clear concave trend shown in Figure 6.11 was found for the dispersion in the thrust direction, with the frequency equal to about 9.4 KHz. By comparing the surface roughness development (Figure 6.7) with the above dispersion pattern, it is seen that consistency exists between them, as summarised in Table 6.2.

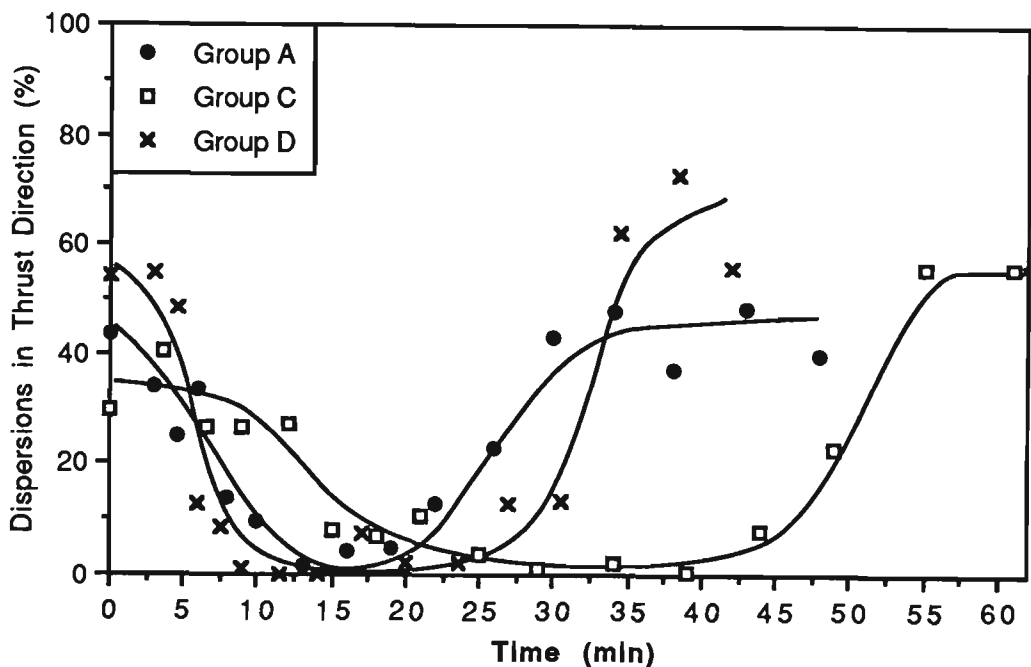


Figure 6.11 Dispersion patterns for the higher feed condition (0.08 mm/rev)

Based on the analysis in Table 6.2, it can be concluded that the behaviour of the dispersion in the thrust direction (9.4 KHz), isolated from the 3-D vibration variations, resembles the rate (slope) of the surface roughness development shown in Figure 6.7. Thus this dispersion could be used as an index for the severity of groove wear at the minor cutting edge under higher feed conditions.

Table 6.2 Relationship between surface roughness and dispersion pattern

Groove Wear Development	Changes of Surface Roughness for the Higher Feed Group	Dispersion Pattern around the Natural Frequency of Tool/Holder Assembly
Initial Stage	increasing rapidly due to the normal tool running-in	appearing in high values during tool running-in period
Steady Stage	remaining constant as the groove depth develops slowly	decreasing to the minimum due to smaller variations involved in the thrust vibration signals
Accelerating Stage	starting to accelerate due to the severity of groove wear indicated by the acceleration of groove wear area (Fig. 6.5)	increasing to the high-value again due to the changes in thrust vibration caused by the severe groove wear

6.5 PHYSICAL INTERPRETATIONS

Clear patterns have been identified relating the vibration in terms of multiple dispersions and corresponding frequencies to the different stages of groove wear development. For the lower feed condition (0.04 mm/rev), more grooves are formed and earlier vibration is induced, giving rise to worse surface finish, while the higher feed condition (0.08 mm/rev) appears to have better wear-resistance. The difference between the lower and higher feed conditions lies in the fact that for a selected tool geometry, the feed becomes a dominant factor to determine the grooves' spacing at the minor cutting edge. It is noticed that, in the case where grooves are formed, the lower feed condition does not produce better surface finish.

For both conditions the dispersion analysis results, based on the stochastic model developed from the experimental data directly, indicate that groove wear development finds its reflection mainly in the thrust vibration. This can be explained as follows. This vibration, i.e. the relative displacement between the workpiece and the tool tip in the radial direction, is a compound effect of the workpiece lateral dynamics and the tool/tool holder dynamics. In the analysis for the lower feed condition it was shown that the dispersions of the thrust vibration reached their peaks at about 150 Hz and 9,300 Hz respectively, with the higher one dominant when the number of grooves began to decrease, that is, the surface roughness began to deteriorate rapidly. These frequencies, as expected, correspond to the natural frequencies of the workpiece and tool/holder assembly, which were determined to be around 155 Hz and 9,340 Hz, respectively, by using conventional excitation tests. These close agreements may indicate that, when a sufficient number of grooves have been formed, the dynamics of the cutting process is excited, so that more severe vibration at the characteristic frequencies is induced.

Similar results were obtained in the dispersion analysis of vibration in the main cutting direction. For the high feed condition, the dispersions in the thrust direction around the natural frequency of tool/holder assembly were again found closely related to the surface roughness development determined by the severity of groove wear at the minor cutting edge. Table 6.3 summarises these physical interrelationships.

Table 6.3 Comparison between dispersion analysis results and physical quantities

For the Lower Feed Condition (0.04 mm/rev)				
	Peak Frequencies detected by using Dispersion Analysis when the number of grooves began to decrease		Natural Frequencies determined by using conventional excitation tests	
Vibration Direction	in the range of low frequency	in the range of high frequency	workpiece system	tool/holder assembly
Thrust	150 Hz	9,300 Hz	155 Hz	9,340 Hz
Main Cutting	145 Hz	2,500 Hz	155 Hz	2,610 Hz
For the Higher Feed Condition (0.08 mm/rev)				
	Characteristic Frequency of Dispersion which resembles the rate of Surface Roughness		Natural Frequency of the tool/holder assembly	
Thrust Vibration	9,400 Hz		9,340 Hz	

6.6 SUMMARY AND CONCLUDING REMARKS

- (1) The purpose of this chapter is to investigate the relationships between off-line measurements of groove wear at the minor cutting edge and the multiple dispersion analysis based on the multivariate time series models of 3-D vibration in finish-machining, such that the latter alone will be capable of on-line monitoring of groove wear development at the minor cutting edge.
- (2) The development patterns of groove wear at the minor cutting edge and the associated surface roughness were investigated under typical cutting conditions. It was found that if a finish-machining condition under which grooves will form at

the minor cutting edge is used, the feed is the dominant factor in determining the development patterns of groove wear.

- (3) Multiple dispersion analysis of the 3-D vibration has been proven to be effective in detecting the critical points at which either the surface finish deteriorates sharply due to the wiping-out of grooves at the minor cutting edge, or the acceleration of surface roughness induced by the rapid increase of groove wear area occurs. The criteria derived from the dispersion analysis are all based on the frequencies which can be physically interpreted. Although these frequencies may vary for different workpiece geometries, and tool/tool holder assemblies, they are not difficult to determine.
- (4) The results of this work further emphasise that groove wear at the minor cutting edge may occur during finish-machining under a fairly wide range of cutting conditions for the commonly-used cutting tools and work materials. Should grooves be formed, the life of the finishing tool will be significantly shortened.
- (5) The monitoring method presented in this chapter offers one avenue by which surface finish may be controlled in automated finish-machining, as an essential component of product quality assurance.

CHAPTER 7

INTEGRATING CHIP CONTROL AND TOOL WEAR ESTIMATION THROUGH NEURAL NETWORKS FOR THE ON-LINE ASSESSMENT OF MACHINING PERFORMANCE

7.1 INTRODUCTION

Chip control and tool wear estimation are closely interrelated during machining processes. Although much work has been done on the analysis and prediction of chip forming patterns including chip shapes and chip breaking in machining [2, 40, 50, 94-95], all assumed ideal machining conditions, i.e. machining with *unworn* cutting tools. It is also known that present theories concerning chip formation in machining and available machinability databases are all established based on unworn tools. In actual machining processes, however, the chip forming patterns vary significantly with tool wear progression, thus resulting in unpredictable performance of the machining operation. In this sense, a truly effective chip control system should not only be capable of predicting chip forming patterns off-line, but also updating them on-line as tool wear develops in the machining process.

During the machining process tool wear formed at different tool faces alters the original tool configuration/geometry, which, in turn, greatly influences chip forming patterns. Therefore, in order to assess chip forming patterns with wear progression, an effective estimation strategy for tool wear at different tool faces is a prerequisite. In Chapter 5, dispersion analysis of 3-D dynamic cutting force derived from multivariate time series models has proven particularly effective for comprehensive tool wear estimation, i.e. more than one type of wear can be estimated simultaneously, thus

providing a possible basis for predicting chip forming patterns during tool wear progression.

Since the interrelationship between chip forming patterns and tool wear progression is extremely complex and the present machining theories are inadequate to describe it analytically, some kind of "black-box" approach becomes appealing, even necessary, for tackling the problem.

One such approach, neural networks, has been applied recently in machining process monitoring or control [11-12, 37-38]. Rangwala and Dornfeld [11] demonstrated the feasibility of using neural networks to integrate information from acoustic emission and force sensors to monitor flank wear, where the features from power spectra were extracted as the inputs to neural networks. In subsequent work, Dornfeld [12] developed a neural network-based tool wear monitoring system by incorporating autoregressive time series model parameters. Chryssolouris and Domroese [37] performed a simulation system to evaluate the learning ability of neural networks and highlighted the use of neural networks as the decision-making component in an intelligent tool wear monitoring system. Rangwala and Dornfeld [38] presented a method for optimising machining conditions based on the neural network architecture, which has shown that the neural network can learn and synthesise knowledge effectively by observing the input variables of cutting conditions and the output variables of cutting force, power, temperature and surface finish.

Therefore, neural networks provide a new approach to resolve a complicated problem through learning by being shown and synthesising knowledge from the observed input and output variables of the process under investigation.

For the chip forming pattern problem, chip shapes produced are observable and readily collectable, while tool wear can be estimated with higher certainties by the monitoring strategy developed in Chapter 5. Therefore, employing neural network techniques, which model a complicated process by extracting knowledge largely based on experimental input-output data, would be feasible to correlate dynamic chip forming patterns with tool wear progression. In addition, once it is trained off-line, the established network algorithm can be implemented on-line.

In Chapter 2, it has been shown that prediction of chip breaking/shapes under the condition of unworn cutting tools can be achieved through a fuzzy membership function ranging from 0 to 1, which provides the initial estimation of chip forming patterns. Neural networks are then trained based on the recorded data of chip breakability/surface roughness in finish-machining with tool wear progression. The latter is characterised by four features extracted from multivariate time series models of 3-D dynamic cutting force signals. Using the results derived from neural network modelling, together with the comprehensive tool wear estimation, an integrated assessment of machining performance may be achieved, which includes chip breaking and chip shapes, surface finish and tool wear states.

7.2 DESCRIPTION OF MACHINING EXPERIMENTS

7.2.1 Machining Conditions

A series of machining experiments concerning chip breaking and chip shapes, surface finish and tool wear was carried out under finish-machining conditions to obtain the data needed for training and testing the neural network to be established. Shown in Table 7.1 are the machining conditions used in the experiments. The cutting

conditions are organised into two groups, i.e. training and testing. The degraded tool tests, viz. using a relatively softer tool as recommended in [86], are adopted to shorten the time-consuming and costly tool wear experiments.

Table 7.1 Machining conditions used in the experiments

Machine Tool	Colchester Mascot 1600 (9.3 KW)	
Tool Insert Type	TNMA160408F (flat-faced tool)	
Tool Material	Carbide : Grade 883, SECO	
Tool Geometry	0°, 5°, -6°, 90°, 60°, 0.8	
Work Material	AISI4140 (BHN=275-320)	
Depth of Cut	d = 0.5 mm	
Cutting Speed and Feed		
	Training Group	Testing Group
	1. V=115 m/min f=0.1 mm/rev	1. V=140 m/min f=0.12 mm/rev
	2. V=145 m/min f=0.1 mm/rev	2. V=165 m/min f=0.06 mm/rev
	3. V=145 m/min f=0.06 mm/rev	3. V=190 m/min f=0.06 mm/rev
	4. V=205 m/min f=0.06 mm/rev	4. V=130 m/min f=0.15 mm/rev
	5. V=170 m/min f=0.10 mm/rev	
	6. V=160 m/min f=0.15 mm/rev	

7.2.2 Comprehensive Tool Wear Patterns

Based on Chapter 5, patterns of major flank, crater and minor flank wear were considered as they reflect the overall tool wear situation and largely influence tool configuration/geometry and the surface quality of a finished product. Patterns of major flank wear VB, crater wear (depth) KT and minor flank wear VB' are summarised and typical results with Training Cutting Condition 1 as representatives are plotted in Figure 7.1.

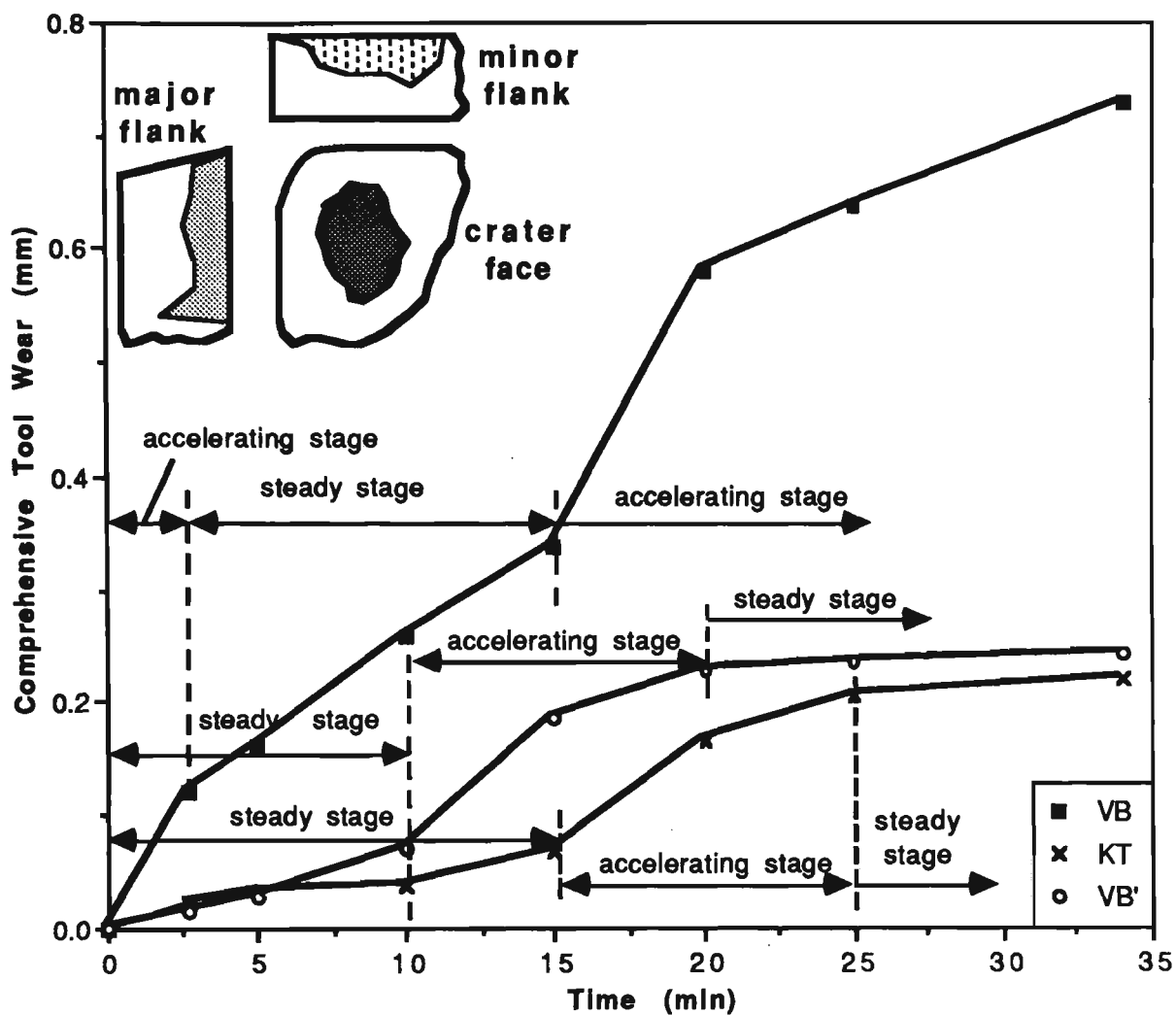


Figure 7.1 Development patterns of comprehensive tool wear

7.2.3 Chip Breakability Assessment

Chip breakability was assessed by using the fuzzy membership function according to the chip shapes/sizes produced in the machining process. Figure 7.2 illustrates the change of chip shapes/sizes with cutting time under Training Cutting Condition 1, and Table 7.2 gives the description of these chips and the corresponding fuzzy membership values assigned.

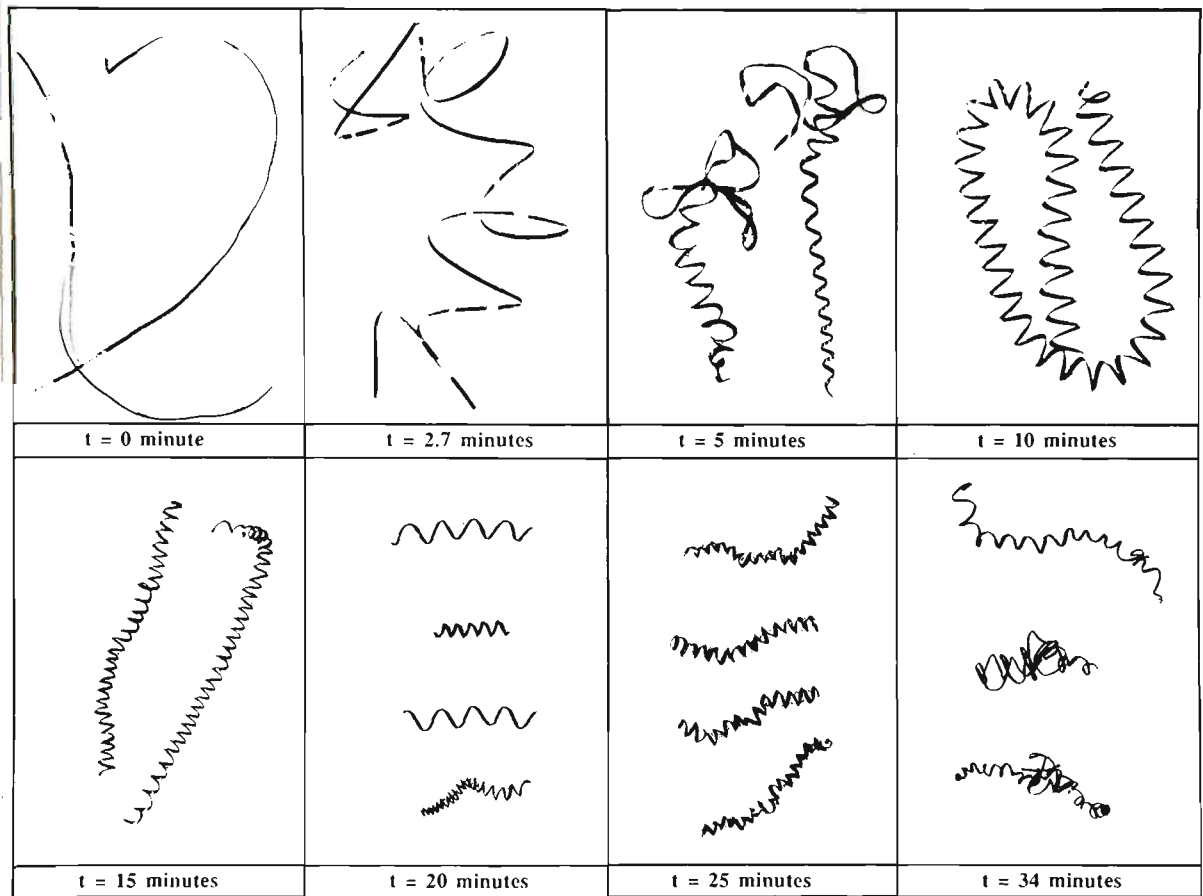


Figure 7.2 Change of chip shapes/sizes with tool wear progression

Table 7.2 Chip forming behaviour in machining process while tool wear

TIME (min)	CHIP SHAPES/SIZES	CHIP BREAKABILITY (MEMBERSHIP VALUE)
0	long and continuous ribbon chips	0.25
2.7	curved ribbon chips	0.30
5	combination of ribbon and continuous cork-screw chips	0.32
10	long and continuous cork-screw chips	0.35
15	long but broken cork-screw chips	0.41
20	short to medium size chips	0.58
25	distorted medium size chips	0.46
34	heavily distorted long but broken chips	0.42

As is seen from Fig 7.2 and Table 7.2, it is clear that tool wear has a significant effect on chip forming behaviour. This is largely due to the fact that when tool wear develops, tool configuration/geometry changes accordingly. In the initial stage of machining, long and continuous chips form, because the tool insert used has no chip breaker. With the increase of machining time, tool wear causes the change of tool configuration/geometry. In particular, the formation of crater wear on the tool rake face acts as a groove-type chip breaker and thus increases chip breakability. As crater wear grows larger its effect as the chip breaker becomes more significant until a fully-utilised chip breaker is realised which breaks chips in the most effective way as seen at $t = 20$ minutes. Further growth of crater wear oversized the chip breaker, resulting in the increase of chip curling curvature which lowers chip breakability. The change of chip breakability as tool wear develops has been observed being consistent under all cutting conditions used, as shown in terms of fuzzy membership values in Figure 7.3 for Training Cutting Conditions 2 to 6.

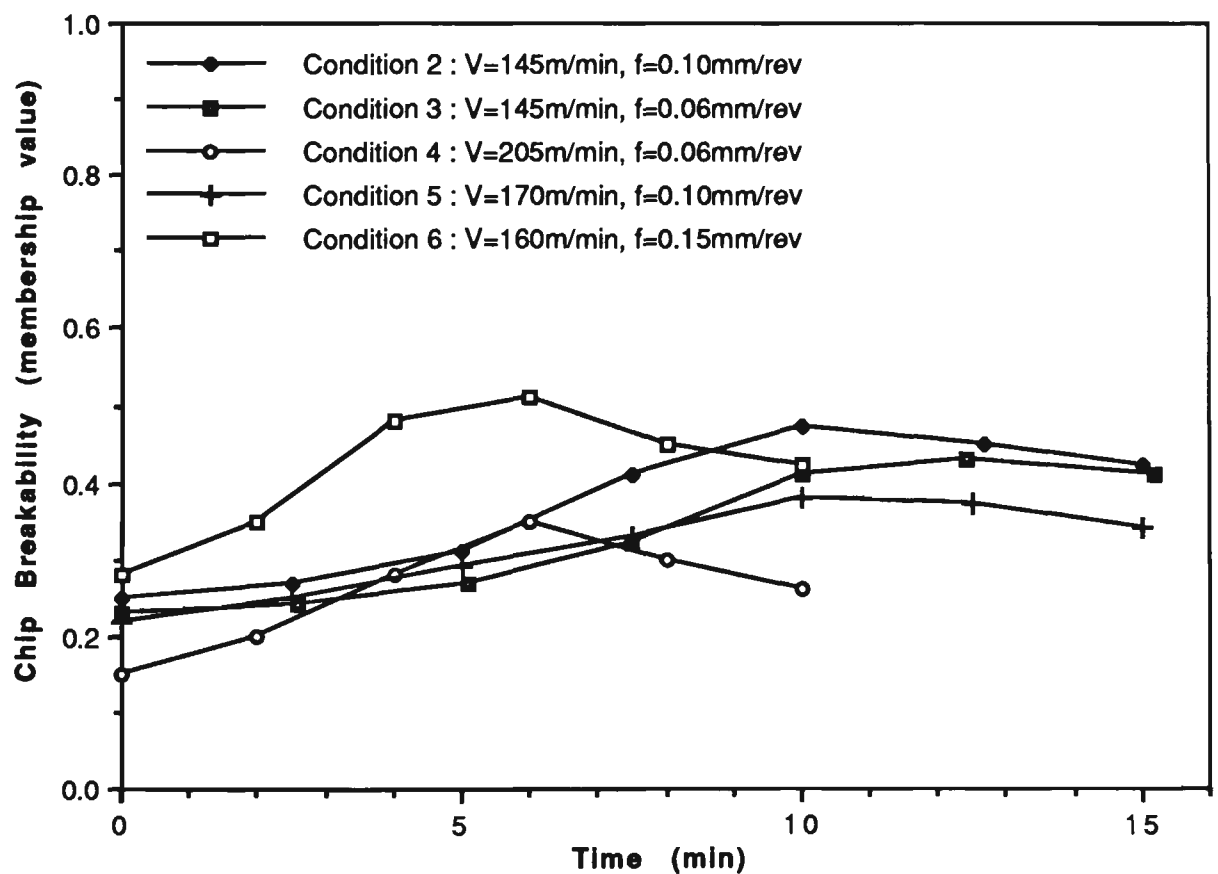


Figure 7.3 Change of chip breakability under Training Cutting Conditions 2-6

Although the above analysis clearly confirms the interrelationship between chip forming patterns and tool wear progression, its analytical modelling proves prohibitively difficult, even impossible. In order to predict the chip forming patterns, a quantitative description is required, which highlights the need for introducing the modelling by neural networks.

7.2.4 Surface Finish Assessment

Surface finish was assessed by the arithmetic mean deviation, R_a , with the use of a portable surface measurement instrument. Although surface finish can be predicted theoretically with some accuracy, its development depends heavily on the severity of tool wear during the machining process, as shown in Figure 7.4 for Training Cutting Condition 1. Compared with the tool wear development shown in Figure 7.1, it is noticeable that the significant increase of surface roughness corresponds to the acceleration stage of minor flank wear.

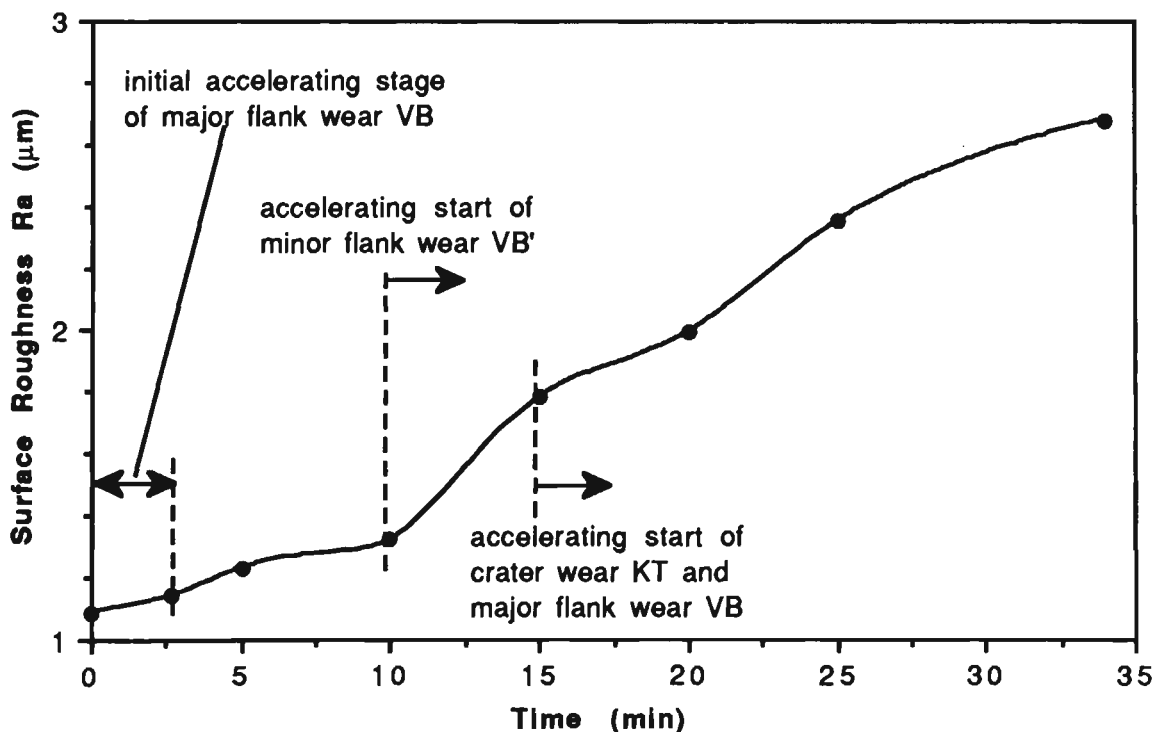


Figure 7.4 Change of surface finish with tool wear rates for Training Cutting Condition 1

Similar results were obtained under Training Cutting Conditions 2 to 6, as shown in Figure 7.5.

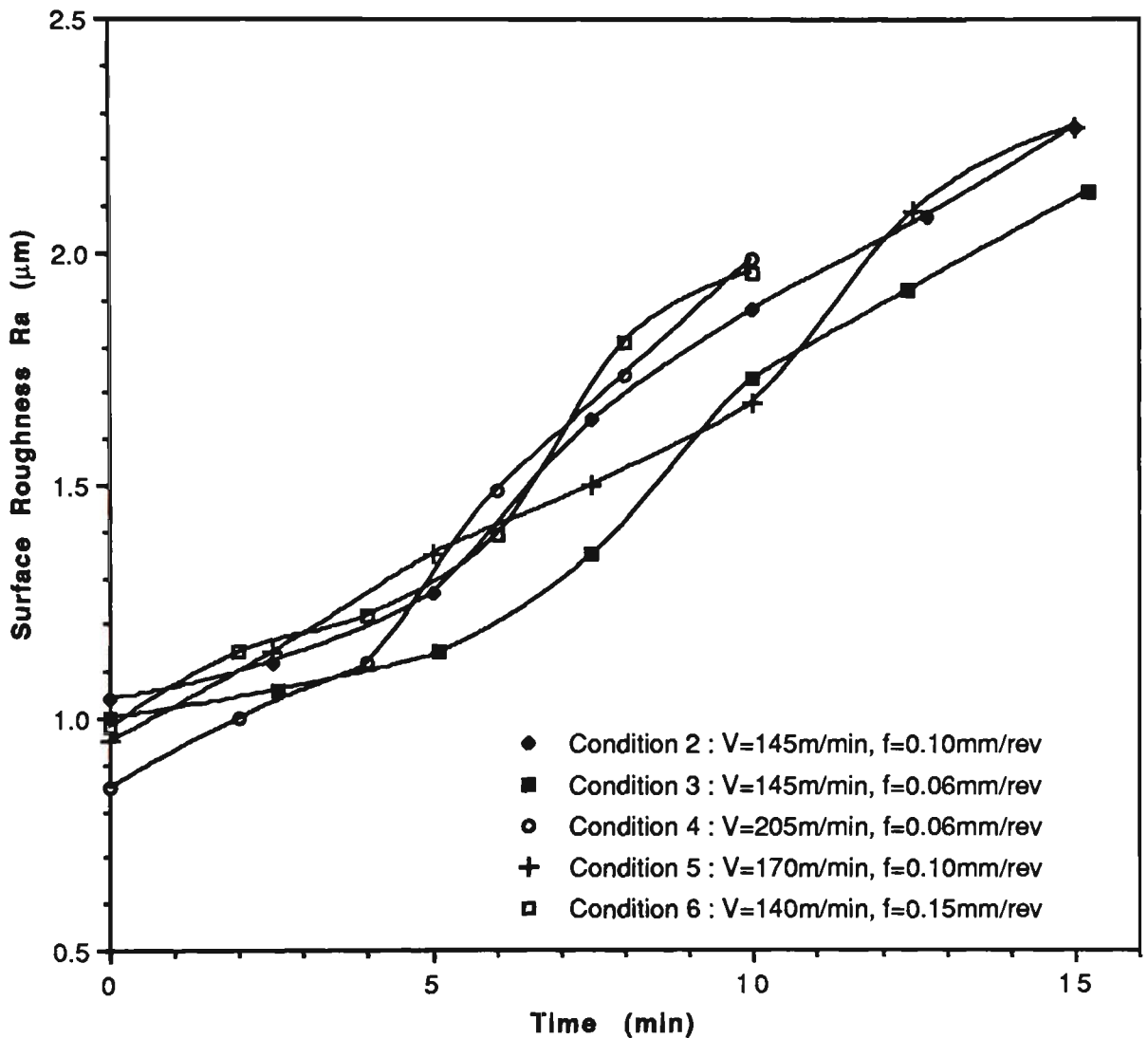


Figure 7.5 Development of surface finish for Training Cutting Conditions 2-6

7.3 FEATURE EXTRACTION FROM 3-D DYNAMIC CUTTING FORCES

In Chapter 5, dispersion analysis based on multivariate time series models has proven to be effective to single out particular features in the 3-D dynamic cutting force signals

corresponding to particular types of tool wear. Four dispersion features extracted from dynamic components of 3-D cutting forces are found to correlate reliably with various types of tool wear development under all training and testing cutting conditions (Table 7.1). The results are summarised below.

The eigenvalues appearing in complex conjugate pairs are of particular interest because they contribute to the oscillating variation of the process. Two dominant percentage dispersions, one in low frequency (LF) related to the idle frequencies of machine-tool and the other in high frequency (HF) related to the natural frequencies of the tool-holder/dynamometer system, are found to exhibit patterns in agreement with wear rate patterns including major flank wear VB, crater wear KT and minor flank wear VB'. As a summary, the relationship between wear rate patterns and dispersion development patterns is shown in Figure 7.6.





TOOL WEAR TYPES	TOOL WEAR RATE PATTERNS			DESCRIPTIONS OF DISPERSION DEVELOPMENT PATTERNS
	Stage I	Stage II	Stage III	
major flank wear (VB)	accelerating	steady	accelerating	D_x (LF) of feed force 
crater wear (KT)	steady	accelerating	steady	D_y (HF) of thrust force 
minor flank wear (VB')	steady	accelerating	steady	D_x (HF) of feed force  D_z (HF) of main cutting force 

Figure 7.6 A typical relationship between tool wear and dispersion patterns

7.4 ARCHITECTURE OF NEURAL NETWORKS

7.4.1 Neural Network Techniques Used

By imitating the computational architecture of the human brain and implementing it into software/hardware, neural networks are capable of learning to recognise non-linear and complicated input-output relationships. Back-propagation (BP) is the most widely used learning algorithm for multilayered feed-forward neural networks [96-98]. BP neural networks can be used to attack any problems that require pattern mapping, i.e., given the input pattern, the network produces the associated output. Once the network has learned the pattern mapping from the input-output training set, for any new or previously unrepresented input it will be capable of producing an output pattern based on the knowledge derived from the recognised input-output relationship.

The typical BP neural network employs one hidden layer of artificial neurons fully connected through weights to the input and output layers. The significance of using the hidden layer is that it allows the non-linear mappings between input and output patterns. Shown in Figure 7.7 is a three-layer neural network with N inputs, M hidden neurons and L output neurons.

In Fig. 7.7, the forward propagation takes place first after an input pattern is presented at the input layer. The errors, i.e. the differences between the output pattern ($O_j, j=1, 2, \dots, L$) and target pattern ($T_j, j=1, 2, \dots, L$) are calculated for all neurons in the output layer and propagated back through the network to update their coming weights. Next an error value is calculated for all the neurons in the hidden layer and the weights are adjusted for all interconnections coming from the input layer. This process is

repeated until the output pattern is close enough to the target pattern or until the error is within the convergence criterion determined in advance. The bias is connected to each neuron in the hidden and output layers and is used to adjust the activation threshold of the artificial neurons during the training process.

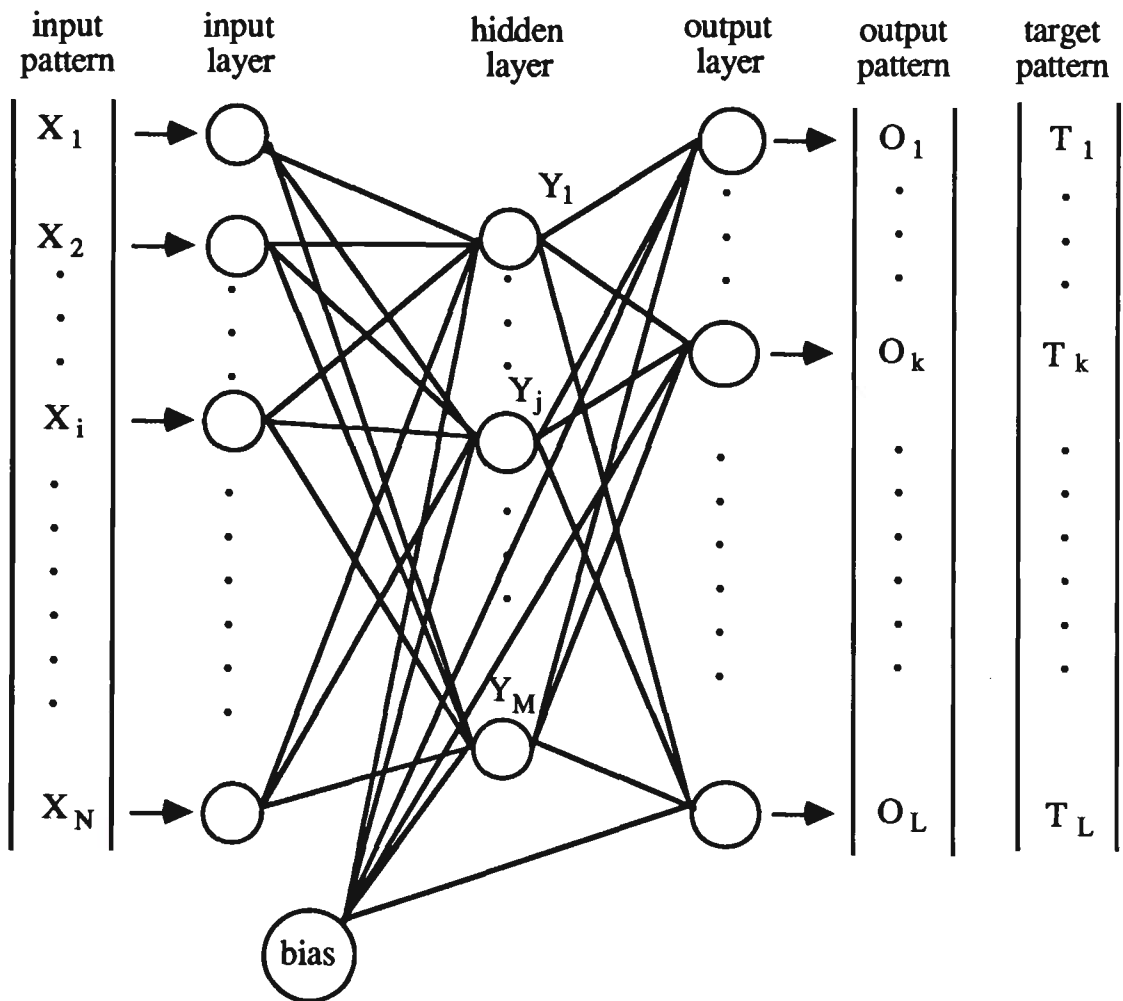


Figure 7.7 Back-propagation neural network with one hidden layer

The function of a neuron in the hidden layer and output layer is shown in Figure 7.8.

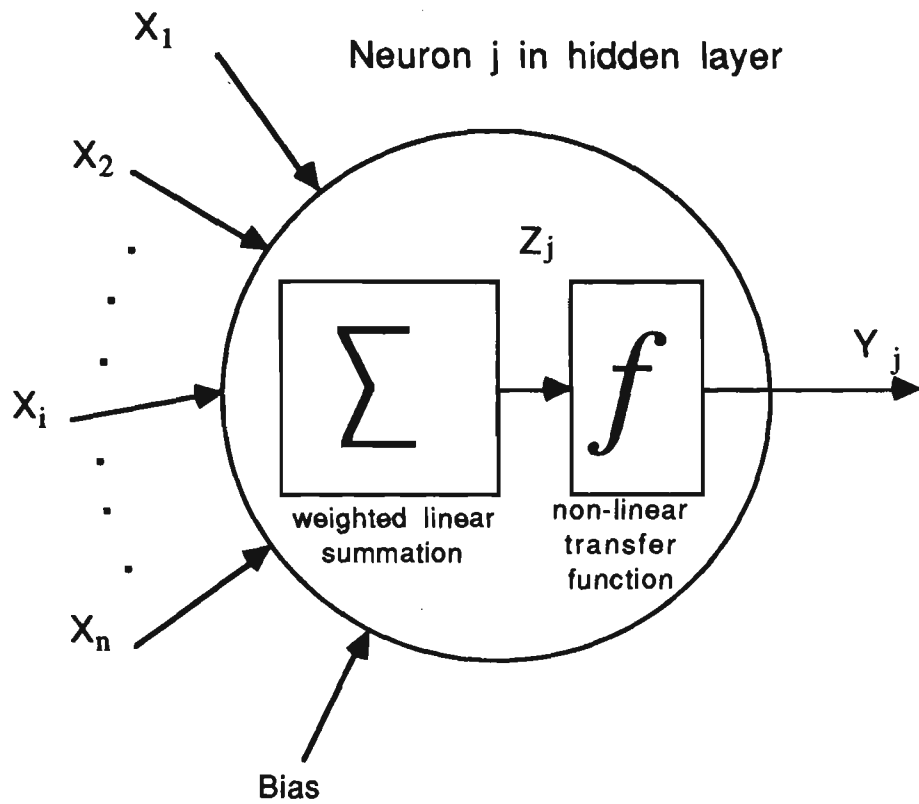


Figure 7.8 The function of artificial neuron

In Fig. 7.8, the total input X_1, \dots, X_n to Neuron j is a weighted linear summation, i.e.,

$$Z_j = \sum_{i=1}^n W_{ji} \cdot X_i + B_j \quad (7.1)$$

where W_{ji} is the weight from the i th input to Neuron j and B_j is the bias of the Neuron j . Then a real output value from Neuron j is activated by a non-linear transfer function $f(Z_j)$,

$$Y_j = f(Z_j) = f\left(\sum_{i=1}^n W_{ji} \cdot X_i + B_j\right) \quad (7.2)$$

There are many transfer functions which might be implemented in the BP neural network, which only requires the functions be differentiable everywhere [97]. Figure 7.9 describes three commonly used non-linear transfer functions.

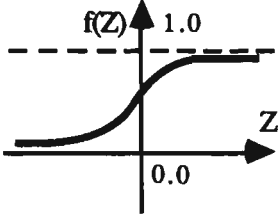
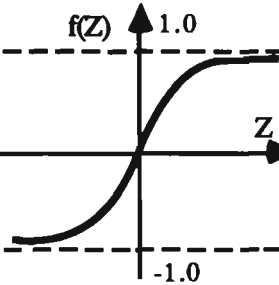
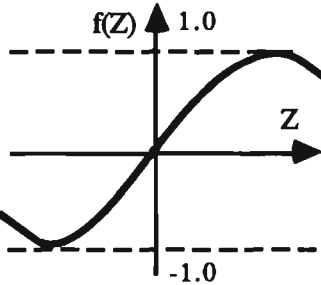
NAME	Sigmoid	TanH (Hyperbolic Tangent)	Sine
TRANSFER FUNCTION	 $f(z) = \frac{1}{1 + e^{-z}}$	 $f(z) = \frac{e^z - e^{-z}}{e^z + e^{-z}}$	 $f(z) = \text{SIN}(z)$

Figure 7.9 Description of three basic transfer functions

7.4.2 Selection of Input Features

The appropriate selection of input features is vital to the success of neural networks and depends on the thorough understanding of the problem in question. As described before, chip breakability and surface finish change with tool wear progression, and therefore the features selected should be sensitive to the specific wear types which influence the chip breakability and surface finish. Major flank wear and crater wear (crater depth) significantly change the tool configuration/geometry, thus resulting in the variation of chip breakability, while minor flank wear is the dominant factor influencing the surface quality of a finished product. Since the dispersion patterns derived from multivariate time series models are sensitive to the rate of the above-mentioned wear types, four associated dispersion features, viz., the low frequency

(LF) dispersion $D_x'(LF)$ of the feed force, and the high frequency (HF) dispersions $D_x'(HF)$ of the feed force, $D_y'(HF)$ of the thrust force and $D_z'(HF)$ of the main cutting force are selected as the input features representing effects of tool wear on chip breakability and surface finish.

In addition, an initial condition for assessing chip forming patterns is required. As described before, assessment of chip shapes/sizes for unworn tools is achieved in terms of a fuzzy membership value, μ . This value is selected as the fifth feature. Two machining parameters, cutting speed and feed, are also selected as the input features due to their close relationship with chip breakability and surface finish. Figure 7.10 shows the schematic diagram of feature selection, and Table 7.3 lists the input-output data under Training Cutting Conditions 1 to 3 as representatives. The input-output data under all the other cutting conditions are given in Appendix D.

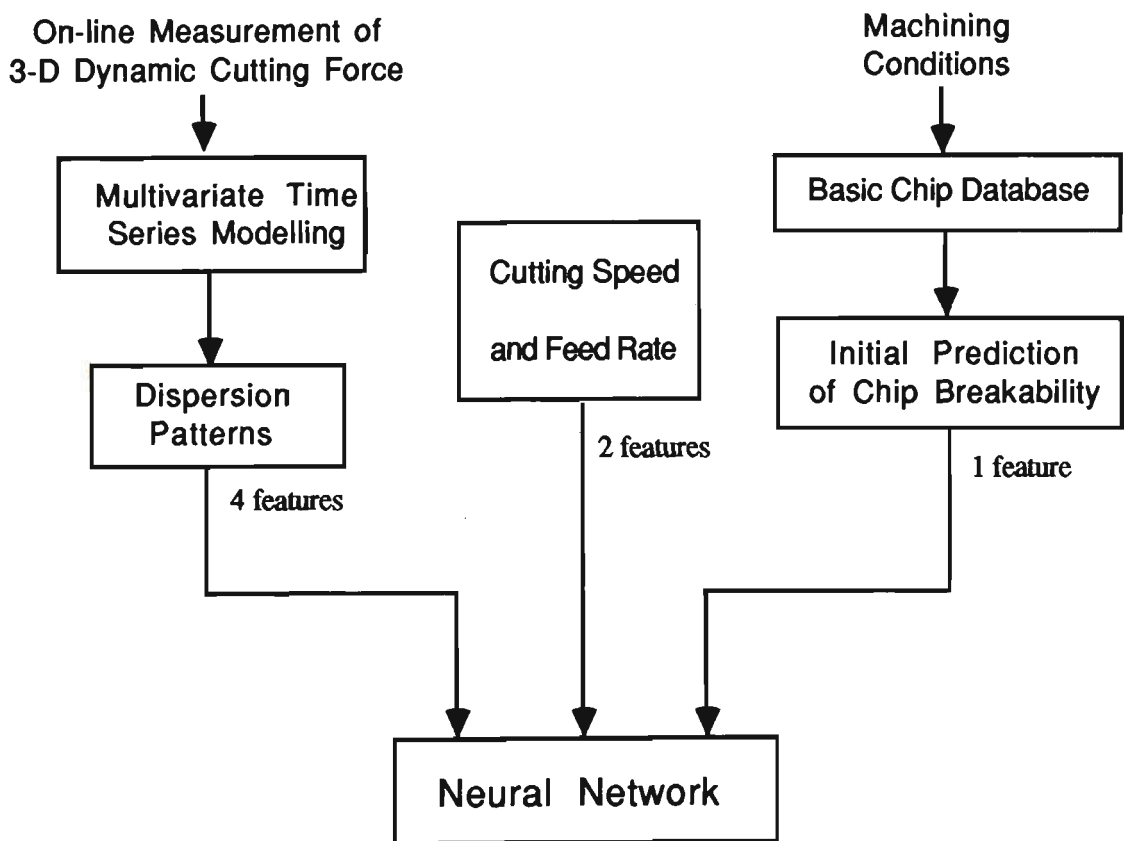


Figure 7.10 Feature selection for neural network

Table 7.3 The training data under Training Cutting Conditions 1-3

	INPUT FEATURES							OUTPUTS	
	Feed (mm/rev)	Speed (m/min)	D'_x (LF) (min^{-1})	D'_x (HF) (min^{-1})	D'_y (HF) (min^{-1})	D'_z (HF) (min^{-1})	$\mu_i(k)$	$\mu_o(k)$	R_a (μm)
Cutting Condition 1	0.1	115	-4.91	3.22	1.50	1.47	0.25	0.25	1.09
	0.1	115	-3.89	2.52	1.31	1.15	0.25	0.30	1.14
	0.1	115	-3.03	1.92	1.14	0.87	0.30	0.32	1.23
	0.1	115	-1.15	0.62	0.78	0.27	0.32	0.35	1.32
	0.1	115	0.73	-0.68	0.42	-0.33	0.35	0.41	1.78
	0.1	115	2.61	-1.98	0.06	-0.93	0.41	0.58	1.99
	0.1	115	4.49	-3.28	-0.30	-1.53	0.58	0.46	2.35
	0.1	115	7.78	-5.62	-0.95	-2.61	0.46	0.42	2.68
Cutting Condition 2	0.1	145	-5.29	3.83	5.22	4.01	0.25	0.25	1.04
	0.1	145	-3.11	2.31	3.84	2.79	0.25	0.27	1.12
	0.1	145	-1.01	0.78	2.54	1.56	0.27	0.31	1.27
	0.1	145	1.01	-0.75	1.29	0.34	0.31	0.41	1.64
	0.1	145	3.11	-2.27	-0.01	-0.89	0.41	0.47	1.88
	0.1	145	5.13	-3.92	-1.26	-2.21	0.47	0.45	2.08
	0.1	145	7.48	-5.32	-2.71	-3.34	0.45	0.42	2.27
Cutting Condition 3	0.06	145	-8.50	4.06	4.89	2.87	0.23	0.23	1.00
	0.06	145	-5.80	2.71	3.88	2.06	0.23	0.24	1.06
	0.06	145	-3.20	1.41	2.90	1.29	0.24	0.27	1.14
	0.06	145	-0.70	0.16	1.97	0.55	0.27	0.32	1.35
	0.06	145	1.90	-1.14	0.99	-0.23	0.32	0.41	1.73
	0.06	145	4.40	-2.39	0.05	-0.97	0.41	0.43	1.92
	0.06	145	7.30	-3.84	-1.04	-1.84	0.43	0.41	2.13

In Table 7.3, $\mu_i(k)$ and $\mu_o(k)$, $k = 1, 2, \dots$, represent the input and output of chip breakability respectively, and

$$\begin{aligned} \mu_i(0) &= \text{predicted value from the basic chip database, and} \\ \mu_i(k) &= \mu_o(k-1) \end{aligned} \quad (7.3)$$

Equation 7.3 assumes that no sudden change in chip breakability will occur as tool wear is normally a process of gradual progression. It is therefore reasonable to use the output of chip breakability from the neural network at previous time interval $\mu_o(k-1)$ as the value of current input $\mu_i(k)$, with the initial chip breakability $\mu_i(0)$ from the established basic chip database for unworn tools.

7.5 ANALYSIS OF RESULTS FROM NEURAL NETWORKS

7.5.1 Training Strategy with Neural Networks

The objective of using neural networks is to predict the development patterns of chip breakability and surface finish at different wear states. Therefore, the input data should be presented to the neural network by group in order to learn the development trend of chip breakability and surface finish during the process of tool wear. The training task in this work is to have the neural network learn the mappings from the given input patterns to the desired output patterns under the Training Cutting Conditions 1 to 6 (Table 7.1) which contain 41 samples in total. As the system under investigation contains only 7 inputs and 2 outputs, one hidden layer is sufficient to establish an effective neural network [98].

How to select the optimum number of hidden neurons is a critical yet complicated issue in Back-propagation networks [99-100]. In this work an experimental approach was taken to the selection of the number of hidden neurons. The training procedure

started with 7 and ended with 14 hidden neurons in line with the number of inputs/outputs. Due to lack of knowledge about what transfer function would give the best performance for the problem in question, three common transfer functions, i.e. sigmoid, hyperbolic tangent (TanH) and sine, are used in each training process. As the training time is not important in the off-line stage for the size of neural networks concerned, the training process was stopped only when no further improvement was observed.

7.5.2 Analysis of Results for Training and Testing Effects

A Macintosh-based package, NeuralWorks Professional II, was used to establish the neural network. Figure 7.11 shows the RMS errors for all the neural networks trained with different number of hidden neurons and different transfer functions. It is seen that with 12 hidden neurons is the minimum RMS error achieved for all three transfer functions. This is in agreement with [12] where the experimental results show that up to a certain number, further increase of hidden neurons does not always lead to a better performance of neural networks. From Fig. 7.11, it can also be concluded that among three transfer functions, TanH gives the minimum RMS errors, i.e. 0.014 which should be thought as sufficiently close to zero [98].

The training effects of the selected 7-12-2 (i.e. 7 inputs, 12 hidden neurons & 2 outputs) neural network with the TanH transfer function are shown in Figures 7.12 & 7.13 for chip breakability and surface finish, respectively. The results indicate that the selected neural network is capable of learning the mappings between the given input patterns and the desired output patterns with quite acceptable accuracy.

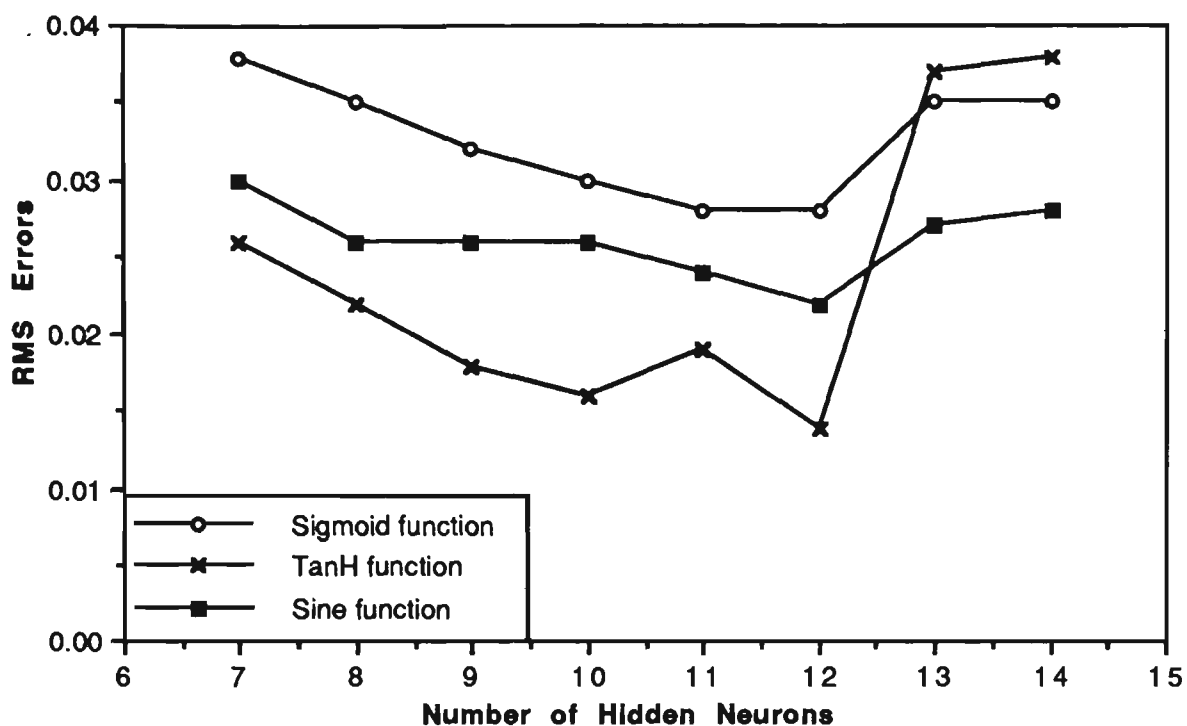
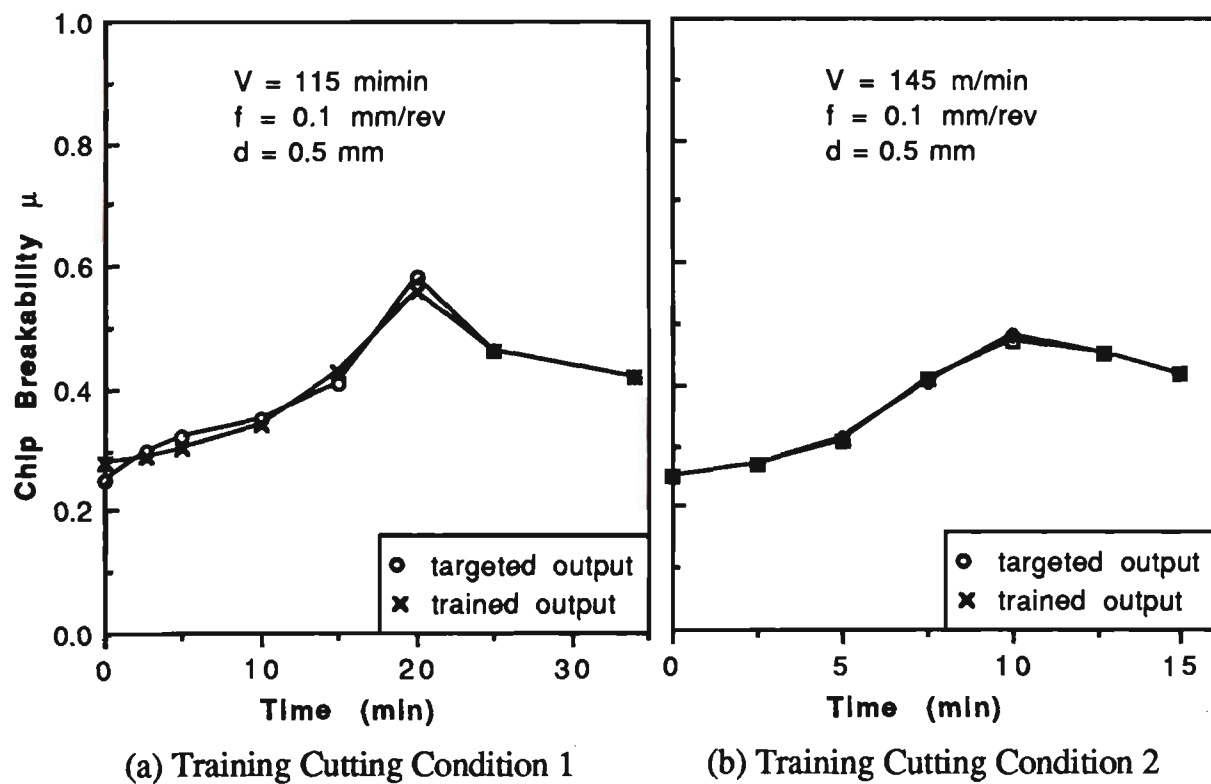
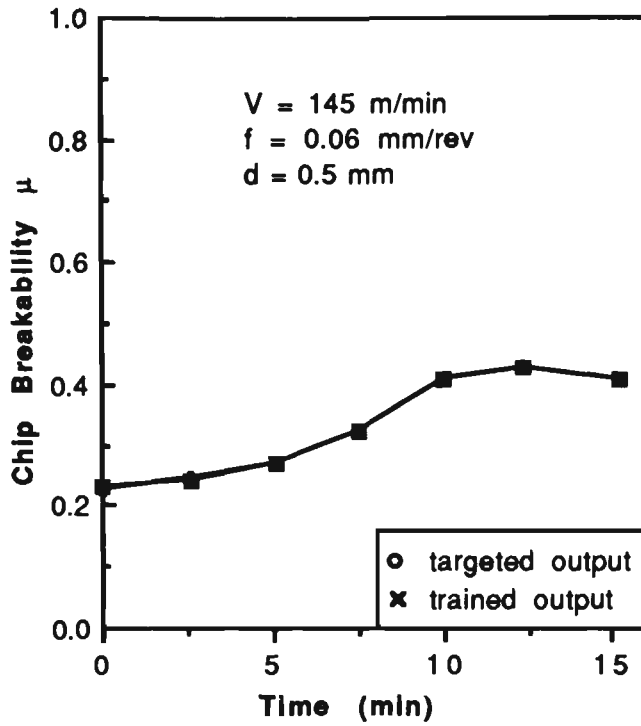


Figure 7.11 Effect of the number of hidden neurons for three transfer functions

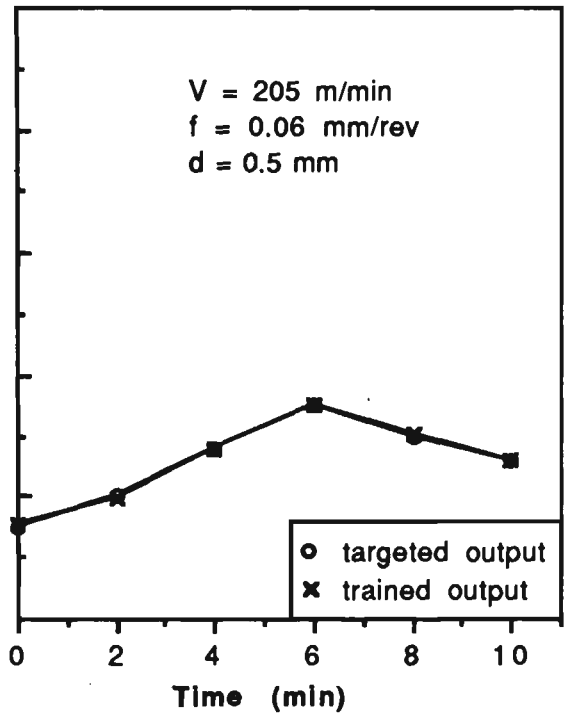


(a) Training Cutting Condition 1

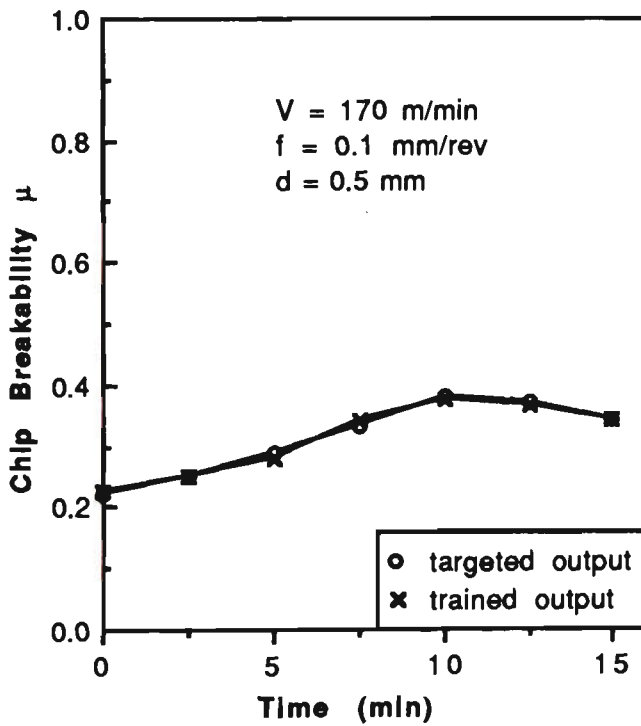
(b) Training Cutting Condition 2



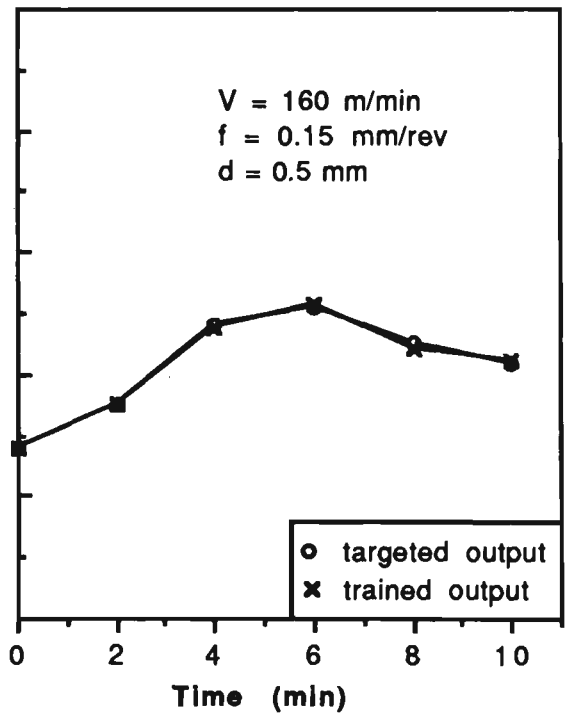
(c) Training Cutting Condition 3



(d) Training Cutting Condition 4

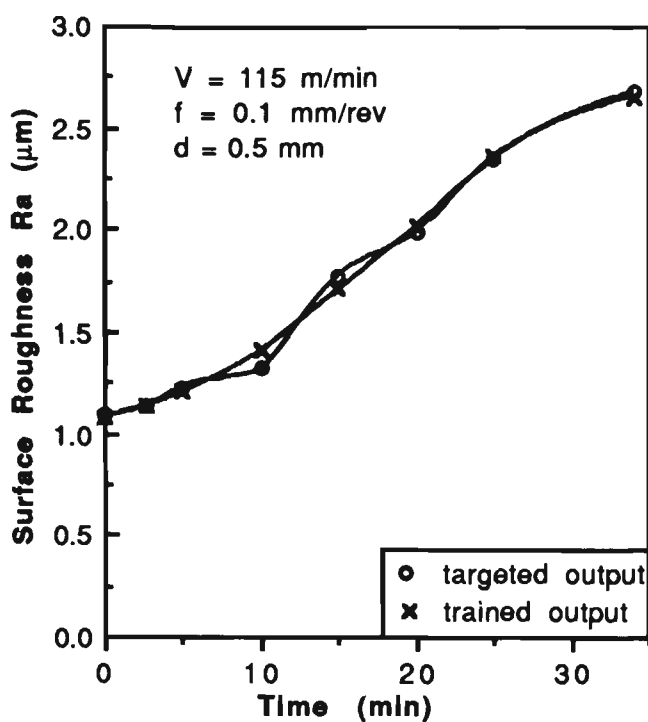


(e) Training Cutting Condition 5

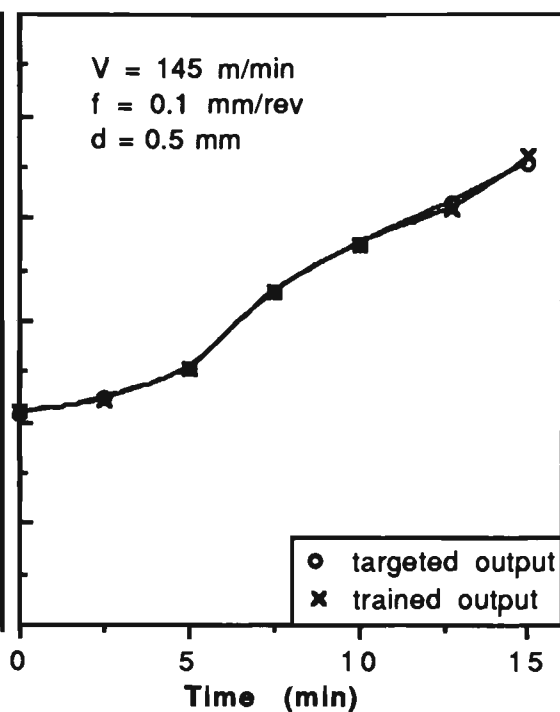


(f) Training Cutting Condition 6

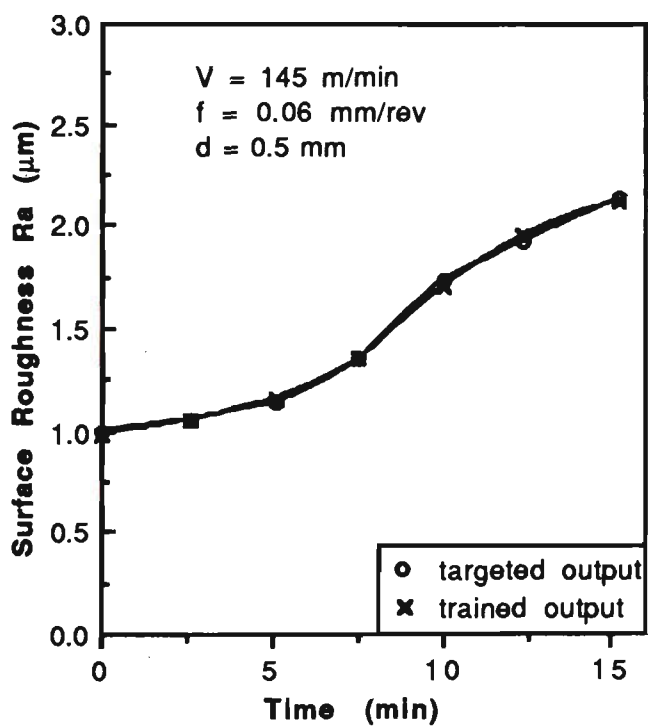
Figure 7.12 Evaluation of training effect of chip breakability



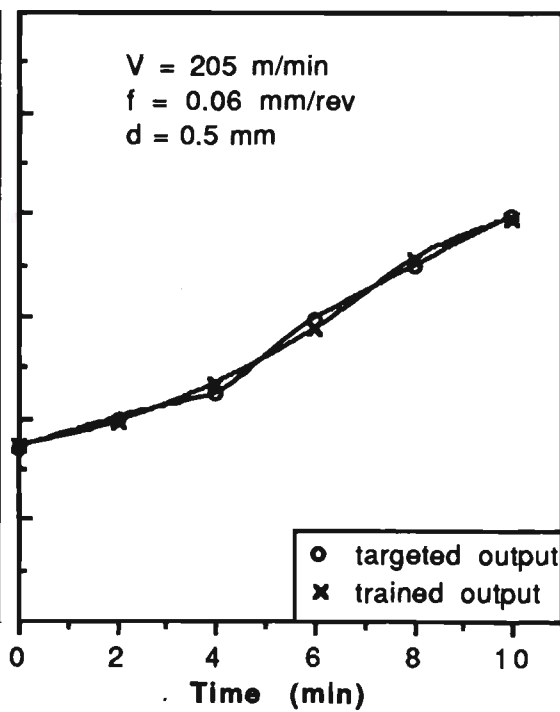
(a) Training Cutting Condition 1



(b) Training Cutting Condition 2



(c) Training Cutting Condition 3



(d) Training Cutting Condition 4

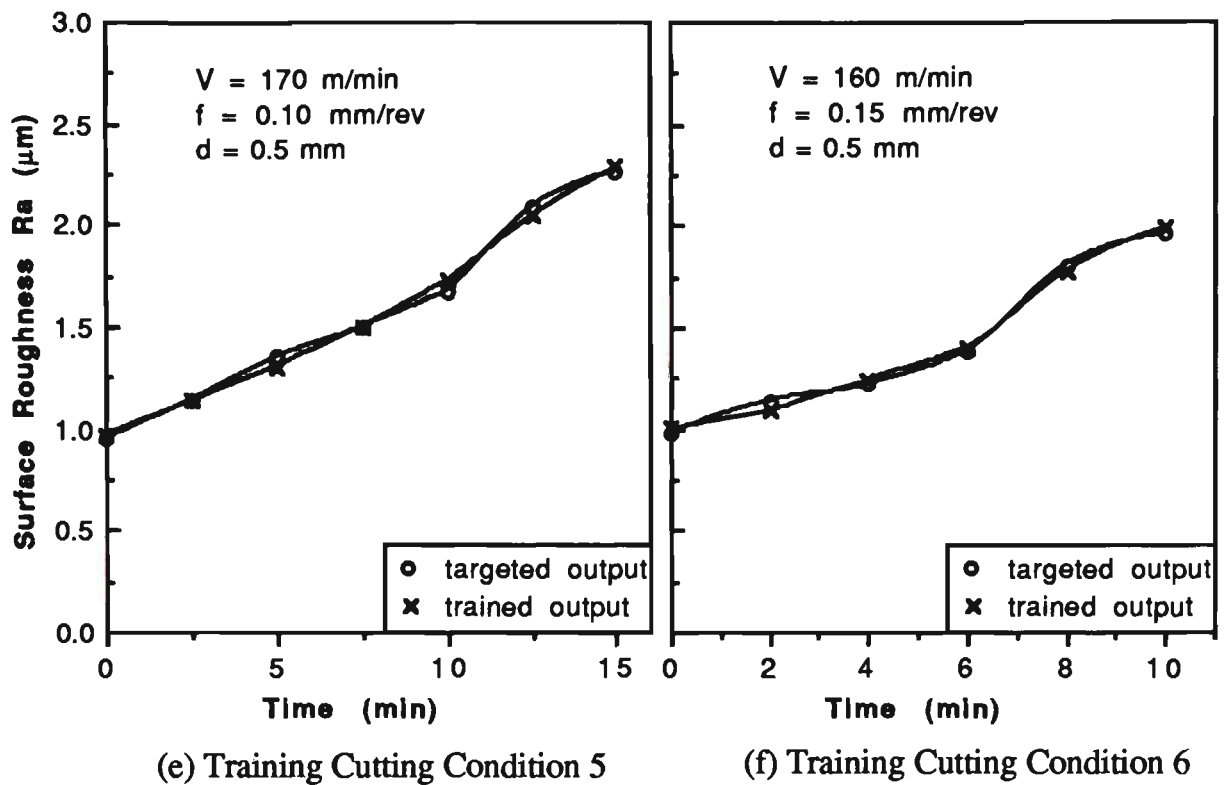


Figure 7.13 Evaluation of training effect of surface finish

Four groups of Testing Cutting Conditions (Table 7.1), which were not used in training of the neural network, are used to test the performance of this 7-12-2 network. Figures 7.14 & 7.15 show the comparisons between the actual outputs and the predicted network outputs for chip breakability and surface finish, respectively. Although the results are not as good as those during the training shown in Figs. 12 & 7.13, they should be considered accurate enough to describe the in-process relationship between chip breakability/surface finish and tool wear states under finish-machining conditions. Therefore, the results from the established neural network, together with comprehensive tool wear estimation, would give a quite satisfactory on-line assessment of machining performance in finish-machining.

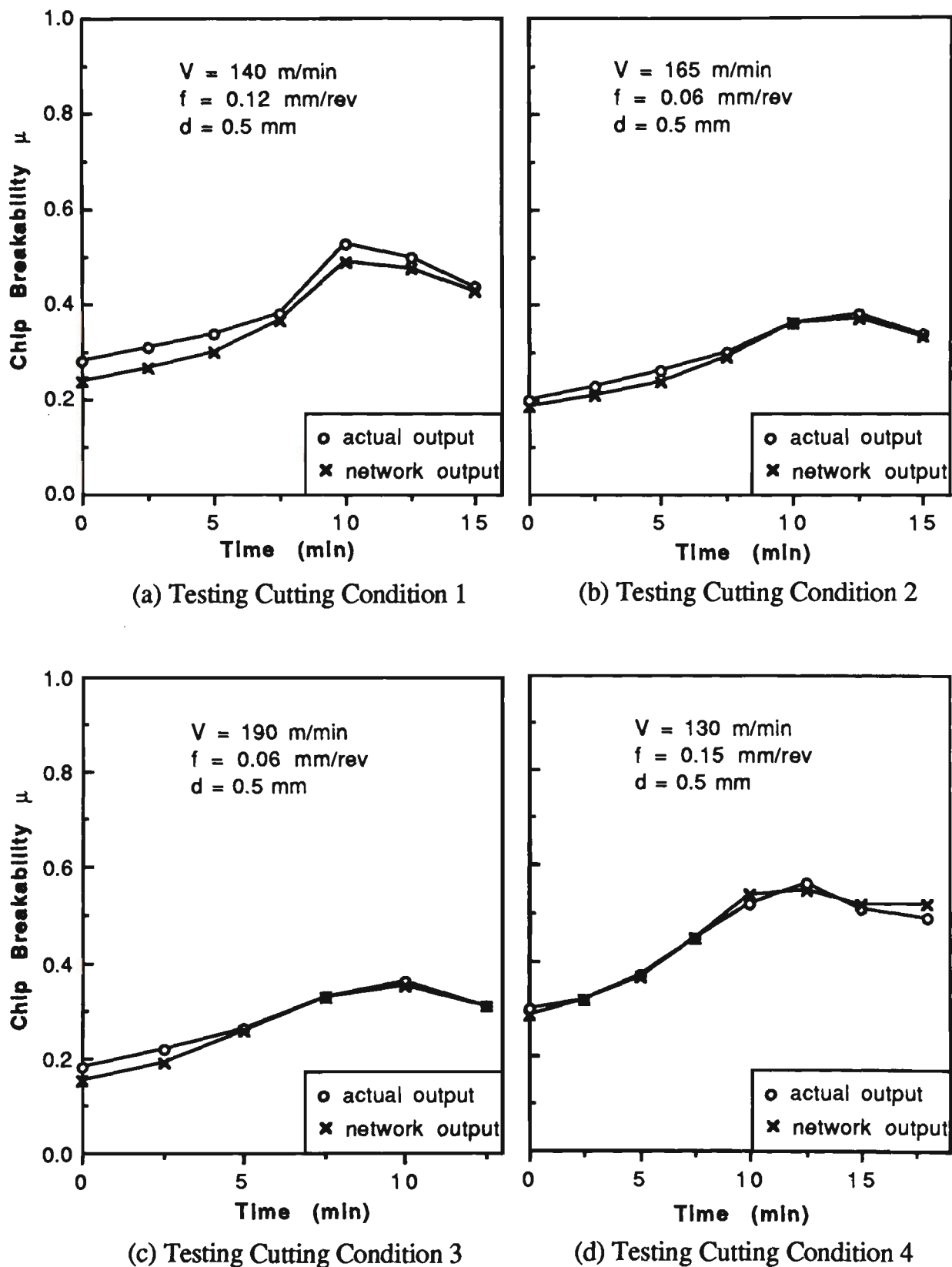


Figure 7.14 Neural network performance in predicting patterns of chip breakability

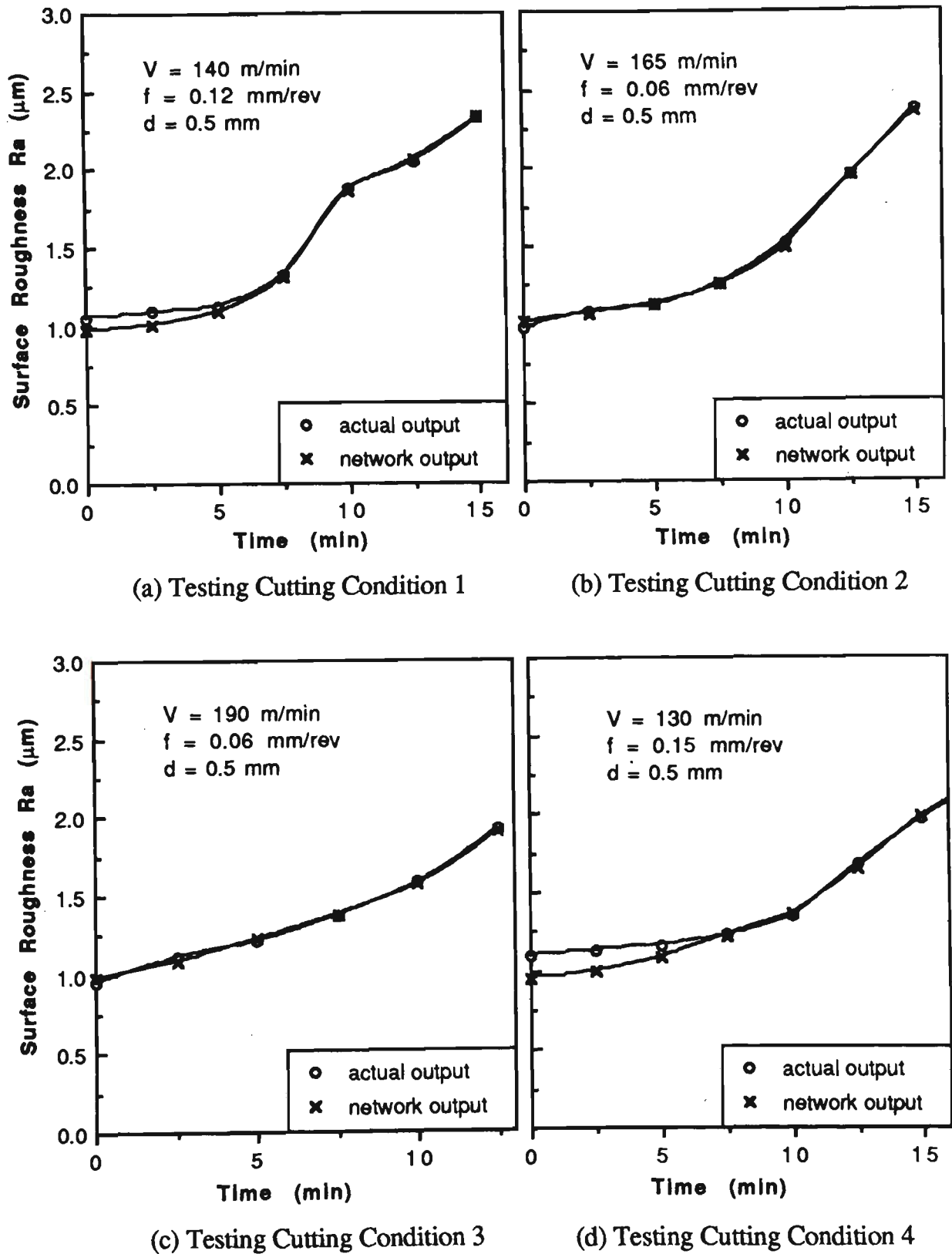


Figure 7.15 Neural network performance in predicting patterns of surface finish

7.6 EXTENSION : FUTURE DIRECTIONS AND DEVELOPMENTS

7.6.1 Real-time Application of Chip Control and Tool Wear Estimation in Automated Machining Systems

Successful applications of chip control and tool wear estimation to the actual automated machining systems rely heavily on the support of a powerful and comprehensive software tool for the purpose of real-time monitoring/control. It is suggested that this software, incorporated with an appropriate hardware, should have the multiple functions of handling large scale database and knowledge base, executing complicated scientific calculation, processing logic reasoning and knowledge synthesising, and performing real-time monitoring and control.

As an example, Figure 7.16 shows a possible project for an integrated system of chip control and tool wear estimation, based on the software "G2 Real-time Expert System" * which may meet the above-mentioned requirements.

* "G2 Real-time Expert System" is developed by Gensym Corporation, Cambridge, MA 02140, U.S.A. This software has recently become available commercially.

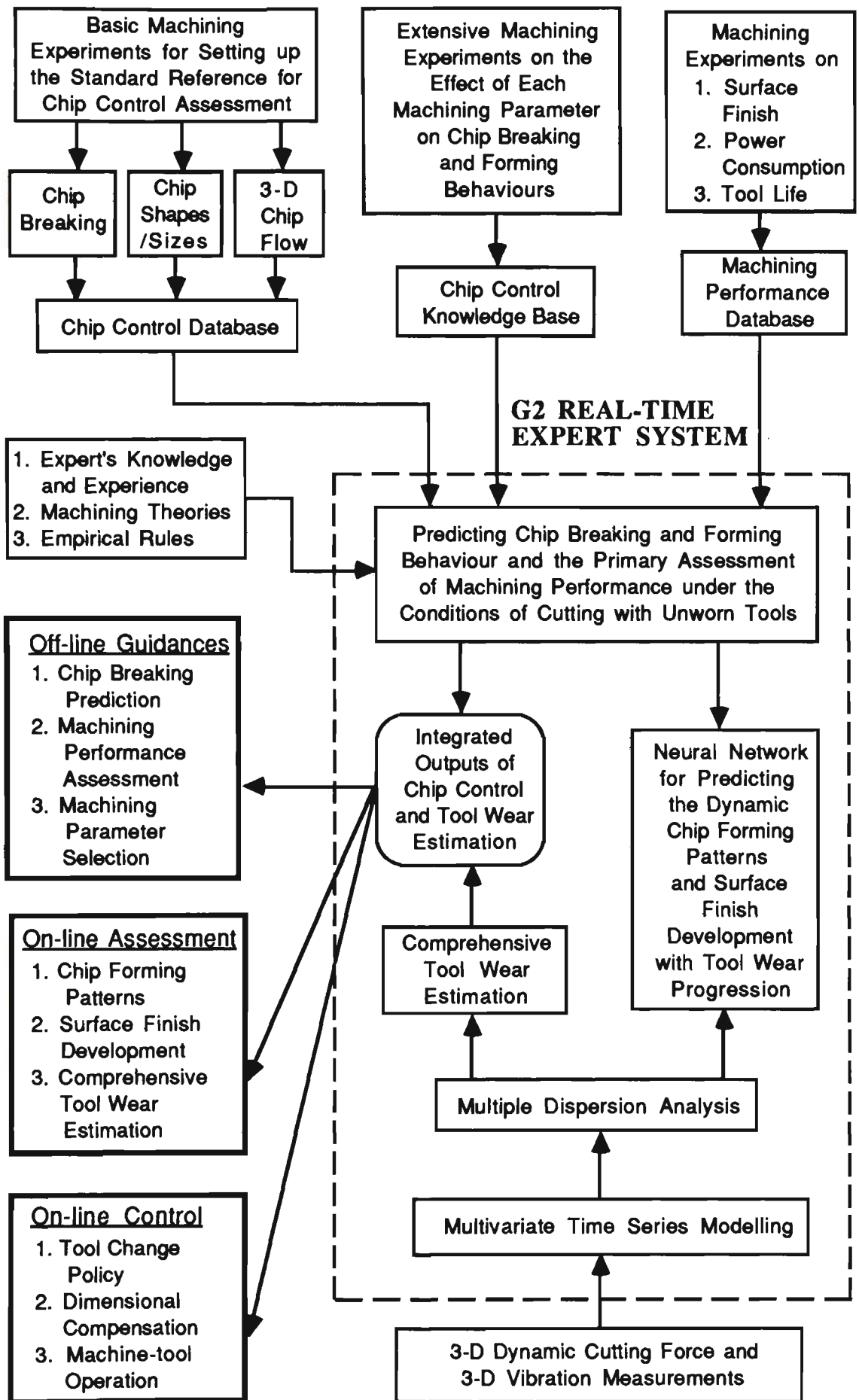


Figure 7.16 Proposed schematic diagram of an integrated system for chip control and tool wear estimation based on the G2 Real-time Expert System

7.6.2 Developing a Self-organising Neural Network

Back propagation neural network techniques have been successfully used to predict dynamic chip forming patterns and surface finish with tool wear progression under the selected machining conditions. However, the major drawback is that the back propagation algorithm is based on a "supervised" learning strategy, which needs desired output patterns in each case. Apparently, it is not feasible to conduct extensive experiments to find the target patterns for numerous combinations of work materials and tool configurations/geometries. Therefore, a strategy of "learning by self-organising" should be developed to replace currently used "learning by being shown". Self-organising learning is much more challenging, however, it can be used to resolve very complicated problems such as aircraft engine monitoring [101]. The significance of a self-organising neural network is its ability to adapt successfully to the environments where rules may change unpredictably, that is, the ability to adapt through direct confrontation with its "experiences" without a teacher to "supervise" [102]. Therefore, employing a self-organising neural network is highly suggested for future work in order to develop an integrated machining process monitoring/control system which is applicable to the actual workshop environments.

7.7 SUMMARY AND CONCLUDING REMARKS

- (1) The interaction of chip forming patterns with tool wear progression is extremely complicated. No effective theories at present can describe their interrelationship analytically. Thus neural networks, which rely largely on input-output data, have proven effective for the problem under investigation in this chapter.

- (2) Based on the previous work described in Chapters 2 and 5, where the chip breaking and forming behaviour when machining with unworn cutting tools and comprehensive tool wear estimation can be predicted, an approach for the in-process assessment of chip breakability and surface finish is achieved by using neural network techniques.
- (3) With the appropriate selection of a neural network structure and non-linear transfer function, the mapping between the given input and output patterns can be quite precisely achieved through training. Thus predictions of chip breakability and surface finish for any new input data, which were not used in training and may come from different cutting conditions, can be achieved with quite acceptable accuracy.
- (4) Although the results of this work are only for a flat-faced tool, they can be extended to more complicated tool configurations by using the methodology presented in this chapter. The method may also be extended to rough-machining conditions where power consumption may have to be included in the neural networks because of its critical effect on machining performance with tool wear progression.
- (5) The integration of the prediction of chip forming pattern, comprehensive tool wear estimation, as well as surface finish, through the use of neural networks provides an effective means for on-line assessment of machining performance in automated machining systems.

CHAPTER 8

CONCLUSIONS

Through theoretical analysis and experimental research, this thesis presents a feasible means for achieving effective chip control and comprehensive tool wear estimation, and for further integrating these two vital concerns into an overall on-line assessment of machining performance. The thesis has resulted in a better understanding of chip control and tool wear estimation in automated machining systems, including the following aspects :

- (a) quantitative chip breakability prediction when machining steels;
- (b) machining performance assessment including chip control, surface finish and power consumption;
- (c) tool chip breaker design with the evaluation of three-dimensional chip flow;
- (d) comprehensive tool wear estimation, viz. major flank wear, crater wear, minor flank wear and groove wear at the minor cutting edge, in oblique machining;
- (e) dynamic chip forming behaviour assessment with tool wear progression.

The major findings of this work are summarised below.

8.1 A NEW APPROACH FOR THE QUANTITATIVE PREDICTION OF CHIP BREAKABILITY AND CHIP FORMING PATTERNS

Prediction of chip breakability/chip forming patterns with sufficient accuracy for arbitrary machining conditions is necessary because no suitable theories for chip breaking in machining are available for use at the shop floor level. Almost every theory that has been presented to date seems to be either of "academic" nature or of a descriptive type with no specific applicable methods recommended. This is attributed to the extremely complex nature of chip formation patterns with varying tool configuration/geometry features and their interactions with work materials under various cutting conditions.

As a new approach, a fuzzy-set mathematical model, in conjunction with a knowledge database and the corresponding set of knowledge rules, has been implemented into an expert system for predicting the "probable" levels of chip breakability in terms of a fuzzy membership value.

The significance of the method for predicting chip breakability presented in this thesis lies in that chip breakability can be quantified through a fuzzy rating system according to the chip shapes/sizes produced, and further predicted through a fuzzy-set model with very reasonable accuracy under any given set of input machining conditions, including work materials, chip breaker configurations, tool geometries and cutting conditions. Therefore, this method is suitable for application in an industrial environment in automated machining systems.

The method for predicting chip breakability has been further extended to incorporate the chip forming patterns and chip acceptability (for chip disposal) to give an

integrated evaluation of chip control in machining. Based on this, a predictive expert system for machining performance assessment with chip control as a major criterion has been developed with due consideration of surface finish and power consumption. Thus, the method presented may be used as a basis for the assessment of "total machinability" in automated machining systems.

8.2 A SCIENTIFICALLY-BASED METHOD FOR THE EFFECTIVE DESIGN OF CHIP BREAKERS

The apparent "try and see" methods adopted by cutting tool manufacturers in the design of chip breakers have to date resulted in hundreds of different chip breaker configurations. Most of them, however, seem to produce desired chips only under specific cutting conditions for selected work materials. When these conditions are changed and/or different work materials are used, chip breakability often becomes quite different.

With the aim of developing a scientifically-based method for designing groove-type chip breakers, a knowledge-based system has been developed based on the analysis of three-dimensional chip flow in oblique machining for a wide range of machining conditions covering various work materials, cutting conditions, tool restricted contact lengths, chip-breaker groove styles/sizes and tool geometries.

The merit of this method lies in that the optimum design of a chip breaker configuration can be achieved based on the criterion of efficient chip breaking at reduced power consumption. All the major factors which influence the effectiveness of chip breaker configurations are quantitatively evaluated by using an experimentally-based database and an integrated knowledge-base. Therefore, the methodology

presented in this thesis may provide an effective alternative to the traditional method of designing groove-type chip breakers and also can be used as a guideline for cutting tool manufacturers when designing any other types of tool chip breakers.

8.3 A NEW STRATEGY FOR COMPREHENSIVE TOOL WEAR ESTIMATION

The conventional method for tool wear estimation is set only based on two common types of wear, i.e., major flank wear and crater wear. No one has made the effort to include the wear states on the minor flank face which are crucial to assure surface quality and dimensional accuracy. Especially in finish-machining, estimation of major flank and/or crater wear alone is no longer adequate to describe the overall wear states.

This work a first attempt to develop a new strategy for comprehensive tool wear estimation, including major flank wear, crater wear, minor flank wear and groove wear at the minor cutting edge. Multivariate time series modelling techniques are successfully applied to decompose data sampled from the machining process, such as the 3-D dynamic cutting force and 3-D tool vibration, in terms of dispersions and/or multiple dispersions. The success of employing dispersion analysis to comprehensive tool wear estimation is attributed to its ability to single out the signal ingredients sensitive to particular types of wear to be estimated.

The strategy of comprehensive tool wear estimation presented in this thesis may provide a feasible means for on-line tool wear monitoring in automated machining systems to assure product quality. The thesis also emphasises, in contrast to currently used criteria, that in finish-machining tool change policy or optimal cutting conditions

should be determined based on wear states on the minor flank face because it is likely that they reach critical points earlier than those on the major flank face and rake face.

8.4 A NEW ATTEMPT AT ESTIMATING CHIP FORMING PATTERNS WITH TOOL WEAR PROGRESSION FOR ON-LINE ASSESSMENT OF MACHINING PERFORMANCE

Chip control and tool wear estimation are two major concerns in automated machining systems. They are closely interrelated during the machining process. The former facilitates the safety of the machining operation, the maintenance of good surface finish on the machined work surface and the convenience of chip disposal, while the latter determines the tool change policy and the quality control strategy, especially in the finish-machining processes.

Since the present theories and knowledge about metal machining are all based on ideal machining conditions with unworn cutting tools, they are inadequate to quantitatively describe the actual chip forming patterns with tool wear progression. When tool wear formed during the machining process becomes considerable, the chip forming patterns vary significantly, or even totally differ, from those predicted for unworn cutting tools, due to the changes in machining process characteristics and tool configurations/geometries. Work has been seldom reported on studying the dynamic chip forming behaviour with tool wear progression, mainly due to the extreme complexity involved.

As a new attempt, neural network techniques are introduced to model the dynamic interrelationship between chip forming patterns and tool wear development. Considering that in finish-machining surface quality is of great importance to the

product being machined, dynamic prediction of surface roughness, which depends primarily on wear states on the minor flank face for a worn tool, is also included.

The advantage of this new approach is that the previously developed methods, such as quantitative prediction of chip breakability and comprehensive estimation of tool wear, can be effectively integrated based on the same signal processing system, which would greatly facilitate meeting the real-time requirement. Therefore, the established tool wear monitoring system, once implemented using the results developed from the neural network, provides a feasible means for on-line assessment of machining performance, including chip breaking/forming patterns, surface finish and overall tool wear progression, which may give a satisfactory evaluation of dynamic machining performance in finish-machining processes.

8.5 SUGGESTION FOR FUTURE WORK

Due to the heavy dependence of tool wear on work materials and tool configurations/geometries, it is impossible to develop a single on-line tool wear recognition algorithm which is effective for arbitrary machining conditions. In order to extend the method developed in this thesis for tool wear estimation to suit a wide range of machining conditions, further efforts are required. It is, however, not feasible to conduct extensive tool wear experiments due to the fact that tool wear experiments are costly and time-consuming. An alternative may be possible by utilising and synthesising the present knowledge and database about tool wear and machining operation, with the aid of an expert system.

The need for developing the techniques of artificial intelligence or expert systems for on-line tool wear monitoring has been highlighted in recently published survey papers about tool wear estimation [5, 103-104]. Such an idea was presented in a recent work [105] by introducing an expert system-supported tool wear monitoring strategy based on a knowledge base. The basic thrust is based on the assumption that the distribution of the forces acting on different tool faces (see Figure 5.9) depends mainly on tool cutting edge angle, tool rake angle, chip breaker type as well as the three-dimensional chip flow. The established multiple dispersion patterns derived from ARMAV models of 3-D dynamic cutting force can be selected to establish the standard tool wear recognition algorithm. When machining conditions are different from the standard ones, a set of tool wear decision-making rules may be determined to modify tool wear recognition algorithm according to the variations of force distribution acting on different tool faces.

However, greater efforts are needed in analysing the complicated relationship between different force distributions on tool faces and multiple dispersion patterns, and in synthesising the knowledge that could be used to develop tool wear decision-making rules. Figure 8.1 proposes a possible scheme for developing such a tool wear monitoring system.

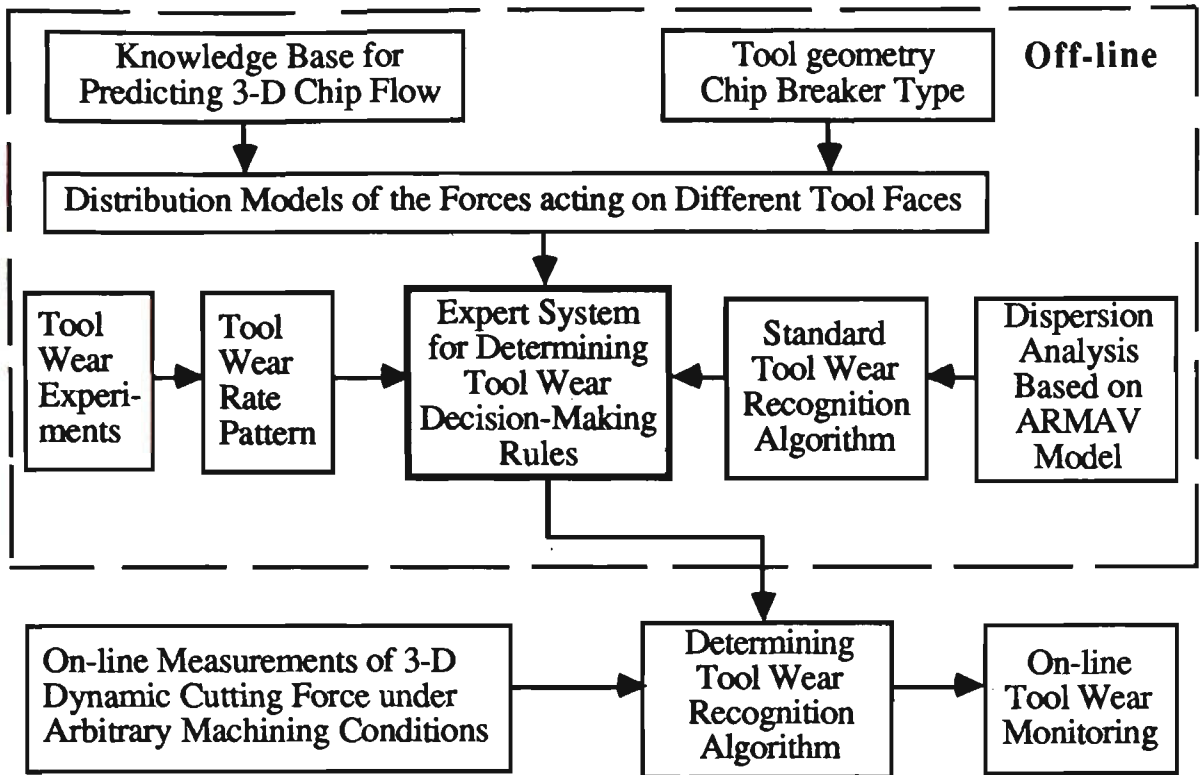


Figure 8.1 A proposed schematic diagram for an expert system-supported tool wear estimation system

REFERENCES

1. J. F. Kahles, "CIRP Technical Reports : Machinability Data Requirements for Advanced Machining Systems", *Ann. CIRP*, **36**(2), pp. 523-529, (1987).
2. I. S. Jawahir, "A Survey and Future Predictions for the Use of Chip Breaking in Unmanned Systems", *Int. J. Adv. Mfg. Tech.*, **3**(4), pp. 87-104, (1988).
3. D. Li and J. Mathew, "Tool Wear and Failure Monitoring Techniques for Turning - A Review", *Int. J. Mach. Tools Manufact.*, **30**, No. 4, pp. 579-598 (1990).
4. J. Tlustý, "A Critical Review of Sensors for Unmanned Machining", *Ann. CIRP*, **32**(2), pp. 563-572 (1983).
5. H.K., Toenshoff, et. al., "Developments and Trends in Monitoring and Control of Machining Processes", *Ann. CIRP*, **37**(2), pp. 611-622 (1988).
6. M., Shiraishi, "Scope of In-process Measurement, Monitoring and Control Techniques in Machining Processes--Part 1 : In-process Techniques for Tools", *Precision Engineering*, **10**(4), pp. 179-189 (1988).
7. S.Y., Liang and D.A., Dornfeld, "Detection of Cutting Tool Wear Using Adaptive Time Series Modeling of Acoustic Emission Signal", *ASME/WAM, Sensors for Manufacturing*, PED - Vol. 26, pp. 27-38 (1987).
8. S.Y., Liang and D.A., Dornfeld, "Tool Wear Detection Using Time Series Analysis of Acoustic Emission", *J. of Eng. for Ind.*, **111**, pp. 199-205 (1989).
9. S.M, Pandit, H. Susuki and C.H. Kahng, "Application of Data Dependent Systems to Diagnostic Vibration Analysis", *J. Mechanical Design*, **102**, 233-241 (1980).
10. S.M. Pandit, and S. Kashou, "A Data Dependent Systems Strategy of On-line Tool Wear Sensing", *J. of Eng. for Ind.*, **104**, pp. 217-223 (1982).

11. S. Rangwala and D. Dornfeld, "Sensor Integration Using Neural Networks for Intelligent Tool Condition Monitoring", *ASME Trans., J. of Eng. for Ind.*, **112**, pp. 219-228 (1990).
12. D.A. Dornfeld, "Neural Network Sensor Fusion for Tool Condition Monitoring", *Ann. CIRP*, **39**(1), pp. 101-105 (1990).
13. Z.J. Yuan, et. al., "In-Process Detection of Tool Wear and Breakage by Autocorrelation Coefficient of Dynamic Cutting Forces in Turning", *Proc. 4th Int. Conf. on Manuf. Eng.*, Brisbane, Australia, pp. 201-205 (1988).
14. A.M. Petrie, T.S. Sifra and A. Ismail, "The Development of An Automated System for On-line Tool Wear Monitoring", *Proc. of 1st Int. Machinery Monitoring & Diagnostics Conference*, U.S.A., pp. 546-552 (1989).
15. Y. Koren et. al., "Monitoring Tool Wear Through Force Measurement", *Proc. of 15th NAMRC*, pp. 463-468 (1987).
16. S.B. Rao, "Tool Wear Monitoring Through the Dynamics of Stable Turning", *ASME Trans., J. of Eng. for Ind.*, **108**, pp. 183-190 (1986).
17. J. Vogel, S. Pamalingam and K. Stelson, "On Tool Post Vibration Monitoring for Tool Condition Identification", *Proc. of 14th NAMRC*, pp. 281-285 (1986).
18. G. Chryssolouris, M. Guillot and M. Domroese, "Tool Wear Estimation for Intelligent Machining", *ASME/WAM, Intelligent Control*, DSC - Vol. 5, pp. 35-43 (1987).
19. F. Giusti, M. Santochi and G. Tantussi, "On-Line Sensing of Flank and Crater Wear of Cutting Tools", *Ann. CIRP*, **36**(1), pp. 41-44 (1987).
20. R. Teti, "Tool Wear Monitoring Through Acoustic Emission", *Ann. CIRP*, **38**(1), pp. 99-102 (1989).
21. K. Danai and A.G. Ulsoy, "A Dynamic State Model for On-line Tool Wear Estimation in Turning", *ASME/WAM, Sensors of Control of Manufacturing*, PED-Vol. 18, pp. 137-148 (1985).

22. K. Okushima, K. Hitomi and S. Ito, "A Study of Super-High Speed Machining", *Ann. CIRP*, **13**, pp. 399-410 (1966).
23. A.J. Pekelharing and R.A. Schuermann, "Wear of Carbide Tools - its effect of surface finish and dimensional accuracy", *The Tool Engineer*, pp. 51-57 (Oct. 1953).
24. A.J. Pekelharing, "Finish Turning", *Ann. CIRP*, **8**, pp. 112-120 (1959).
25. B.H. Lambert, "Two Years of Finish-Turning Research at the Technological University, Delft", *Ann. CIRP*, **10**, pp. 246-255 (1961-62).
26. A.J. Pekelharing, "Some Special Aspects of Carbide Tool Wear", *International Production Engineering Research Conference*, ASME, New York (1963).
27. S. Takata, and T. Sata, "Model Referenced Monitoring and Diagnosis -- Application to Manufacturing System", *Computers in Industry*, **7**, pp. 31-43 (1986).
28. K. Eman and S.M. Wu, "A Feasibility Study of On-Line Identification of Chatter in Turning Operations", *J. of Eng. for Ind.*, **102**, pp. 315-321 (1980).
29. X.D. Fang, Y. Yao and G. Arndt, "Tool Wear Estimation by Multidimensional Autoregressive Spectral Analysis", *Proc. 1990 Pacific Conference on Manufacturing*, Sydney & Melbourne, Australia, Vol. 2, pp. 834-841 (1990).
30. Y. Yao, X.D. Fang and G. Arndt, "Comprehensive Tool Wear Estimation in Finish-Machining via Multivariate Time-Series Analysis of 3-D Cutting Forces", *Ann. CIRP*, **39**(1), pp. 57-60 (1990).
31. S.M. Pandit, "Analysis of Vibration Records by Data Dependent Systems", *Shock and Vibration Bulletin*, **47**(4), pp. 161-174 (1977).
32. Y. Yao, X.D. Fang and G. Arndt, "On-line Estimation of Groove Wear in the Minor Cutting Edge for Finish-Machining", accepted for publication in *Ann. CIRP*, **40**(1) (1991).

33. P. Bandyopadhyay and S.M. Wu, "Signature Analysis of Drilling Dynamics for On-Line Drill Life Monitoring", *ASME/WAM, Sensors and Controls for Manufacturing*, pp. 101-110 (1985).
34. M.S. Lan and Y. Naerheim, "In-Process Detection of Tool Breakage in Milling", *ASME Trans., J. of Eng. for Ind.*, **108**, pp. 191-197 (1986).
35. S.M. Pandit and S.M. Wu, Time Series and System Analysis with Applications, John Wiley, USA (1983).
36. R.H. Jones, "Multivariate Autoregression Estimation using Residuals", Applied Time Series Analysis, Academic Press Inc., pp. 139-162, (1978).
37. G. Chryssolouris and M. Domroese, "Sensor Integration for Tool Wear Estimation in Machining", *Proc. WAM/ASME, Symposium on Sensor and Control for Manufacturing*, pp. 115-123, (1988).
38. S. Rangwala and D. Dornfeld, "Learning and Optimization of Machining Operations Using Computing Abilities of Neural Networks", *IEEE Trans. on Systems, Man and Cybernetics*, **19**(2), pp. 299-314 (1989).
39. K. Nakayama, "Chip Curl in Metal Cutting Process", *Bulletin of the Faculty of Engineering, Yokohama National Univ.* **11**, pp. 1-13 (1962).
40. K. Nakayama, "Chip Control in Metal Cutting", *Bull. Japan. Soc. of Prec. Eng.* **18**(2), pp. 97-103 (1984).
41. B. Worthington and M. H. Rahman, "Predicting Breaking with Groove Type Breakers", *Int. J. MTDR*, **19**, pp. 121-132 (1979).
42. E. K. Henriksen, 'Balanced Design Will Fit the Chip Breaker to the Job : Chip Breaker Dimensions are Critical in Taming Chips', *American Machinist*, **98**(4), pp. 118-124 (1954).
43. E. K. Henriksen, "Findings and Directions in Chip Breakers Research", *Proc. 23rd Annual Meeting of ASTE*, Los Angles, California (14-18 March 1955).
44. L. V. Colwell, "Predicting the Angle of Chip Flow for Single-Point Cutting Tools", *Trans. ASME* , **76**(2), pp. 199-204 (1954).

45. G. V. Stabler, "The Chip Flow Law and its Consequences", *Proc. 5th Int. MTDR Conf.*, pp. 243-251 (September 1964).
46. N. H. Cook, P. Jhaveri and N. Nayak, "The Mechanism of Chip Curl and its Importance in Metal Cutting", *Trans. ASME*, pp. 374-380 (1963).
47. K. Nakayama, "A Study on Chip Breaker", *Bulletin of JSME*, **5**(15), pp. 142-150 (1962).
48. K. Nakayama, "Pure Bending Test of Chip - An Approach to the Prediction of Cutting Force", *Bulletin of the Faculty of Engineering, Yokohama National Univ.*, **12**, pp.1-14 (1963).
49. K. Nakayama, "Origins of Side Curl of Chip in Metal Cutting", *Bull. Japan Soc. of Prec. Eng.*, **6**(3), pp. 99-101 (1972).
50. K. Nakayama and M. Ogawa, "Basic Rules on the Form of Chip in Metal Cutting", *Ann. CIRP*, **27**(1), pp. 17-21 (1978).
51. K. Nakayama and M. Arai, "The Breakability of Chip in Metal Cutting", *Proc. Int. Conf. on Manuf. Eng.*, Melbourne, Australia, pp. 6-10 (1980).
52. K. Nakayama, M. Arai and T. Kondo, "Cutting Tools with Curved Rake Face - A Means for Breaking Thin Chips", *Ann. CIRP*, **30**(1), pp. 5-8 (1981).
53. B. Worthington and A. H. Redford, "Chip Curl and the Action of the Groove Type Chip Former", *Int. J. MTDR*, **13**, pp. 257-270 (1973).
54. B. Worthington, "The Effect of Rake Face Configuration on the Curvature of the Chip in Metal Cutting", *Int. J. MTDR*, **15**, pp. 223-239 (1975).
55. B. Worthington, "The Operation and Performance of a Groove-type Chip Forming Device", *Int. J. Prod. Res.*, **14**(5), pp. 529-558 (1976).
56. W. Johnson, "Some Slip-line Fields for Swaging or Expanding, Indenting, Extruding and Machining for Tools with Curved Dies", *Int. J. Mech. Sci.*, **4**, pp. 323-347 (1962).

57. E. Usui and K. Hoshi, "Slip-line Fields in Metal Machining Which Involve Centered Fans", *Proc. Int. Prod. Eng. Res. Conf. ASME*, Pittsburgh, pp. 61-71 (September 1963).
58. E. Usui, K. Kikuchi and K. Hoshi, "The Theory of Plasticity Applied to Machining with Cut-Away Tools" *Trans. ASME*, pp. 95-104 (May 1964).
59. I. S. Jawahir, "The Chip Control Factor in Machinability Assessments : Recent Trends", *Journal of Mechanical Working Technology*, **17**, pp. 213-224 (1988).
60. I. S. Jawahir and P. L. B. Oxley, "Efficient Chip Breaking at Reduced Power Consumption - An Experimental Analysis", *Proc. 4th Int. Conf. on Manufacturing Engineering*, Brisbane, Australia, pp. 97-102 (May 1988).
61. I. S. Jawahir, "The Tool Restricted Contact Effect as a Major Influencing Factor in Chip Breaking : An Experimental Analysis", *Ann. CIRP*, **37**(1), pp. 121-126 (1988).
62. I. S. Jawahir and P. L. B. Oxley, "New Developments in Chip Control Research; Moving Towards Chip Breakability Predictions for Unmanned Manufacture", *Proc. Int. Conf. ASME - MI'88, ASME Publ.*, Atlanta, USA, Vol. 1, pp. 311-320 (April 1988).
63. I. S. Jawahir, "On the Controllability of Chip Breaking Cycles and Modes of Chip Breaking in Metal Machining", *Ann. CIRP*, **39**(1), pp. 47-51 (1990).
64. C. L. Hsu, "An Expert System Approach for Selection and Optimization of Machining Process Parameters", PhD Thesis, University of Illinois at Chicago, U.S.A. (1985).
65. H. P. Wang and R. A. Wysk, "An Expert System for Machining Data Selection", *Comput. & Indus. Engg*, **10**(2), pp. 99-107 (1986).
66. F. Giusti et al, "COATS : An Expert Module for Optimal Tool Selection", *Ann. CIRP*, **35**(1), pp. 337-340 (1986).

67. I. S. Jawahir and X. D. Fang, "A Knowledge-based Approach for Improved Performance with Grooved Chip Breakers in Metal Machining", *Proc. 3rd Int. Conf. on Advances in Manufacturing Technology*, Singapore, pp. 130-144 (August 1989).
68. C. Spaans, "The Fundamentals of Three-Dimensional Chip Curl, Chip Breaking and Chip Control", Doctoral Thesis, TH Delft, (1971).
69. W. K. Luk, "The Direction of Chip Flow in Oblique Cutting", *Int. J. Prod. Res.*, **10**(1), pp. 67-76 (1972).
70. C. Y. Jiang, Y. Z. Zhang, Z. J. Chi, "Experimental Research of the Chip Flow Direction and its Application to the Chip Control", *Ann. CIRP*, **33**(1), pp. 81-84 (1984).
71. H. T. Young, P. Mathew and P. L. B. Oxley, "Allowing for Nose Radius Effects in Predicting the Chip Flow Direction and Cutting Forces in Bar Turning", *Proc. Inst. Mech. Engrs.*, **201**(C3), pp. 213-226 (1987).
72. J. Wang and P. Mathew, "Predicting the Chip Flow Direction for Nose Radius Tools under Oblique Machining Conditions", University of New South Wales Report, Australia, 1988/IE/2 (1988).
73. V.I.Sisoev, Fundamentals of Metal Cutting and Cutting Tools, Mashgiz, Moscow (1962).
74. J. S. Bator, "Power Reduction through Efficient Chip Control", *Cutting Tool Engineering*, pp. 4-8 (July/August 1975).
75. A. Ber, S. Kaldor and E. Lenz, "New Concept in Chip-breaker Design Leads to a Wider Range of Chip-Breaking", SME Technical Paper, MR 79-307 (1979).
76. S. Kaldor, A. Ber and E. Lenz, "On the mechanism of chip breaking", *Trans. ASME*, **101** pp. 241-249 (1979).
77. L. De Chiffre, "Cutting Tools with Restricted Contact", *Int. J. Mach. Tool Des. Res.*, **22**(4), pp. 321-332 (1982).

78. L. De Chiffre, "Metal Cutting - Mechanics and Applications", D. Sc. Thesis, Technical University of Denmark (1990).
79. I. S. Jawahir, "An investigation of Three-dimensional Chip Flow in Machining of Steels with Grooved Chip Forming Tool Insert", *Trans. NAMRC*, Vol. 19, pp. 222-231 (1991).
80. S. Rangwala and D. Dornfeld, "Integration of Sensors via Neural Networks for Detection of Tool Wear States", *ASME/WAM, Intelligent and Integrated Manufacturing Analysis & Synthesis*, PED - Vol. 25, pp. 109-120 (1987).
81. A. Del Taglia, et. al., "An Approach to On-line Measurement of Tool Wear by Spectrum Analysis", *Proc. of Int. MTDRC*, pp. 141-148 (1976).
82. C.Y. Jiang, Y.Z. Zhang and H.J. Xu, "In-Process Monitoring of Tool Wear Stage by the Frequency Band-Energy Method", *Ann. CIRP*, 36(1), pp. 45-48 (1987).
83. T. Sata, et. al, "Learning and Recognition of the Cutting States by the Spectrum Analysis", *Ann. CIRP*, 22(1), pp 41-42 (1973).
84. K.F. Eman and S.M. Wu, "Present and Future Trends in Stochastic Analysis of Cutting and Structural Dynamics", *Proc. of 15th NAMRC*, pp. 426-432 (1987).
85. W.R. DeVries, D.A. Dornfeld and S.M. Wu, "Bivariate Time Series Analysis of the Effective Force Variation and Friction Coefficient Distribution in Wood Grinding", *ASME Trans., J. of Eng. for Ind.*, 100, pp 181-185 (May 1978).
86. B. Mills and A. H. Redford, Machinability of Engineering Materials, Applied Science Publishers (1983).
87. A.J. Pikelharing and C.A., Van Luttervelt, CIRP Terminology and Procedures for Turning Research, Technical Secretary CIRP Group C, Delft, (1969).
88. B. Wu, et. al., "The Dynamic Component of Cutting Force and its Application in Cutting State Identification", *J. of Nanjing Institute of Technology*, 17, No. 6 (I), pp. 55-65 (1987).

89. H. Akaike, "A New Look at the Statistical Model Identification", *IEEE Trans. Automat. Contr.*, AC-19, pp. 716-723 (1974).
90. V. Solaja, "Wear of Carbide Tools and Surface Finish Generated in Finish Turning of Steel", *Wear*, 2, pp. 40-58 (1958/1959).
91. M.C. Shaw, and J.A. Crowell, "Finish Machining", *Ann. CIRP*, 13, pp. 5-22 (1965).
92. A.J. Pekelharing and H.J. Hovinga, "Wear at the End Cutting Edge of Carbide Tools in Finish and Rough Turning", *Proc. of 8th Int. MTDR Conf*, pp. 643-651 (1967).
93. S.M. Pandit, "Data Dependent Systems : Modeling Analysis and Optimal Control via Time Series", PhD Thesis, University of Wisconsin, Madison, WI, U.S.A. (1973).
94. X. D. Fang and I. S. Jawahir, "An Expert System Based on A Fuzzy Mathematical Model for Chip Breakability Assessments in Automated Machining", *Proc. Int. Conf., ASME, MI'90*, Vol. IV, Atlanta, Georgia, U. S. A., pp. 31-37 (March 1990).
95. X. D. Fang and I. S. Jawahir, "On Predicting Chip Breakability in Machining of Steels with Carbide Tool Inserts Having Complex Chip Groove Geometries", to appear in *J. Materials Processing Technology*, 26, Issue 2, selected from the papers in *Proc. 7th International Conference on Computer-Aided Production Engineering*, Tennessee, USA, pp. 37-48 (1991).
96. D. Rumelhart and J. McClelland, Parallel Distributed Processing, Vol. 1, MIT Press, Cambridge, MA (1986).
97. P.D. Wasserman, Neural Computing : Theory and Practice, Van Nostrand Reinhold, New York (1989).
98. J.E. Dayhoff, Neural Network Architectures, Van Nostrand Reinhold, New York (1990).

99. S.C. Huang and Y.F. Huang, "Bounds on the Number of Hidden Neurons in Multilayer Perceptrons", *IEEE Trans. on Neural Networks*, 2(1), pp. 47-55 (1991).
100. S.Y. Kung and J.N. Hwang, "Bounds on the Number of Hidden Neurons in Multilayer Perceptrons", *Proc. IEEE Int. Conf. on Neural Networks*, Vol. I, San Diego, California, pp. 363-370 (1988).
101. P.D. Hewitt, P.J.C. Skitt and R.C. Witcomb, "A Self-organising Feedforward Network Applied to Acoustic Data", *New Development in Neural Computing*, ed. J.G. Taylor and C.L.T. Mannion, Adam Hilger, Bristol and New York, pp. 71-78 (1989).
102. G.A. Carpenter and S. Grossberg, "The ART of Adaptive Pattern Recognition by a Self-organising Neural Network", *Artificial Neural Networks Concept Learning*, ed. J. Diederich, IEEE Computer Society Press, pp. 69-80 (1990).
103. Usui, E., "Progress of 'Predictive' Theories in Metal Cutting", *JSME Int. J.*, Series III, 31, No. 2, pp. 363-369 (1988).
104. Monostori, L., "Signal Processing and Decision Making in Machine Tool Monitoring Systems", *Proc. 16th NAMRC*, pp. 277-284 (1988).
105. X. D. Fang and Y. Yao, "Expert System-Supported On-line Tool Wear Monitoring", *Proc. of International Conference on Artificial Intelligence in Engineering - AIE'90*, Sponsored by I.E.E.(UK), Kuala Lumpur, Malaysia, pp. 77-84 (August 1990).

APPENDIX A

STANDARD FUZZY MEMBERSHIP VALUES FOR CHIP BREAKABILITY

Table A-1 Standard fuzzy membership values $\mu(x)$ for chip breakability

Work Material : CS1020

Chip Breaker : ENZ-type

Tool Geometry : 0° , 5° , -6° , 90° , 60° , 0.8

Cutting Speed (m/min)	Depth of Cut (mm)	Feed (mm/rev)					
		0.06	0.1	0.2	0.3	0.4	0.5
50	4.0	0.49	0.40	0.56	0.77	0.82	0.86
	3.0	0.51	0.41	0.58	0.77	0.86	0.91
	2.0	0.53	0.47	0.46	0.73	0.83	0.87
	1.0	0.58	0.51	0.38	0.43	0.46	0.47
	0.5	0.43	0.41	0.40	0.41	0.42	0.44
	0.25	0.45	0.43	0.43	0.40	0.41	0.42
75	4.0	0.23	0.21	0.49	0.74	0.83	0.87
	3.0	0.25	0.23	0.50	0.73	0.80	0.83
	2.0	0.27	0.23	0.45	0.73	0.80	0.83
	1.0	0.41	0.26	0.38	0.43	0.45	0.46
	0.5	0.40	0.38	0.38	0.40	0.41	0.43
	0.25	0.44	0.40	0.40	0.40	0.40	0.41
100	4.0	0.16	0.19	0.48	0.71	0.75	0.82
	3.0	0.17	0.19	0.48	0.71	0.80	0.84
	2.0	0.19	0.19	0.45	0.71	0.77	0.81
	1.0	0.23	0.21	0.35	0.42	0.45	0.45
	0.5	0.26	0.28	0.37	0.40	0.41	0.43
	0.25	0.31	0.35	0.39	0.38	0.39	0.40
150	4.0	0.11	0.16	0.47	0.68	0.72	0.80
	3.0	0.13	0.16	0.47	0.68	0.77	0.81
	2.0	0.16	0.16	0.41	0.69	0.74	0.80
	1.0	0.16	0.31	0.41	0.41	0.43	0.43
	0.5	0.21	0.24	0.36	0.39	0.40	0.42
	0.25	0.26	0.30	0.38	0.37	0.38	0.40
200	4.0	0.09	0.13	0.43	0.64	0.68	0.76
	3.0	0.11	0.13	0.43	0.64	0.73	0.77
	2.0	0.13	0.13	0.37	0.65	0.70	0.75
	1.0	0.16	0.13	0.27	0.37	0.40	0.40
	0.5	0.18	0.20	0.32	0.35	0.36	0.38
	0.25	0.22	0.26	0.33	0.33	0.34	0.36

Table A-2 Standard fuzzy membership values $\mu(x)$ for chip breakability
 Work Material : K1040
 Chip Breaker : ENZ-type
 Tool Geometry : 0° , 5° , -6° , 90° , 60° , 0.8

Cutting Speed (m/min)	Depth of Cut (mm)	Feed (mm/rev)					
		0.06	0.1	0.2	0.3	0.4	0.5
50	4.0	0.47	0.37	0.68	0.76	0.81	0.85
	3.0	0.50	0.39	0.66	0.76	0.85	0.90
	2.0	0.53	0.44	0.49	0.73	0.82	0.86
	1.0	0.58	0.50	0.37	0.43	0.45	0.45
	0.5	0.59	0.56	0.39	0.40	0.41	0.43
	0.25	0.50	0.55	0.50	0.40	0.41	0.42
75	4.0	0.22	0.20	0.64	0.73	0.71	0.83
	3.0	0.24	0.22	0.62	0.73	0.82	0.86
	2.0	0.26	0.22	0.49	0.73	0.79	0.82
	1.0	0.40	0.25	0.36	0.43	0.45	0.46
	0.5	0.50	0.38	0.38	0.40	0.41	0.43
	0.25	0.50	0.46	0.40	0.40	0.40	0.41
100	4.0	0.15	0.18	0.60	0.70	0.74	0.81
	3.0	0.16	0.18	0.59	0.70	0.79	0.83
	2.0	0.18	0.18	0.49	0.70	0.76	0.80
	1.0	0.22	0.20	0.34	0.42	0.44	0.44
	0.5	0.25	0.28	0.36	0.39	0.40	0.42
	0.25	0.30	0.34	0.38	0.38	0.39	0.40
150	4.0	0.10	0.15	0.42	0.67	0.71	0.79
	3.0	0.12	0.15	0.43	0.67	0.76	0.80
	2.0	0.15	0.15	0.37	0.68	0.73	0.79
	1.0	0.18	0.15	0.30	0.40	0.43	0.43
	0.5	0.20	0.23	0.35	0.38	0.39	0.41
	0.25	0.25	0.29	0.36	0.37	0.38	0.40
200	4.0	0.08	0.12	0.38	0.63	0.67	0.75
	3.0	0.10	0.12	0.39	0.63	0.72	0.76
	2.0	0.12	0.12	0.32	0.64	0.69	0.74
	1.0	0.15	0.12	0.26	0.36	0.39	0.39
	0.5	0.17	0.19	0.31	0.34	0.35	0.37
	0.25	0.21	0.25	0.32	0.33	0.34	0.36

Table A-3 Standard fuzzy membership values $\mu(x)$ for chip breakability
 Work Material : EN25
 Chip Breaker : ENZ-type
 Tool Geometry : $0^\circ, 5^\circ, -6^\circ, 90^\circ, 60^\circ, 0.8$

Cutting Speed (m/min)	Depth of Cut (mm)	Feed (mm/rev)					
		0.06	0.1	0.2	0.3	0.4	0.5
50	4.0	0.26	0.27	0.45	0.73	0.78	0.82
	3.0	0.30	0.31	0.45	0.73	0.82	0.87
	2.0	0.35	0.36	0.45	0.67	0.79	0.83
	1.0	0.40	0.38	0.34	0.40	0.42	0.43
	0.5	0.45	0.39	0.36	0.37	0.38	0.40
	0.25	0.48	0.43	0.42	0.39	0.40	0.41
75	4.0	0.19	0.17	0.45	0.70	0.74	0.80
	3.0	0.21	0.19	0.45	0.70	0.79	0.83
	2.0	0.23	0.19	0.45	0.70	0.76	0.79
	1.0	0.37	0.22	0.33	0.40	0.42	0.43
	0.5	0.38	0.35	0.35	0.37	0.38	0.40
	0.25	0.42	0.38	0.37	0.39	0.39	0.40
100	4.0	0.12	0.15	0.42	0.67	0.76	0.80
	3.0	0.13	0.15	0.42	0.67	0.76	0.80
	2.0	0.15	0.15	0.42	0.67	0.73	0.77
	1.0	0.19	0.17	0.31	0.39	0.41	0.41
	0.5	0.22	0.25	0.33	0.36	0.37	0.39
	0.25	0.27	0.32	0.36	0.37	0.38	0.39
150	4.0	0.07	0.12	0.40	0.64	0.68	0.76
	3.0	0.09	0.12	0.41	0.64	0.73	0.77
	2.0	0.12	0.12	0.35	0.65	0.70	0.76
	1.0	0.15	0.12	0.27	0.37	0.40	0.40
	0.5	0.17	0.20	0.32	0.35	0.36	0.38
	0.25	0.22	0.28	0.35	0.36	0.37	0.39
200	4.0	0.06	0.10	0.36	0.60	0.64	0.72
	3.0	0.07	0.09	0.37	0.60	0.69	0.73
	2.0	0.09	0.09	0.31	0.61	0.66	0.71
	1.0	0.12	0.09	0.23	0.33	0.36	0.36
	0.5	0.14	0.16	0.28	0.31	0.32	0.34
	0.25	0.20	0.24	0.31	0.32	0.33	0.35

Table A-4 Standard fuzzy membership values $\mu(x)$ for chip breakability
 Work Material : CS1020
 Chip Breaker : ENA-type
 Tool Geometry : 0° , 5° , -6° , 90° , 60° , 0.8

Cutting Speed (m/min)	Depth of Cut (mm)	Feed (mm/rev)					
		0.06	0.1	0.2	0.3	0.4	0.5
50	4.0	0.48	0.56	0.70	0.78	0.85	0.90
	3.0	0.49	0.56	0.74	0.83	0.90	0.94
	2.0	0.49	0.55	0.72	0.80	0.89	0.91
	1.0	0.48	0.46	0.65	0.72	0.80	0.84
	0.5	0.60	0.46	0.37	0.38	0.40	0.42
	0.25	0.60	0.48	0.38	0.38	0.39	0.40
75	4.0	0.25	0.32	0.68	0.75	0.83	0.89
	3.0	0.25	0.33	0.71	0.81	0.89	0.93
	2.0	0.28	0.33	0.66	0.75	0.85	0.87
	1.0	0.28	0.32	0.60	0.67	0.78	0.80
	0.5	0.46	0.36	0.36	0.36	0.40	0.42
	0.25	0.55	0.45	0.36	0.36	0.39	0.40
100	4.0	0.20	0.30	0.65	0.72	0.80	0.88
	3.0	0.20	0.30	0.68	0.80	0.88	0.92
	2.0	0.25	0.30	0.62	0.72	0.81	0.84
	1.0	0.26	0.29	0.55	0.64	0.74	0.78
	0.5	0.34	0.36	0.36	0.36	0.40	0.42
	0.25	0.32	0.36	0.36	0.36	0.38	0.39
150	4.0	0.12	0.25	0.60	0.70	0.79	0.87
	3.0	0.15	0.26	0.65	0.75	0.87	0.91
	2.0	0.18	0.26	0.59	0.70	0.78	0.82
	1.0	0.19	0.25	0.50	0.60	0.71	0.76
	0.5	0.30	0.34	0.34	0.35	0.38	0.39
	0.25	0.32	0.36	0.35	0.35	0.37	0.37
200	4.0	0.20	0.30	0.65	0.72	0.80	0.88
	3.0	0.20	0.30	0.68	0.80	0.88	0.92
	2.0	0.25	0.30	0.62	0.72	0.81	0.84
	1.0	0.26	0.29	0.55	0.64	0.74	0.78
	0.5	0.34	0.36	0.36	0.36	0.40	0.42
	0.25	0.32	0.36	0.36	0.36	0.38	0.39

Table A-5 Standard fuzzy membership values $\mu(x)$ for chip breakability
 Work Material : K1040
 Chip Breaker : ENA-type
 Tool Geometry : $0^\circ, 5^\circ, -6^\circ, 90^\circ, 60^\circ, 0.8$

Cutting Speed (m/min)	Depth of Cut (mm)	Feed (mm/rev)					
		0.06	0.1	0.2	0.3	0.4	0.5
50	4.0	0.48	0.47	0.69	0.77	0.84	0.89
	3.0	0.48	0.46	0.73	0.82	0.89	0.93
	2.0	0.48	0.46	0.71	0.79	0.88	0.90
	1.0	0.48	0.46	0.64	0.71	0.79	0.83
	0.5	0.61	0.55	0.38	0.39	0.39	0.39
	0.25	0.53	0.58	0.38	0.38	0.39	0.40
75	4.0	0.25	0.32	0.67	0.74	0.82	0.88
	3.0	0.25	0.33	0.70	0.80	0.88	0.92
	2.0	0.28	0.33	0.65	0.74	0.84	0.86
	1.0	0.28	0.32	0.59	0.66	0.77	0.79
	0.5	0.54	0.35	0.37	0.37	0.41	0.43
	0.25	0.52	0.52	0.36	0.36	0.39	0.40
100	4.0	0.20	0.30	0.64	0.71	0.79	0.87
	3.0	0.20	0.30	0.67	0.78	0.87	0.91
	2.0	0.25	0.30	0.61	0.71	0.80	0.83
	1.0	0.25	0.29	0.54	0.63	0.73	0.77
	0.5	0.35	0.35	0.37	0.37	0.41	0.43
	0.25	0.43	0.36	0.36	0.36	0.38	0.39
150	4.0	0.11	0.25	0.59	0.69	0.78	0.86
	3.0	0.14	0.26	0.64	0.74	0.86	0.90
	2.0	0.17	0.26	0.58	0.69	0.77	0.81
	1.0	0.18	0.25	0.49	0.59	0.70	0.75
	0.5	0.30	0.33	0.34	0.35	0.38	0.39
	0.25	0.32	0.36	0.35	0.35	0.37	0.37
200	4.0	0.20	0.30	0.64	0.71	0.79	0.87
	3.0	0.20	0.30	0.67	0.78	0.87	0.91
	2.0	0.25	0.30	0.61	0.71	0.80	0.83
	1.0	0.25	0.29	0.54	0.63	0.73	0.77
	0.5	0.35	0.35	0.37	0.37	0.41	0.43
	0.25	0.43	0.36	0.36	0.36	0.38	0.39

Table A-6 Standard fuzzy membership values $\mu(x)$ for chip breakability
 Work Material : EN25
 Chip Breaker : ENA-type
 Tool Geometry : 0° , 5° , -6° , 90° , 60° , 0.8

Cutting Speed (m/min)	Depth of Cut (mm)	Feed (mm/rev)					
		0.06	0.1	0.2	0.3	0.4	0.5
50	4.0	0.30	0.32	0.64	0.75	0.82	0.87
	3.0	0.32	0.34	0.68	0.80	0.87	0.91
	2.0	0.32	0.32	0.64	0.77	0.86	0.88
	1.0	0.32	0.30	0.59	0.69	0.77	0.81
	0.5	0.40	0.43	0.36	0.38	0.39	0.45
	0.25	0.45	0.38	0.37	0.37	0.38	0.39
75	4.0	0.22	0.29	0.38	0.72	0.80	0.86
	3.0	0.22	0.30	0.40	0.78	0.86	0.90
	2.0	0.25	0.30	0.38	0.72	0.83	0.84
	1.0	0.25	0.29	0.35	0.64	0.75	0.77
	0.5	0.28	0.33	0.35	0.35	0.39	0.41
	0.25	0.43	0.36	0.35	0.35	0.37	0.38
100	4.0	0.17	0.27	0.36	0.69	0.77	0.85
	3.0	0.17	0.27	0.38	0.77	0.85	0.89
	2.0	0.22	0.27	0.36	0.69	0.78	0.81
	1.0	0.22	0.26	0.34	0.61	0.71	0.75
	0.5	0.28	0.33	0.35	0.36	0.39	0.39
	0.25	0.34	0.35	0.35	0.35	0.37	0.38
150	4.0	0.08	0.22	0.34	0.67	0.76	0.84
	3.0	0.11	0.23	0.35	0.72	0.84	0.88
	2.0	0.14	0.23	0.33	0.67	0.75	0.79
	1.0	0.16	0.22	0.32	0.57	0.68	0.73
	0.5	0.27	0.31	0.33	0.35	0.38	0.39
	0.25	0.29	0.33	0.34	0.34	0.36	0.36
200	4.0	0.17	0.27	0.36	0.69	0.77	0.85
	3.0	0.17	0.27	0.38	0.77	0.85	0.89
	2.0	0.22	0.27	0.36	0.69	0.78	0.81
	1.0	0.22	0.26	0.34	0.61	0.71	0.75
	0.5	0.28	0.33	0.35	0.36	0.39	0.39
	0.25	0.34	0.35	0.35	0.35	0.37	0.38

Table A-7 Standard fuzzy membership values $\mu(x)$ for chip breakability
 Work Material : CS1020
 Chip Breaker : ENT-type
 Tool Geometry : 0° , 5° , -6° , 90° , 60° , 0.8

Cutting Speed (m/min)	Depth of Cut (mm)	Feed (mm/rev)					
		0.06	0.1	0.2	0.3	0.4	0.5
50	4.0	0.42	0.32	0.63	0.79	0.89	0.92
	3.0	0.42	0.31	0.62	0.80	0.91	0.95
	2.0	0.43	0.31	0.61	0.77	0.82	0.88
	1.0	0.43	0.25	0.51	0.70	0.79	0.81
	0.5	0.51	0.38	0.39	0.40	0.43	0.45
	0.25	0.48	0.45	0.38	0.38	0.40	0.43
75	4.0	0.22	0.31	0.61	0.77	0.87	0.91
	3.0	0.22	0.30	0.60	0.78	0.89	0.94
	2.0	0.22	0.30	0.59	0.75	0.80	0.86
	1.0	0.27	0.24	0.47	0.68	0.74	0.78
	0.5	0.51	0.38	0.37	0.39	0.42	0.44
	0.25	0.45	0.45	0.38	0.38	0.40	0.43
100	4.0	0.22	0.30	0.59	0.75	0.85	0.90
	3.0	0.22	0.30	0.58	0.76	0.87	0.93
	2.0	0.22	0.30	0.57	0.73	0.78	0.84
	1.0	0.23	0.23	0.44	0.66	0.70	0.75
	0.5	0.32	0.34	0.33	0.38	0.41	0.43
	0.25	0.39	0.38	0.36	0.36	0.38	0.41
150	4.0	0.18	0.29	0.57	0.73	0.83	0.89
	3.0	0.18	0.29	0.57	0.74	0.84	0.92
	2.0	0.18	0.28	0.55	0.71	0.76	0.82
	1.0	0.20	0.22	0.42	0.62	0.66	0.76
	0.5	0.28	0.32	0.30	0.37	0.40	0.42
	0.25	0.36	0.35	0.36	0.36	0.37	0.41
200	4.0	0.14	0.26	0.53	0.69	0.79	0.85
	3.0	0.26	0.17	0.37	0.70	0.80	0.88
	2.0	0.14	0.25	0.51	0.67	0.72	0.78
	1.0	0.17	0.19	0.38	0.58	0.62	0.68
	0.5	0.25	0.28	0.26	0.33	0.36	0.38
	0.25	0.32	0.31	0.33	0.33	0.34	0.40

Table A-8 Standard fuzzy membership values $\mu(x)$ for chip breakability
 Work Material : K1040
 Chip Breaker : ENT-type
 Tool Geometry : $0^\circ, 5^\circ, -6^\circ, 90^\circ, 60^\circ, 0.8$

Cutting Speed (m/min)	Depth of Cut (mm)	Feed (mm/rev)					
		0.06	0.1	0.2	0.3	0.4	0.5
50	4.0	0.42	0.46	0.49	0.77	0.87	0.90
	3.0	0.42	0.40	0.46	0.78	0.89	0.93
	2.0	0.43	0.40	0.46	0.75	0.80	0.86
	1.0	0.43	0.40	0.43	0.68	0.76	0.79
	0.5	0.55	0.38	0.35	0.40	0.43	0.45
	0.25	0.55	0.46	0.38	0.38	0.40	0.43
75	4.0	0.20	0.30	0.45	0.75	0.85	0.89
	3.0	0.20	0.30	0.45	0.76	0.87	0.92
	2.0	0.20	0.22	0.45	0.73	0.78	0.84
	1.0	0.25	0.28	0.45	0.66	0.72	0.76
	0.5	0.35	0.34	0.35	0.39	0.42	0.44
	0.25	0.40	0.38	0.38	0.38	0.40	0.43
100	4.0	0.20	0.25	0.45	0.73	0.83	0.88
	3.0	0.20	0.25	0.45	0.74	0.85	0.91
	2.0	0.20	0.22	0.45	0.71	0.76	0.82
	1.0	0.21	0.22	0.45	0.64	0.68	0.73
	0.5	0.30	0.32	0.31	0.38	0.41	0.43
	0.25	0.37	0.36	0.36	0.36	0.38	0.41
150	4.0	0.15	0.20	0.38	0.71	0.81	0.87
	3.0	0.15	0.20	0.39	0.72	0.82	0.90
	2.0	0.15	0.18	0.38	0.69	0.74	0.80
	1.0	0.18	0.18	0.38	0.60	0.64	0.70
	0.5	0.26	0.30	0.27	0.37	0.40	0.42
	0.25	0.34	0.33	0.36	0.36	0.37	0.41
200	4.0	0.12	0.15	0.34	0.67	0.77	0.83
	3.0	0.12	0.15	0.35	0.68	0.78	0.86
	2.0	0.12	0.14	0.34	0.65	0.70	0.76
	1.0	0.15	0.15	0.34	0.56	0.60	0.66
	0.5	0.23	0.26	0.30	0.33	0.36	0.38
	0.25	0.30	0.30	0.33	0.33	0.34	0.39

Table A-9 Standard fuzzy membership values $\mu(x)$ for chip breakability
 Work Material : EN25
 Chip Breaker : ENT-type
 Tool Geometry : $0^\circ, 5^\circ, -6^\circ, 90^\circ, 60^\circ, 0.8$

Cutting Speed (m/min)	Depth of Cut (mm)	Feed (mm/rev)					
		0.06	0.1	0.2	0.3	0.4	0.5
50	4.0	0.28	0.29	0.45	0.74	0.84	0.87
	3.0	0.30	0.30	0.47	0.75	0.86	0.90
	2.0	0.31	0.28	0.47	0.72	0.77	0.83
	1.0	0.32	0.28	0.42	0.65	0.73	0.76
	0.5	0.35	0.28	0.32	0.39	0.41	0.43
	0.25	0.38	0.37	0.37	0.37	0.39	0.42
75	4.0	0.17	0.27	0.41	0.72	0.82	0.86
	3.0	0.17	0.27	0.43	0.73	0.84	0.89
	2.0	0.17	0.25	0.42	0.70	0.75	0.81
	1.0	0.22	0.25	0.39	0.63	0.69	0.73
	0.5	0.32	0.31	0.28	0.38	0.40	0.42
	0.25	0.36	0.35	0.37	0.37	0.39	0.42
100	4.0	0.17	0.22	0.39	0.70	0.80	0.85
	3.0	0.12	0.22	0.40	0.71	0.82	0.88
	2.0	0.12	0.19	0.40	0.68	0.73	0.79
	1.0	0.18	0.19	0.38	0.59	0.65	0.70
	0.5	0.27	0.29	0.25	0.37	0.39	0.41
	0.25	0.34	0.33	0.35	0.35	0.37	0.40
150	4.0	0.08	0.17	0.38	0.68	0.78	0.84
	3.0	0.10	0.17	0.38	0.69	0.79	0.87
	2.0	0.12	0.15	0.38	0.66	0.71	0.77
	1.0	0.15	0.15	0.35	0.48	0.61	0.67
	0.5	0.23	0.27	0.22	0.36	0.38	0.40
	0.25	0.31	0.30	0.35	0.35	0.36	0.40
200	4.0	0.06	0.12	0.31	0.64	0.74	0.80
	3.0	0.09	0.12	0.32	0.65	0.75	0.83
	2.0	0.09	0.11	0.31	0.62	0.67	0.73
	1.0	0.12	0.12	0.31	0.53	0.57	0.63
	0.5	0.21	0.22	0.22	0.32	0.32	0.34
	0.25	0.27	0.26	0.33	0.33	0.33	0.38

APPENDIX B

REPRESENTATIVE DATA OF SURFACE FINISH WHEN MACHINING WITH DIFFERENT TOOL CHIP BREAKERS

Table B-1 Surface roughness R_a (μm) for work material CS1020

Tool Geometry : $0^\circ, 5^\circ, -6^\circ, 90^\circ, 60^\circ, 0.8$

Depth of Cut : $d = 0.5 \text{ mm}$

Machine Tool : Colchester Mascot 1600 (9.3 KW)

Cutting Speed (m/min)	Feed (mm/rev)	Tool Chip Breaker					
		EFJ- type	EFB- type	ENA- type	ENG- type	ENK- type	ENJ- type
100	0.06	1.69	1.38	1.28	1.27	1.95	1.90
	0.08	1.38	1.29	1.22	1.20	1.61	1.49
	0.10	1.22	1.17	1.29	1.26	1.29	1.24
	0.12	1.30	1.20	1.32	1.32	1.38	1.35
	0.15	1.37	1.38	1.41	1.60	1.62	1.60
	0.20	1.63	1.66	1.84	1.99	1.82	1.88
	0.25	2.42	2.38	2.57	2.59	2.61	2.70
	0.30	3.54	3.41	3.87	3.87	3.79	3.96
150	0.06	1.15	1.08	1.17	1.12	1.21	1.20
	0.08	1.17	1.10	1.20	1.18	1.23	1.22
	0.10	1.20	1.15	1.26	1.23	1.28	1.26
	0.12	1.24	1.17	1.31	1.26	1.32	1.31
	0.15	1.30	1.33	1.37	1.50	1.64	1.58
	0.20	1.62	1.48	1.77	1.88	1.81	1.87
	0.25	2.29	2.28	2.19	2.31	2.09	2.31
	0.30	3.22	3.01	3.37	3.19	3.20	3.29
200	0.06	1.04	0.95	1.08	1.07	1.11	1.09
	0.08	1.10	0.99	1.13	1.12	1.15	1.12
	0.10	1.16	1.04	1.17	1.13	1.18	1.17
	0.12	1.20	1.12	1.24	1.18	1.25	1.24
	0.15	1.25	1.18	1.31	1.29	1.31	1.30

Table B-2 Surface roughness R_a (μm) for work material K1040Tool Geometry : $0^\circ, 5^\circ, -6^\circ, 90^\circ, 60^\circ, 0.8$ Depth of Cut : $d = 0.5 \text{ mm}$

Machine Tool : Colchester Mascot 1600 (9.3 KW)

Cutting Speed (m/min)	Feed (mm/rev)	Tool Chip Breaker					
		EFJ- type	EFB- type	ENA- type	ENG- type	ENK- type	ENJ- type
100	0.06	1.91	1.82	1.49	2.03	1.81	2.19
	0.08	1.72	1.20	1.25	1.43	1.29	1.80
	0.10	1.32	1.26	1.28	1.27	1.33	1.31
	0.12	1.41	1.30	1.42	1.30	1.36	1.38
	0.15	1.65	1.31	1.66	1.51	1.70	1.59
	0.20	1.82	1.70	1.91	1.94	1.97	1.96
	0.25	2.59	2.27	2.39	2.34	2.29	2.34
	0.30	3.60	3.26	2.99	3.21	3.21	3.39
150	0.06	1.14	1.11	1.19	1.16	1.18	1.15
	0.08	1.19	1.14	1.24	1.19	1.24	1.22
	0.10	1.25	1.15	1.27	1.27	1.31	1.30
	0.12	1.32	1.21	1.35	1.34	1.39	1.37
	0.15	1.39	1.28	1.49	1.60	1.59	1.61
	0.20	1.69	1.69	1.80	1.84	1.86	1.91
	0.25	2.18	2.20	2.31	2.24	2.35	2.44
	0.30	2.97	2.88	3.01	2.86	3.02	3.26
200	0.06	1.06	0.98	1.09	1.08	1.12	1.10
	0.08	1.10	1.11	1.12	1.10	1.16	1.13
	0.10	1.13	1.15	1.16	1.17	1.20	1.17
	0.12	1.24	1.20	1.21	1.22	1.23	1.24
	0.15	1.27	1.25	1.29	1.32	1.29	1.29

Table B-3 Surface roughness R_a (μm) for work material EN25Tool Geometry : $0^\circ, 5^\circ, -6^\circ, 90^\circ, 60^\circ, 0.8$ Depth of Cut : $d = 0.5$ mm

Machine Tool : Colchester Mascot 1600 (9.3 KW)

Cutting Speed (m/min)	Feed (mm/rev)	Tool Chip Breaker					
		EFJ- type	EFB- type	ENA- type	ENG- type	ENK- type	ENJ- type
100	0.06	0.76	0.73	0.82	0.80	0.89	0.84
	0.08	0.78	0.74	0.85	0.84	0.92	0.87
	0.10	0.81	0.78	0.89	0.86	0.97	0.91
	0.12	0.97	0.84	0.98	0.95	1.01	0.99
	0.15	1.10	1.19	1.28	1.27	1.29	1.32
	0.20	1.61	1.49	1.62	1.71	1.80	1.88
	0.25	2.45	2.13	2.38	2.58	2.49	2.61
	0.30	3.36	2.78	2.97	3.11	2.88	3.24
150	0.06	0.74	0.70	0.78	0.78	0.84	0.82
	0.08	0.77	0.72	0.79	0.81	0.88	0.83
	0.10	0.80	0.75	0.83	0.84	0.91	0.87
	0.12	0.89	0.79	0.88	0.87	0.93	0.92
	0.15	1.23	1.10	1.27	1.19	1.34	1.31
	0.20	1.60	1.44	1.60	1.71	1.85	1.89
	0.25	2.38	1.92	2.21	2.32	2.25	2.61
	0.30	3.25	2.59	2.89	2.88	2.91	3.11
200	0.06	0.70	0.68	0.72	0.73	0.78	0.76
	0.08	0.73	0.71	0.76	0.74	0.83	0.79
	0.10	0.78	0.73	0.78	0.82	0.88	0.84
	0.12	0.83	0.78	0.87	0.86	0.91	0.89
	0.15	0.89	0.84	0.95	0.96	1.04	1.08

APPENDIX C

OVERALL GROOVE WEAR DATA FROM GROOVE WEAR EXPERIMENTS

Table C-1 Overall groove wear data under cutting condition Group A
 Machine Tool : HITEC-20SII CNC Lathe (18 KW)
 $V = 160$ m/min, $f = 0.08$ mm/rev, $d = 0.25$ mm

Cutting Time (minute)	Number of Groove	Groove Depth (μm)	Maximum Groove Length (μm)	Groove Wear Area (mm^2)	Nose wear (μm)	Surface Roughness R_a (μm)
0.0	0	0	0	0	0	0.86
0.5						0.92
1.0						0.95
1.5						1.29
2.0						1.59
3.0	2	5	91	0.49	4	1.68
4.0						1.74
5.0						1.77
6.0	3	5.5	105	0.84	5	1.79
7.5						1.78
8.5						1.80
10	3	6	140	2.10	6	1.81
12						1.79
14						1.82
16	3	6.5	155	2.39	8	1.80
18						1.77
20						1.77
22	4	6.9	165	3.51	10	1.78
25						1.99
27						2.23
30	4	8.2	185	4.25	13	2.41
33						2.70
35.5						2.89
38	5	9.3	225	7.60	17	2.98
41						3.25
45						3.29
48	5	10.7	260	7.80	20	3.37

Table C-2 Overall groove wear data under cutting condition Group B
 Machine Tool : HITEC-20SII CNC Lathe (18 KW)
 $V = 160$ m/min, $f = 0.04$ mm/rev, $d = 0.25$ mm

Cutting Time (minute)	Number of Groove	Groove Depth (μm)	Maximum Groove Length (μm)	Groove Wear Area (mm^2)	Nose wear (μm)	Surface Roughness R_a (μm)
0.0	0	0	0	0	0	0.40
0.5						0.44
1.0						0.47
1.5						0.70
2.0						0.98
3.0	4	5.0	65	0.52	4.5	1.36
4.0						1.58
5.0						1.71
6.0	5	5.0	113	1.31	6	1.79
7.5						1.82
8.5						1.85
10	7	5.5	150	3.45	7	1.82
12						1.82
14						1.80
16	8	5.8	160	4.20	8.5	1.84
18.5						2.98
21						3.51
23	4	4.7	175	4.26	12	3.40
25						3.30
27.5						3.20
30	5	6.8	225	6.53	15	3.31
33						3.22
37						3.13
40	5	5.3	250	7.50	18	3.14
43						3.50
47						3.55
50	1	5.2	265	8.32	21	3.58

Table C-3 Overall groove wear data under cutting condition Group C
 Machine Tool : HITEC-20SII CNC Lathe (18 KW)
 $V = 125$ m/min, $f = 0.08$ mm/rev, $d = 0.25$ mm

Cutting Time (minute)	Number of Groove	Groove Depth (μm)	Maximum Groove Length (μm)	Groove Wear Area (mm^2)	Nose wear (μm)	Surface Roughness R_a (μm)
0.0	0	0	0	0	0	1.02
0.5						1.02
1.0						1.05
1.5						1.40
2.5						1.68
3.5	2	5.0	67	0.35	4.5	1.79
5.0						1.80
7.0						1.83
9.0	2	6.0	82	0.60	5	1.82
11						1.83
13						1.82
15	3	6.5	135	2.06	7	1.82
17						1.83
19						1.84
21	3	6.7	158	2.56	9	1.87
23						1.84
26						1.85
29	3	6.7	165	2.72	12.5	1.86
32						1.83
35						1.79
39	4	6.8	205	4.40	15	1.79
43						1.91
46						2.38
49	5	10.3	310	4.62	19	2.77
53						2.98
57						3.19
61	5	10.5	330	10.5	23	3.28

Table C-4 Overall groove wear data under cutting condition Group D
 Machine Tool : HITEC-20SII CNC Lathe (18 KW)
 $V = 190$ m/min, $f = 0.08$ mm/rev, $d = 0.25$ mm

Cutting Time (minute)	Number of Groove	Groove Depth (μm)	Maximum Groove Length (μm)	Groove Wear Area (mm^2)	Nose wear (μm)	Surface Roughness R_a (μm)
0.0	0	0	0	0	0	0.79
0.5						0.82
1.0						0.87
1.5						1.17
2.0						1.42
3.0	2	4.5	72	0.38	6	1.58
4.0						1.65
5.0						1.69
6.0	3	4.5	85	0.85	7	1.70
7.0						1.72
8.0						1.72
9	3	4.5	112	1.66	8.5	1.73
10.5						1.74
12						1.76
14	3	5.0	135	2.30	10	1.77
16						1.79
18						1.80
20	3	5.3	160	2.50	11.5	1.82
22						1.85
25						1.89
27	4	7.3	180	3.96	17.5	1.94
29						2.09
31						2.23
34.5	4	8.7	220	4.90	20	2.49
37						2.68
39.5						2.89
42	5	9.6	280	8.75	24	3.19

Table C-5 Overall groove wear data under cutting condition Group E
 Machine Tool : HITEC-20SII CNC Lathe (18 KW)
 $V = 190$ m/min, $f = 0.04$ mm/rev, $d = 0.25$ mm

Cutting Time (minute)	Number of Groove	Groove Depth (μm)	Maximum Groove Length (μm)	Groove Wear Area (mm^2)	Nose wear (μm)	Surface Roughness R_a (μm)
0.0	0	0	0	0	0	0.35
0.5						0.37
1.0						0.40
1.5						0.70
2.0						0.99
3.0	4	4.5	75	0.94	6	1.34
4.0						1.56
5.0						1.74
6.0	5	4.5	95	1.12	7	1.73
7.5						1.76
9						1.79
11	7	4.8	145	3.22	7.5	1.81
13						1.86
15						1.85
17	7	6.1	160	3.68	10	1.84
18.5						2.59
21						2.99
23	2	4.3	200	6.24	15	3.51
25						3.62
27						3.69
30	1	2.8	240	6.48	18	3.62
32						3.57
35						3.58
37	1	2.65	275	7.80	21	3.60
39						3.59
41						3.58
44	1	2.30	318	9.99	25	3.60

APPENDIX D

INPUT/OUTPUT TRAINING AND TESTING DATA
IN NEURAL NETWORK EXPERIMENTS

Table D-1 The training data under Training Cutting Conditions 4-6

	INPUT FEATURES							OUTPUTS	
	Feed Speed (mm/rev) (m/min)	D'_x (LF) (min^{-1})	D'_x (HF) (min^{-1})	D'_y (HF) (min^{-1})	D'_z (HF) (min^{-1})	$\mu_i(k)$	$\mu_o(k)$	R_a (μm)	
Cutting Condition 4	0.06	205	-8.09	2.07	4.53	2.17	0.15	0.15	0.85
	0.06	205	-4.57	1.23	2.38	1.35	0.15	0.20	1.00
	0.06	205	-1.05	0.39	0.23	0.53	0.20	0.28	1.12
	0.06	205	2.47	-0.45	-1.93	-0.29	0.28	0.35	1.49
	0.06	205	5.99	-1.29	-4.08	-1.11	0.35	0.30	1.74
	0.06	205	9.51	-2.13	-8.59	-1.93	0.30	0.26	1.99
Cutting Condition 5	0.10	170	-4.82	3.16	3.44	0.53	0.22	0.22	0.94
	0.10	170	-2.82	2.06	2.09	0.18	0.22	0.25	1.15
	0.10	170	-0.82	0.96	0.74	-0.17	0.25	0.29	1.35
	0.10	170	-1.18	-0.14	-0.61	-0.52	0.29	0.33	1.50
	0.10	170	3.18	-1.24	-1.96	-0.87	0.33	0.38	1.68
	0.10	170	5.18	-2.34	-3.31	-1.22	0.38	0.37	2.09
	0.10	170	7.18	-3.44	-4.66	-1.57	0.37	0.34	2.27
Cutting Condition 6	0.15	160	-3.65	3.32	6.75	1.31	0.28	0.28	0.98
	0.15	160	-1.17	1.66	4.83	0.87	0.28	0.35	1.14
	0.15	160	1.31	0.00	2.91	0.43	0.35	0.48	1.22
	0.15	160	3.79	-1.66	0.99	0.01	0.48	0.51	1.39
	0.15	160	6.27	-3.32	-0.93	-0.45	0.51	0.45	1.81
	0.15	160	8.75	-4.98	-2.85	-0.89	0.45	0.42	1.96

Table D-2 The testing data under Testing Cutting Conditions 1-2

	INPUT FEATURES							OUTPUTS	
	Feed (mm/rev)	Speed (m/min)	D'_x (LF) (min^{-1})	D'_x (HF) (min^{-1})	D'_y (HF) (min^{-1})	D'_z (HF) (min^{-1})	μ_i (k)	μ_o (k)	R_a (μm)
Testing Condition 1	0.12	140	-9.78	6.01	2.55	1.52	0.28	0.28	1.06
	0.12	140	-6.51	4.14	1.40	1.15	0.28	0.31	1.09
	0.12	140	-3.23	2.26	0.25	0.77	0.31	0.34	1.13
	0.12	140	0.05	0.39	-0.90	0.40	0.34	0.38	1.33
	0.12	140	3.32	-1.49	-2.05	0.02	0.38	0.53	1.87
	0.12	140	6.60	-3.37	-3.20	-0.36	0.53	0.50	2.05
	0.12	140	9.87	-5.24	-4.35	-0.73	0.50	0.44	2.33
Testing Condition 2	0.06	165	-0.97	3.44	6.03	1.26	0.20	0.20	0.98
	0.06	165	-6.22	2.34	4.03	0.86	0.20	0.23	1.08
	0.06	165	-3.37	1.24	2.03	0.46	0.23	0.26	1.12
	0.06	165	-0.52	0.14	0.03	0.06	0.26	0.30	1.26
	0.06	165	2.33	-0.96	-1.97	-0.34	0.30	0.36	1.52
	0.06	165	5.18	-2.06	-3.97	-0.74	0.36	0.38	1.94
	0.06	165	8.03	-3.16	-5.97	-1.14	0.38	0.34	2.37

Table D-3 The testing data under Testing Cutting Conditions 3-4

	INPUT FEATURES							OUTPUTS	
	Feed (mm/rev)	Speed (m/min)	D'_x (LF) (min^{-1})	D'_x (HF) (min^{-1})	D'_y (HF) (min^{-1})	D'_z (HF) (min^{-1})	μ_i (k)	μ_o (k)	R_a (μm)
Testing Condition 3	0.06	190	-12.9	1.23	8.59	0.63	0.18	0.18	0.95
	0.06	190	-9.00	0.58	6.31	0.37	0.18	0.22	1.11
	0.06	190	-5.12	-0.07	4.03	0.10	0.22	0.26	1.21
	0.06	190	-1.24	-0.80	1.75	-0.17	0.26	0.33	1.37
	0.06	190	2.64	-1.37	-0.53	-0.43	0.33	0.36	1.58
	0.06	190	6.53	-2.02	-2.81	-0.70	0.36	0.31	1.92
Testing Condition 4	0.15	130	-4.54	3.87	6.69	2.38	0.30	0.30	1.10
	0.15	130	-3.02	2.72	4.64	1.78	0.30	0.32	1.13
	0.15	130	-1.49	1.57	2.59	1.18	0.32	0.37	1.16
	0.15	130	0.04	0.42	0.54	0.58	0.37	0.45	1.22
	0.15	130	1.56	-0.73	-1.51	-0.02	0.45	0.52	1.34
	0.15	130	3.09	-1.88	-3.56	-0.62	0.52	0.56	1.67
	0.15	130	4.61	-3.03	-5.61	-1.22	0.56	0.51	1.96
	0.15	130	6.44	-4.41	-8.07	-1.94	0.51	0.49	2.23